

University of Windsor

Scholarship at UWindor

Electronic Theses and Dissertations

Theses, Dissertations, and Major Papers

10-30-2020

Methods Development for the Fluorescent Determination of Inorganic Phosphate and Phospho-Proteins

Angela Awada
University of Windsor

Follow this and additional works at: <https://scholar.uwindsor.ca/etd>

Recommended Citation

Awada, Angela, "Methods Development for the Fluorescent Determination of Inorganic Phosphate and Phospho-Proteins" (2020). *Electronic Theses and Dissertations*. 8434.
<https://scholar.uwindsor.ca/etd/8434>

This online database contains the full-text of PhD dissertations and Masters' theses of University of Windsor students from 1954 forward. These documents are made available for personal study and research purposes only, in accordance with the Canadian Copyright Act and the Creative Commons license—CC BY-NC-ND (Attribution, Non-Commercial, No Derivative Works). Under this license, works must always be attributed to the copyright holder (original author), cannot be used for any commercial purposes, and may not be altered. Any other use would require the permission of the copyright holder. Students may inquire about withdrawing their dissertation and/or thesis from this database. For additional inquiries, please contact the repository administrator via email (scholarship@uwindsor.ca) or by telephone at 519-253-3000ext. 3208.

**Methods Development for the Fluorescent Determination of Inorganic Phosphate
and Phospho-Proteins**

By

Angela Awada

A Thesis
Submitted to the Faculty of Graduate Studies
through the Department of Chemistry and Biochemistry
in Partial Fulfillment of the Requirements for
the Degree of Master of Science
at the University of Windsor

Windsor, Ontario, Canada

2020

© 2020 Angela Awada

**Methods Development for the Fluorescent Determination of Inorganic Phosphate
and Phospho-Proteins**

by

Angela Awada

APPROVED BY:

J. Gagnon
School of the Environment

K. E. Taylor
Department of Chemistry and Biochemistry

B. Mutus, Advisor
Department of Chemistry and Biochemistry

September 1st, 2020

DECLARATION OF ORIGINALITY

I hereby certify that I am the sole author of this thesis and that no part of this thesis has been published or submitted for publication.

I certify that, to the best of my knowledge, my thesis does not infringe upon anyone's copyright nor violate any proprietary rights and that any ideas, techniques, quotations, or any other material from the work of other people included in my thesis, published or otherwise, are fully acknowledged in accordance with the standard referencing practices. Furthermore, to the extent that I have included copyrighted material that surpasses the bounds of fair dealing within the meaning of the Canada Copyright Act, I certify that I have obtained a written permission from the copyright owner(s) to include such material(s) in my thesis and have included copies of such copyright clearances to my appendix.

I declare that this is a true copy of my thesis, including any final revisions, as approved by my thesis committee and the Graduate Studies office, and that this thesis has not been submitted for a higher degree to any other University or Institution.

ABSTRACT

The micronutrient orthophosphate loss into the aquatic environment is one of the primary drivers of harmful algal blooms (HABs) which result in the contamination of drinking water and negatively affects recreation and tourism industries. The aim of this study was to develop fluorescence-based P_i sensors with sensitivity in the low micromolar range.

Various solid supports were surveyed as potential sensor optimizing components. Quinacrine mustard dihydrochloride bound to Sephadex[®] LH-20 yielded fluorescence detection of inorganic phosphate concentrations between 0.5-1.25 mM. Quercetin-Al (III), shared a direct negative fluorescence relationship with inorganic phosphate concentrations between 0-1 mM, in aqueous solutions of pH 5. Binding studies of quercetin-Zr (IV) led to an extended investigation for the detection of phospho-biomolecules.

Phosphorylation of proteins are prevalent post-translational modifications responsible for signal transduction pathways and gene expression. As such, our quercetin-Zr (IV) probe was studied as a simple and cost-effective stain for phosphorylated proteins immobilized on nitrocellulose membrane. Our studies also explored the potential of an aqueous phosphatase assay with the *o*-aminobenzoyl-phosphoserine as a potential probe. These studies yielded significant fluorescence differences between phosphorylated and nonphosphorylated *L*-serine amino acid conjugates in the presence of lanthanide metal, europium (III). These findings can be further utilized for the optimization of inorganic phosphate and phospho-protein/peptide assays.

DEDICATION

To my mother.

ACKNOWLEDGEMENTS

First and foremost, I would like to extend my gratitude to my supervisor and mentor, Dr. Bulent Mutus, for his guidance and unwavering support throughout my graduate studies. Thank you for giving me the opportunity to conduct research in your lab as both an undergraduate and graduate student and to grow as a researcher and individual. I am humbled by your knowledge and grateful to have worked alongside you.

My appreciation is further extended to committee members, Dr.'s Keith Taylor and Joel Gagnon for their valuable input, critical evaluation of my work and meaningful insight towards the success of this research project.

I would like to thank Dr. Matthew Revington for his help and guidance in conducting the NMR studies, it was a pleasure to have worked with you. I would like to also thank Dr. Sam Johnson for taking the time to evaluate and study the NMR spectral data with me. I would also like to thank Jean Claude Barrette and Dr. Gagnon for allowing me to use the laser ablation facilities at GLIER, those winter walks woke me up faster than coffee. And I would like to thank Dr. Vacratsis and Justin Roberto for their collaboration and insight on phospho-proteins, your contribution truly expanded our research and understanding of our probe. I would also like to thank Dr. Sirinart Ananvoranich for kindly sharing her fluorescence imager throughout my studies.

For the tireless efforts and smooth operations of the Department of Chemistry and Biochemistry, I give thanks to Beth Kickham, Marlene Bezaire,

Jayne Pierce, and Joe Lichaa. Thank you all for your administrative services and going above and beyond to assist students and faculty. Your energy and spirits added great value to my graduate experience.

A lab is simply a shell without its researchers, for that I want to extend a warm appreciation to all the Mutus lab members I had the opportunity to work alongside of both past and present, it was truly a pleasure.

Finally, I want to acknowledge my family, especially my mother and brother, David, for their patience and support throughout my studies. To Joana, a true cheerleader on the other side of the world, Zeinab, for keeping me company during long days and Ilhan, for always being a light and reminder of good faith.

TABLE OF CONTENTS

DECLARATION OF ORIGINALITY	iii
ABSTRACT.....	iv
ACKNOWLEDGEMENTS	vi
LIST OF FIGURES	x
LIST OF APPENDICES.....	xiii
LIST OF ABBREVIATIONS/SYMBOLS.....	xvi
CHAPTER 1	1
INORGANIC PHOSPHATE AND PRINCIPLES OF FLUORESCENCE.....	1
1. The fluorescence phenomenon	2
1.1 Förster resonance energy transfer - FRET	10
1.2. The application of fluorescence spectroscopy to analyte detection	12
1.3. Developing chemical sensors for environmental studies	13
1.4. Fluorescence dyes for inorganic phosphate detection.....	15
1.5. Research objectives and rationale	23
CHAPTER 2	24
PHOSPHO-PROTEIN SENSORS.....	24
2. Fluorescent probes for phospho-peptides and phospho-proteins	25
2.1. Fluorophores used for phospho-protein detection	28
2.2. Alkaline phosphatase	30
2.3. o-amino-benzoyl/Isatoic anhydride.....	32
2.4. Research objectives and rationale	34
CHAPTER 3	35
MATERIALS AND METHODS.....	35
3.1. Survey for potential inorganic phosphate sensors.....	36
3.2. Optimizing potential inorganic phosphate probes	39
3.3. Exploring the use of probes for phosphoprotein detection	40

3.4. Investigating potential probes for an aqueous phosphatase assay	45
CHAPTER 4	47
RESULTS	47
4.1. Survey for potential inorganic phosphate sensors.....	48
4.2. Investigating solid supports for potential inorganic phosphate sensor systems.....	52
4.3. The determination of phosphate content on cellulose-phosphate	57
4.4. Investigating fluorogenic quercetin-metal probes for potential inorganic phosphate aqueous assays	69
4.5. Characterizing the flavonoid-metal complex of quercetin-Zr (IV).....	84
4.6. Surveying the quercetin-Zr (IV) probe for the detection of phospho-amino acids and phospho-proteins	96
4.7. o-amino-benzoyl labelled amino acids for the use of a phosphatase assay	105
4.8. Results summary	120
CHAPTER 5	122
DISCUSSION	122
5. The investigation of an inorganic phosphate sensor	123
5.1. Investigating phospho-protein sensors using quercetin-Zr (IV)	127
5.2. The development of a conjugated fluorescence phosphatase assay	130
5.3. Discussion summary	134
CHAPTER 6	135
CONCLUSION AND FUTURE DIRECTIONS	135
REFERENCES/BIBLIOGRAPHY	140
APPENDICES	156
VITA AUCTORIS	216

LIST OF FIGURES

Figure 1. 1. Jablonski diagram for the absorption and fluorescence of molecules.	3
Figure 1. 2. Emission spectra of DNS (4-dimethylamino-4'-nitrostilbene) in solvents of increasing polarity.....	5
Figure 1. 3. FITC-PEG-lipid fluorescent properties in various pH environments.....	7
Figure 1. 4. Emission spectra of four α -helix quenching model in the presence of halothane.....	9
Figure 1. 5. Energy transfer between tryptophan donor emission with dansyl acceptor absorption.....	11
Figure 1. 6. Lake Erie capture of hazardous algal bloom containing microcystin toxins...14	
Figure 1. 7. Molecular structures of phosphate species with pKa values [35].....	16
Figure 1. 8. Propidium iodide structure.	18
Figure 1. 9. Quinacrine dihydrochloride structure.....	20
Figure 1. 10. Quercetin chemical structure.....	22
Figure 2. 1. The general schematic of the phosphorylation and dephosphorylation of proteins.....	27
Figure 2. 2. The hydrolysis reactions of monoester phosphate on protein catalyzed by alkaline phosphatase. (Assembled with bioRENDER.).....	31
Figure 2. 3. Isatoic anhydride reaction scheme with L-threonine or O-phospho-L-threonine.	33
Figure 4. 1. Survey of propidium iodide (PI) fluorescence emission studies in varying solutions.....	49
Figure 4. 2. Survey of quinacrine mustard dihydrochloride (QM) fluorescence emission studies in varying solutions.....	51
Figure 4. 3. Quinacrine mustard dihydrochloride (QM) fluorescence emission studies in Tris-HCl (0.1 M, pH 7) using Sephadex LH-20.	53
Figure 4. 4. Quinacrine mustard dihydrochloride (QM) fluorescence emission studies in Tris-HCl (0.1 M, pH 7) using calcium phosphate.....	55
Figure 4. 5. Quinacrine mustard dihydrochloride (QM) fluorescence emission studies in 50 mg of calcium phosphate.	56
Figure 4. 6. General schematic of cellulose-phosphate hypothesized interaction with cationic fluorophore.	58
Figure 4. 7. FTIR spectra of cellulose and synthesized cellulose-phosphate disks.	60
Figure 4. 8. Phosphorus elemental analysis of cellulose and synthesized cellulose-phosphate using laser ablation techniques.	62
Figure 4. 9. Inorganic phosphate concentrations for cellulose (C) and cellulose-phosphate (CP) disks after sulfuric acid digestion.	64
Figure 4. 10. General schematic of cellulose-phosphate hypothesized interaction with quercetin-Al (III).....	66
Figure 4. 11. Cellulose-phosphate disks stained with quercetin-Al (III) (25 μ M, 50 μ M) washed with increasing concentrations of inorganic phosphate.	68
Figure 4. 12. UV-vis spectra of quercetin (25 μ M) in varying pH environments.....	70

Figure 4. 13. UV-vis spectra of quercetin-nickel (II) (25 μ M, 50 μ M) in varying pH environments.....	71
Figure 4. 14. UV-vis spectra of quercetin-iron (III) (25 μ M, 50 μ M) in varying pH environments.....	72
Figure 4. 15. UV/vis spectra of quercetin-aluminum (III) (25 μ M, 50 μ M) in varying pH environments.....	74
Figure 4. 16. Fluorescence emission spectra of quercetin-aluminum (III) (25 μ M, 50 μ M, pH 2) with P_i titrations (ex: 425 nm).	75
Figure 4. 17. Fluorescence emission spectra of quercetin-aluminum (III) (25 μ M, 50 μ M, pH 5) with P_i titrations (ex: 425 nm).	76
Figure 4. 18. Fluorescence emission spectra of quercetin-aluminum (III) (25 μ M, 50 μ M, pH 2) with P_i titrations (ex: 440 nm).	77
Figure 4. 19. Fluorescence emission spectra of quercetin-aluminum (III) (25 μ M, 50 μ M, pH 5) with P_i titrations (ex: 440 nm).	78
Figure 4. 20. UV/vis spectra of quercetin-zirconium (IV) (25 μ M, 50 μ M) in varying pH environments.....	80
Figure 4. 21. Fluorescence emission spectra of quercetin-zirconium (IV) (25 μ M, 50 μ M, pH 9) with P_i titrations (ex: 455 nm).	81
Figure 4. 22. Fluorescence emission spectra of quercetin-zirconium (IV) (25 μ M, 50 μ M, pH 9) with P_i titrations (ex: 465 nm).	82
Figure 4. 23. Fluorescence emission spectra of quercetin-zirconium (IV) (25 μ M, 50 μ M, pH 9) with P_i titrations (ex: 470 nm).	83
Figure 4. 24. UV/vis spectra of quercetin (20 μ M) with zirconium (IV) chloride titrations.	85
Figure 4. 25. Fluorescence emission intensities of quercetin and zirconium (IV) chloride using steady-state kinetics.....	86
Figure 4. 26. Fluorescence emission spectra of quercetin-zirconium (IV) (10 μ M, 40 μ M, pH 9) with P_i titrations (ex: 465 nm).	88
Figure 4. 27. Fluorescence emission spectra of quercetin-zirconium (IV) (10 μ M, 100 μ M, pH 9) with P_i titrations (ex: 465 nm).	89
Figure 4. 28. The postulated chemical reaction between quercetin ligand and zirconium (IV).....	91
Figure 4. 29. H^1 NMR spectra for quercetin and zirconium (IV) chloride.	92
Figure 4. 30. H^1 NMR spectra of quercetin-zirconium (IV) (2.5 mM, 1.22 mM) and inorganic phosphate (P_i).....	94
Figure 4. 31. ^{31}P NMR spectra of inorganic phosphate and zirconium (IV) chloride.....	95
Figure 4. 32. Fluorescence emission spectra of quercetin-zirconium (IV) (10 μ M, 20 μ M, pH 9) with L-serine titrations.....	97
Figure 4. 33. Fluorescence emission spectra of quercetin-zirconium (IV) (10 μ M, 20 μ M, pH 9) with O-phospho-L-serine titrations.....	98
Figure 4. 34. Quercetin-Zr (IV) fluorescently stained nitrocellulose dot blot of protein samples.....	100
Figure 4. 35. Integrated density of fluorescently stained quercetin-Zr(IV) stained nitrocellulose dot blot of protein samples.	101

Figure 4. 36. Quercetin-Zr (IV) fluorescently stained nitrocellulose membrane dot blot of alkaline phosphatase treated protein samples.	103
Figure 4. 37. Integrated density of fluorescently stained quercetin-Zr(IV) stained nitrocellulose dot blot of alkaline phosphatase treated protein samples.	104
Figure 4. 38. Isatoic anhydride reaction scheme with L-serine or O-phospho-L-serine...	106
Figure 4. 39. ¹ H NMR spectra of isatoic anhydride, OAb-L-serine and OAb-O-phospho-L-serine.	107
Figure 4. 40. ¹ H NMR spectra of the aromatic regions of isatoic anhydride, OAb-L-serine and O-phospho-L-serine.	108
Figure 4. 41. UV/vis spectra of the normalization of OAb-L-serine and OAb-O-phospho-L-serine.	110
Figure 4. 42. Fluorescent emission spectra of normalized OAb-L-serine and OAb-O-phospho-L-serine.	111
Figure 4. 43. ZrCl ₄ precipitation assay of OAb-L-serine and OAb-O-phospho-L-serine.	113
Figure 4. 44. Emission properties of precipitation assay of ZrCl ₄ with OAb-S and OAb-PS.	115
Figure 4. 45: Aqueous assay of OAb-S/-PS with the titration of europium (III) chloride (650 μM, pH 4).	117
Figure 4. 46: Aqueous assay of OAb-S/-PS with the titration of europium (III) chloride (904 μM, pH 7).	118
Figure 4. 47. Aqueous assay of OAb-S/-PS with the titration of europium (III) chloride (854 μM, pH 9).	119

LIST OF APPENDICES

Figure A. 1: Fluorescence emission spectra of quercetin (25 μ M, pH 4) with P_1 titrations (ex: 375 nm).....	157
Figure A. 2: Fluorescence emission spectra of quercetin-Ni (II) (25 μ M, 50 μ M, pH 2) with P_1 titrations (ex: 335 nm).....	158
Figure A. 3: Fluorescence emission spectra of quercetin-Ni (II) (25 μ M, 50 μ M, pH 9) with P_1 titrations (ex: 335 nm).....	159
Figure A. 4: Fluorescence emission spectra of quercetin-Ni (II) (25 μ M, 50 μ M, pH 5) with P_1 titrations (ex: 335 nm).....	160
Figure A. 5: Fluorescence emission spectra of quercetin-Ni (II) (25 μ M, 50 μ M, pH 2) with P_1 titrations (ex: 380 nm).....	161
Figure A. 6: Fluorescence emission spectra of quercetin-Ni (II) (25 μ M, 50 μ M, pH 5) with P_1 titrations (ex: 380 nm).....	162
Figure A. 7: Fluorescence emission spectra of quercetin-Ni (II) (25 μ M, 50 μ M, pH 9) with P_1 titrations (ex: 380 nm).....	163
Figure A. 8: Fluorescence emission spectra of quercetin-Al (III) (25 μ M, 50 μ M, pH 2) with P_1 titrations (ex: 320 nm).....	164
Figure A. 9: Fluorescence emission spectra of quercetin-Al (III) (25 μ M, 50 μ M, pH 5) with P_1 titrations (ex: 320 nm).....	165
Figure A. 10: Fluorescence emission spectra of quercetin-Al (III) (25 μ M, 50 μ M, pH 9) with P_1 titrations (ex: 320 nm).....	166
Figure A. 11: Fluorescence emission spectra of quercetin-Al (III) (25 μ M, 50 μ M, pH 12) with P_1 titrations (ex: 320 nm).....	167
Figure A. 12: Fluorescence emission spectra of quercetin-Al (III) (25 μ M, 50 μ M, pH 2) with P_1 titrations (ex: 380 nm).....	168
Figure A. 13: Fluorescence emission spectra of quercetin-Al (III) (25 μ M, 50 μ M, pH 5) with P_1 titrations (ex: 380 nm).....	169
Figure A. 14: Fluorescence emission spectra of quercetin-Al (III) (25 μ M, 50 μ M, pH 9) with P_1 titrations (ex: 380 nm).....	170
Figure A. 15: Fluorescence emission spectra of quercetin-Al (III) (25 μ M, 50 μ M, pH 12) with P_1 titrations (ex: 380 nm).....	171
Figure A. 16: Fluorescence emission spectra of quercetin-Al (III) (25 μ M, 50 μ M, pH 9) with P_1 titrations (ex: 425 nm).....	172
Figure A. 17: Fluorescence emission spectra of quercetin-Al (III) (25 μ M, 50 μ M, pH 12) with P_1 titrations (ex: 425 nm).....	173
Figure A. 18: Fluorescence emission spectra of quercetin-Al (III) (25 μ M, 50 μ M, pH 9) with P_1 titrations (ex: 440 nm).....	174
Figure A. 19: Fluorescence emission spectra of quercetin-Al (III) (25 μ M, 50 μ M, pH 12) with P_1 titrations (ex: 440 nm).....	175
Figure A. 20: Fluorescence emission spectra of quercetin-Fe (III) (25 μ M, 50 μ M, pH 7) with P_1 titrations (ex: 330 nm).....	176
Figure A. 21: Fluorescence emission spectra of quercetin-Fe (III) (25 μ M, 50 μ M, pH 11) with P_1 titrations (ex: 330 nm).....	177

Figure A. 22: Fluorescence emission spectra of quercetin-Fe (III) (25 μ M, 50 μ M, pH 7) with P ₁ titrations (ex: 445 nm).....	178
Figure A. 23: Fluorescence emission spectra of quercetin-Fe (III) (25 μ M, 50 μ M, pH 11) with P ₁ titrations (ex: 445 nm).....	179
Figure A. 24: Fluorescence emission spectra of quercetin-Zr (IV) (25 μ M, 50 μ M, pH 3) with P ₁ titrations (ex: 325 nm).....	180
Figure A. 25: Fluorescence emission spectra of quercetin-Zr (IV) (25 μ M, 50 μ M, pH 9) with P ₁ titrations (ex: 325 nm).....	181
Figure A. 26: Fluorescence emission spectra of quercetin-Zr (IV) (25 μ M, 50 μ M, pH 12) with P ₁ titrations (ex: 325 nm).....	182
Figure A. 27: Fluorescence emission spectra of quercetin-Zr (IV) (25 μ M, 50 μ M, pH 3) with P ₁ titrations (ex: 455 nm).....	183
Figure A. 28: Fluorescence emission spectra of quercetin-Zr (IV) (25 μ M, 50 μ M, pH 12) with P ₁ titrations (ex: 455 nm).....	184
Figure A. 29: Fluorescence emission spectra of quercetin-Zr (IV) (25 μ M, 50 μ M, pH 3) with P ₁ titrations (ex: 465 nm).....	185
Figure A. 30: Fluorescence emission spectra of quercetin-Zr (IV) (25 μ M, 50 μ M, pH 12) with P ₁ titrations (ex: 465 nm).....	186
Figure A. 31: Fluorescence emission spectra of quercetin-Zr (IV) (25 μ M, 50 μ M, pH 3) with P ₁ titrations (ex: 470 nm).....	187
Figure A. 32: Fluorescence emission spectra of quercetin-Zr (IV) (25 μ M, 50 μ M, pH 12) with P ₁ titrations (ex: 470 nm).....	188
Figure B. 1: Immunoblot of alkaline phosphatase treated MTMR2 using rabbit anti-pSer ⁵⁸ antibody.	189
Figure B. 2: Thin Layer Chromatography performed on SiliaPlate™ TLC aluminum backed TLC plates for IA (isatoic anhydride).	190
Figure B. 3: Thin Layer Chromatography performed on SiliaPlate™ TLC aluminum backed TLC plates for o-aminobenzoyl-L-serine.	191
Figure B. 4: Thin Layer Chromatography performed on SiliaPlate™ TLC aluminum backed TLC plates for o-aminobenzoyl-phospho-L-serine.	192
Figure B. 5: Aqueous assay of OAb-S/-PS with the titration of aluminum (III) chloride (1.92 mM, pH 4).	193
Figure B. 6: Aqueous assay of OAb-S/-PS with the titration of aluminum (III) chloride (980 μ M, pH 7).	194
Figure B. 7: Aqueous assay of OAb-S/-PS with the titration of aluminum (III) chloride (1.92 mM, pH 9).	195
Figure B. 8: Aqueous assay of OAb-S/-PS with the titration of cobalt (II) chloride (650 μ M, pH 4).	196
Figure B. 9: Aqueous assay of OAb-S/-PS with the titration of cobalt (II) chloride (1.17 mM, pH 7).....	197
Figure B. 10: Aqueous assay of OAb-S/-PS with the titration of cobalt (II) chloride (2.83 mM, pH 9).....	198
Figure B. 11: Aqueous assay of OAb-S/-PS with the titration of copper (II) chloride (1.17 mM, pH 4).....	199

Figure B. 12: Aqueous assay of OAb-S/-PS with the titration of copper (II) chloride (2.10 mM, pH 7).....	200
Figure B. 13: Aqueous assay of OAb-S/-PS with the titration of copper (II) chloride (2.83 mM, pH 9).....	201
Figure B. 14: Aqueous assay of OAb-S/-PS with the titration of iron (III) sulfate (980 μ M, pH 4).	202
Figure B. 15: Aqueous assay of OAb-S/-PS with the titration of iron (III) sulfate (1.36 mM, pH 7).....	203
Figure B. 16: Aqueous assay of OAb-S/-PS with the titration of iron (III) sulfate (1.36 mM, pH 9).....	204
Figure B. 17: Aqueous assay of OAb-S/-PS with the titration of lanthanum (III) chloride (1.15 mM, pH 4).	205
Figure B. 18: Aqueous assay of OAb-S/-PS with the titration of lanthanum (III) chloride (589 μ M, pH 7).	206
Figure B. 19: Aqueous assay of OAb-S/-PS with the titration of lanthanum (III) chloride (1.15 mM, pH 9).	207
Figure B. 20: Aqueous assay of OAb-S/-PS with the titration of nickel (II) chloride (210 μ M, pH 4).	208
Figure B. 21: Aqueous assay of OAb-S/-PS with the titration of nickel (II) chloride (980 μ M, pH 7).	209
Figure B. 22: Aqueous assay of OAb-S/-PS with the titration of nickel (II) chloride (1.92 mM, pH 9).....	210
Figure B. 23: Aqueous assay of OAb-S/-PS with the titration of vanadium (III) chloride (1.8 mM, pH 4).	211
Figure B. 24: Aqueous assay of OAb-S/-PS with the titration of vanadium (III) chloride (588 μ M, pH 7).	212
Figure B. 25: Aqueous assay of OAb-S/-PS with the titration of vanadium (III) chloride (1.15 mM, pH 9).	213
Appendix C (Copyright permissions)	214

LIST OF ABBREVIATIONS/SYMBOLS

APP	Alkaline Phosphatase
C	Cellulose
Cali	Calyculin A
CaP	Calcium Phosphate
CMC	Carboxymethyl Cellulose
CP	Cellulose-Phosphate
DMSO	Dimethyl Sulfoxide
em	Emission Wavelength
ex	Excitation Wavelength
GAPP	Germ Cell Alkaline Phosphatase
HABs	Harmful Algal Blooms
HEK293	Human Embryonic Kidney Cells
IAPP	Intestinal Alkaline Phosphatase
Ib	Isosbestic Point
IP	Immunoprecipitation
K	Dissociation Constant
K_b	Binding Constant
LBKAPP	Liver Bone Kidney Alkaline Phosphatase
LH-20	Sephadex
LH-20-QM	LH-20-Quinacrine Mustard
MeOH	Methanol
MTMR2	Myotubularin Related-Protein 2
OAb-PS	<i>o</i> -Aminobenzoyl-Phospho-L-Serine
OAb-S	<i>o</i> -Aminobenzoyl-L-Serine
OAb-S/-PS	<i>o</i> -Aminobenzoyl-Serine or <i>o</i> -Aminobenzoyl-Phosphoserine
P	Orthophosphate
PAPP	Placental Alkaline Phosphatase
phospho-serine	O-Phospho-L-Serine
PI	Propidium Iodide
P_i	Inorganic Phosphate
ppm	Parts Per Million
PSS	Poly (Sodium 4-Styrenesulfonate)
QM	Quinacrine Mustard Dihydrochloride Hydrate
Quercetin-Zr	Quercetin-Zirconium (IV)
Quercetin-Zr (IV)	Quercetin-Zirconium (IV)
Quercetin-Zr-Pi	Precipitated Quercetin-Zirconium-Phosphate
rpm	Revolutions Per Minute
SDS-PAGE	Sodium Dodecyl Sulfate Polyacrylamide Gel Electrophoresis
Serine	L-Serine

STMP	Sodium Trimetaphosphate
Tris-HCl	Tris Hydrochloric Acid Buffer
μE	Excited State
μG	Ground State
λ_{em}	Emission Wavelength
λ_{ex}	Excitation Wavelength

CHAPTER 1

INORGANIC PHOSPHATE AND PRINCIPLES OF FLUORESCENCE

1. The fluorescence phenomenon

Fluorescence spectroscopy has become one of the most prevailing high-sensitivity applications for the detection and quantification of molecules. The fluorescence phenomenon studies the emission of light from excited singlet states, or the luminescence, of any molecule [1]. These molecules absorb radiation at specific wavelengths. As this occurs, molecules become electronically excited and electrons are promoted from the ground state (μG) to the excited state (μE) [2]. As electrons transition back down to the ground state, energy in the form of photons is released to form immediate emissions (**figure 1.1**). Emission spectra are also computed and used to study molecular fluorescent properties [1]. Emission spectra are plotted as fluorescence intensity (a.u) versus wavelength (nm). There are various properties in fluorescent systems that constitute and characterize emission spectra. These properties involve and are not limited to chemical compositions of fluorophores, intra- and intermolecular interactions between fluorophores and solvents, pH environments and quantum yield [3].

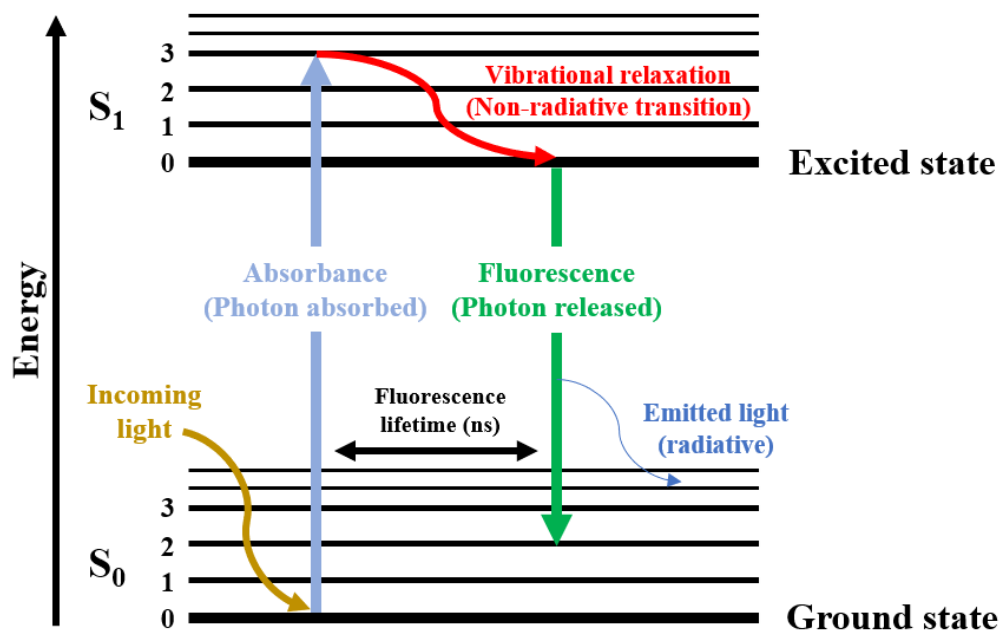


Figure 1. 1. Jablonski diagram for the absorption and fluorescence of molecules.

An incident light excites the molecule at a wavelength which it can absorb a photon and transition from the ground state (S_0) to the higher electronic excited state (S_1). Electrons undergo an internal conversion by vibrational relaxation (red arrow), before a photon is emitted from the lowest (singlet) excited state. (adapted from [1, 4])

Solvents adopt a critical role as fluorescent media; their pH, polarity and electrostatic properties have profound effects on the fluorescence profiling of any fluorophore [5]. Studies have shown that solvent permittivity allows ion pairing even by long-range electrostatic forces [6]. These effects can be a result of simple changes in solvent environments. There is an extensive volume of scientific research that has supported the sensitivity of polar solvents and how their properties can induce an alignment of solvent and fluorophore dipoles. In the excited state (μE), fluorophores have the largest dipole moment and after excitation, solvent dipoles reorient and relax, while excess vibrational energy is absorbed by the polar solvent stabilizes the excited state (μE). This lowers the energy of the excited state (μE) and prompts longer emission wavelengths. Solvent polarity has been found to be most sensitive for polar fluorophores, on account of their large dipole moments in the excited state (μE) (**figure 1.2**) [1, 5, 7].

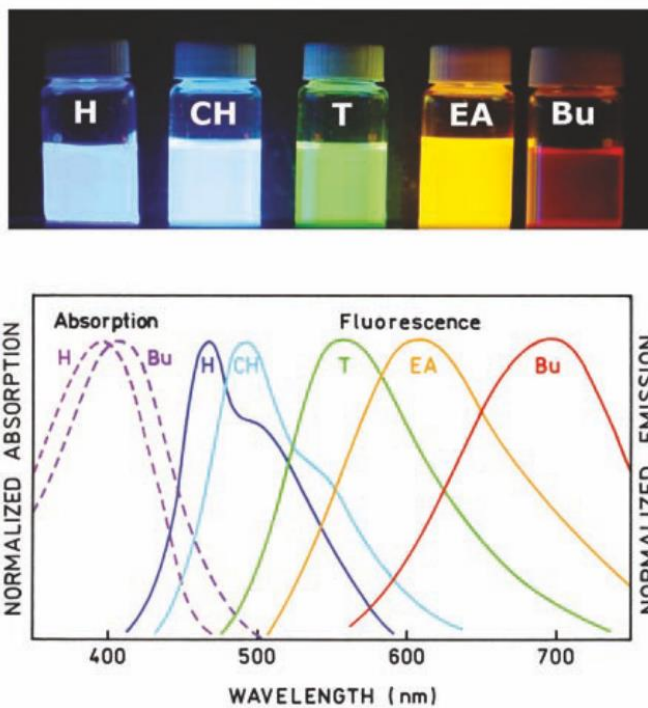


Figure 1. 2. Emission spectra of DNS (4-dimethylamino-4'-nitrostilbene) in solvents of increasing polarity.

H, hexane; CH, cyclohexane; T, toluene; EA, ethyl acetate; Bu, n-butanol. (Copyright © Springer Nature) [1]

In addition to solvent polarity, the effects of pH and hydrogen bonding are fundamental properties to help understand solvent-fluorophore interactions [6]. Increasing concentrations of polar solvents have been linked to hydrogen bonding in solvent-fluorophore interactions, showing gradual increases in emission wavelengths (λ_{em}) (**figure 1.3**) [1]. Manipulating pH environments in fluorescent systems changes absorption wavelengths of fluorogenic species, in turn changing excitation sites. Identifying these emissive species are imperative for the study of potential probes and sensors [8].

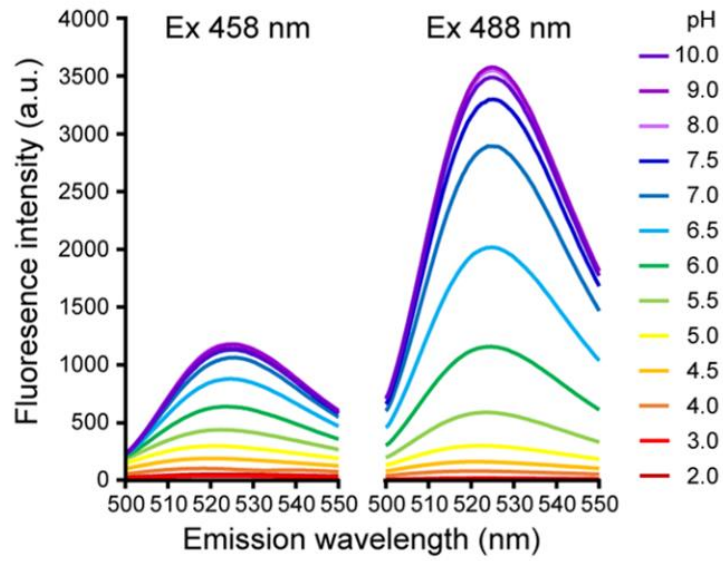


Figure 1. 3. FITC-PEG-lipid fluorescent properties in various pH environments.

FITC-PEG-lipid (fluorescein isothiocyanate – poly(ethylene glycol-)phospholipid) emission fluorescence spectra performed in pH 2.0 - 10.0 buffer solutions [9]. Creative commons permissions seen here: <https://creativecommons.org/licenses/by/4.0/>

Fluorescence quenching is a process where molecules experience a decrease in fluorescence intensity [10]. Among trivial forms of quenching, molecular interactions which inaugurate these effects are designated as collision/dynamic, static or self-quenching. Collision quenching is often prevalent when the excited-state fluorogenic species becomes deactivated when in close contact with another molecule present in the sample solution [11]. As this type of quenching occurs, the fluorophore returns to the ground state (μG) without the emission of a photon. The molecule causing this type of quenching is known as the 'quencher'. Some of the most well-known collision quenchers include amines, halogens, oxygen, and electron-deficient molecules. Static/contact quenching is mechanism that involves the quenching of molecules in the ground states (μG) without the impact of collision; together they form non-fluorescent complexes. These complexes often have unique absorption/excitation wavelengths. High probe concentrations can yield hydrophobic effects, leading to aggregation and molecular stacking. Static quenching is also observed in 'self-quenching'. Self-quenching is when both the fluorophore and the quencher are the same molecules [1, 12].

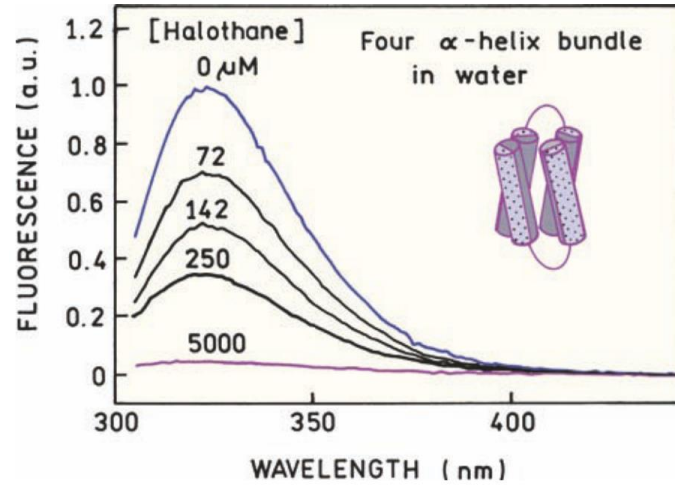


Figure 1. 4. Emission spectra of four α -helix quenching model in the presence of halothane. Reduced fluorescence of four α -helix in 5 mM halothane. (Copyright © Springer Nature) [1]

1.1 Förster resonance energy transfer - FRET

Förster resonance energy transfer (FRET) is a technique that relies on the transfer of energy from a donor fluorophore to an acceptor fluorophore [13]. The non-radiative transfer between these fluorophores is called, FRET pairs. FRET is an effective tool used to measure the distance between the donor fluorophore to that of the acceptor fluorophore. FRET occurs when the emission spectra of the donor fluorophore and the absorption spectra of the acceptor fluorophore are apart by a distance less than 10 nm and are overlapped by 30% [14]. When a ground state acceptor fluorophore is near an excited donor fluorophore, the excited state energy is transferred. This transfer of energy leads to increased emission fluorescence intensities of the acceptor while the donor excited state lifetime and fluorescence intensity decrease. This energy transfer is a product of dipole-dipole interactions. Alongside dipole interactions, resonance energy transfer relies on donor quantum yields, donor and acceptor fluorophore distances and spectral overlap [1, 14–16].

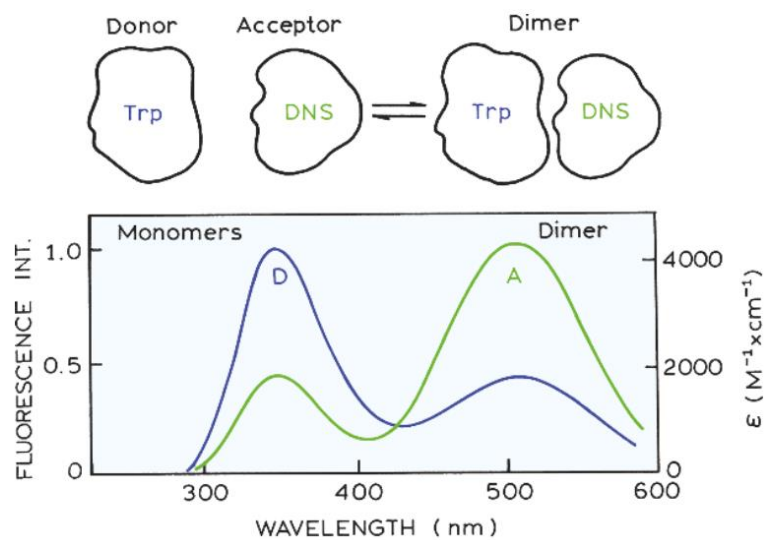


Figure 1. 5. Energy transfer between tryptophan donor emission with dansyl acceptor absorption.

Tryptophan (Trp) donor and dansyl group (DNS) acceptor monomers form dimers used to calculate donor-to-acceptor distances. (Copyright © Springer Nature) [1]

The efficiency of this process was modelled in the equation by Förster, shown below, where E, (efficiency) equals the inverse sixth power of the distance between the donor and acceptor fluorophores [13]. R_0 depends on the spectral properties of the probes and their orientation and represents the distance where half the energy is transferred to the acceptor fluorophore. Ultimately, using E and R_0 , the distances between the probes can be estimated while most effectively determining changes in conformation because E depends on the probes orientation [14].

$$E = \frac{1}{\left(1 + \left(\frac{R}{R_0}\right)^6\right)}$$

Equation 1. 1. The Förster resonance energy transfer efficiency expressed as function of distances.

1.2. The application of fluorescence spectroscopy to analyte detection

The area of research exploring fluorogenic detection of chemical and biochemical analytes has become one of the fastest growing and most active avenues to address the use of costly and less precise methods. Fluorescence techniques do not require reference beams; rather, samples are measured directly and for this reason this technique has proven to be more precise and accurate in comparison to absorbance techniques [1, 5, 17]. This high-sensitivity technique has grown from applications in clinical settings from the use of imaging and spectroscopic detections of nucleic acids and proteins to the improvement of chemical sensors for environmental studies [17–20].

IUPAC defines chemical sensors as systems that can transform chemical information based on total composition analysis to determining the concentrations of

precise sample components [1, 21, 22]. The advantage of these developments comes from their cost-effectiveness, versatility, and the monitoring of fluorescent samples in real-space and real-time.

1.3. Developing chemical sensors for environmental studies

Environmental studies of wastewater treatment and management have been requiring methods for high-sensitivity detection and quantification of chemical concentrations in water bodies [19, 20]. Excess nutrients of phosphorus and nitrogen, existing in the forms of inorganic phosphate and nitrates, caused the rapid growth of algae, leading to algal blooms that can release toxins and produce anoxic conditions. These processes are detrimental to aquatic life and contaminate sources of water for humans and fish populations, resulting in pollution [23, 24]. Algal blooms have contributed to economic losses of the fishing and the recreation and tourism industries, estimated annual losses for the Lake Erie economy have averaged \$34 million and \$28 million, respectively [25, 26]. Developing simple methods to detect chemical concentrations of both phosphate and nitrate would be an essential tool to monitor and control nutrient levels in aquatic environments.



Figure 1. 6. Lake Erie capture of hazardous algal bloom containing microcystin toxins. Algae seen south of entry of Detroit River [27].

With increased inorganic phosphate concentrations in water bodies becoming a growing issue, the development of an inorganic phosphate fluorescence assay would allow for the most accurate means to testing concentrations in the field. According to Ontario Provincial Water Quality Objectives, the concentrations of total phosphorus detection should not exceed 20 $\mu\text{g/L}$ (0.21 μM). As such, an effective fluorescent inorganic phosphate sensor, should be able to measure between 0.1 μM – 10 μM for the avoidance of nuisance algae in lakes [28].

1.4. Fluorescence dyes for inorganic phosphate detection

Selecting fluorophores for specific sensors requires a variety of considerations. An example would be identifying the overall net charges of prospective probes. When targeting specific molecules with anionic or cationic properties, receptors or binding sites on the fluorophore should possess high affinity for the target species [6, 29–31]. Although there are challenges to designing probes for molecular specificity, nonetheless, there have been successful methods to achieve optimized conditions for electrostatic and hydrogen-bond interactions [32].

In the preparation of developing an inorganic phosphate sensor, the molecular species must be understood. Inorganic phosphate has a molar mass of 94.97 g/mol. The ion forms a tetrahedral arrangement, comprising of a phosphorus central atom and four surrounding oxygen atoms. Phosphate possesses three pK_a values, $\text{pK}_{a1} = 2.148$, $\text{pK}_{a2} = 7.198$ and $\text{pK}_{a3} = 12.35$ [33]. Under specific pH conditions, inorganic phosphate exists as phosphoric acid, dihydrogen phosphate, monohydrogen phosphate and phosphate (tribasic) [34].

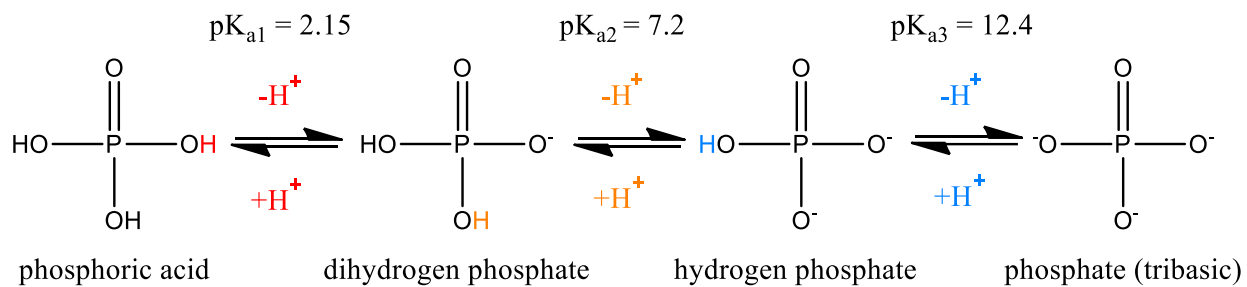


Figure 1. 7. Molecular structures of phosphate species with pKa values [35].

1.4.1. Cationic probes

Fluorophores that have cationic properties can be used for binding target anionic molecules [5]. Previous work using cationic dyes, such as; acridine orange have shown fluorescence quenching with the addition of the negatively charged polymer, carboxymethylcellulose (CMC) [36]. Potential ways of forming a fluorogenic assay with cationic fluorophores would be to develop a simple method that displays a direct positive relationship between the fluorescence of a cationic probe complex with the addition of the anionic molecule of interest.

1.4.1.1. Propidium iodide

Propidium iodide (PI) is a fluorophore with a molecular weight of 668.39 g/mol. PI is primarily used for staining DNA, because its cationic properties allow the fluorophore to intercalate along the phosphate backbone of nucleic acids [18]. PI is used to distinguish between dead and live cells because of its impermeability to cells of unscathed plasma membranes. Propidium iodide has an excitation wavelength (λ_{ex}) of 493 nm and emission wavelength (λ_{em}) of 632 nm [18, 37].

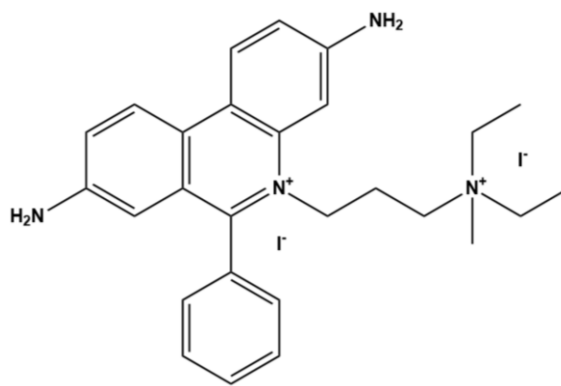


Figure 1. 8. Propidium iodide structure.

Propidium iodide (PI) with cationic sites [18, 37].

1.4.1.1. Quinacrine (mustard) dihydrochloride hydrate

Quinacrine dihydrochloride (QM) is a positively charged fluorophore with a molecular weight of 472.8 g/mol that has been used extensively for staining metaphase chromosomes by intercalation of the double helix in DNA and by selectively binding to guanine residues [38]. QM has an estimated $pK_{a1} = 9.4$ and $pK_{a2} = 10.7$, ensuring that it is almost always in its cationic state between the pH ranges of 5 to 9. Quinacrine dihydrochloride has an excitation wavelength (λ_{ex}) of 436 nm and an emission wavelength (λ_{em}) of 525 nm [38, 39].

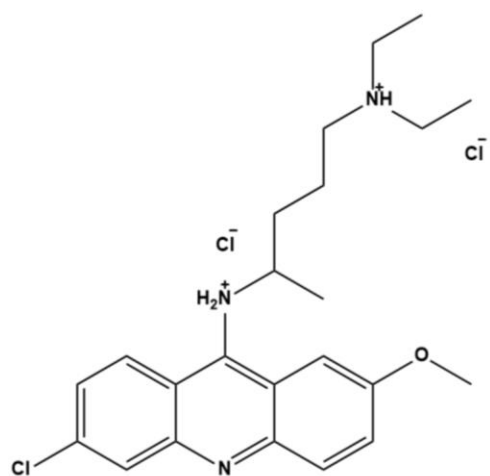
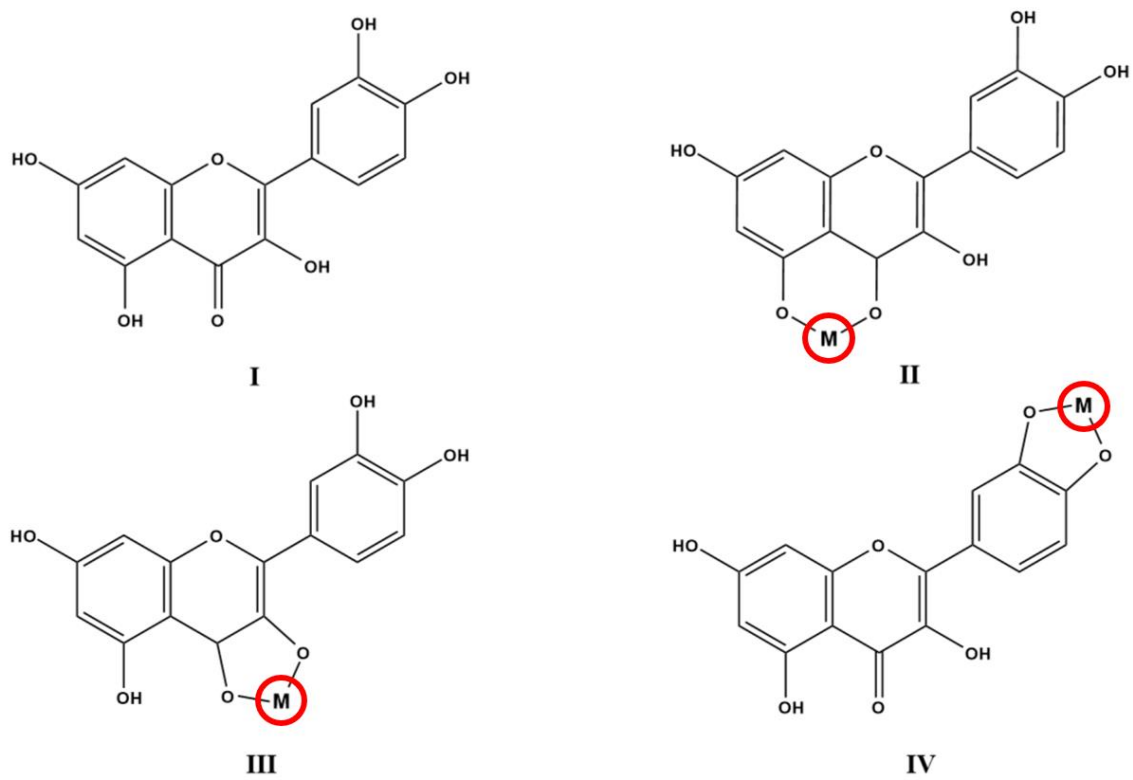


Figure 1. 9. Quinacrine dihydrochloride structure.
Quinacrine dihydrochloride with cationic sites [38–40].

1.4.1.2. Quercetin (3,3',4',5,7-pentahydroxyflavone)

Quercetin (QC) is a flavonoid found in plants, fruits and leaves that possesses anti-inflammatory and antioxidant properties as secondary metabolites [41]. Quercetin has a molecular weight of 302.27 g/mol and has five pK_a values, 7.17, 8.26, 10.13, 12.30 and 13.11 [42]. Alongside its ability to combat free radicals, this flavonoid can interact with transition metals to form cationic metal-associated binding complexes [10, 43, 44]. When one of the three metal associated binding sites is occupied, the new flavonoid-metal complex has been observed to increase in fluorescence. These metal-ligand complexes have new excitation and emission wavelengths specific to the metal bound and the coordination site that is occupied [44]. These natural metal-chelators can be optimized for the purpose of developing new biosensors.



*Figure 1. 10. Quercetin chemical structure.
Quercetin flavonoid with highlighted metal binding ligand sites [43].*

1.5. Research objectives and rationale

An overabundance of nutrients, such as phosphorus and nitrogen, originating from agriculture runoffs of wastewater, fertilizer, and sewage, has attributed and perpetuated algal blooms or eutrophication [45, 46]. These algal blooms are decomposed by bacteria leading to a depletion of oxygen levels in water, killing fish populations [25]. The demand for cost-effective and precise methods to monitor and quantify nutrient concentrations in aquatic environments is of interest to numerous industries and public health [45].

The objective of this research project is to develop a simple and cost-effective fluorescence inorganic phosphate sensor. The inorganic phosphate detection limits of interest are between 0 μM – 10 μM [28]. A focus will be placed on cationic fluorophores, surveying sensors that have previously been utilized in solid support or staining systems. Propidium iodide, quinacrine mustard dihydrochloride and quercetin-metal probes were the cationic fluorophores investigated in aqueous solutions. UV-vis spectroscopy will be used to determine absorption wavelengths of fluorophores in varying pH environments, while fluorescence spectroscopy will monitor fluorophore intensity relationships in the presence of inorganic phosphate.

Sephadex[®] LH-20, calcium phosphate and cellulose-phosphate will be used as solid supports to immobilize fluorophores and assess fluorescence in the presence of inorganic phosphate. Analytical methods of laser ablation, FTIR (Fourier-transform infrared spectroscopy) and sulfuric acid digestion will address the synthesis of cellulose-phosphate [47]. ¹HNMR (proton nuclear magnetic resonance) and ³¹PNMR (phosphorus nuclear magnetic resonance) will be used investigate metal binding sites of the fluorogenic probe, quercetin [44].

CHAPTER 2

PHOSPHO-PROTEIN SENSORS

2. Fluorescent probes for phospho-peptides and phospho-proteins

There is an abundance of ways to use specific fluorescent probes. Congruent with optimizing probes for specific analyte binding, there are fast growing methods to improve the detection of proteins and peptides using fluorescence. There have been a wide variety of fluorescent staining methods evolved for protein detection through immunoprecipitation and western blotting, specific fluorescent tags using SDS-PAGE and immobilized metal affinity columns for protein extractions [41, 48–50]. Amongst improving protocols for specific protein detection, are the demands for developing cost-effective and simple assays for phospho-proteins and phospho-peptides.

Phospho-proteins are proteins that have undergone one of the most abundant and imperative post-translational modifications in biological systems protein phosphorylation [50]. Protein phosphorylation and dephosphorylation are reversible reactions and mechanisms that involve the addition and removal of phosphate [51].

These processes are highly involved in cellular functions such as signal transduction and gene expression [52]. The enzymes responsible for phosphorylation, which can activate proteins, and dephosphorylation, which can deactivate proteins, are kinases and phosphatases, respectively [53]. In eukaryotic proteins, amino acid residues serine, histidine, tyrosine, and threonine experience phosphorylation most frequently, while prokaryotic proteins also experience phosphorylation on lysine and arginine residues [54–56]. Unique conformational changes caused by phosphorylation may include shifts in protein properties, where non-polar, hydrophobic amino acid residues cause portions of proteins to exhibit polar, hydrophilic properties [57]. Humans have an approximate 230,000 potential phosphorylation sites, under the influence of kinases and phosphatases,

these post-translational modifying enzymes propagate cell signaling pathways while aberrant modifications may lead to many diseases, seen in cancers and degenerative diseases such as, Alzheimer's and Parkinson's [58, 59].

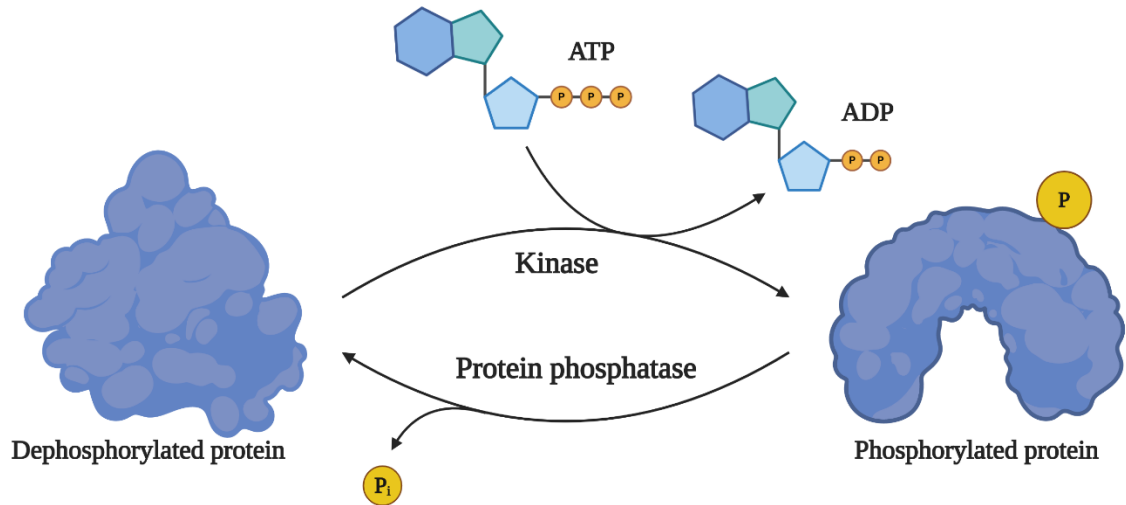


Figure 2. 1. The general schematic of the phosphorylation and dephosphorylation of proteins.

Kinase catalyzes the addition of phosphate from ATP (adenosine triphosphate) to phosphorylate proteins, while protein phosphatase catalyzes the hydrolysis reaction of monoester phosphate, dephosphorylating proteins. (Assembled with bioRENDER.)

Considering the precedent effects of phosphorylation/dephosphorylation, simple methods for identifying and detecting these modified proteins would contribute to the understanding of imperative cell signaling events. Developing and optimizing fluorophores for phosphate specificity would provide researchers with a cost-effective and precise assay for phospho-proteins and phospho-peptides.

2.1. Fluorophores used for phospho-protein detection

Optimizing fluorophores for the detection of phosphate and phospho-proteins has been a long-standing goal in research assay development. In efforts to produce highly specific phosphate assays, researchers have developed methods for phosphate detection using fluorescence in pre-existing laboratory techniques, such as, SDS-PAGE gel stains, western blots and in aqueous protein samples [17, 41, 53, 60].

Parallel to measuring the phosphate content in protein/peptide samples, these fluorescence methods can also aid in quantifying the activity of phosphatase enzymes in treatments [61–63]. When in the presence of phospho-tyrosine, terbium has been known to form fluorescent complexes. With this, terbium-phospho-tyrosine complexes can be used to measure the activity of protein-tyrosine phosphatase activity, where the effectiveness of the phosphatase would have a direct negative relationship with the terbium-phospho-tyrosine fluorescence [64].

Fluorophores have also been optimized for the detection of phospho-proteins on electroblot membranes. This method uses a small-molecule organic fluorophore, Pro-Q® Diamond dye. Pro-Q® Diamond dye can provide phosphoprotein results in 1h waiting times, for a detection limit of 2 to 4 ng [60]. The stain non-covalently binds precisely to

the phosphate moiety. This same group has applied this dye to microarrays for phosphoprotein detection. Microarray is a technique that is used to evaluate and visualize the activity of proteins and substrate presence [61]. In this application, peptides are immobilized onto a monolayer alkanethiolates [60].

Phosphoprotein detection using fluorescence has also been used in labelling through ATP-biotin mediation. This application begins with the incubation of ATP-biotin labelling, peptides and proteins undergo separation by SDS-PAGE, before SDS-PAGE gels are incubated in IRDye 680 streptavidin and an infrared imaging system is used to observe NIR fluorescence for the detection of phosphoproteins [49].

In the development of phosphoprotein sensor assays, it is almost synonymous to approach the possibility of manipulating fluorophores for the use of kinase/phosphatase assays; such as, an adenosine 3',5'-cyclic monophosphate dependent protein kinase and phosphoprotein phosphatase fluorometric assay [65]. This assay uses tryptophan fluorescence in synthesized peptides to distinguish between phosphorylated and non-phosphorylated peptides, where the phosphorylated tryptophan is cited to have a direct and positive fluorescence relationship with the addition of a phosphate moiety [65].

Flavonoids are among the monitored anti-oxidants in biological systems [66]. Quercetin, (3,5,7,4',5'-pentahydroxyflavon)), an antioxidant agent that increases in fluorescence once formed in a metal-ligand binding complex, has been cited to detect phosphoproteins in SDS-PAGE gels. When quercetin forms a complex with aluminum (III), this fluorophore has a limit of detection of 16 to 32 ng. It was reported that α -casein,

β -casein and phosvitin were detected after a 90-minute stain, a two-fold less sensitive stain than Pro-Q® Diamond dye [41].

2.2. Alkaline phosphatase

Alkaline phosphatase (APP) is a membrane-bound glycoprotein. This enzyme exists diversely and abundantly in nature. At basic pH, alkaline phosphatase catalyzes the hydrolysis reactions of protein monoester phosphate (**figure 2.2**) [67].

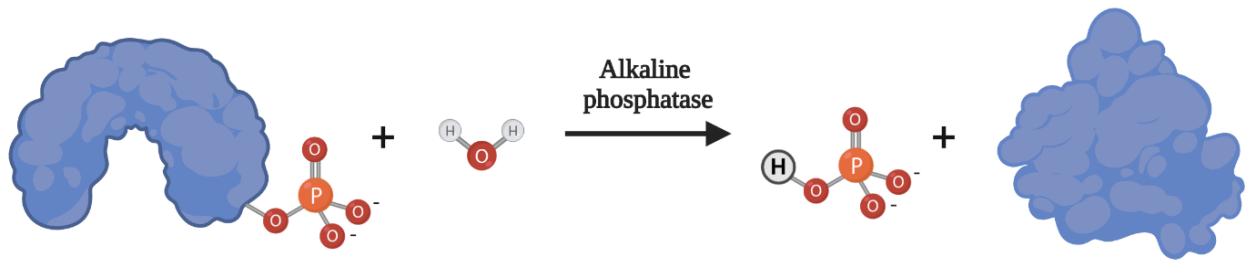


Figure 2. 2. The hydrolysis reactions of monoester phosphate on protein catalyzed by alkaline phosphatase. (Assembled with bioRENDER.)

Found in both prokaryotes and eukaryotic organisms, APP is categorized among four isozymes, solely dependent on the localized protein expression, and termed accordingly, intestinal alkaline phosphatase (IAPP), placental alkaline phosphatase (PAPP), germ cell alkaline phosphatase (GAPP) and liver/bone/kidney alkaline phosphatase (LBKAPP) [67, 68]. Intestinal APP gene is mapped on the long arm of chromosome 2, is *partially* heat stable. Contrary to other APPs sialic acid does not cleave its carbohydrate side chains. Placental APP is a heat stable enzyme with gene encoding mapped to chromosome 2. PAPP is highly expressed in the placenta. Liver/bone/kidney APP is expressed in different tissues, in turn, is nonspecific in its localized protein expression. This property has shown to allow different post-translational modifications based on thermostability and electrophoretic mobility. The germ APP gene, like IAPP and PAPP, was mapped on chromosome 2. Although, GAPP is expressed in low levels in neoplastic and embryonal tissues, it possesses heat stable properties. It is even expressed in placental tissue at low levels [67].

2.3. o-amino-benzoyl/Isatoic anhydride

Isatoic anhydride (IA) is a versatile organic compound. This compound is a derivative of anthranilic acid which when hydrolyzed gives rise to different compound constituents [69]. IA reacts primarily with ammonia, amides, and primary and secondary amines to form *o*-aminobenzoyl derivatives (**figure 2.3**). Alternative forms of cleavage of the anhydride ring yield mechanisms for different reaction fates with electro- or nucleophilic reagents [70].

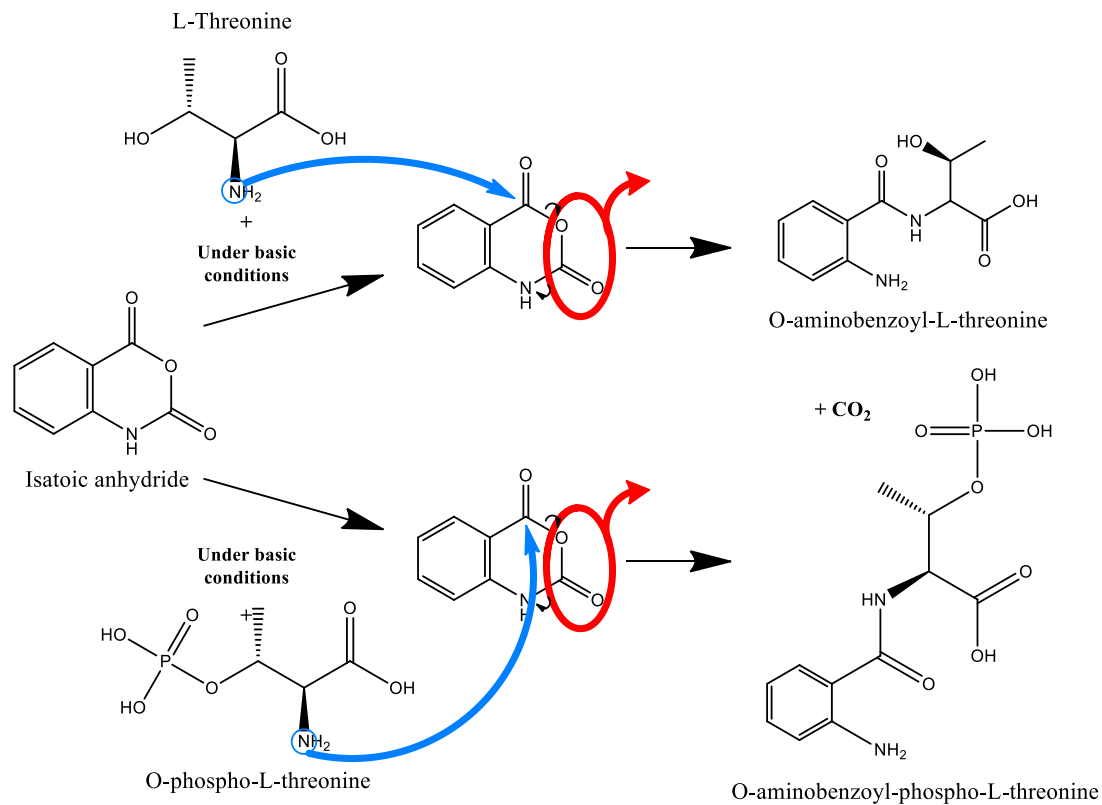


Figure 2. 3. Isatoic anhydride reaction scheme with L-threonine or O-phospho-L-threonine.

Isatoic anhydride under basic conditions forms a fluorescent amino acid conjugate. The quinazoline derivative, o-aminobenzoyl, reacts by a nucleophilic attack by the nitrogen atom on the α -carbon of the L-threonine or O-phospho-L-threonine [71].

2.4. Research objectives and rationale

Protein phosphorylation is a post-translational modification that plays a compulsory role in regulatory and signal transduction cascades catalyzed by protein kinases [56]. Phosphorylation primarily occurs on tyrosine, threonine, and serine amino acid residues, with 86.4% of phosphorylation occurring on serine [57]. (-OH) groups on these amino acids carry out the nucleophilic attack on the phosphate supplying molecule and form a phospho-amino acid. This process is especially imperative for gene expression [54, 56]. Modifying and developing an aqueous phosphatase assay would assist in studying this modification in specific proteins.

The aim of this research project is to develop a simple fluorescence phosphoprotein stain and aqueous phosphatase assay. These objectives will involve the investigation of the flavonoid-metal, quercetin-Zr (IV) and isatoic anhydride derivative, *o*-aminobenzoyl [44, 71]. These probes will be surveyed on solid supports and in aqueous media. An emphasis will be placed on quercetin-Zr (IV) for the staining of phospho-proteins immobilized on nitrocellulose membrane. Non-phosphorylated and phosphorylated proteins will be immobilized on nitrocellulose membrane to address the phosphate binding specificity of quercetin-Zr (IV). Meanwhile, development of an aqueous phosphatase assay will explore the fluorescence of *o*-aminobenzoyl-amino acid/phospho-amino acid conjugates. Anion exchange chromatography (Sephadex[®] QAE), TLC (Thin Layer Chromatography) and ¹HNMR will be used to observe the separation and verification of conjugated *o*-aminobenzoyl-amino acid molecules [72]. It is the hope that these techniques allow for the production of ***robust*** and ***cost-effective*** phosphate sensors, applicable to the field and molecular biological studies.

CHAPTER 3

MATERIALS AND METHODS

Materials

All reagents and antibodies were purchased from Sigma-Aldrich (Oakville, ON, Canada) unless otherwise stated in the methods section. All solutions were prepared with MilliQ water (Advantage A10 Water Purification System, Millipore Sigma, Etobicoke, ON, Canada). All the steady-state fluorescence studies were performed on Cary Eclipse fluorescence spectrophotometer (Agilent Technologies, Mississauga, ON, Canada) or SpectraMax® M5E microplate reader (Molecular Devices, San Jose, California, United States). All absorbance studies were performed on Cary 8453 UV/Vis spectrophotometer (Agilent Technologies, Mississauga, ON, Canada) or SpectraMax® Plus 384 microplate reader (Molecular Devices, San Jose, California, United States).

Methods

3.1. Survey for potential inorganic phosphate sensors

3.1.1. Propidium iodide and quinacrine mustard dihydrochloride hydrate spectral properties:

15 μM propidium iodide in tris buffer (0.1 M, pH 7) and varying concentrations of inorganic phosphate (P_i) (150 μM – 266 μM) using K_2HPO_4 were titrated and fluorescence emission was monitored at 632 nm upon excitation at 493 nm. The same procedure was repeated in propidium iodide 0.1% carboxymethyl cellulose (CMC) or 0.1% poly(sodium 4-styrenesulfonate (PSS)).

An identical protocol was followed for 18 μM quinacrine mustard dihydrochloride hydrate (QM), in tris buffer (0.1 M, pH 7), 0.1% CMC or 0.1% PSS. The fluorescence emission at 500 nm was monitored upon excitation at 436 nm.

3.1.2. Sephadex LH-20 for QM binding complex and spectral properties:

Sephadex LH-20 was hydrated in MilliQ and transferred to Econo-Column® (1.5 x 10 cm, Bio-Rad, Mississauga, ON, Canada) and washed thoroughly with MilliQ. 20 mM QM was applied to the packed column. The column was washed thoroughly with 400 mL of MilliQ and was resuspended five times. 250 µL of Sephadex LH-20-QM, 500 µL of tris buffer (0.1 M, pH 7) and 100 µL of varying P_i concentrations (0 mM – 1.25 mM) were added to five separate microcentrifuge tubes (Axygen®). All tubes were vortexed for 1 minute and centrifuged at 2000 rpm. 500 µL of supernatants was monitored for QM fluorescence (λ_{ex} : 436 nm, λ_{em} : 500 nm).

An identical protocol was conducted using QM (20 µM, 700 µL) and calcium phosphate (Ca₃(PO₄)₂, 0.5 g and 1.0 g) in the place of Sephadex LH-20-QM [73].

3.1.3. Synthesis, laser ablation and FTIR of cellulose-phosphate using filter paper for binding complex:

Following pre-existing synthesis methods, 1 cm Whatman® filter paper disks were washed generously and subjected to the basic synthesis conditions for cellulose-phosphate [47, 74]. Controlled samples were made without the addition of sodium trimetaphosphate (STMP). Cellulose and cellulose-phosphate disks were mounted onto microscope slides and subjected to laser ablation (70 secs, 50%, 20 Hz) using PhotonMachines 193 nm short pulse width Analyte Excite excimer laser ablation system (Isomass Scientific Inc., Calgary, AB, Canada). Samples were also characterized with Fourier-transform infrared spectroscopy (FTIR) using the Bruker Alpha FTIR Spectrometer (Plantinum-ATR attachment) (Bruker Ltd, Milton, ON, Canada).

3.1.4. Organic phosphate sulfuric acid digestion of cellulose and cellulose-phosphate:

Cellulose and cellulose-phosphate disks (ranging from 0-6 disks) were placed into separate vials of 0.7% ammonium persulfate and 250 mM sulfuric acid. Vials of samples and internal standards (0-10 μM) of P_i were boiled 1 hour. The malachite green assay was used to measure total P_i concentrations (λ_{Abs} : 630 nm).

3.1.5. Inorganic phosphate titrations of cellulose and cellulose-phosphate, quercetin-Al (III) probing and fluorescence imaging:

Cellulose and cellulose-phosphate disks were stained using pre-existing methods for quercetin-Al (III) (pH 4) for 1 hour [41]. Disks were thoroughly rinsed in tris buffer (0.1 M, pH 4.5) before incubating for 1 hour in varying concentrations of P_i (0-250 μM) [41]. All samples were washed with tris buffer, protected from light, and imaged for fluorescence signaling using FluoroChem® Q quantitative imaging system (Alpha Innotech, San Leandro, California, United States).

3.1.6. Cellulose-phosphate quercetin-Al (III) probe assay:

Cellulose and cellulose-phosphate disks were incubated in varying quercetin-Al (III) probe concentrations (1-30 μM) and monitored for fluorescence (λ_{ex} : 420 nm and λ_{em} : 510 nm) [41].

3.2. Optimizing potential inorganic phosphate probes

3.2.1. Characterizing quercetin and quercetin-metal ligand binding complexes using

UV-vis:

25 μM of quercetin working reagent (40% methanol, 20% 1,2-propanediol and 0.1 M tris buffer pH 2-12) and 50 μM of aluminum (III) chloride, iron (III) sulfate, nickel (II) chloride hexahydrate or zirconium (IV) chloride were monitored for absorbance in the pH ranges of 2 to 12 [41].

3.2.2. Quercetin and quercetin-metal inorganic phosphate titration spectral properties:

25 μM of quercetin working reagents and 50 μM of aluminum (III) chloride, iron (III) sulfate, nickel (II) chloride hexahydrate or zirconium (IV) chloride were titrated with P_i (0 μM – 1000 μM). Maximum absorption wavelengths for quercetin and quercetin-metals were used to monitor fluorescence at corresponding pH ranges.

3.2.3. Quercetin spectral properties with zirconium (IV) chloride titrations:

25 μM quercetin working reagent (pH 9) was titrated with zirconium (IV) chloride (0-338 μM) until the sample solution achieved saturation. All titrations were excited at 465 nm and monitored for fluorescence.

3.2.4. Quercetin-Zr (IV) ligand binding characterization using NMR:

^1H NMR spectra of 2.5 mM quercetin working reagent (40% MeOD, 44 mM tris buffer, pH 9) and zirconium(IV) chloride (in D_2O) titrations (0-1.22 mM) were compared as well as, ^1H NMR spectra of quercetin-Zr(IV) (2.5 mM : 1.22 mM) and P_i (in D_2O)

titrations (0-5.75 mM) using 500 MHz Bruker NMR (Bruker Ltd, Milton, ON, Canada). Quercetin stock solutions were made in deuterated dimethyl sulfoxide (DMSO).

³¹P NMR spectra of 50 mM P_i and zirconium (IV) chloride titrations (0-20 mM) were compared. After saturation of P_i (45 mM) and zirconium (IV) chloride (4.5 mM) occurred, the supernatant of the sample was compared.

3.3. Exploring the use of probes for phosphoprotein detection

3.3.1. Quercetin-Zr (IV) probe and L-serine and O-phospho-L-serine spectra properties:

A 10 μM quercetin, 20 μM zirconium working reagent was titrated with L-serine (0-3.3 nM) or O-phospho-L-serine (0-1.9 nM) and excited at 465 nm and monitored for fluorescence.

3.3.2. Casein extraction and phosphoprotein preparation:

10 grams of skim milk (Selection) was dissolved in 600 mL of MilliQ and warmed to 43°C. A 2.4 M solution of glacial acetic acid was added dropwise with constant stirring until curd formation was apparent. After 15 minutes of constant stirring, the precipitate was filtered and washed thoroughly with MilliQ and isopropanol [73, 75, 76]. Precipitate was dried overnight at 21°C and dissolved in tris buffer (0.1 M, pH 12) for storage [73]. A Bradford assay was performed for quantification of protein concentration.

Please note: JR indicates that the following methods were performed in collaboration with Justin Roberto from the Vacratsis Research Group (University of Windsor, Windsor, Ontario, Canada).

3.3.3. Protein expression in mammalian cell culture (JR):

Human embryonic kidney cells (HEK293) (ATCC) were grown in Dulbecco's Modified Eagle's Medium/Nutrient F-12 Ham (DMEM-F12 HAM; Corning) supplemented with 10% FBS (Gibco) and antibiotics (100 units/mL penicillin, 100 µg/mL streptomycin) at 5% CO₂ and 37°C. Cells were maintained at 70% confluency in 100 mm or 150 mm culture dishes (Starstedt, Inc).

3.3.4. Transient transfection of MTMR2 (JR):

Lipid phosphatase MTMR2 (myotubularin related protein 2) in HEK293 was transiently expressed in HEK293. Cells were plated 24-hours prior to polyethyleneimine (PEI) transfection at 500,000 cells/mL grown in antibiotic-free media. At the time of transfection, two separate reactions containing PEI and media, or DNA and media were prepared. The DNA mixture 10 µg of either pCMV-FLAG-empty vector or pCMV-FLAG-MTMR2 DNA was added to 100 µL of non-supplemented media incubated for 10 min in the dark at room temperature. Meanwhile, PEI mixtures had 40 µL of 1 mg/mL PEI was added to 100 µL of non-supplemented media also being incubated at 10 min in the dark. Following this incubation, the contents of each mixture were combined, and incubated for 13 mins in the room dark. The combined mixture was then added onto the cells in a dropwise motion and incubated at 37 °C for 6 hours. Following this incubation, cells were

washed with PBS (Hyclone) and incubated with fresh antibiotic- and FBS-containing media, where they would remain until lysis (~18 hours).

3.3.5. Phosphatase inhibitor treatment and lysis (JR):

In the attempt to elevate MTMR2 phosphorylation, cells were treated with phosphatase inhibitor, calyculin A (CalA). Transfected cells were treated with 5 nM CalA (CalBioChem) for 30 min prior to transfection. Cells were collected and spun at 5000 rpm for 5 min at 4°C, and the pellet was resuspended with cold PBS and centrifuged again. Pellets were then prepared for lysis.

CalA-treated cells' pellets were resuspended in lysis buffer (50 mM tris-HCl, 1% Triton X-100, 150 mM NaCl, 0.1% SDS, pH 7.4) supplemented with protease and phosphatase inhibitors and incubated on ice for 5 minutes. Untreated cells were washed with cold PBS and collected with lysis buffer and incubated on ice for 5 minutes. Lysates were spun at 15,000 rpm for 10 minutes at 4°C. Supernatants were collected and protein concentrations were determined via Bradford assay.

3.3.6. MTMR2 isolation via FLAG-immunoprecipitation (JR):

ANTI-FLAG M2 monoclonal antibody was used to isolate FLAG-MTMR2 from cell lysates. Equal amounts of clarified lysates (~400 µg) were added onto anti-FLAG M2 mouse monoclonal resins and incubated overnight. Following incubation, samples were spun at 5,000 rpm for 1 minute and three washes were performed using IP (immunoprecipitation) wash buffer (50 mM tris-HCl, 1% Triton X-100, 150 mM NaCl, 0.1% SDS, pH 7.4). Samples were treated with 35 µL of reduced 6X loading dye (0.35 M

tris-HCl, 10% SDS, 0.3% β -mercaptoethanol, 30% glycerol, 0.012% bromophenol blue, 3% dithiothreitol, pH 6.8) and boiled for 5 minutes [77].

3.3.7. Immunoblotting (JR):

The phosphorylation status of MTMR2 from whole cell lysates and immunoprecipitations was evaluated using immunoblotting using sodium dodecyl sulfate-polyacrylamide gel electrophoresis (SDS-PAGE). Protein samples were resolved on 10% gels for 2 hours 20 minutes at 140 V in 1X SDS-PAGE running buffer (0.192 M, 0.025 M tris-base, 0.01% SDS, pH 8.3).

Following separation, proteins were transferred to polyvinylidene difluoride (PVDF) membrane (Millipore Corp.) or nitrocellulose (Millipore) using cold 1X transfer buffer (20% methanol, 0.192 M glycine, 0.025 M tris-base, pH 8.3) for 1 hour at 100 V. Membranes were blocked with 5% skim milk or bovine serum albumin (BSA) for phosphoblots, in 1X Tris-Buffered Saline (1X TBS; 0.068 M NaCl, 8.3 mM Tris-base, pH 7.6) containing 0.1% Tween®-20 (1X TBSt; Fisher Scientific) at room temperature for 1 hour with gentle agitation.

Blots were probed overnight with primary antibody at 4°C with gentle agitation. Primary antibodies used were mouse anti-FLAG and mouse anti-MTMR2 (Santa Cruz) at 1:3000 in 2.5% milk and TBSt, and rabbit anti-MTMR2^{pSer58} at 1:1000 in 2.5% BSA and TBSt. Blots were washed with TBSt for 5 minutes three times and incubated for 45 minutes at room with secondary antibody. Goat anti-mouse-HRP secondary antibody was made in 2.5% milk at 1:5000 and goat anti-rabbit-HRP (BioRad) was made in 2.5% BSA at 1:5000. Blots were washed with TBSt three times for 5 minutes. Bands were visualized via

chemiluminescence using the SuperSignal[®] West Femto Maximum Sensitivity Substrate (Thermo Fisher) according to the manufacturer's instructions.

3.3.8. *Quercetin-Zr (IV) staining of SDS-PAGE gel with phosphoproteins:*

The following protocol was based on the Thermo Scientific standards for dephosphorylation of proteins [78]. Protein samples, bovine serum albumin (BSA, Sigma), phosphoproteins MTMR2 (myotubularin related protein 2) and casein had been normalized (1 $\mu\text{g} / \mu\text{L}$). Following Thermo Scientific parameters, 1 μL of alkaline phosphatase (APP; Thermo Fisher Scientific, Waltham, Massachusetts, United States) and 2 μL of 10x FAST alkaline phosphatase buffer (10X FAST; Thermo Scientific) was added 1 $\mu\text{g} / \mu\text{L}$ of protein samples in a 20 μL total reaction volume. All samples were incubated at 37°C for 1 hour. The reactions were stopped with reduced SDS dye [77]. Controls had undergone the same experimental parameters without the use of APP or 10x FAST. 1 μL of each sample was dot blotted in triplicates onto nitrocellulose membrane. Protein samples were dot blotted on nitrocellulose membrane before the addition of SDS dye [77]. 20 μL of each reduced protein sample was separated using sodium dodecyl sulfate-polyacrylamide gel electrophoresis (SDS-PAGE) at 140V for 2 hours and 20 minutes in SDS-PAGE running buffer (0.192 M, 0.025 M tris-base, 0.01% SDS, pH 8.3). Separated proteins were transferred to nitrocellulose or polyvinylidene difluoride (PVDF) membrane using cold transfer buffer (20% methanol, 0.192 M glycine, 0.025 M tris-base, pH 8.3) for 1 hour at 100 V. Both membranes were probed with quercetin-Zr(IV) for 30 minutes and washed three times for 5 minutes using TBSt (TBS; 0.068 M NaCl, 8.3 mM Tris-base, pH 9) containing 0.5% Tween[®]-20 (TBSt 0.5%; Fisher Scientific). Nitrocellulose, PVDF

membranes, and SDS-gels were imaged using the excitation cy2 and emission cy3 settings on the FluoroChem® Q quantitative imaging system (Alpha Innotech).

3.4. Investigating potential probes for an aqueous phosphatase assay

3.4.1. Synthesis and Normalization of o-aminobenzoyl-L-serine and o-aminobenzoyl-O-phospho-L-serine:

180 mM of isatoic anhydride (IA; recrystallized from isopropanol) and 720 mM L-serine or O-phospho-L-serine were dissolved in tris buffer (0.5 M, pH 9) and left to react at 21°C under constant stirring, protected from light for 48 hours. The reaction mixtures were applied onto columns (Econo-Column®, 1.5 x 10 cm) packed with hydrated QAE-Sephadex. The columns were washed with 100 mL of water and eluted with NaCl (0.5 M). *o*-aminobenzoyl-L-serine (OAb-S) and *o*-aminobenzoyl-phospho-L-serine (OAb-PS) were stored in 1 mL aliquots and frozen at -20°C [79]. OAb-S or OAb-PS were normalized (Abs: 0.43, $\lambda_{\text{max}} = 312 \text{ nm}$, $\epsilon_{\text{M}} = 2800 \text{ M}^{-1} \text{ cm}^{-1}$) using UV-vis. Normalized samples were excited at 320 nm and monitored for fluorescence.

3.4.2. Thin Layer Chromatography (TLC) of eluted IA, OAb-S and OAb-PS:

Thin-layer chromatography was performed for the elution samples of IA, OAb-S and OAb-PS using SiliaPlate™ TLC aluminum backed TLC plates (200 μM thickness). The mobile phase was composed of acetone:water:methanol (10:10:1) [72].

3.4.3. NMR of IA, OAb-S and OAb-PS

¹H NMR spectra of 4.2 mM of IA, OAb-S or OAb-PS were made in tris buffer (pH 9) and compared.

3.4.4. Precipitation assay of OAb-S and OAb-PS using zirconium (IV) chloride

In a 96-well plate, 5-25 mM of zirconium (IV) chloride and 75 μ M of OAb-S and OAb-PS were made with tris buffer (0.5 M, pH 9). Samples were excited at 320 nm and monitored for fluorescence.

3.4.5. Titration of OAb-S and OAb-PS with lanthanides and transition metals

2.8 μ M of OAb-S or OAb-PS in tris buffer (0.5 M, pH 4,7 or 9) was titrated with aluminum (III) chloride (0-1.9 mM), cobalt (II) chloride (0-2.8 mM), copper (II) chloride (0-3.0 mM), europium (III) chloride (0-0.9 mM), iron (III) chloride (0-1.4 mM), lanthanum (III) chloride heptahydrate (0-1.2 mM), nickel (II) chloride (0-2.1 mM) or vanadium (III) chloride (0-1.8 mM). All samples were excited at 320 nm and monitored for fluorescence.

CHAPTER 4

RESULTS

4.1. Survey for potential inorganic phosphate sensors

4.1.1. Spectral data for propidium iodide in polar solvents in the presence of P_i

Propidium iodide (PI) is a cationic fluorophore primarily used for staining DNA by intercalating along the phosphate backbone [18, 37]. PI (15 μM) in Tris-HCl (0.1 M, pH 7) was first monitored for fluorescence in (λ_{ex} : 493 nm) (**figure 4.1, black line**), then titrated with 150 μM of inorganic phosphate (P_i) (**figure 4.1, grey line**). A small change in PI fluorescence due to quenching was observed [1]. No further changes in PI fluorescence was detected with increased concentrations of P_i .

Transitioning to more polar solvents, PI (15 μM) in carboxymethyl cellulose (0.1%, pH 7) (**figure 4.1, dark green line**) was monitored for fluorescence (λ_{ex} : 493 nm) and titrated with P_i (150 μM), similar findings to PI in Tris-HCl were observed (**figure 4.1, light green line**) [24, 36].

PI (15 μM) in poly(sodium-4-styrenesulfonate) (PSS, 0.1%, pH 7) was monitored for fluorescence (λ_{ex} : 493 nm) (**figure 1, dark orange line**) and titrated with P_i (0-266 μM) (**figure 1, lighter orange lines**) [80, 81]. Increased concentrations of P_i were found to have fluorescence-quenching effects on PI. No further quenching was observed with concentrations of P_i greater than 266 μM .

Although quenching can be used to quantify concentrations of P_i , fluorescent quenching sensors are hindered by their limiting ranges of detection and possible measurement interferences by contaminants [82].

**Inorganic Phosphate Titrations of 15 μM PI in Tris (0.1 M, pH 7),
0.1% CMC (pH 7) and 0.1% PSS (pH 7)**

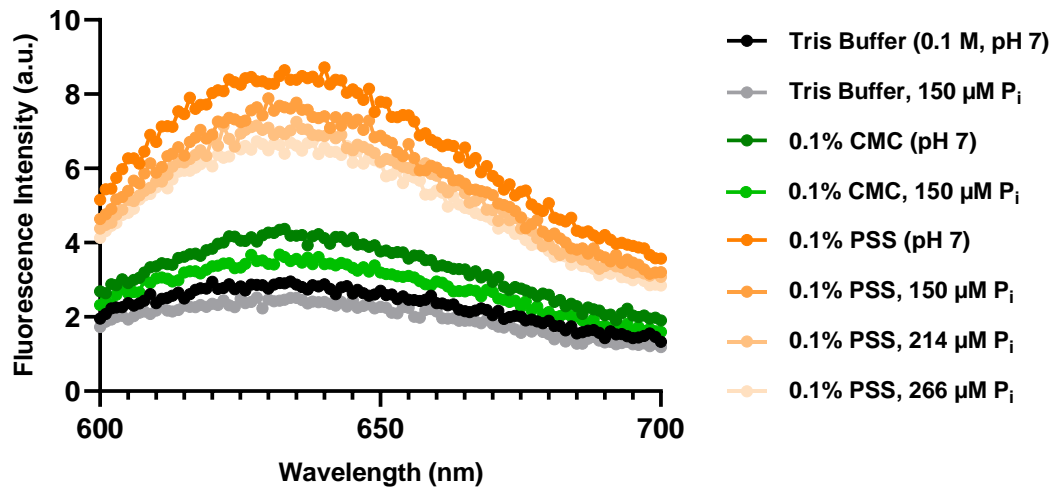


Figure 4. 1. Survey of propidium iodide (PI) fluorescence emission studies in varying solutions.

A constant concentration of PI (15 μM) was added to a 500 μL cuvette and monitored in varying neutral solvents of Tris-HCl (0.1M, pH 7), carboxymethyl cellulose (CMC, 0.1%, pH 7) and poly(sodium 4-styrenesulfonate) (PSS, 0.1%, pH 7). Each PI sample was titrated with inorganic phosphate (P_i) using a KH_2PO_4 solution until no change in fluorescence intensity was detected. The survey of PI in Tris-HCl and CMC was titrated with P_i (0-150 μM) (shown in the black and grey for Tris-HCl and green for CMC). For the survey of PI in PSS, the sample was titrated with P_i (0-266 μM) (shown in orange). All samples were excited at 493 nm and monitored for fluorescence between 600-700 nm. An emission maximum was observed at 632 nm for all samples.

4.1.2. Fluorescence spectral data for quinacrine in polar solvents in the presence of P_i

Quinacrine mustard dihydrochloride (QM) is a positively charged fluorophore used for staining metaphase chromosomes by intercalation of the double helix in DNA [38–40]. QM (18 μ M) was monitored for fluorescence in increasingly polar environments, Tris-HCl (0.1 M, pH 7), 0.1% carboxymethyl cellulose (CMC, 0.1%) and poly(sodium-4-styrenesulfonate) (PSS, 0.1%, pH 7) (**figure 4.2**) [24, 80].

QM (18 μ M) in Tris-HCl (0.1 M, pH 7) was monitored for fluorescence (λ_{ex} : 436 nm) (**figure 2, black line**) then titrated with P_i (83 μ M) (**figure 4.2, grey line**) [40]. Fluorescence-quenching effects were observed, however, no further changes in the fluorescence of QM were recorded with P_i concentrations greater than 83 μ M. Similar results were observed for QM (18 μ M) in CMC (0.1%, pH 7) (**figure 4.2, red line**), and with P_i titrations (**figure 2, pink line**).

QM (18 μ M) in PSS (0.1%, pH 7) was monitored for fluorescence (λ_{ex} : 436 nm) (**figure 2, dark green line**). The sample was titrated with P_i (83-267 μ M) (light green lines). Increasing concentrations of P_i were proportional to increased fluorescence. No fluorescence increases were observed for P_i concentrations above 267 μ M.

**Inorganic Phosphate Titrations of 18 μM Quinacrine in Tris (0.1 M, pH 7),
0.1% CMC and 0.1% PSS**

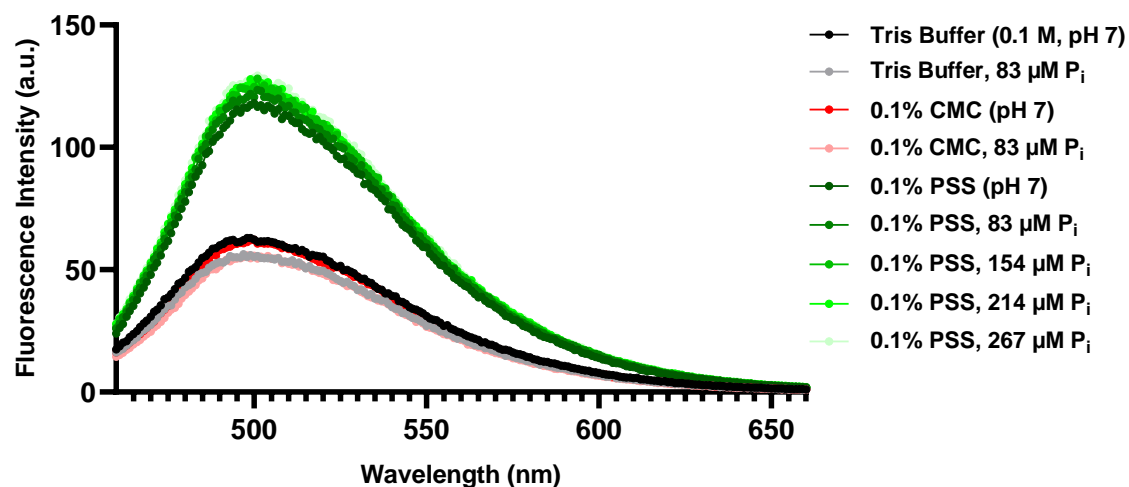


Figure 4. 2. Survey of quinacrine mustard dihydrochloride (QM) fluorescence emission studies in varying solutions.

A constant concentration of QM (18 μM) was added to a 500 μL cuvette and monitored in varying neutral solvents of Tris-HCl (0.1M, pH 7), carboxymethyl cellulose (CMC, 0.1%, pH 7) and poly(sodium 4-styrenesulfonate) (PSS, 0.1%, pH 7). Each QM sample was titrated with inorganic phosphate (P_i) using a KH_2PO_4 solution until no change in fluorescence intensity was detected. The survey of QM in Tris-HCl and CMC was titrated with P_i (0-83 μM) (shown in the black and grey for Tris-HCl and red for CMC). For the survey of QM in PSS, the sample was titrated with P_i (0-267 μM) (shown in green). The lighter green emission properties correlate to the increased titration of P_i . All samples were excited at 436 nm and monitored for fluorescence between 460-660 nm. An emission maximum was observed at 500 nm for all samples.

4.2. Investigating solid supports for potential inorganic phosphate sensor systems

4.2.1. Fluorescence emission properties of LH-20-QM in the presence of P_i

Sephadex[®] LH-20 is a cross-linked dextran bead with hydrophilic and lipophilic properties [83]. These characteristics allow the beads to take up polar components in solvents [83]. Knowing this, we hypothesized that Sephadex[®] LH-20 could bind the polar fluorophore, QM. When titrated with P_i , the QM could potentially dissociate from the LH-20 thus the fluorescence of unbound QM would increase in intensity proportional to the $[P_i]$.

QM (20 mM) was applied to a hydrated resin of Sephadex[®] LH-20, the column was disturbed and rinsed thoroughly with MilliQ water (400 mL), five times (**figure 4.3**). The column remained fluorescent. Next, equal volumes of Sephadex[®] LH-20-QM (250 μ L) were aliquoted into 1.5 mL microcentrifuge tubes (Axygen[®]) of Tris-HCl (500 μ L, 0.1 M, pH 7) and P_i (100 μ L, 0-1.25 mM). Samples were vortexed and centrifuged (2000 rpm). The supernatant (500 μ L) of each sample was monitored for fluorescence (λ_{ex} : 436 nm) and an increase in fluorescence proportional to $[P_i]$ (0-1.25 mM) was detected [40]. A 1.4-fold change was observed ($P_i = 1.25$ mM), possible methods to improve the detection limits of P_i could involve manipulating Tris-HCl (0.1 M, pH 7) volumes (**figure 4.3**).

Inorganic Phosphate Titrations in LH-20-QM, Tris (0.1 M, pH 7)

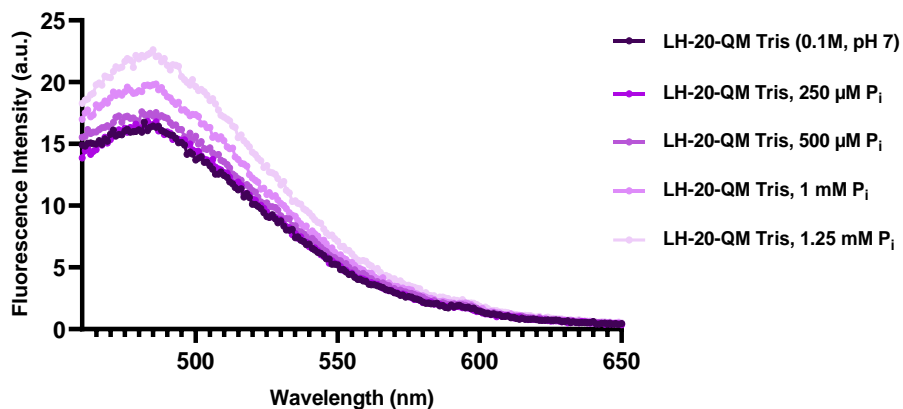


Figure 4. 3. Quinacrine mustard dihydrochloride (QM) fluorescence emission studies in Tris-HCl (0.1 M, pH 7) using Sephadex LH-20.

A solution of QM (20 mM) was applied to a packed column of Sephadex LH-20. The image of the Econo-Column® (1.5 x 10 cm) on the right captures QM entering the packed Sephadex LH-20 to form Sephadex LH-20-QM. The column was washed with 400 mL of MilliQ and resuspended five times. 250 μ L of Sephadex-LH-20-QM, 500 μ L of Tris-HCl (0.1 M, pH 7) and 100 μ L of varying concentrations of inorganic phosphate (P_i ; 0-1.25 mM) were added to five separate 1.5 mL microcentrifuge tubes (Axygen®). All samples were vortexed for one minute and centrifuged at 2000 rpm before each sample's supernatant was aliquoted into 500 μ L cuvettes. The emission spectra with increasing concentrations of P_i correlate to the lighter shades of purple in the figure. All samples were excited at 436 nm and monitored for fluorescence emission between 460 – 650 nm. An emission maximum was observed at 485 nm for all samples.

4.2.2. Fluorescence emission properties of calcium-phosphate-QM in the presence of P_i

Calcium phosphate is a polar white solid, that was hypothesized to covalently bind with QM [84]. We anticipated that bound QM would be displaced by titrations of P_i and that fluorescence increases would be proportional to P_i concentrations.

In (**figure 4.4**), masses of calcium phosphate (0.5 and 1 gram) were vortexed, centrifuged (2000 rpm) and monitored for fluorescence (λ_{ex} : 436 nm). Supernatant samples with twice the mass of the calcium phosphate showed lower fluorescence intensities. This supported the hypothesis of the calcium phosphate and QM complexation.

Following this, we sought to examine the fluorescence intensities of aqueous samples incubated QM (20 μM) bound to calcium phosphate (50 mg) with varying concentrations of P_i (0.01 – 1 mM), shown in (**figure 4.5**). The titrations of P_i did not support any increases in fluorescence. As a result, P_i cannot be used under these conditions to liberate QM from calcium phosphate and/or bind free phosphate to observe fluorescence intensities proportional to P_i concentrations (0.01-1 mM).

Calcium phosphate Titrations of 20 μM Quinacrine in Tris (0.1 M, pH 7)

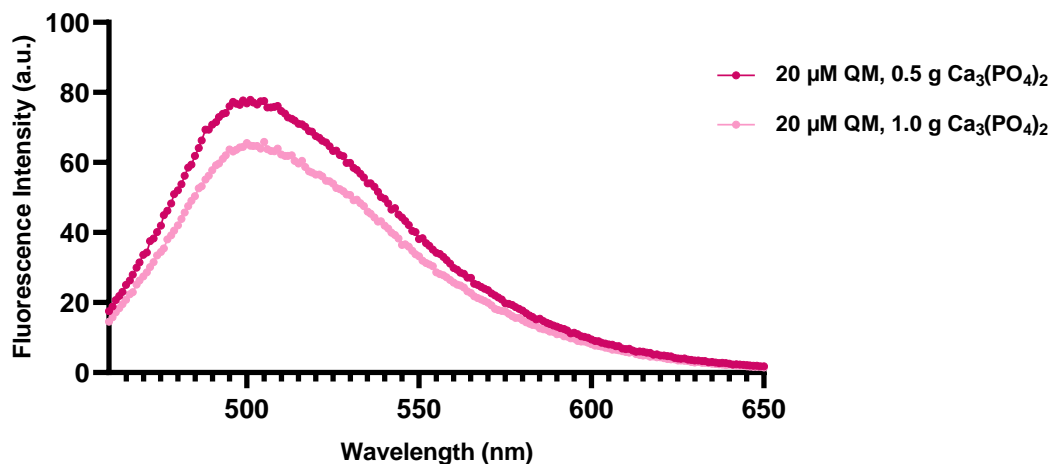


Figure 4. 4. Quinacrine mustard dihydrochloride (QM) fluorescence emission studies in Tris-HCl (0.1 M, pH 7) using calcium phosphate.

0.5 or 1.0 grams of $\text{Ca}_3(\text{PO}_4)_2$ and a constant volume (800 μL) of QM (20 μM) in Tris-HCl (0.1 M, pH 7) was added to 1.5 mL microcentrifuge tubes (Axygen®). Samples were vortexed for one minute and centrifuged at 2000 rpm before each sample's supernatant was aliquoted into a 500 μL cuvette. Samples were excited at 436 nm and monitored for fluorescence emission between 460 – 650 nm. An emission maximum was observed at 485 nm for all samples. The emission properties of QM with the highest fluorescence emission intensity was incubated in 0.5 grams of $\text{Ca}_3(\text{PO}_4)_2$ (the dark pink line). The emission properties of QM with the lower fluorescent emission intensity was incubated in 1.0 gram of $\text{Ca}_3(\text{PO}_4)_2$.

**Emission Spectra for the P_i Titrations of
Quinacrine-Calcium phosphate (pH 7, excited at 436 nm)**

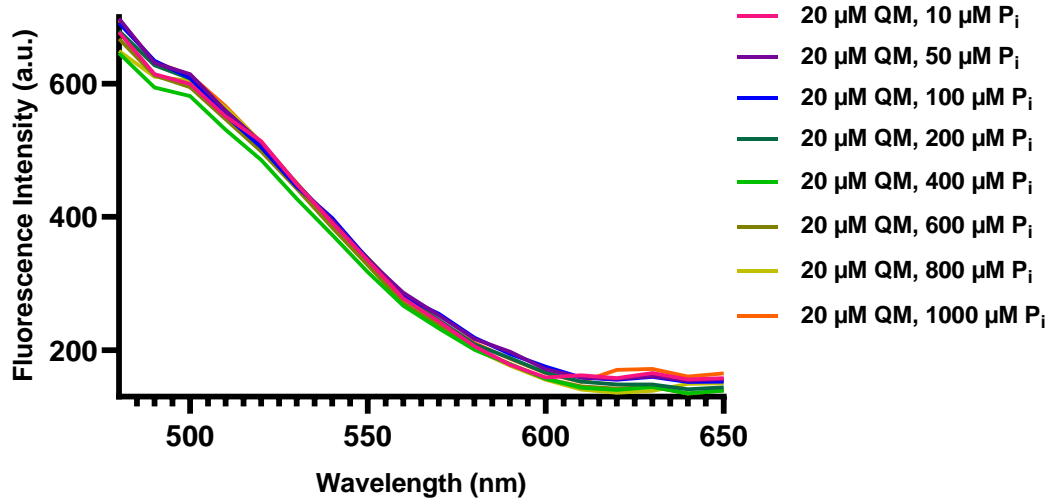


Figure 4. 5. Quinacrine mustard dihydrochloride (QM) fluorescence emission studies in 50 mg of calcium phosphate.

50 milligrams of $Ca_3(PO_4)_2$ was massed into eight separate 1.5 mL microcentrifuge tubes (Axygen®). A constant volume (700 μL) of QM (20 μM) in Tris-HCl (0.1 M, pH 7) and 100 μL of varying concentrations of P_i (0.01-1 mM) was added to each tube. Samples were vortexed for one minute, centrifuged at 2000 rpm and 200 μL were plated in a clear 96-well plate. Samples with increasing concentrations of P_i were aliquoted (down rows A to H) in triplicates. Wells A1-A3 held the QM- $Ca_3(PO_4)_2$ samples titrated with 10 μM P_i , A1-A3 (50 μM P_i), B1-B3 (100 μM P_i), C1-C3 (200 μM P_i), D1-D3 (400 μM P_i), E1-E3 (600 μM P_i), F1-F3 (800 μM P_i) and G1-G3 (1 mM P_i). Samples were excited at 436 nm and monitored for fluorescence emission between 470 – 650 nm. An emission maximum was observed at 500 nm for all samples, $n = 3$.

4.3. The determination of phosphate content on cellulose-phosphate

4.3.1. Phosphorus analysis of cellulose-phosphate by FTIR

In our previous studies utilizing Sephadex[®] LH-20 as a solid support system, an increase in QM fluorescence occurred in the presence of free P_i; here, we hypothesized that a fluorescent solid support of cellulose-phosphate-fluorophore could exist via the ionic binding of the phosphate group and cationic fluorophore [47]. And with the titration of free P_i, this solid support would experience a loss of fluorescence, ultimately due to the displacement of fluorophore, reflecting an increased aqueous fluorescence intensity of the fluorophore, proportional to the free P_i concentrations introduced into the system. A schematic of this hypothesis is shown below.

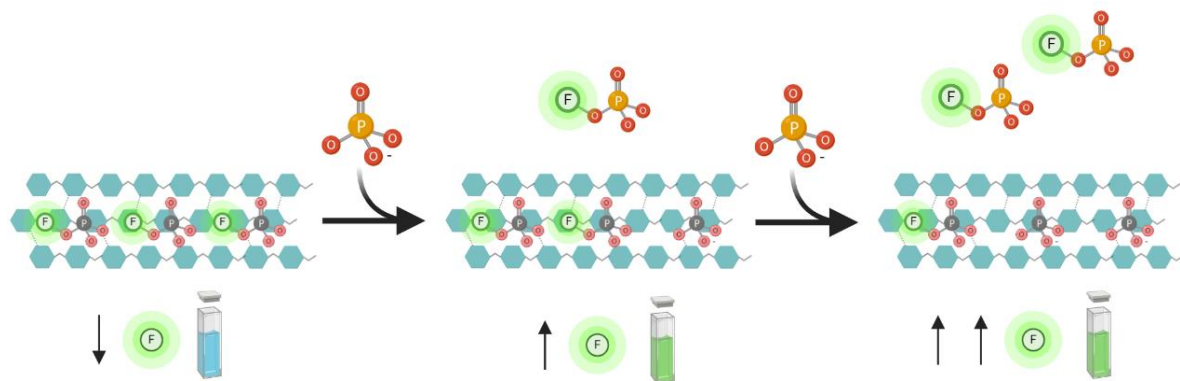


Figure 4. 6. General schematic of cellulose-phosphate hypothesized interaction with cationic fluorophore.

Cellulose-phosphate solid support is fluorescent by the ionic bond formed between an oxygen atom on the organophosphate and the metal atom of the fluorophore. The titration of inorganic phosphate disrupts the fluorophore-organophosphate bond and cellulose phosphate experiences a loss in fluorescence, while an increase in solution fluorescence occurs proportional to the concentration of inorganic phosphate titrated into the aqueous system. This schematic is assumed under neutral conditions.

Initially, analytical methods were performed to determine the success of synthesized cellulose-phosphate before its application as a solid support.

Using Fourier-transform infrared spectroscopy (FTIR) cellulose and cellulose-phosphate disks were analyzed for phosphorus peaks. Cellulose-phosphate disks were synthesized by incubating Whatman[®] filter paper and sodium trimetaphosphate (STMP) under basic conditions [47, 85]. Samples were analyzed using the Bruker Alpha FTIR Spectrometer (Platinum-ATR attachment). Cellulose and cellulose-phosphate samples shared absorbance readings for PH and PH₂ stretches, at 2386.1 cm⁻¹ and 2321.7 cm⁻¹, respectively, while absorbance peaks at 2182.9, 2100.9 and 1745.8 cm⁻¹ signified stretches of O = P – OH (**figure 4.7**) [86].

Cellulose-phosphate samples detected strongest peaks for phosphorus containing compounds, PH, PH₂ and phosphine oxide, OPOHR₂ (**figure 4.7**) [86]. These results suggested that phosphate was successfully bound to cellulose (to yield cellulose-phosphate). Phosphine oxide vibrational peaks for cellulose samples could be attributed to free phosphate contamination [86].

Although, FTIR detected stretches for phosphorus containing compounds, insignificant differences between cellulose and cellulose-phosphate would suggest that this technique is not practical for the detection of covalently bound inorganic phosphate on cellulose. Inconclusive results could also be due to measuring non-uniform cellulose fibres, interfering with the accuracy of sample readings.

Charaterization of Cellulose and Cellulose-phosphate using FTIR

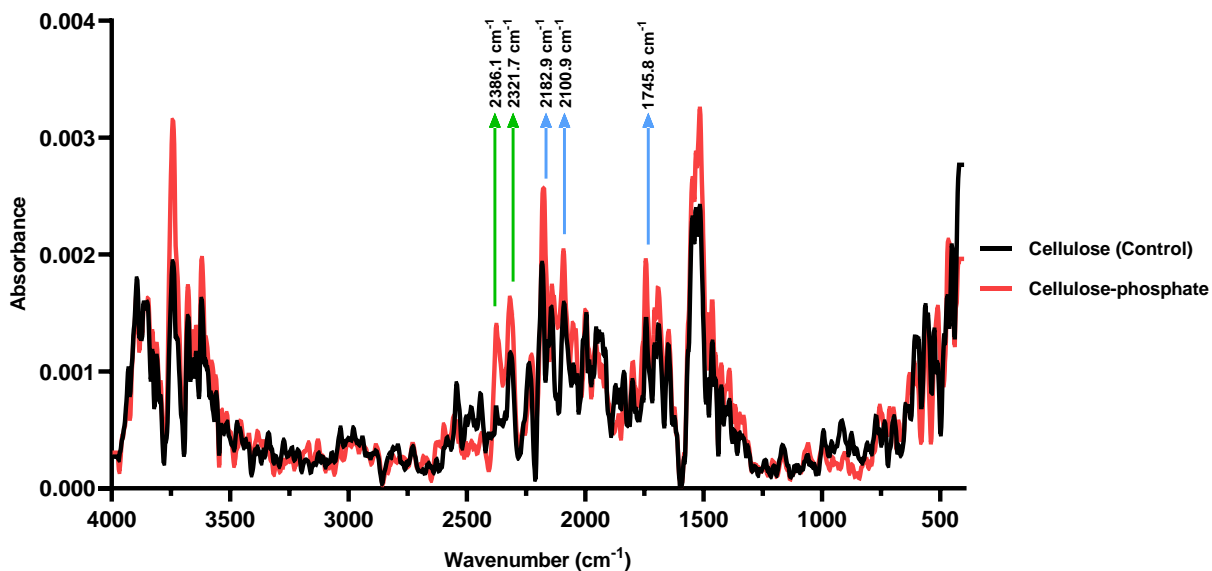


Figure 4. 7. FTIR spectra of cellulose and synthesized cellulose-phosphate disks.

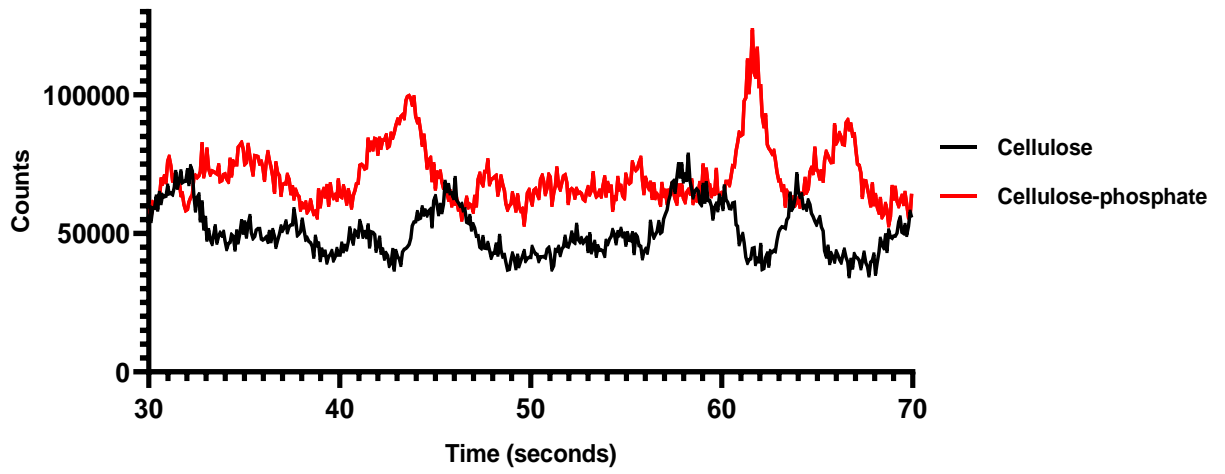
Fourier-transform infrared spectroscopy (FTIR) was used to analyze the absorption of cellulose (control, back line) and synthesized cellulose-phosphate (red line) from a basic treatment with sodium trimetaphosphate (STMP). The cellulose (control, 6.3 mm diameter) and cellulose-phosphate disks were read using the Bruker Alpha FTIR Spectrometer (Platinum-ATR attachment).

4.3.2. Phosphorus elemental analysis of cellulose-phosphate with laser ablation

Following FTIR, laser ablation was used to detect phosphorus concentrations through sublimation (counts/second) [87, 88]. This technique involves the removal of small fractions of substrate material by a pulsed laser beam. Cellulose (control) and cellulose-phosphate disks (6.3 mm) were mounted onto a glass microscope slide. Samples were ablated using a line pattern (50 % laser power, 20 Hz laser pulse, 70 seconds ablation duration) [89]. This technique was successful in detecting significant differences in phosphorus content ($p\text{-value} < 0.0001$, **figure 4.8**) between samples, with a 1.4-fold change (based on average counts between 30-70s).

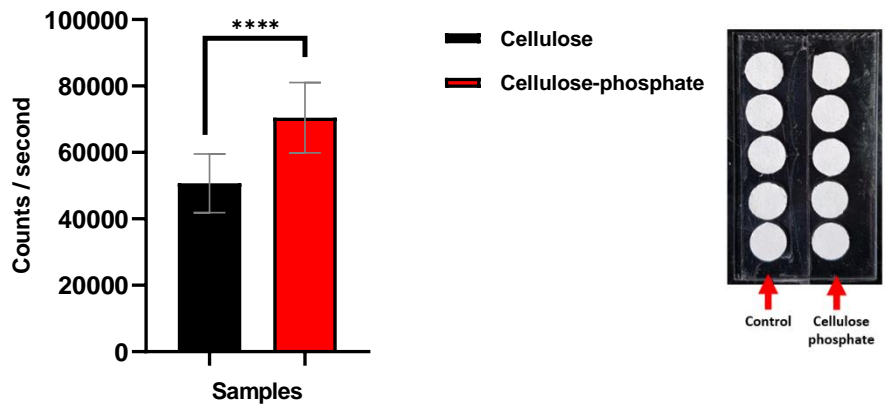
This controlled technique is often utilized for *trace-element analyses* of metals, ceramics and rocks or even to selectively remove material layers, as such, may be deemed not most suitable for the detection of phosphorus containing compounds on cellulose [87, 88, 90]. Next, samples were treated using the method of sulfuric acid digestion and quantified for phosphate concentrations using a total phosphate assay [91].

Elemental Analysis of Synthesized Cellulose-phosphate using Laser Ablation



(a)

Elemental Analysis Comparison of Synthesized Cellulose-phosphate using Laser Ablation



(b)

Figure 4. 8. Phosphorus elemental analysis of cellulose and synthesized cellulose-phosphate using laser ablation techniques.

(a) 6.3 mm disks of cellulose (control, black line) and synthesized cellulose-phosphate (red line) were placed on a microscope slide layered with double-sided tape (shown on the right-hand side of figure 7.b)). The slide was placed into a staging chamber and vacuumed to reduce air contamination. Samples were ablated using a line pattern (50%, 20 Hz, 70 seconds). The average counts of phosphorus between 30-70 seconds were used. (b) Cellulose (black bar) and cellulose phosphate (red bar) samples were averaged for phosphorus counts/second. Cellulose (μ : 50714.8 counts/second) and cellulose-phosphate (μ : 70435.1 counts/second) had a p-value of <0.0001 using an unpaired t-test. The error bars represent SEM, $n=40$.

4.3.3. Sulfuric acid digestion of cellulose-phosphate and the quantification of phosphate concentrations using the Malachite Green assay

Sulfuric acid digestion is a method that is often used for the determination of organophosphates [91]. This method involves the incubation of samples in strong acidic solvents and induces the breakdown of sample matrices. For our sulfuric acid digestion, cellulose and cellulose-phosphate disks were placed into two groups of 6 vials, each vial had increasing amounts of each sample, i.e. cellulose vial 1 had one disk, cellulose vial 2 had two disks...vial 6 had six disks, etc. All samples were incubated in ammonium persulfate (0.7%) and sulfuric acid (250 mM) solutions [91]. Vials of samples and internal standards (0-10 μM) of P_i were boiled 1 hour. The malachite green assay was used to measure total orthophosphate concentrations (λ_{Abs} : 630 nm, ϵ : 14,899 $\text{cm}^{-1} \text{M}^{-1}$) [92].

Digested cellulose samples did not show increasing trends of phosphate with increasing disks, while cellulose-phosphate yielded increasing concentrations of total phosphate (**figure 4.9**). This protocol was successful in providing evidence of the covalently bound cellulose-phosphate.

Malachite Green Assay Phosphate Concentrations of Cellulose and Synthesized Cellulose-phosphate after Sulfuric Acid Digestion

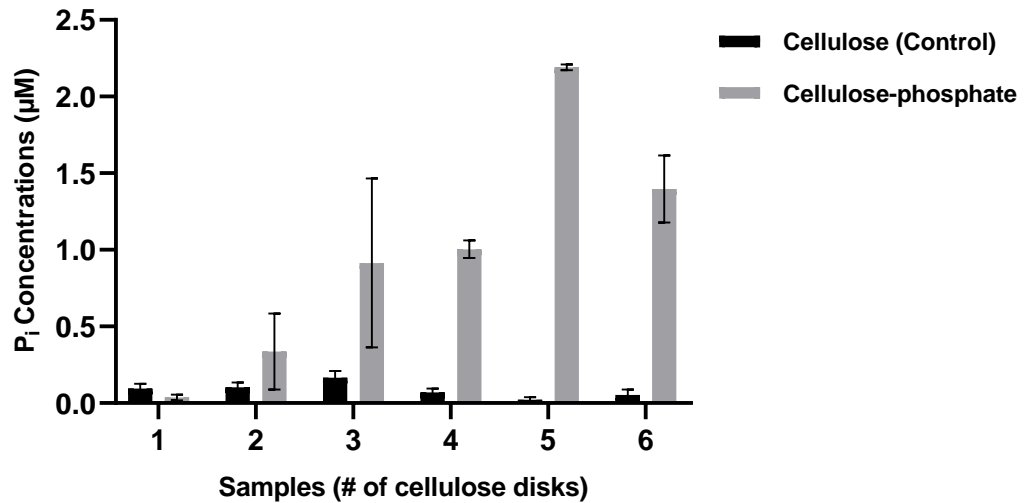


Figure 4. 9. Inorganic phosphate concentrations for cellulose (C) and cellulose-phosphate (CP) disks after sulfuric acid digestion.

Sulfuric acid treatments were carried out in vials with increasing amounts of disk (6.3 mm) samples to reveal P_i concentrations (sample 1: C = 95 nM, CP = 36.2 nM, sample 2: C = 102 nM, CP = 335 nM, sample 3: C = 166 nM, CP = 914 nM, sample 4: C = 70.1 nM, CP = 1 μ M, sample 5: C = 226 nM, CP = 2.19 μ M and sample 6: C = 52.2 nM, CP = 1.40 μ M. The error bars represent SEM, n=3.

4.3.4. Surveying quercetin-Al (III) on cellulose-phosphate disks as a P_i Sensor

Next, a fluorogenic probe, quercetin-Al (III) (25 μ M, 50 μ M, pH 4.5), was explored for potential P_i sensing using cellulose-phosphate [41]. Quercetin is a flavonoid, that when bound to a metal in one of three binding sites, experiences an increase in fluorescence [43, 44]. This probe was documented in the literature to detect phospho-proteins on SDS-PAGE (sodium dodecyl sulfate polyacrylamide gel electrophoresis) gels [41]. We hypothesized that cellulose-phosphate can bind quercetin-Al (III) via the ionic bonding of aluminum (III) and the phosphate (via oxygen atoms) on cellulose [42]. By probing the cellulose-phosphate disks with quercetin-Al (III), we could then introduce P_i and detect a loss of fluorescence on cellulose-phosphate. P_i concentrations would be proportional to fluorescence signaling, made possible by the liberation of the quercetin-Al (III) probe.

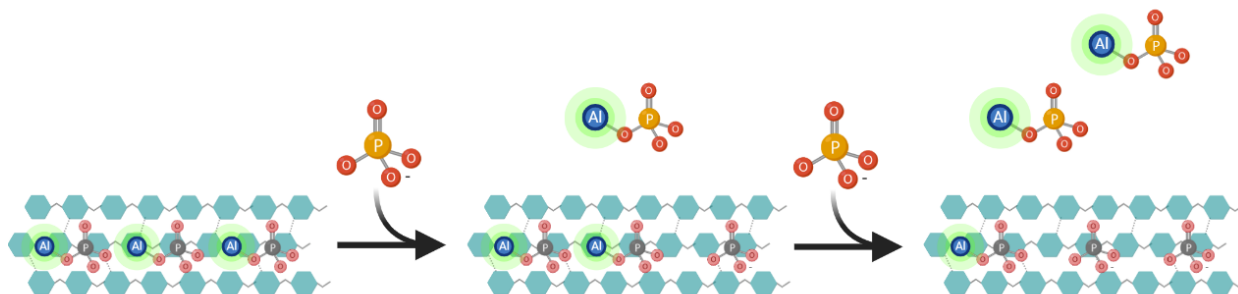
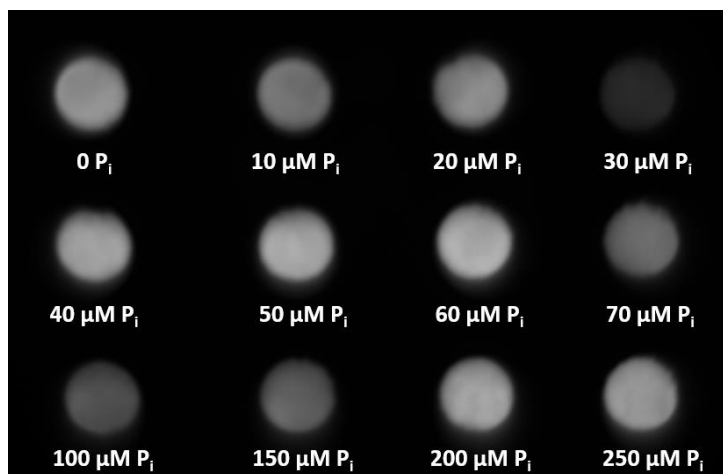


Figure 4. 10. General schematic of cellulose-phosphate hypothesized interaction with quercetin-Al (III).

Cellulose-phosphate solid support is fluorescent by the ionic bond formed between an oxygen atom on the organophosphate and the aluminum (III) atom of the fluorophore. The titration of inorganic phosphate disrupts the quercetin-Al (III)-organophosphate bond and cellulose phosphate experiences a loss in fluorescence, while an increase in fluorescence occurs proportional to the concentration of inorganic phosphate titrated into the aqueous system. This schematic is assumed under neutral conditions.

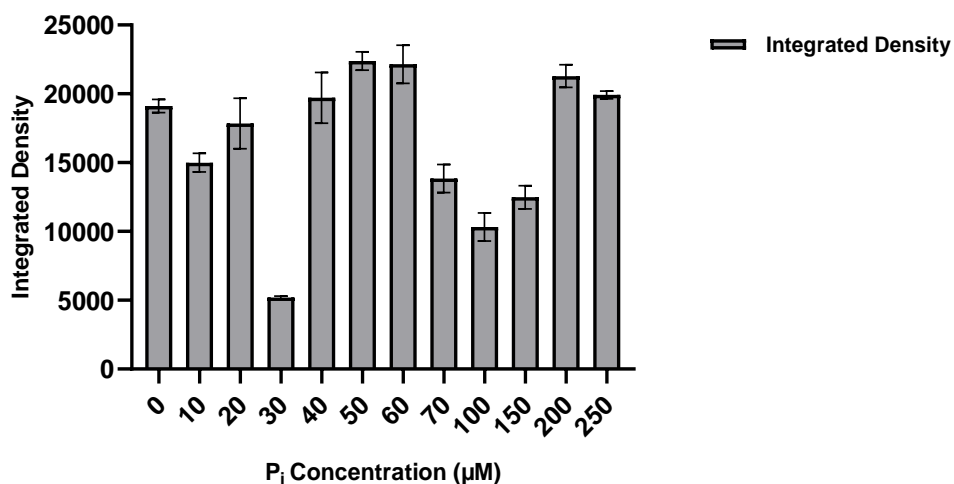
Cellulose-phosphate disks were incubated in quercetin-Al (III) (25 μ M, 50 μ M, pH 4.5) for one hour, rinsed with Tris-HCl (0.1 M, pH 4.5) followed by an incubation in P_i (0-250 μ M) for one hour. Samples were imaged for fluorescence (ex: cy2, em: cy3) and no relationship was reported between the concentration of P_i used and the fluorescence of each disk (**figure 4.11**).

This method still requires incubating quercetin-Al (III) probed cellulose-phosphate in varying concentrations of P_i and monitoring the aqueous samples for fluorescence (λ_{ex} : 365 nm) [41].



(a)

Quercetin-Al (III) Staining of Cellulose-phosphate Disks with Increasing Inorganic Phosphate Concentrations



(b)

Figure 4. 11. Cellulose-phosphate disks stained with quercetin-Al (III) (25 μM, 50 μM) washed with increasing concentrations of inorganic phosphate.

(a) Cellulose-phosphate disks (6.3 mm) were incubated in quercetin-Al (III) (25 μM, 50 μM, 40% MeOH, 20% 1,2-propanediol, pH 4) for one hour in a clear 12-well plate protected from light. Samples were thoroughly rinsed with Tris-HCl (0.1 M, pH 4.5) before incubation in P_i (0-250 μM) for one hour. Samples were imaged using cy2 excitation and cy3 emission settings on the FluoroChem® Q quantitative imaging system (Alpha Innotech). (b) The fluorescence integrated density for the cellulose-phosphate disks treated with quercetin-Al (III) and incubated in P_i (0-250 μM) were calculated using ImageJ[93]. The error bars represent SEM, n=3.

4.4. Investigating fluorogenic quercetin-metal probes for potential inorganic phosphate aqueous assays

4.4.1. Quercetin-metal studies using nickel (II) chloride and iron (III) sulfate

Quercetin was studied in aqueous environments by measuring absorption and fluorescence properties. This flavonoid possesses three metal binding sites, it was hypothesized that different quercetin metal complexations would have different absorption maxima, yielding unique fluorescence emission properties [1, 42, 44].

In an effort to identify a metal-ligand complex that could be used to detect P_i , quercetin and quercetin-metal probes were monitored for absorbance in different pH environments (2-12) (**figures 4.12-15, 4.20**) [42]. Using UV-vis spectroscopy, the absorption maxima at specific wavelengths for the quercetin-metals was used to excite and monitor fluorescence in the presence of varying P_i concentrations (0-1 mM) [1]. Only the pH environments that had the highest absorbance at a unique wavelength, were titrated with P_i . Utilizing an absorbance spectra is an accessible form of identifying excited states of a molecule, this phenomena reported excitation wavelengths of the quercetin-metal probes we developed [1].

Quercetin-Ni (II) and quercetin-Fe (III) were monitored for absorbance (**figures 4.13 and 4.14**). Quercetin-Ni (II) displayed absorption maxima in pH 2 (380 nm), pH 5 (380 nm) and pH 9 (335 nm) while quercetin-Fe (III) displayed absorption maxima in pH 7 (445 nm) and 11 (330 nm). All samples were titrated with P_i (0-1 mM) and were monitored for fluorescence ($\lambda_{\text{abs}} = \lambda_{\text{ex}}$). No relationship was observed for the fluorescence properties of quercetin-Ni (II) or quercetin-Fe (III) and P_i concentrations (**Appendix A**).

Absorbance Spectra of Quercetin (25 μM) at Varying pH

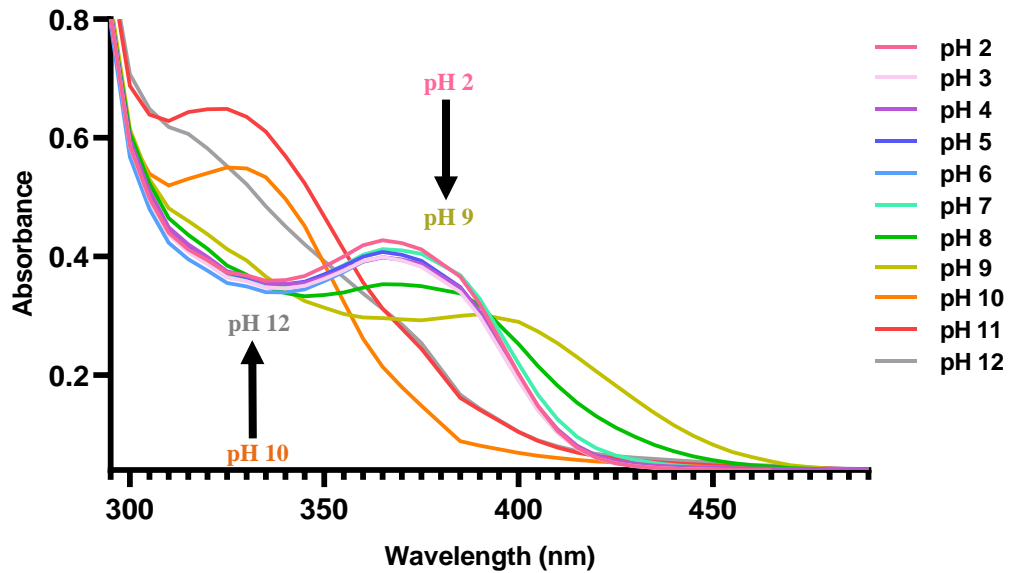


Figure 4. 12. UV-vis spectra of quercetin (25 μM) in varying pH environments.

Quercetin (25 μM , 40% MeOH, 20% 1,2-propanediol) was made in Tris-HCl (40 mM) in varying pH environments (2-12). In a clear 96-well plate, triplicates of each sample were aliquoted (200 μL). Samples were monitored for absorbance 295 – 490 nm. Absorption maximums were observed at 325, 365 and 400 nm. At 325 nm, peaks were shown for pH samples 10 (Abs: 0.55) and 11 (Abs: 0.65), at 365nm, pH 2 (Abs: 0.43), pH 3 (Abs: 0.4), pH 4 (Abs: 0.4), pH 5 (Abs: 0.41), pH 6 (Abs: 0.4), pH 7(Abs: 0.41) and pH 8 (Abs: 0.35) and at 400 nm, pH 9 (Abs: 0.29). For wavelengths 325, 365 and 400 nm, pH samples 11, 2 and 9 held the highest absorption peaks. The arrows show the trends of pH environments at specific absorption maximum wavelengths, $n = 3$.

Absorbance Spectra of Quercetin-Ni (II) (25 μ M, 50 μ M) at Varying pH

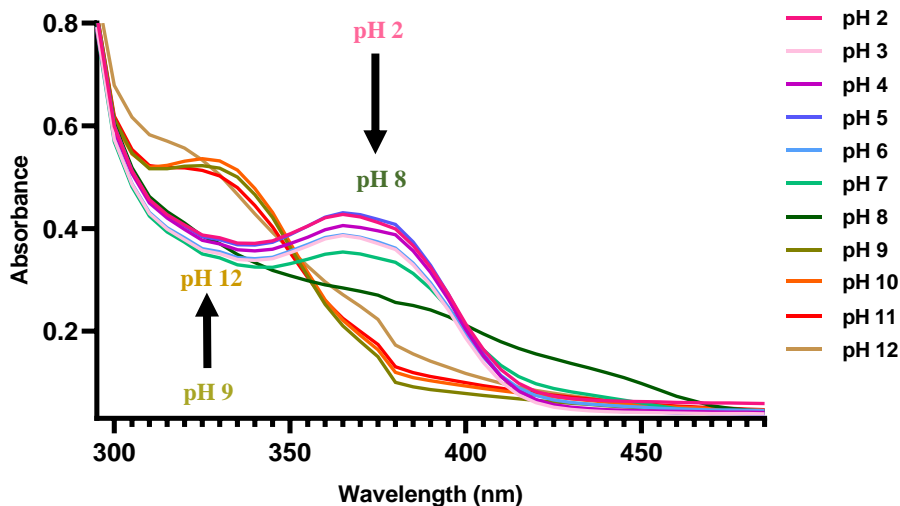


Figure 4. 13. UV-vis spectra of quercetin-nickel (II) (25 μ M, 50 μ M) in varying pH environments.

Quercetin-Ni (II) (25 μ M, 50 μ M, 40% MeOH, 20% 1,2-propanediol) was made in Tris-HCl (40 mM) in varying pH environments (2-12). In a clear 96-well plate, triplicates of each sample were aliquoted (200 μ L). Samples were monitored for absorbance from 295 – 485 nm. Absorption maximums were observed at 320, 325 and 365 nm. At 320 nm, peaks were shown for pH samples 12 (Abs: 0.56), at 325nm, pH 9 (Abs: 0.52), pH 10 (Abs: 0.54) and pH 11 (Abs: 0.51) and at 365 nm, pH 2 (Abs: 0.43), pH 3 (Abs: 0.39), pH 4 (Abs: 0.41), pH 5 (0.43), pH 6 (Abs: 0.39) and pH 7 (Abs: 0.35). For wavelengths, 320 nm and 325 nm, samples pH 12 and pH 10 held the highest absorption peaks, respectively, while pH 2 and pH 5 had the highest absorption peaks at 365 nm. The arrows show the trends of pH environments at specific absorption maximum wavelengths, $n = 3$.

Absorbance Spectra of Quercetin-Fe (III) (25 μ M, 50 μ M) at Varying pH

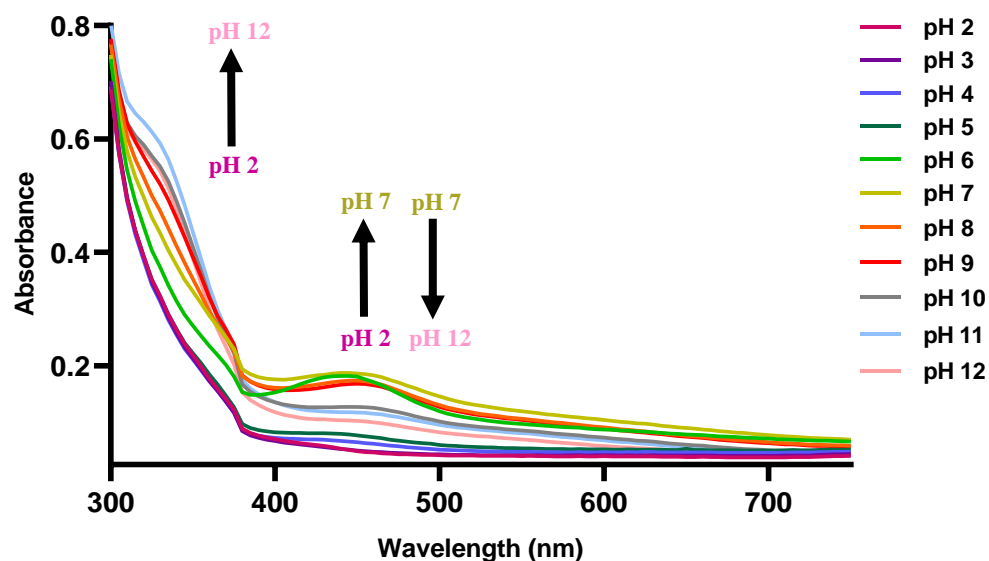


Figure 4. 14. UV-vis spectra of quercetin-iron (III) (25 μ M, 50 μ M) in varying pH environments.

Quercetin-Fe (III) (25 μ M, 50 μ M, 40% MeOH, 20% 1,2-propanediol) was made in Tris-HCl (40 mM) in varying pH environments (2-12). In a clear 96-well plate, triplicates of each sample were aliquoted (200 μ L). Samples were monitored for absorbance from 300 – 750 nm. Absorption maximums were observed at 325 and 445 nm. At 325 nm, pH 11 had shown an absorption peak of 0.61, while all samples aside from pH 2 had displayed absorption peaks at 445 nm (pH 3 (Abs: 0.052), pH 4 (Abs: 0.066), pH 5 (Abs: 0.079), pH 6 (Abs: 0.18), pH 7 (Abs: 0.19), pH 8 (Abs: 0.17), pH 9 (Abs: 0.17), pH 10 (Abs: 0.13), pH 11 (Abs: 0.12) and pH 12 (Abs: 0.10)). Samples pH 11 (Abs: 0.61) and pH 7 (Abs: 0.19) held the high absorption peaks at 325 and 445 nm, respectively, $n = 3$.

4.4.2. Quercetin-metal studies using aluminum (III) chloride

Quercetin-Al (III) was monitored for absorbance in pH environments 2-12. We observed absorption maxima in pH 2 (360 nm), pH 5 (360 nm), pH 9 (440 nm) and pH 12 (325 nm) (**figure 4.15**). These samples were titrated with P_i (0-1 mM) and were monitored for fluorescence ($\lambda_{\text{abs}} = \lambda_{\text{ex}}$). The first quercetin-metal and P_i relationship was observed using quercetin-Al (III).

Quercetin-Al (III) in pH 2, 5 (λ_{ex} : 425 nm) and 9 (λ_{ex} : 440 nm), demonstrated a direct negative relationship with increasing P_i concentrations (**figures 4.16-19**). A fluorescence emission standard curve was constructed using the P_i titrations reported in pH 5 (λ_{ex} : 425 nm).

In **figure 4.17 (b)**, for the titration of P_i, using the *Equation 4.1*, two binding constants were observed, $K_{b1} = 9.5 \pm 4.7 \text{ nM}$ and $K_{b2} = 26.4 \pm 1.9 \text{ nM}$ [94].

$$\text{Log} [(F_0 - F)/F] = \log K_b + n \log [\text{ligand}]$$

Equation 4. 1

Where F₀ and F represent the fluorescence intensity of quercetin-Al (III) in the absence and presence of P_i, respectively, n represents the number of binding sites and K_b represents the binding constant.

Absorbance Spectra of Quercetin-Al (III) (25 μ M, 50 μ M) at Varying pH

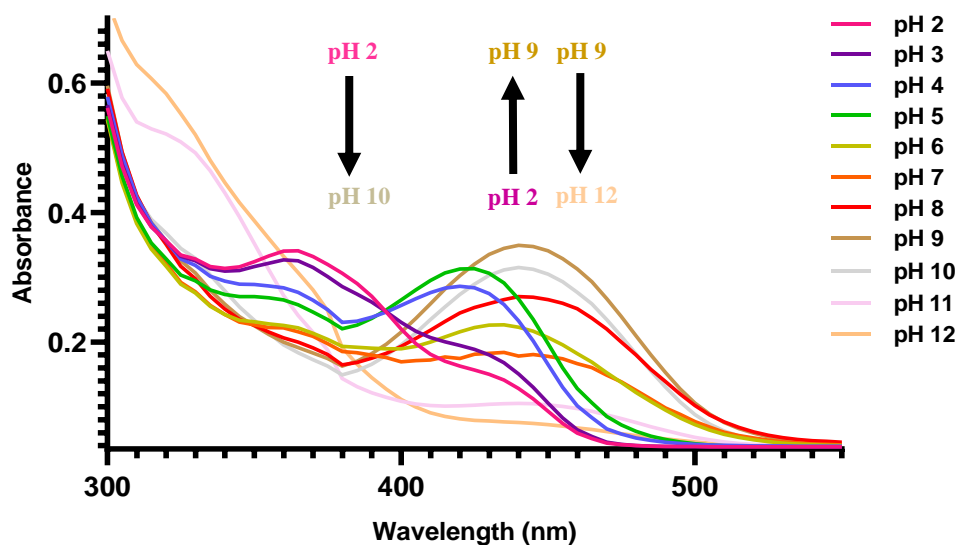


Figure 4. 15. UV/vis spectra of quercetin-aluminum (III) (25 μ M, 50 μ M) in varying pH environments.

Quercetin-Al (III) (25 μ M, 50 μ M, 40% MeOH, 20% 1,2-propanediol) was made in Tris-HCl (0.1 M) in varying pH environments (2-12). In a clear 96-well plate, triplicates of each sample were aliquoted (200 μ L). Samples were monitored for absorbance and scanned from 300 – 550 nm. Absorption maximums were observed at 325, 360, 425 and 440 nm. At 325 nm, absorption peaks are shown for pH 11 (Abs: 0.5) and pH 12 (Abs: 0.55). At 360 nm, absorption peaks are shown for pH 2 (Abs: 0.34), pH 3 (Abs: 0.33), pH 4 (Abs: 0.28), pH 5 (Abs: 0.27), pH 6 (Abs: 0.23), pH 7 (Abs: 0.22), pH 8 (Abs: 0.21), pH 9 (Abs: 0.2) and pH 10 (Abs: 0.2). At 425 nm, absorption peaks are shown for pH 2 (Abs: 0.16), pH 3 (Abs: 0.19), pH 4 (Abs: 0.28) and pH 5 (Abs: 0.31). At 440 nm, absorption peaks are shown for pH 6 (Abs: 0.22), pH 7 (Abs: 0.18), pH 8 (Abs: 0.27), pH 9 (Abs: 0.35), pH 10 (Abs: 0.32) and pH 11 (Abs: 0.11). Samples pH 12 (Abs: 0.55), pH 2 (0.34), pH 5 (Abs: 0.31) and pH 9 (Abs: 0.35) held the high absorption peaks at 325, 360, 425 and 440 nm, respectively, $n = 3$.

**Emission Spectra of P_i Titrations of Quercetin-Al (III)
(pH 2, excited at 425 nm)**

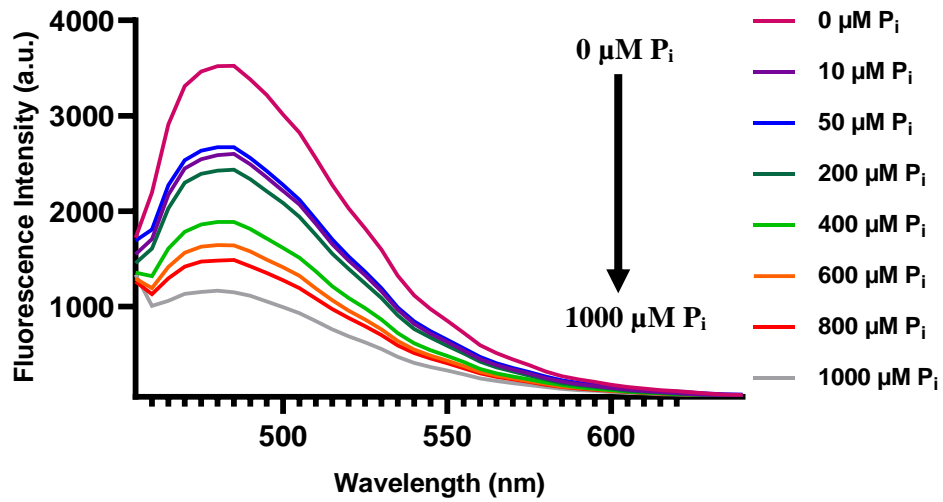
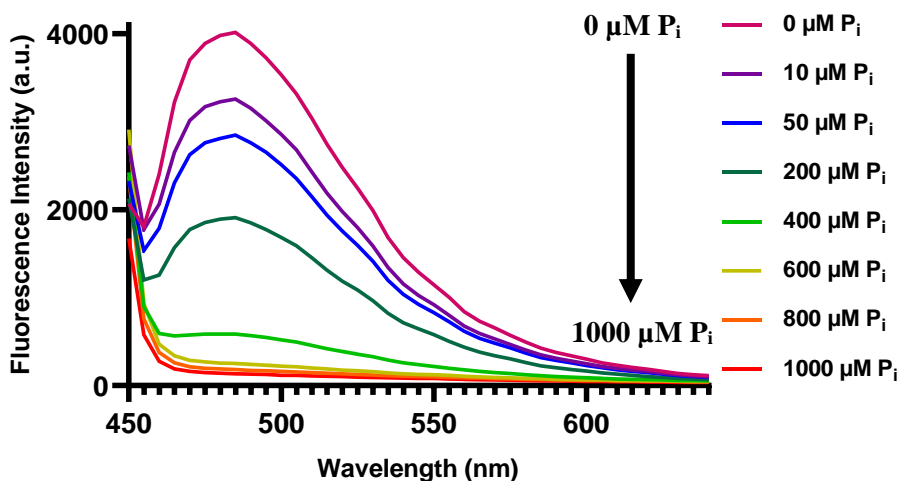


Figure 4. 16. Fluorescence emission spectra of quercetin-aluminum (III) (25 μM , 50 μM , pH 2) with P_i titrations (ex: 425 nm).

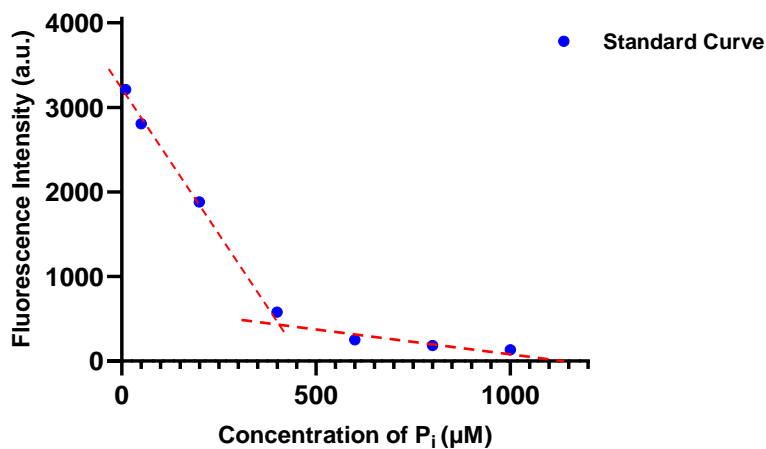
Quercetin-Al (III) (25 μM , 50 μM , 40% MeOH, 20% 1,2-propanediol) was made in Tris-HCl (40 mM, pH 2). In a clear 96-well plate, triplicates of each sample were aliquoted (180 μL) and stock concentrations of P_i (0-1mM, 20 μL) were added. Samples were excited at 425 nm and monitored for fluorescence emission between 445 – 645 nm, every 5 seconds. An emission maximum was observed at 480 nm for all samples, $n = 3$.

**Emission Spectra of P_i Titrations of Quercetin-Al (III)
(pH 5, excited at 425 nm)**



(a)

**Quercetin-Al (III) Emission Spectra Standard Curve
(pH 5, excited at 425 nm)**



(b)

Figure 4. 17. Fluorescence emission spectra of quercetin-aluminum (III) (25 μ M, 50 μ M, pH 5) with P_i titrations (ex: 425 nm).

(a) Quercetin-Al (III) (25 μ M, 50 μ M, 40% MeOH, 20% 1,2-propanediol) was made in Tris-HCl (40 mM, pH 5). In a clear 96-well plate, triplicates of each sample were aliquoted (180 μ L) and stock concentrations of P_i (0-1mM, 20 μ L) were added. Samples were excited at 425 nm and monitored for fluorescence emission between 450 – 640 nm, every 5 seconds. An emission maximum was observed at 480 nm for all samples. (b) Fluorescence emission standard curve of quercetin-aluminum (III) (25 μ M, 50 μ M, pH 5) with P_i (ex: 425 nm). The fluorescence emission spectral data for quercetin-Al (III) (25 μ M, 50 μ M, pH 5) with P_i (0-1 mM) was used to construct the linear trend with the titration of P_i (0.2 – 1 mM), $n = 3$.

**Emission Spectra of P_i Titrations of Quercetin-Al (III)
(pH 2, excited at 440 nm)**

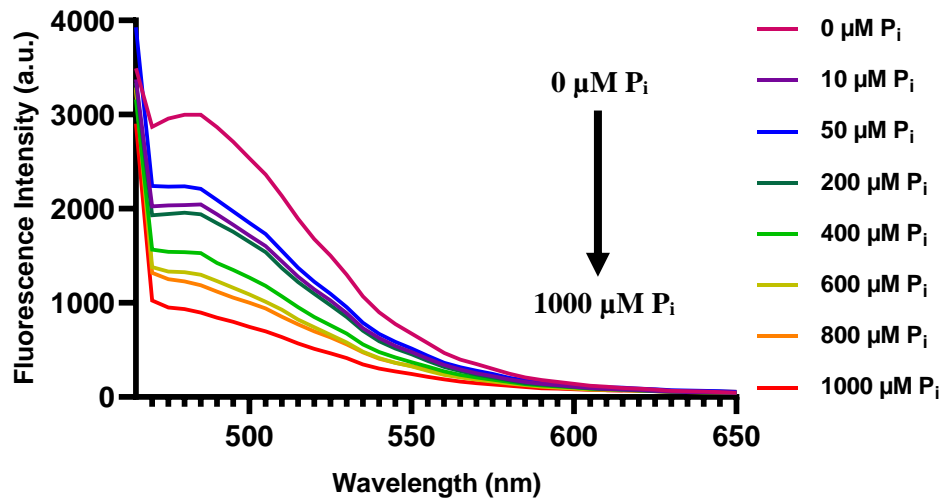


Figure 4. 18. Fluorescence emission spectra of quercetin-aluminum (III) (25 μM , 50 μM , pH 2) with P_i titrations (ex: 440 nm).

Quercetin-Al (III) (25 μM , 50 μM , 40% MeOH, 20% 1,2-propanediol) was made in Tris-HCl (40 mM, pH 2). In a clear 96-well plate, triplicates of each sample were aliquoted (180 μL) and stock concentrations of P_i (0-1mM, 20 μL) were added. Samples were excited at 440 nm and monitored for fluorescence emission between 465 – 650 nm, every 5 seconds. An emission maximum was observed at 485 nm for all samples, $n = 3$.

**Emission Spectra of P_i Titrations of Quercetin-Al (III)
(pH 5, excited at 440 nm)**

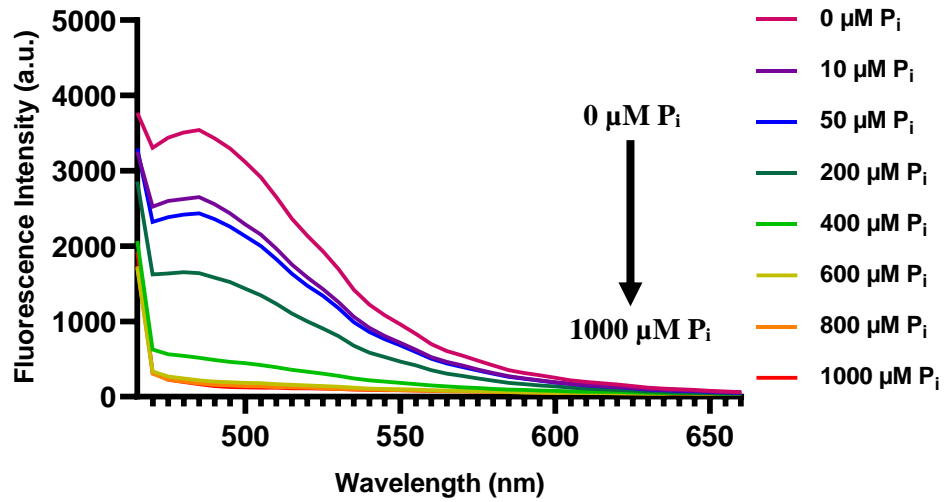


Figure 4. 19. Fluorescence emission spectra of quercetin-aluminum (III) (25 μ M, 50 μ M, pH 5) with P_i titrations (ex: 440 nm).

Quercetin-Al (III) (25 μ M, 50 μ M, 40% MeOH, 20% 1,2-propanediol) was made in Tris-HCl (40 mM, pH 5). In a clear 96-well plate, triplicates of each sample were aliquoted (180 μ L) and stock concentrations of P_i (0-1mM, 20 μ L) were added. Samples were excited at 440 nm and monitored for fluorescence emission between 465 – 660 nm, every 5 seconds. An emission maximum was observed at 485 nm for all samples, $n = 3$.

4.4.3. Quercetin-zirconium (IV) UV-vis characterization and P_i fluorescence studies

Another quercetin-metal fluorogenic probe was studied using zirconium (IV) chloride. Quercetin-Zr (IV) (25 μ M, 50 μ M) was monitored for absorbance in pH environments of 3-13 (**figure 4.20**) [20]. Absorption maxima were reported at 325 nm (pH 12), 450 nm (pH 3), 465 nm (pH 9) and 470 nm (pH 12). All samples were titrated with P_i (0-1 mM) and monitored for fluorescence ($\lambda_{\text{abs}} = \lambda_{\text{ex}}$).

The fluorescence emission properties of quercetin-Zr (IV) had a direct positive relationship with increasing concentrations of P_i (0-1 mM). This relationship was reported in pH 9 environments (λ_{ex} : 455, 465 and 470 nm) (**figures 4.21-23**). Future studies of quercetin-Zr (IV) with P_i would investigate this relationship monitored the fluorescence of precipitated quercetin-zirconium (IV) in alkaline environments and bound P_i [95].

Absorbance Spectra of Quercetin-Zr (IV) (25 μ M, 50 μ M) at Varying pH

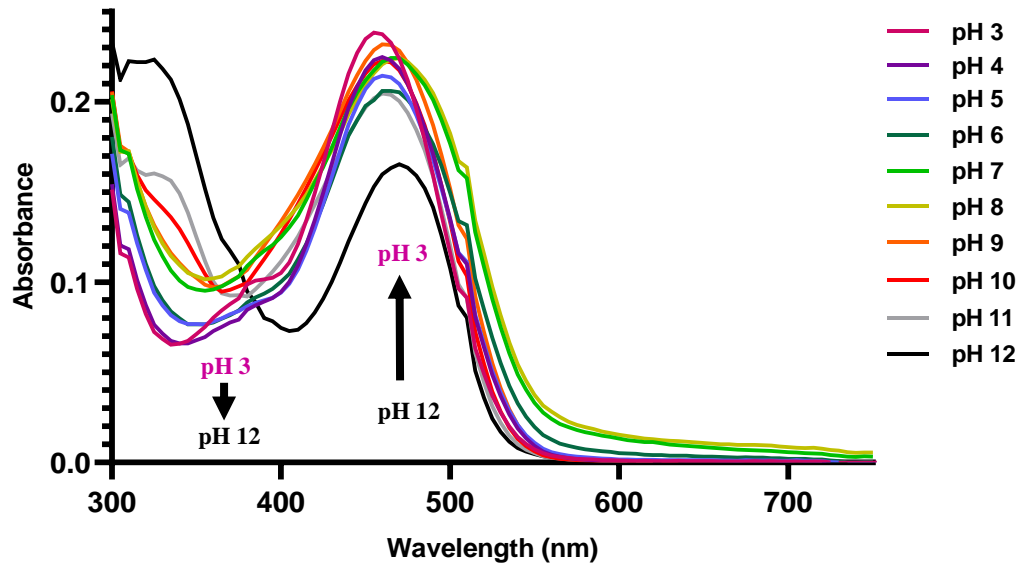


Figure 4. 20. UV/vis spectra of quercetin-zirconium (IV) (25 μ M, 50 μ M) in varying pH environments.

Quercetin-Zr (IV) (25 μ M, 50 μ M, 40% MeOH, 20% 1,2-propanediol) was made in Tris-HCl (40 mM) in varying pH environments (3-12). In a clear 96-well plate, triplicates of each sample were aliquoted (200 μ L). Samples were monitored for absorbance and scanned from 300 – 750 nm. Absorption maximums were observed at 325, 450, 465 and 470 nm. At 325 nm, absorption peaks are shown for pH 10 (Abs: 0.15), pH 11 (Abs: 0.16) and pH 12 (Abs: 0.22). At 450 nm, the absorption peak was shown for pH 3 (Abs: 0.24). At 465 nm, absorption peaks are shown for pH 4 (Abs: 0.22), pH 5 (Abs: 0.21), pH 6 (Abs: 0.21), pH 7 (Abs: 0.22), pH 8 (Abs: 0.22), pH 9 (Abs: 0.23), pH 10 (Abs: 0.22), pH 11 (Abs: 0.20) and pH 12 (Abs: 0.13). At 470 nm, absorption peaks are shown for pH 12 (Abs: 0.17). Samples pH 12 (Abs: 0.22), pH 3 (Abs: 0.24), pH 9 (Abs: 0.23) and pH 12 (Abs: 0.17) held the high absorption peaks at 325, 450, 465 and 470 nm, respectively, $n = 3$.

**Emission Spectra of P_i Titrations of Quercetin-Zr (IV)
(pH 9, excited at 455 nm)**

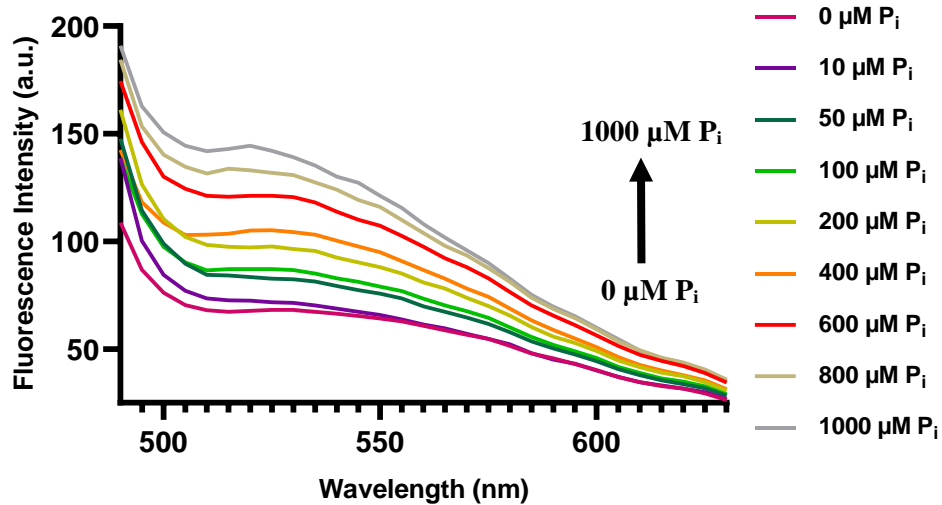


Figure 4. 21. Fluorescence emission spectra of quercetin-zirconium (IV) (25 μM , 50 μM , pH 9) with P_i titrations (ex: 455 nm).

Quercetin-Zr (IV) (25 μM , 50 μM , 40% MeOH, 20% 1,2-propanediol) was made in Tris-HCl (40 mM, pH 5). In a clear 96-well plate, triplicates of each sample were aliquoted (180 μL) and stock concentrations of P_i (0-1mM, 20 μL) were added. Samples were excited at 455 nm and monitored for fluorescence emission between 490 – 630 nm, every 5 seconds. An emission maximum was observed at 520 nm for all samples, $n = 3$.

**Emission Spectra of P_i Titrations of Quercetin-Zr (IV)
(pH 9, excited at 465 nm)**

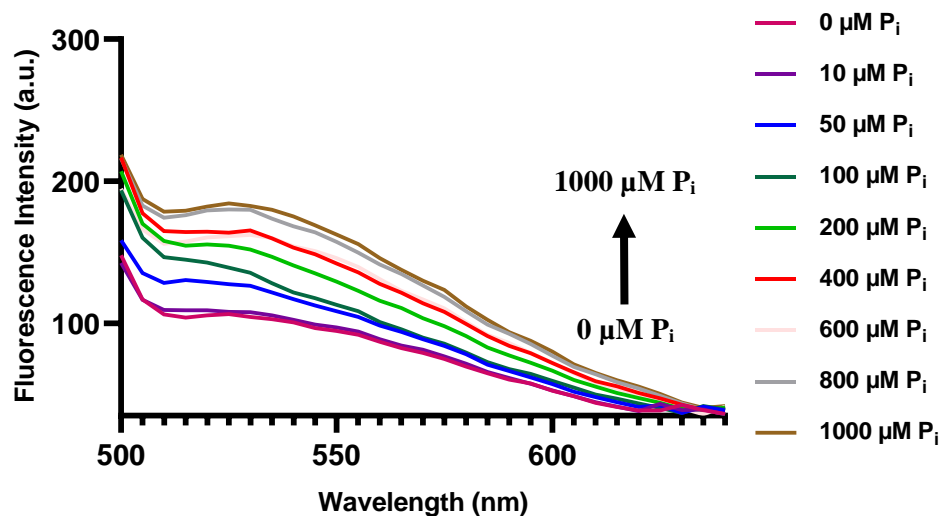


Figure 4. 22. Fluorescence emission spectra of quercetin-zirconium (IV) (25 μM , 50 μM , pH 9) with P_i titrations (ex: 465 nm).

Quercetin-Zr (IV) (25 μM , 50 μM , 40% MeOH, 20% 1,2-propanediol) was made in Tris-HCl (40 mM, pH 5). In a clear 96-well plate, triplicates of each sample were aliquoted (180 μL) and stock concentrations of P_i (0-1mM, 20 μL) were added. Samples were excited at 465 nm and monitored for fluorescence emission between 495 – 640 nm, every 5 seconds. An emission maximum was observed at 525 nm for all samples, $n = 3$.

**Emission Spectra of P_i Titrations of Quercetin-Zr (IV)
(pH 9, excited at 470 nm)**

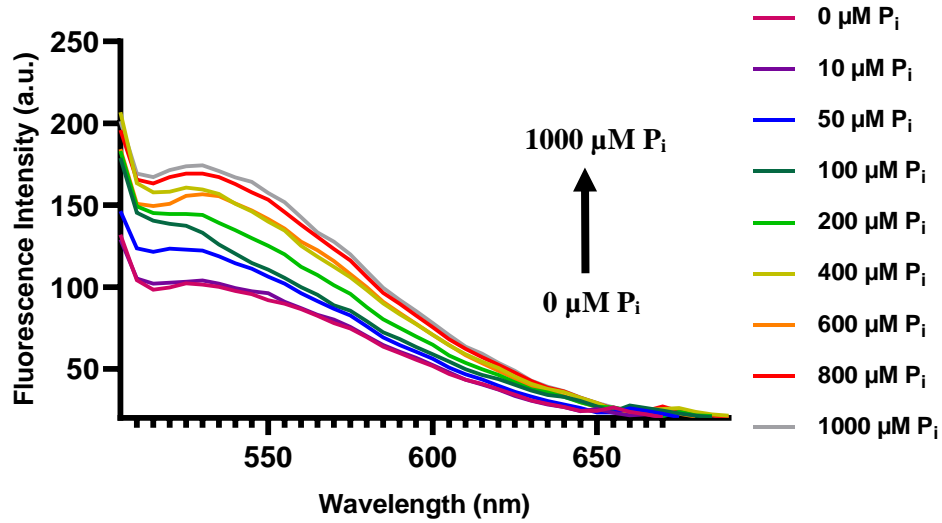


Figure 4. 23. Fluorescence emission spectra of quercetin-zirconium (IV) (25 μM , 50 μM , pH 9) with P_i titrations (ex: 470 nm).

Quercetin-Zr (IV) (25 μM , 50 μM , 40% MeOH, 20% 1,2-propanediol) was made in Tris-HCl (40 mM, pH 5). In a clear 96-well plate, triplicates of each sample were aliquoted (180 μL) and stock concentrations of P_i (0-1mM, 20 μL) were added. Samples were excited at 470 nm and monitored for fluorescence emission between 500 – 690 nm, every 5 seconds. An emission maximum was observed at 530 nm for all samples, $n = 3$.

4.5. Characterizing the flavonoid-metal complex of quercetin-Zr (IV)

4.5.1. Quercetin-Zr (IV) ¹HNMR studies and zirconium (IV) chloride binding affinity

The flavonoid-metal complex of quercetin-Zr (IV) was characterized using UV/vis spectroscopy, fluorescence titration studies, ¹HNMR and ³¹PNMR to optimize P_i sensitivity.

The research thus far had supported that quercetin-Zr (IV) in pH 9 environments allotted a direct positive relationship with P_i (0-1 mM). Quercetin-Zr (IV) ratios from 1:1 to 1:10 were monitored for absorbance (**figure 4.24**). All sample ratios reported absorbance peaks between ~ **450-470 nm**. The absorption wavelength reported for median probe ratios (1:4, 1:5 and 1:6), 465 nm, was used. Quercetin (20 μM, pH 9) was titrated with zirconium (IV) chloride (0-316 μM) and monitored for fluorescence until a saturation curve was observed (λ_{ex}: 465nm) (**figure 4.25**). Increased concentrations of zirconium (IV) chloride were proportional to the fluorescence emission properties of quercetin (20 μM) (λ_{em}: 540 nm).

The binding constant for quercetin-Zr (IV) was calculated from a fit of data of **figure 4.25** to the modified Benesi–Hildebrand equation (shown below, **Equation 4.2**): **K = 20.0 ± 0.7 nM (figure 4.25)**. F_{max}, F_x, and F₀ are the emission intensities of quercetin at [ZrCl₄] of complete interaction, at an intermediate [ZrCl₄] and in the absence of ZrCl₄, respectively, where M is the [ZrCl₄] and n is the number of Zr⁴⁺ ions bound per quercetin [96].

$$\frac{(F_{max} - F_0)}{(F_x - F_0)} = 1 + \left(\frac{1}{K}\right)\left(\frac{1}{[M]^n}\right)$$

Equation 4. 2

Absorbance Spectra of Quercetin (20 μM) with ZrCl_4 Titrations

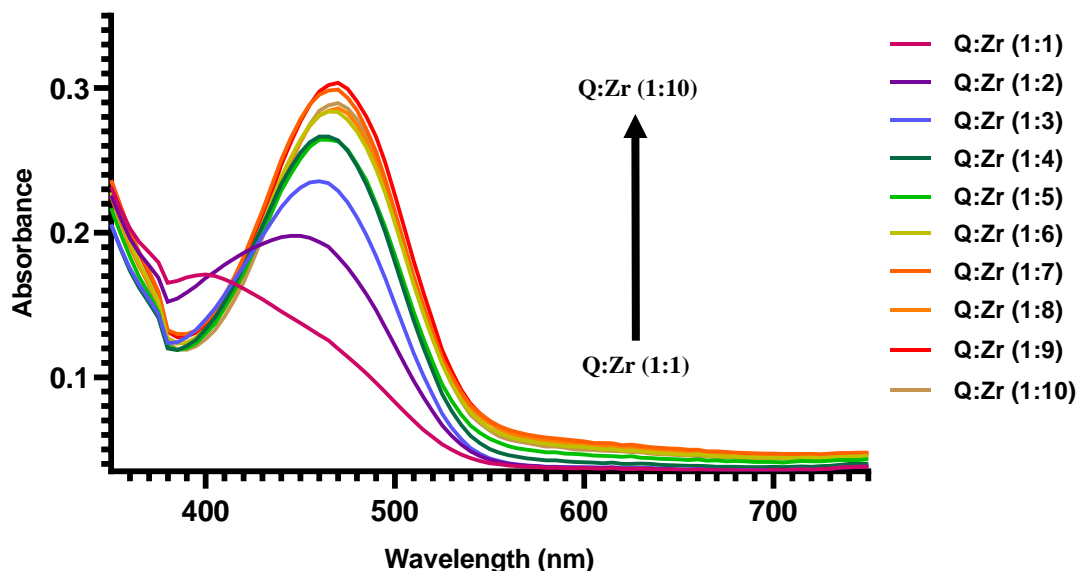


Figure 4. 24. UV/vis spectra of quercetin (20 μM) with zirconium (IV) chloride titrations.

In a clear 96-well plate, triplicate samples of quercetin (20 μM , 40% MeOH, 20% 1,2-propanediol) in Tris-HCl (40 mM, pH 9) titrated with varying concentrations of zirconium (IV) chloride (0-200 μM) were aliquoted. Samples were monitored for absorbance (350 -750 nm) every 10 seconds. Absorption maximums were observed from 450 – 465 nm with the increased concentrations of zirconium (IV) chloride. At 400 nm, an absorption peak was observed for Q:Zr(IV) (1:1, Abs: 0.17). At 450 nm, an absorption peak was shown for Q:Zr(IV) (1:2, Abs: 0.20). At 460 nm, an absorption peak was shown for Q:Zr(IV) (1:3, Abs: 0.24). At 465 nm, absorption peaks are shown Q:Zr(IV) (1:4, Abs: 0.26), (1:5, Abs: 0.26) and (1:6, Abs: 0.28). At 470 nm, absorption peaks are shown Q:Zr(IV) (1:7, Abs: 0.29), (1:8, Abs: 0.29), (1:9, Abs: 0.30) and (1:10, Abs: 0.29). Samples Q:Zr(IV) (1:2, Abs: 0.20), (1:3, Abs: 0.24), (1:6, Abs: 0.28) and (1:9, Abs: 0.30) held the high absorption peaks at 450, 460, 465 and 470 nm, $n = 3$.

**Emission Properties of Quercetin with Zirconium (IV) chloride
in Tris (0.1 M, pH 9, excited at 465 nm)**

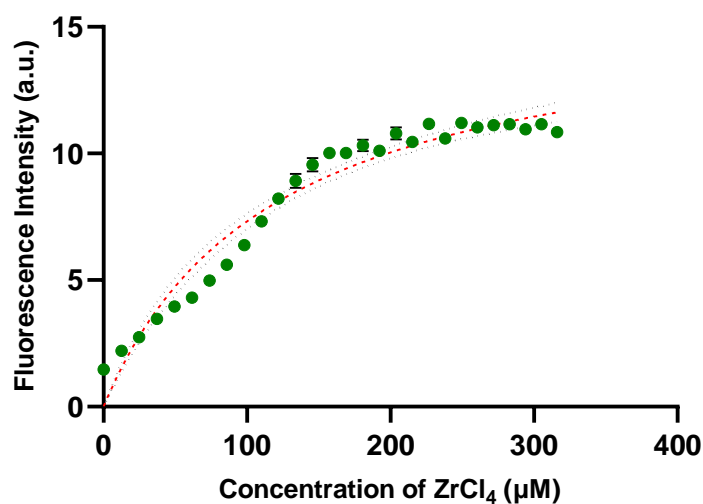


Figure 4. 25. Fluorescence emission intensities of quercetin and zirconium (IV) chloride using steady-state kinetics.

In a 1 mL cuvette, varying concentrations of zirconium (IV) chloride (0-316 μM) and a constant concentration of quercetin (25 μM, 40% MeOH, 20% 1,2-propanediol) in Tris-HCl (40 mM, pH 9) were added. The sample was excited at 465 nm and monitored for fluorescence emission between every zirconium (IV) chloride titration. Emission maximums were observed at 540 nm. Binding interactions were extrapolated using the modified Benesi–Hildebrand equation: $K = 20.0 \pm 0.7$ nM. Black dotted lines show the 99% confidence or prediction bands for the truest curve. Samples were excited at 465 nm and emission maximums were observed at 540 nm.

4.5.2. Surveying quercetin-Zr (IV) concentrations (10 μ M, 40 μ M or 10 μ M, 100 μ M) in the presence of P_i

Using **figure 4.25**, we identified the approximate concentration ratios of quercetin-Zr (IV) at 50% fluorescence saturation (1:4 / 25 μ M : 107.5-128.5 μ M) and total saturation (1:10 / 25 μ M : 200 μ M) [1, 97].

In a clear 96-well plate, triplicate samples of quercetin-Zr (IV) (10 μ M : 40 μ M, pH 9) were titrated with P_i (0-120 μ M) and monitored for fluorescence (λ_{ex} : 465 nm) (**figure 4.26**). An increase in fluorescence proportional to [P_i] was reported (later studies would suggest this was due to the precipitated quercetin-Zr (IV)- P_i detected). The same protocol was repeated using quercetin-Zr (IV) (10 μ M : 100 μ M, pH 9), a gradual quenching effect was observed (**figure 4.27**). This is the first reporting of quercetin-Zr (IV) showing an aqueous fluorescence quenching effect with increased concentrations of P_i [1].

Emission Spectra of the Inorganic Phosphate Titration of Quercetin-Zr (IV) (10 μ M, 40 μ M) in Tris (0.1 M, pH 9, excited at 465 nm)

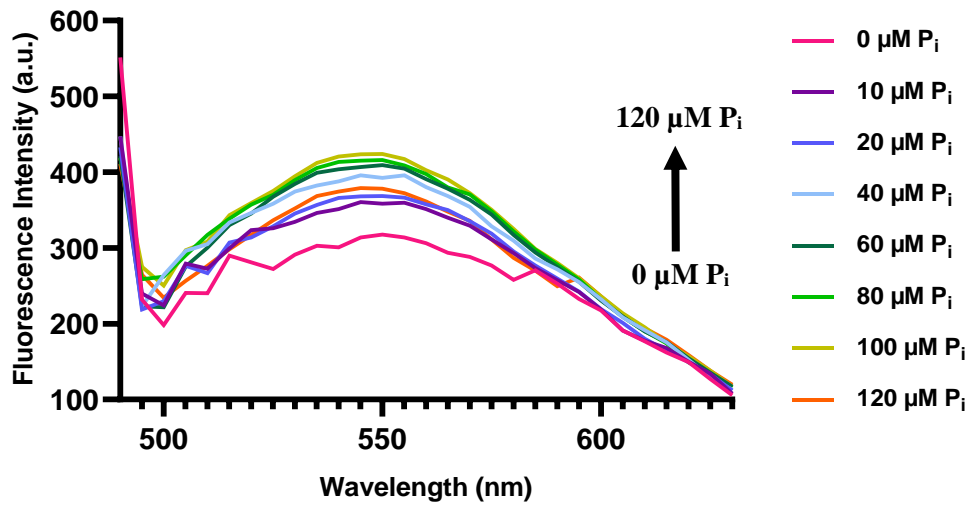


Figure 4. 26. Fluorescence emission spectra of quercetin-zirconium (IV) (10 μ M, 40 μ M, pH 9) with P_i titrations (ex: 465 nm).

Quercetin-Zr (IV) (10 μ M, 40 μ M, 40% MeOH, 20% 1,2-propanediol) was made in Tris-HCl (40 mM, pH 9). In a clear 96-well plate, triplicates of each sample were aliquoted (180 μ L) and stock concentrations of P_i (0- 120 μ M, 20 μ L) were added. Samples were excited at 465 nm and monitored for fluorescence between 490 – 630 nm, every 5 seconds. An emission maximum was observed at 545 nm for all samples, $n = 3$.

Emission Spectra of the Inorganic Phosphate Titration of Quercetin-Zr (IV) (10 μ M, 100 μ M) in Tris (0.1 M, pH 9, excited at 465 nm)

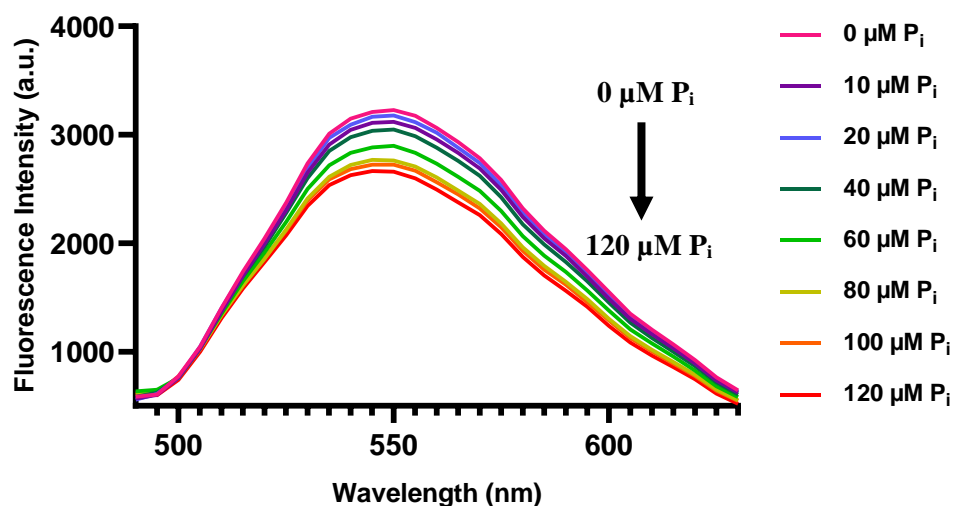


Figure 4. 27. Fluorescence emission spectra of quercetin-zirconium (IV) (10 μ M, 100 μ M, pH 9) with P_i titrations (ex: 465 nm).

Quercetin-Zr (IV) (10 μ M, 100 μ M, 40% MeOH, 20% 1,2-propanediol) was made in Tris-HCl (40 mM, pH 9). In a clear 96-well plate, triplicates of each sample were aliquoted (180 μ L) and stock concentrations of P_i (0- 120 μ M, 20 μ L) were added. Samples were excited at 465 nm and monitored for fluorescence between 490 – 630 nm, every 5 seconds. An emission maximum was observed at 545 nm for all samples, $n = 3$.

4.5.3. Investigating zirconium (IV) occupancy on the quercetin ligand molecule

In the literature, charge specific metals have been reported to exist in a quercetin-metal stoichiometric ratio of 1:1 and 2:1 [42, 44]. Non-linear fits of quercetin and metal titrations with ionic charges of at least three have been reported to exist in a 2:1 stoichiometric ratio. We postulated that two quercetin molecules would exist as bidentate ligands, binding the zirconium (IV) atom (**figure 4.28**) [43, 44].

¹HNMR (Proton Nuclear Magnetic Resonance), an analytical technique often used for determining sample content and molecular structures, was used to monitor quercetin spectra (2.5 mM, 40% MeOD, pH 9) with successive titrations of zirconium (IV) chloride (0-1.22 mM) (**figure 4.29**) [10, 41]. This experiment possessed limitations due to the interference of paramagnetic effects by zirconium (IV) chloride, as such, ¹HNMR spectra was not observed for quercetin and zirconium (IV) at concentration ratios above 2:1.5 [98, 99]. Quercetin had deshielding properties on the aromatic protons highlighted on the benzopyrone, at C₆ and C₈ (**figure 4.29**), in the presence of zirconium (IV)[99, 100]. C₆ and C₈ peaks of quercetin began at 5.4 and 5.57 ppm (0 mM ZrCl₄) and experienced downfield chemical shifts (towards higher ppm values) to ~5.49 and 5.67 ppm (1.22 mM ZrCl₄), respectively[101]. No other chemical shifts on quercetin were observed, suggesting protons on C₆ and C₈ achieve resonance at higher frequencies, related to the quercetin-Zr (IV) complexation occurring at the nearest metal binding site [101].

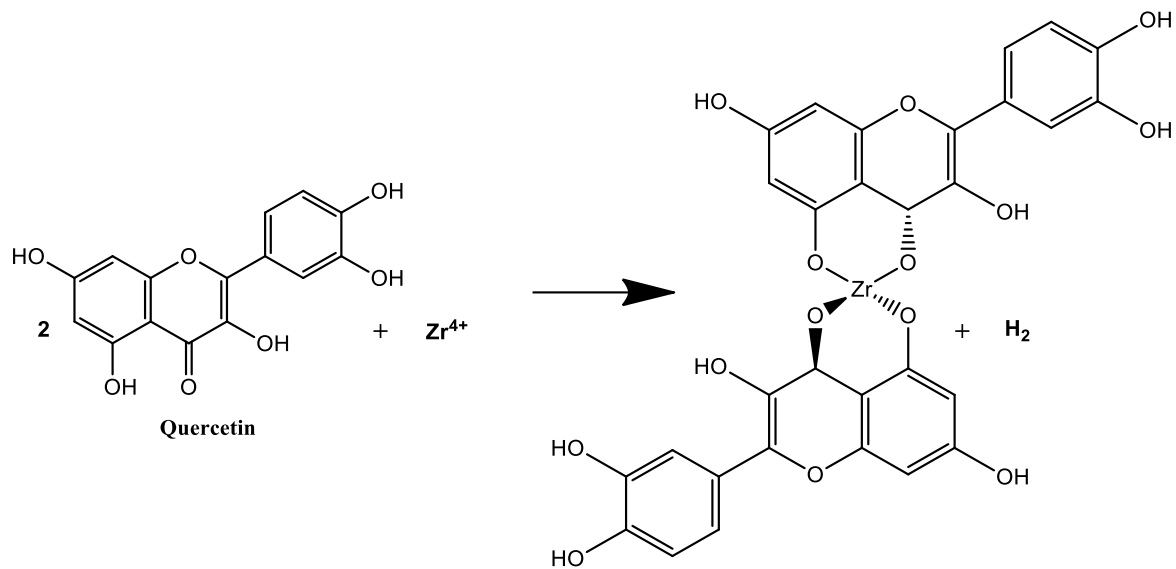


Figure 4. 28. *The postulated chemical reaction between quercetin ligand and zirconium (IV). Quercetin acts as bidentate ligand on the central atom, Zr^{4+} . This reaction yielded two hydrogen atoms from the hydroxyl group on the quercetin ligand molecule [42].*

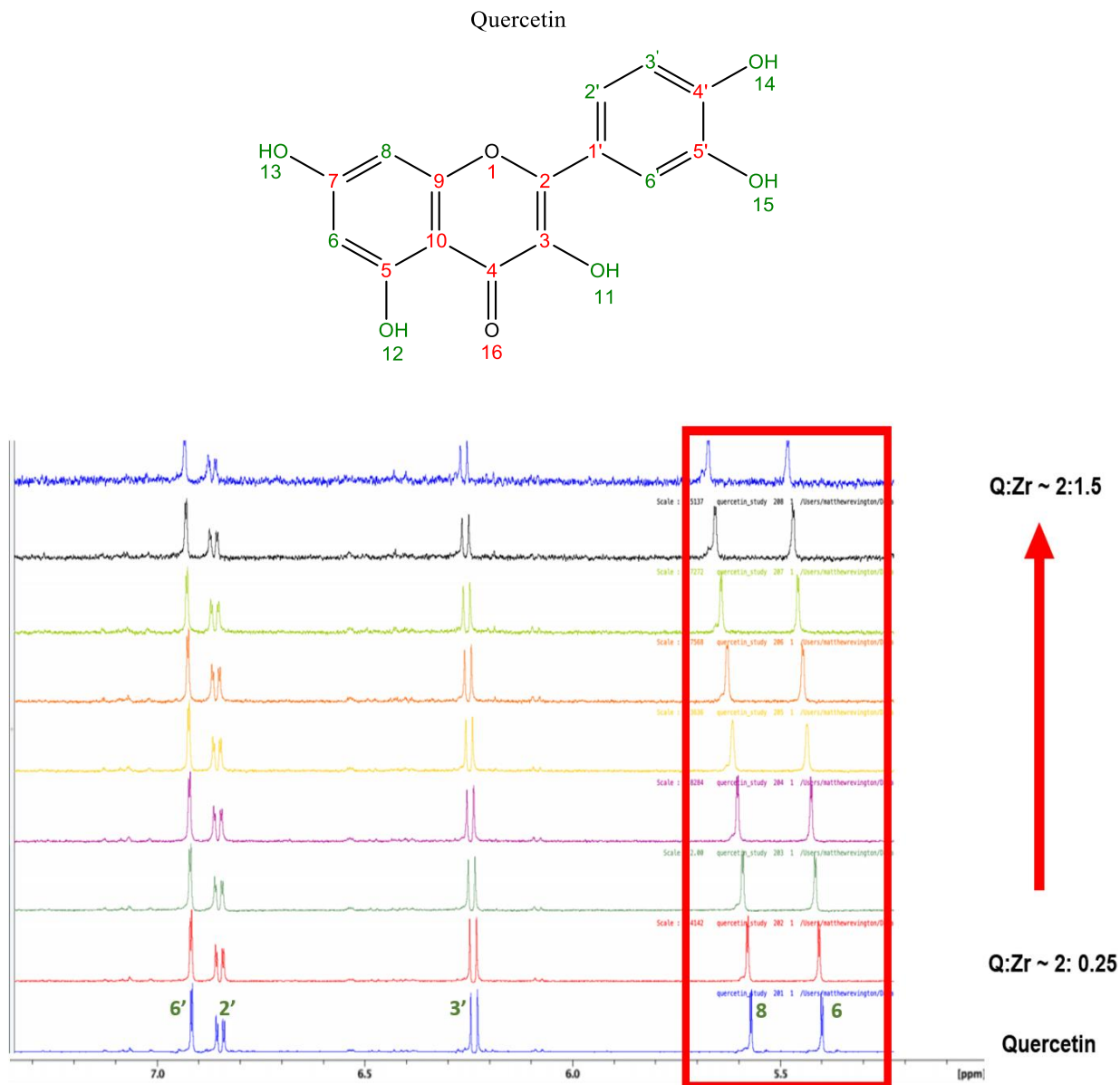


Figure 4. 29. H^1 NMR spectra for quercetin and zirconium (IV) chloride.

H^1 NMR was used to analyze 600 μ L of quercetin (2.5 mM, 40% MeOD) in Tris-HCl (44 mM, pH 9), further analysis was conducted with the titration of zirconium (IV) chloride (50 mM, in D_2O). Equal amounts of zirconium (IV) chloride (3 μ L, 0-1.22 mM) were titrated into the quercetin solution and varying ratios (quercetin : zirconium (IV) chloride) were analyzed. The highlighted doublets identify the aromatic protons, located at ~ 6.05 and 6.30 ppm. These peaks correspond to C_6 and C_8 on the quercetin structure. With the titration of zirconium (IV) chloride, these peaks shifted to the left.

4.5.4. Monitoring the molecular structure of quercetin-Zr (IV) in the presence of P_i using ¹HNMR

Next, quercetin-Zr (IV) samples with concentration ratios of 10:5 (2.5 mM, 1.22 mM, pH 9) were monitored in the presence of P_i (0-5.75 mM) using ¹HNMR (**figure 4.30**). Titrations of P_i led to shielding, where chemical shifts transitioned upfield (lower ppm values) [101]. C₆ and C₈ peaks of quercetin began at 5.52 and 5.75 ppm (1.22 mM ZrCl₄) and experienced chemical shifts to ~5.35 and 5.54 ppm, respectively. These upfield chemical shifts due to the introduction of P_i would suggest that the protons on C₆ and C₈ are experiencing an increase in electron density and resonance is achieved with the decreased pull on outer electrons [101]. We found, when P_i (0-5.75 mM, in D₂O) was titrated into quercetin-Zr (IV) (2.5 mM, 1.22 mM, in 40% MeOD, pH 9), an immediate colour change (neon → dark orange) and sample phase separation began to form (white precipitate) [1]. This visual chemical reaction that was never observed when using μM concentrations. A hypothesis was made about quercetin-Zr (IV) precipitating when P_i was ionically bound. To test this new hypothesis, P_i (600 μL, 50 mM, in D₂O) was monitored with ³¹P NMR. Zirconium (IV) chloride (3 μL, 0-20 mM, in D₂O) was titrated into our sample and a white precipitate began to form, like the sample shown in **figure 4.30**. The top phase (supernatant) from the sample, zirconium (IV) : P_i (45 mM : 4.5 mM), was isolated and monitored by ³¹P NMR (**figure 4.31**) [99, 101]. A loss of phosphorus signal was reported. This supported that the ionic binding of zirconium (IV) and P_i yielded a precipitate reaction and could be the cause of the positive direct fluorescence relationship observed between quercetin-Zr (IV) and P_i at pH 9 (λ_{ex}: 465 nm) (**figures 4.21-23**).

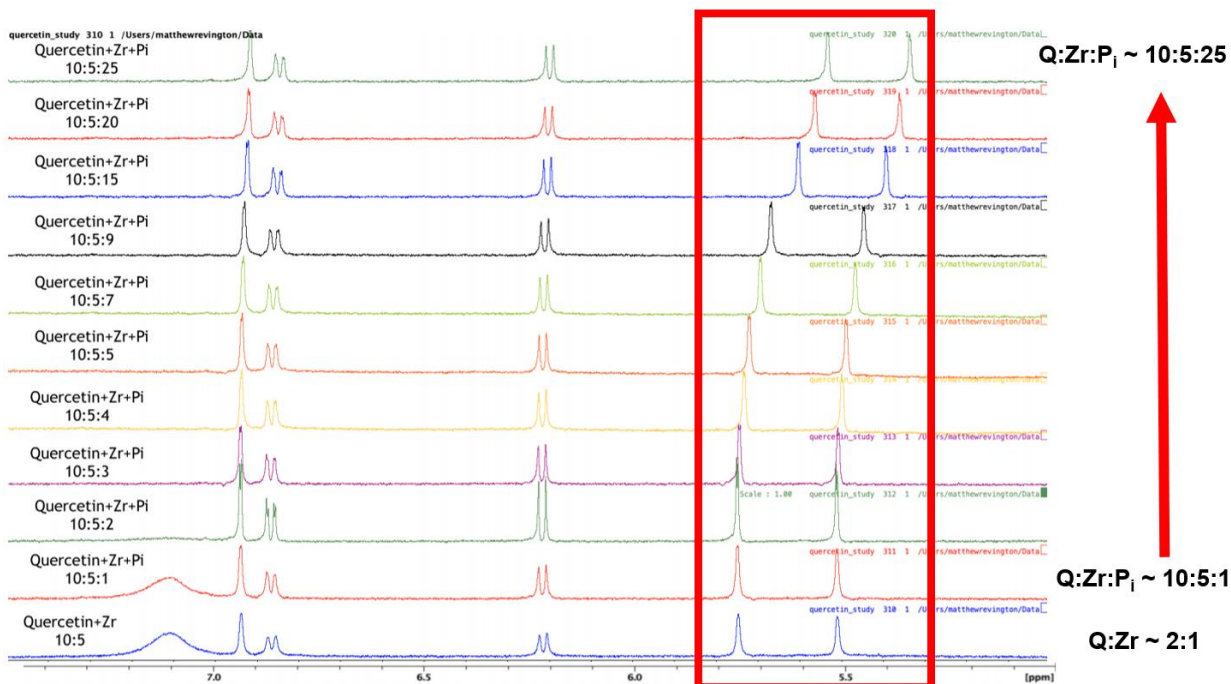


Figure 4. 30. ^1H NMR spectra of quercetin-zirconium (IV) (2.5 mM, 1.22 mM) and inorganic phosphate (P_i).

^1H NMR was used to analyze 600 μL of quercetin (2.5 mM, 40% MeOD) in Tris-HCl (44 mM, pH 9) and zirconium (IV) chloride (1.22 mM, in D_2O). Equal amounts of P_i (1.5 μL , 0-5.75 mM, in D_2O) were titrated into quercetin-zirconium (IV) (2.5 mM, 1.22 mM). Shifting doublet peaks correspond to C_6 and C_8 on the quercetin structure. Increasing concentrations of P_i led to upfield chemical shifts of the aromatic proton peaks.

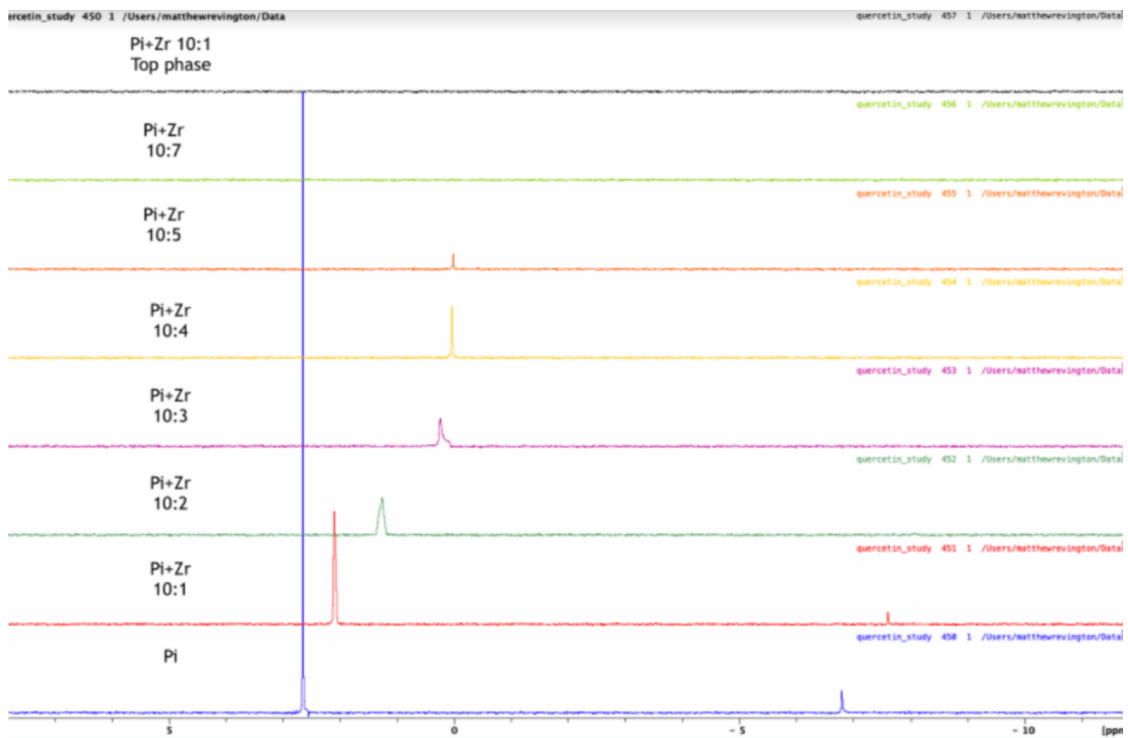


Figure 4. 31. ^{31}P NMR spectra of inorganic phosphate and zirconium (IV) chloride.

^{31}P NMR was used to identify the spectra of $600\ \mu\text{L}$ of P_i (50 mM, in D_2O) at ~ 2.7 ppm. Further analysis was conducted with the titration of zirconium (IV) chloride (50 mM). Equal amounts of zirconium (IV) chloride ($3\ \mu\text{L}$, 0-20 mM) were titrated into P_i (50 mM). Increasing concentrations of zirconium (IV) led to a white precipitate. The supernatant (top phase) of sample $\text{P}_i : \text{Zr}$ (10:1, 45 mM : 4.5 mM) sample was isolated and monitored for a ^{31}P NMR spectra. No signal was detected ($\text{P}_i + \text{Zr}$ (IV) 10:1).

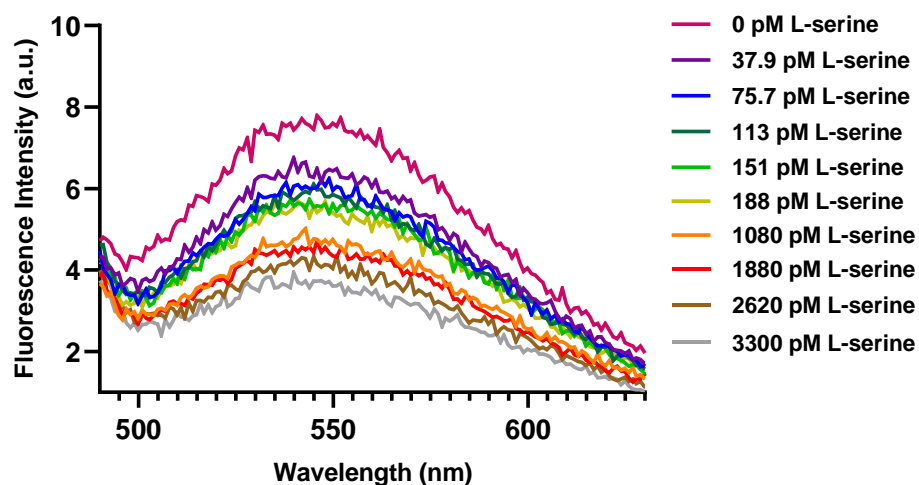
4.6. Surveying the quercetin-Zr (IV) probe for the detection of phospho-amino acids and phospho-proteins

4.6.1. Fluorescence emission studies of L-serine and O-phospho-L-serine using quercetin-Zr (IV)

Protein phosphorylation is a post-translational modification that acts as a regulatory mechanism for cellular transduction signaling [56, 102]. These signals can be responsible for the hyperactivity, malfunction or the overexpression of proteins found in many diseases [50, 56, 103]. A simple method using a fluorescent probe specific for the rapid detection of phosphorylated peptides/proteins would greatly aid the research of these regulatory mechanisms. 33% of protein phosphorylation occurs on serine (S), threonine (T), and tyrosine (Y) residues, while phosphorylated residues of serine make up 86.4% [57].

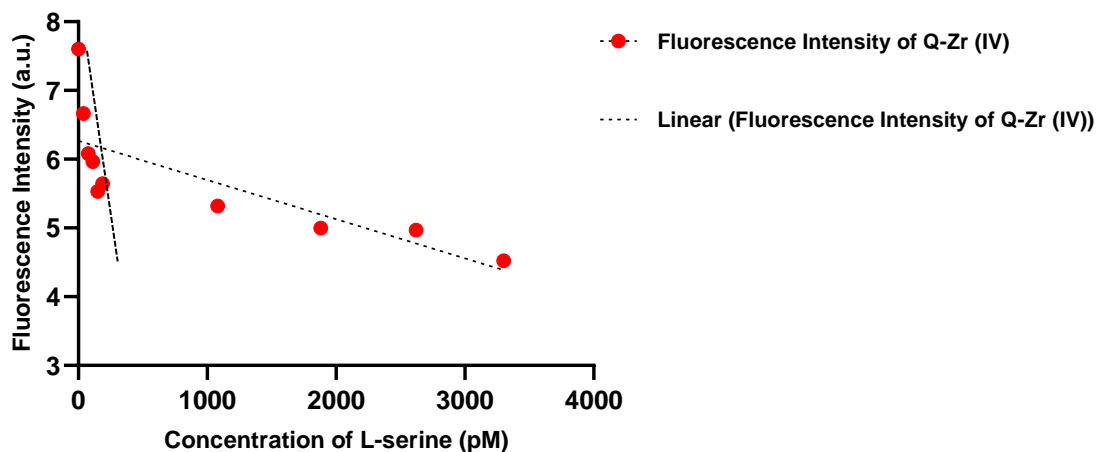
Our quercetin-Zr (IV) (10 μ M, 20 μ M, pH 9) probe was titrated with L-serine (0-3.3 mM) and monitored for fluorescence (λ_{ex} : 465 nm) (**figure 4.32**). The same protocol was performed using O-phospho-L-serine (0-1.9 nM) (**figure 4.33**). A fluorescence quenching effect was observed in the presence of either amino acid titration [1]. In **figure 4.32 (b)**, for the titration of L-serine, using *Equation 4.1*, two binding constants were observed, $K_{b1} = 2.7 \text{ fM}$ and $K_{b2} = 0.23 \text{ fM}$, the same phenomenon was examined in **figure 4.33 (b)**, for the titration of O-phospho-L-serine. O-phospho-L-serine yielded the following binding constants, $K_{b1} = 2.2 \text{ fM}$ and $K_{b2} = 0.2 \text{ fM}$ [94]. Quercetin-Zr (IV) was reported to approach fluorescence quenching saturation with lower concentrations of the amino acid, O-phospho-L-serine.

**L-serine titrations in Quercetin-Zr (IV) (10 μ M, 20 μ M)
in Tris buffer HCl (0.1 M, pH 9)**



(a)

**L-serine titrations in Quercetin-Zr (IV) (10 μ M, 20 μ M)
in Tris buffer HCl (0.1 M, pH 9)**

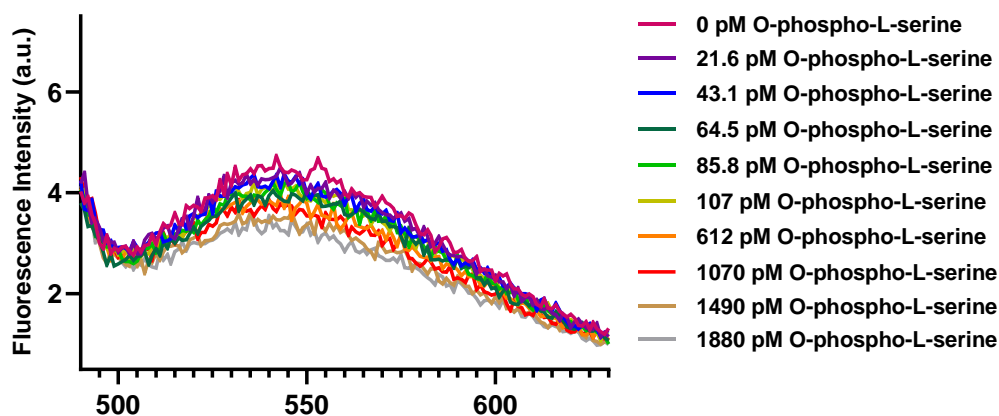


(b)

Figure 4. 32. Fluorescence emission spectra of quercetin-zirconium (IV) (10 μ M, 20 μ M, pH 9) with L-serine titrations.

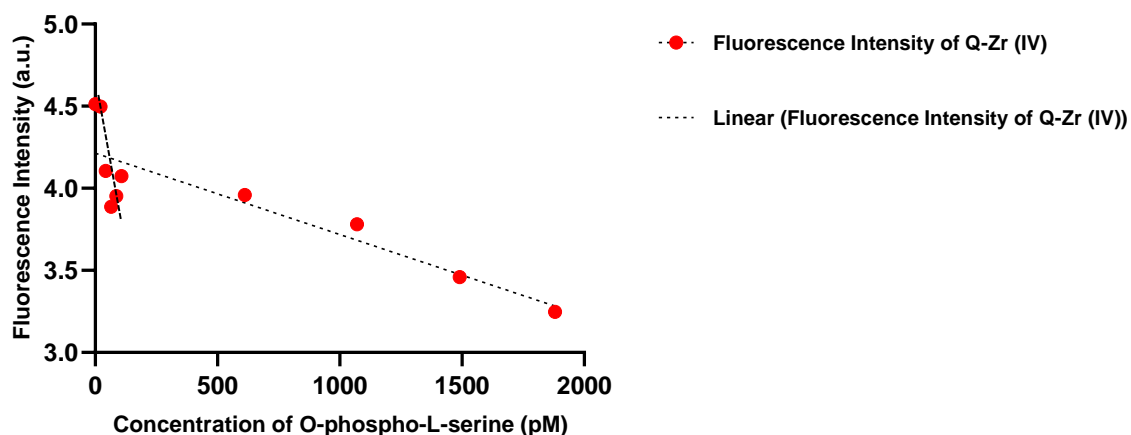
Quercetin-Zr (IV) (10 μ M, 20 μ M, 40% MeOH, 20% 1,2-propanediol) was made in Tris-HCl (40 mM, pH 9) and monitored for fluorescence in a 1 mL cuvette. Further emission spectral studies were conducted with the titration of L-serine amino acid (0-3.3 nM). All samples were excited at 465 nm and had an emission maximum of 545 nm. Titrations were conducted until sample saturation was achieved. b) Standard curve of the fluorescence emission intensities of L-serine amino acid (0-3.3 nM) titrations in quercetin-Zr (IV) (10 μ M, 20 μ M) in Tris-HCl (40 mM, pH 9). $K_{b1} = 2.7$ fM and $K_{b2} = 0.23$ fM.

**O-phospho-L-serine titrations in Quercetin-Zr (IV) (10 μ M, 20 μ M)
in Tris buffer HCl (0.1 M, pH 9)**



(a)

**O-phospho-L-Serine titrations in Quercetin-Zr (IV) (10 μ M, 20 μ M)
in Tris buffer HCl (0.1 M, pH 9)**



(b)

Figure 4. 33. Fluorescence emission spectra of quercetin-zirconium (IV) (10 μ M, 20 μ M, pH 9) with O-phospho-L-serine titrations.

(a) Quercetin-Zr (IV) (10 μ M, 20 μ M, 40% MeOH, 20% 1,2-propanediol) was made in Tris-HCl (40 mM, pH 9) and monitored for fluorescence in a 1 mL cuvette. Further emission spectral studies were conducted with the titration of O-phospho-L-serine amino acid (0-1.9 nM). All samples were excited at 465 nm and had an emission maximum of 545 nm. Titration were conducted until sample saturation was achieved. (b) Standard curve of the fluorescence emission intensities of L-serine amino acid (0-1.9 nM) titrations in quercetin-Zr (IV) (10 μ M, 20 μ M) in Tris-HCl (40 mM, pH 9). $K_{b1} = 2.2$ fM and $K_{b2} = 0.2$ fM.

4.6.2. Monitoring fluorescence signaling of quercetin-Zr (IV) on phospho-proteins

The application of dyes has become quite versatile in research, where probes are prevalent in the development of aqueous and solid-support assay [104, 105]. In the efforts to observe the specificity of quercetin-Zr (IV) to phospho-proteins on a solid support, we dot blotted triplicate samples of non-phosphorylated (BSA, bovine serum albumin) and phosphorylated proteins (including MTMR2, specific for pSer⁵⁸ residues) on nitrocellulose membrane (**figure 4.34**) [106]. Nitrocellulose membrane was dried with the protein samples and incubated in quercetin-Zr (IV) (25 μ M, 50 μ M, 40% MeOH, 20% 1,2-propanediol, 40 mM Tris-HCl, pH 9) for 30 minutes and washed three times with TBST (Tris-HCl saline, 0.5% tween, pH 9) for five minutes, per wash [60, 107, 108]. We observed fluorescence signaling of phosphorylated proteins and no signaling for the non-phosphorylated protein (BSA) (**figure 4.34**).

The integrated densities of each protein sample (dot blot area) was calculated and summarized in **figure 4.35** [93]. The following phosphorylated protein samples were significant to the non-phosphorylated protein sample, BSA; casein (*p-value: 0.0003*), control (empty vector) (*p-value: 0.0002*), WT MTMR2 (*p-value: 0.0010*), control + cali (*p-value: 0.0015*) and WT MTMR2 + cali (*p-value: 0.0036*) [41, 109].

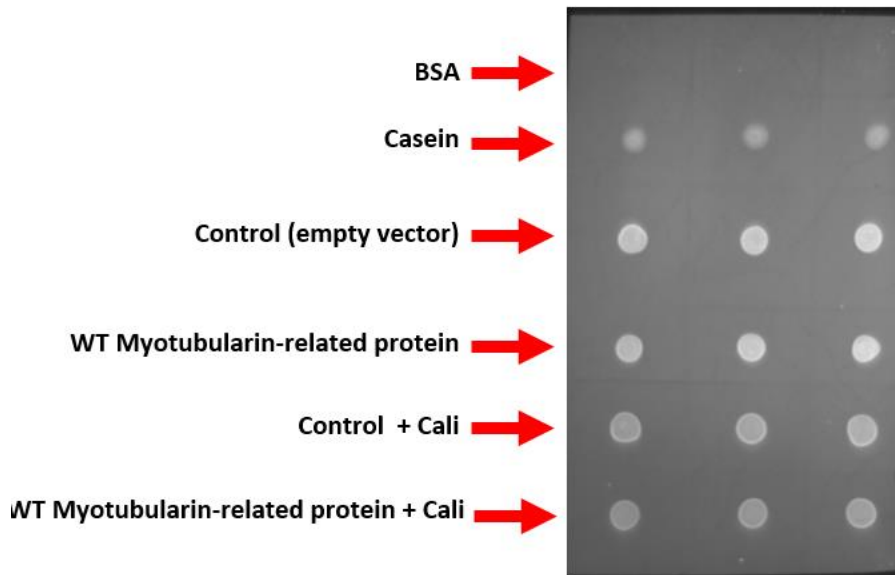


Figure 4. 34. Quercetin-Zr (IV) fluorescently stained nitrocellulose dot blot of protein samples.
 On a nitrocellulose membrane, 1 μL of the following protein samples (top to bottom of figure): bovine serum albumin (1.37 $\mu\text{g}/\mu\text{L}$), casein (0.33 $\mu\text{g}/\mu\text{L}$), control (empty vector) (1.33 $\mu\text{g}/\mu\text{L}$), wild-type myotubularin-related protein (1.47 $\mu\text{g}/\mu\text{L}$), Cali* (Calyculin A) control (1.17 $\mu\text{g}/\mu\text{L}$) and Cali* myotubularin-related protein (1.12 $\mu\text{g}/\mu\text{L}$), were dot blotted in triplicates. The membrane was set to dry and incubated in quercetin-Zr (IV) probe (25 μM , 50 μM , 40% MeOH, 20% 1,2-propanediol, 44 mM Tris-HCl (pH 9)) for 30 minutes. Following the stain, the membrane was wash three times in TBST (Tris-HCl saline, 0.5% tween, pH 9) for five minutes per wash. The membrane was imaged using excitation cy2 and emission cy3 settings on the FluoroChem® Q quantitative imaging system (Alpha Innotech).

Fluorescent Protein Detection using Quercetin-Zr (IV) on Nitrocellulose Membrane

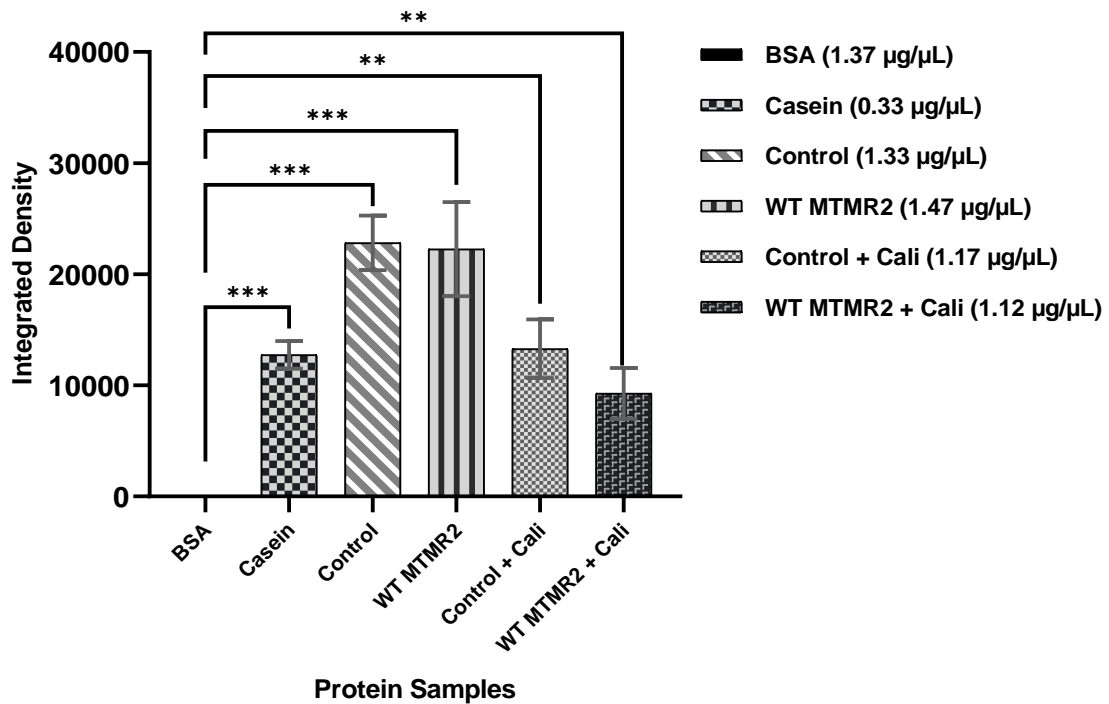


Figure 4. 35. Integrated density of fluorescently stained quercetin-Zr(IV) stained nitrocellulose dot blot of protein samples.

The following proteins samples had been dot blotted (1 μL) on nitrocellulose membrane, bovine serum albumin (1.37 $\mu\text{g}/\mu\text{L}$), casein (0.33 $\mu\text{g}/\mu\text{L}$), control (empty vector) (1.33 $\mu\text{g}/\mu\text{L}$), wild-type myotubular-related protein (1.47 $\mu\text{g}/\mu\text{L}$), Cali* control (1.17 $\mu\text{g}/\mu\text{L}$) and Cali* myotubular-related protein (1.12 $\mu\text{g}/\mu\text{L}$). Fluorescent signalling was apparent for all protein samples aside from bovine serum albumin. The membrane was set to dry and incubated in quercetin-Zr (IV) probe (25 μM , 50 μM , 40% MeOH, 20% 1,2-propanediol, 44 mM Tris-HCl (pH 9)) for 30 minutes. Following the stain, the membrane was wash three times in TBST (Tris-HCl saline, 0.5% tween, pH 9) for five minutes per wash. The membrane was imaged using excitation cy2 and emission cy3 settings on the FluoroChem® Q quantitative imaging system (Alpha Innotech). Using ImageJ the recorded integrated densities were used to compare fluorescent properties of each protein sample[93]. P-values were calculated using an unpaired t-test. The error bars represent SEM, n = 3.

4.6.2.1. Monitoring fluorescence signaling of quercetin-Zr (IV) on alkaline phosphatase treated phospho-proteins

Following the fluorescence signaling detected for immobilized phospho-proteins on nitrocellulose membrane using quercetin-Zr (IV) as a staining probe, fresh protein samples had undergone an alkaline phosphatase (APP) treatment [67]. The ability of alkaline phosphatase to catalyze hydrolysis reactions of mono-ester phosphate was used to detect changes in fluorescence signaling of treated phospho-proteins [67].

All protein samples (non-phosphorylated and phosphorylated) were normalized (0.5 $\mu\text{g}/\mu\text{L}$) and aliquoted (1 μL) onto nitrocellulose membrane (**figure 4.36**) [107]. Protein samples without APP treatment (in triplicates, left side, **figure 4.36**) and APP treated protein samples (in triplicates, right side, **figure 4.36**) were reported to have fluorescence signaling. These results can be attributed to the lack of phospho-protein specificity of the quercetin-Zr (IV) probe. No visual fluorescence signaling was detected for the non-phosphorylated protein, BSA, without and with APP treatment, however integrated densities did yield significant differences (**figure 4.36**).

Future work could involve a sample protein/APP separation step, because the alkaline phosphatase used consisted of phospho-amino acid residues (**appendix B: figure B.1**) [109]. This would explain the reported fluorescence integrated densities of the APP treated BSA protein sample.

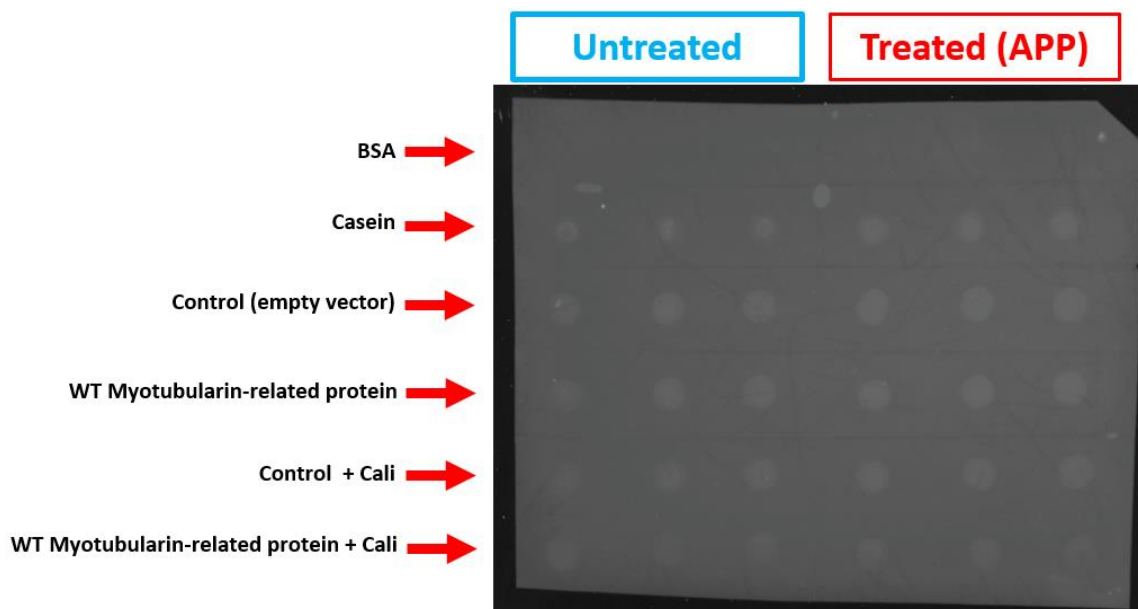


Figure 4. 36. Quercetin-Zr (IV) fluorescently stained nitrocellulose membrane dot blot of alkaline phosphatase treated protein samples.

From top to bottom, the following protein samples were normalized to have a final concentration of 0.5 $\mu\text{g}/\mu\text{L}$: bovine serum albumin, casein, control (empty vector), wild-type myotubularin-related protein, Cali* control and Cali* myotubularin-related protein. Untreated protein samples (triplicates on the left side of the membrane) and treated protein samples (triplicates on the right side of the membrane) were dot blotted (1 μL) on the nitrocellulose membrane. The membrane was set to dry and incubated in quercetin-Zr (IV) probe (25 μM , 50 μM , 40% MeOH, 20% 1,2-propanediol, 44 mM Tris-HCl (pH 9)) for 30 minutes. Following the stain, the membrane was washed three times in TBST (Tris-HCl saline, 0.5% tween, pH 9) for five minutes per wash. The membrane was imaged using excitation cy2 and emission cy3 settings on the FluoroChem® Q quantitative imaging system (Alpha Innotech).

Fluorescence Protein Detection using Q-Zr (IV) Probe on Alkaline Phosphatase Treated Samples on Nitrocellulose Membrane

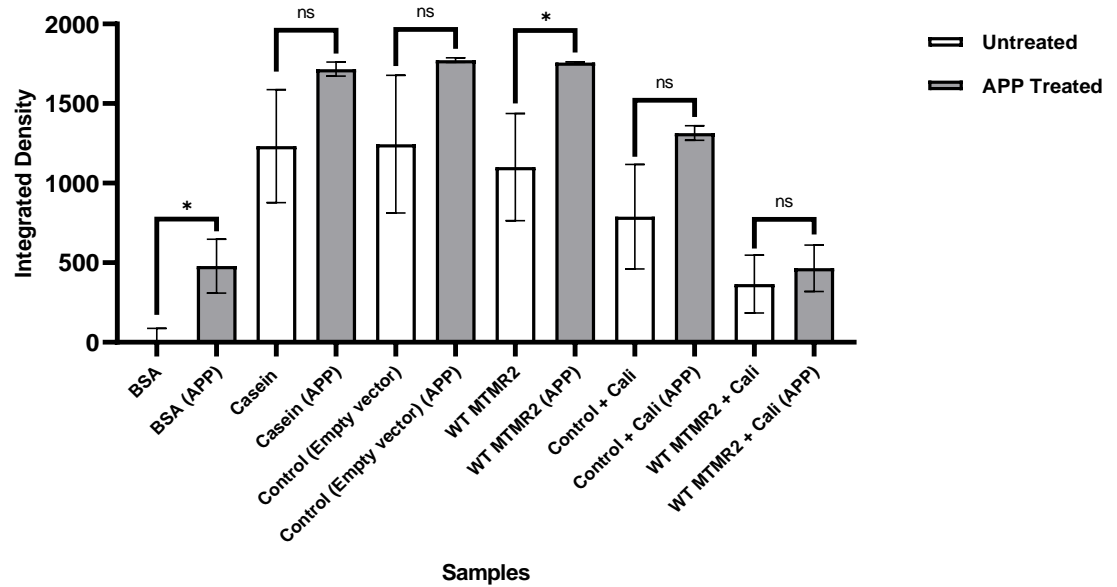


Figure 4. 37. Integrated density of fluorescently stained quercetin-Zr(IV) stained nitrocellulose dot blot of alkaline phosphatase treated protein samples.

Untreated and alkaline phosphatase treated samples of the following proteins had been dot blotted (1 μ L, 0.5 μ g/ μ L) on nitrocellulose membrane: bovine serum albumin, casein, control (empty vector), wild-type myotubular-related protein, Cali* control and Cali* myotubular-related protein. The membrane was set to dry and incubated in quercetin-Zr (IV) probe (25 μ M, 50 μ M, 40% MeOH, 20% 1,2-propanediol, 44 mM Tris-HCl (pH 9)) for 30 minutes. Following the stain, the membrane was wash three times in TBST (Tris-HCl saline, 0.5% tween, pH 9) for five minutes per wash. The membrane was imaged using excitation cy2 and emission cy3 settings on the FluoroChem® Q quantitative imaging system (Alpha Innotech). Using ImageJ the recorded integrated densities were used to compare fluorescent properties of each protein sample[93]. P-values were calculated using a unpaired t-test. The error bars represent SEM, n = 3.

4.7. *o*-amino-benzoyl labelled amino acids for the use of a phosphatase assay

4.7.1. The analytical determination of OAb-L-serine and OAb-phospho-L-serine using ¹HNMR

Isatoic anhydride (IA) is a molecule that can prepare quinazoline and quinazoline derivatives by reacting with nitrogen nucleophiles, yielding *o*-aminobenzoyl (OAb) derivatives, which can form fluorescent protein conjugates [69–71, 110]. We hypothesized that the incubation of amino acids, L-serine (S) or O-phospho-L-serine (PS), could form OAb-S and OAb-PS (**figure 4.38**) [70, 71]. These samples would then yield unique and significant fluorescence emission properties which could further be used to optimize a fluorescence phosphatase assay, thus developing a simple and rapid assessment of non-phosphorylated and phosphorylated peptides/proteins [72].

We began with incubating L-serine or O-phospho-L-serine (720 mM) with isatoic anhydride (180 mM, pH 9, 25°C, 48 hours) [72]. Samples were applied onto Sephadex-QAE columns, washed thoroughly (100 mL MilliQ) and eluted with NaCl (0.5 M). 4.2 mM of IA, OAb-S or OAb-PS made in Tris-HCl (0.1 M, pH) were compared using ¹HNMR to rectify the success of each amino acid synthesis to the *o*-amino-benzoyl derivative [72]. The successful synthesis of OAb-S and OAb-PS was supported by the methanediyl group (-CH₂) chemical shifts for L-serine (**3.9 ppm**) and O-phospho-L-serine (**~4.1 ppm**) (**figure 4.39**) and by the presence of aromatic proton resonances (**figure 4.40**) [100].

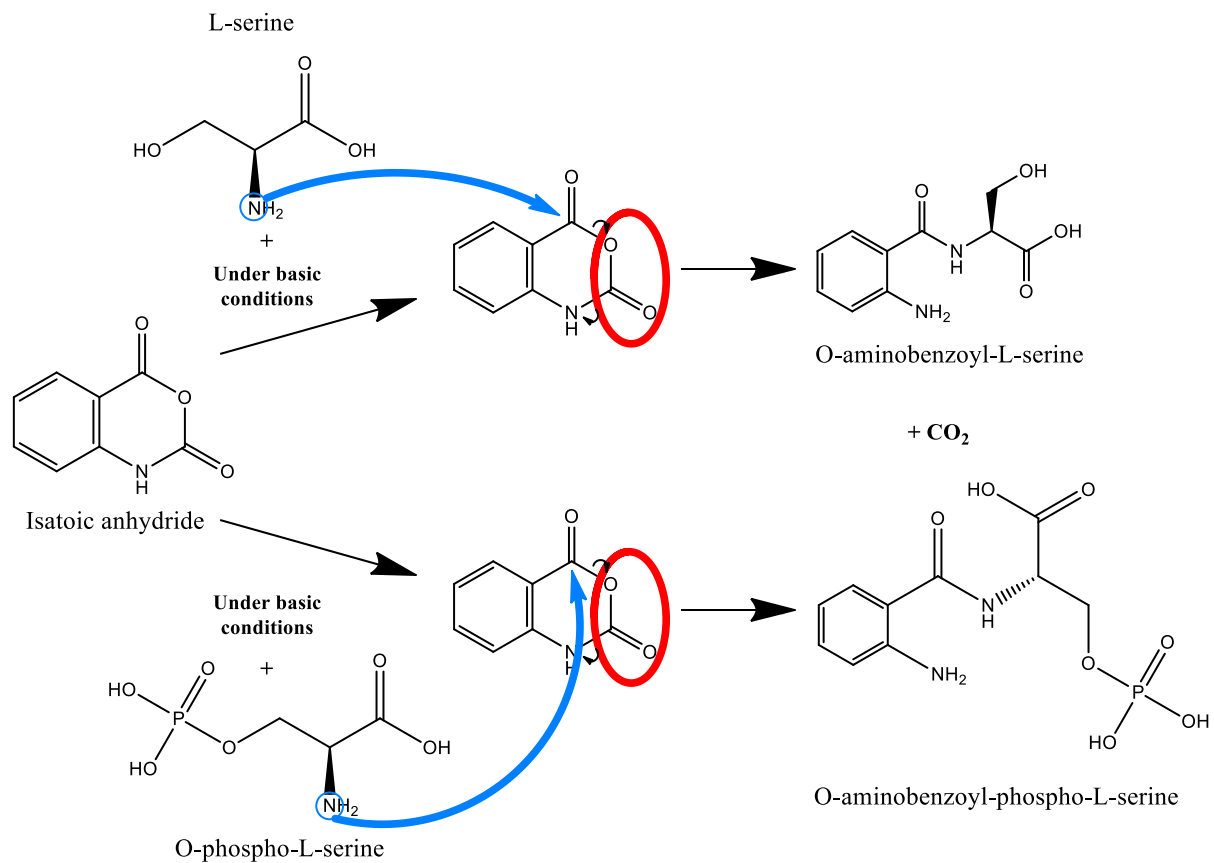


Figure 4. 38. Isatoic anhydride reaction scheme with L-serine or O-phospho-L-serine.

Isatoic anhydride under basic conditions forms a fluorescent amino acid conjugate. The quinazoline derivative, o-aminobenzoyl, reacts by a nucleophilic attack by the nitrogen atom on the α -carbon of the L-serine or O-phospho-L-serine.

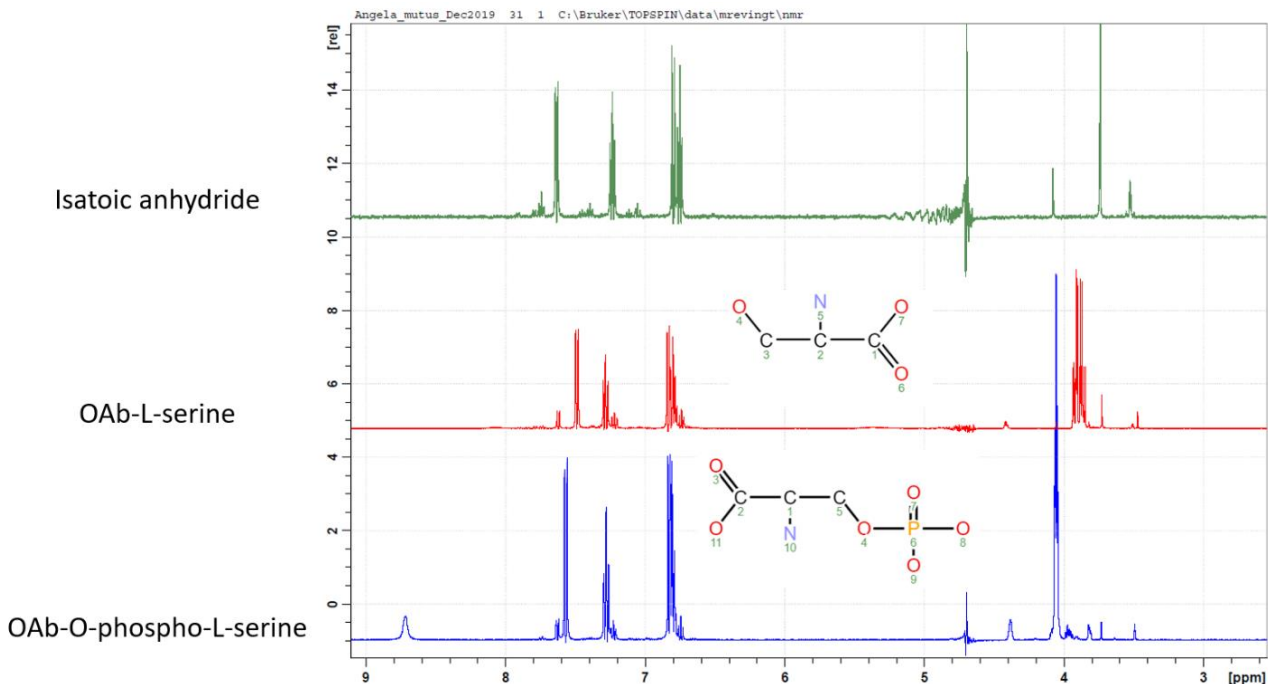


Figure 4. 39. ^1H NMR spectra of isatoic anhydride, OAb-L-serine and OAb-O-phospho-L-serine.

Samples of isatoic anhydride, OAb-L-serine and OAb-O-phospho-L-serine, were dissolved and/or synthesized in Tris-HCl (0.5 M, pH 9). Samples were subject to a Sephadex QAE column and eluted (0.5M NaCl in MilliQ) before being diluted in a Tris-HCl (0.1M, pH 9) using 1:9 dilution factor of neat sample to solvent. 600 μL of isatoic anhydride, OAb-L-serine or OAb-O-phospho-L-serine were analyzed using ^1H NMR. Samples of synthesized OAb- L-serine- displays serine chemical shifts (~ 3.9 ppm) and synthesized OAb-O-phospho-L-serine show evidence of phospho-serine chemical shifts (~ 4.1 ppm).

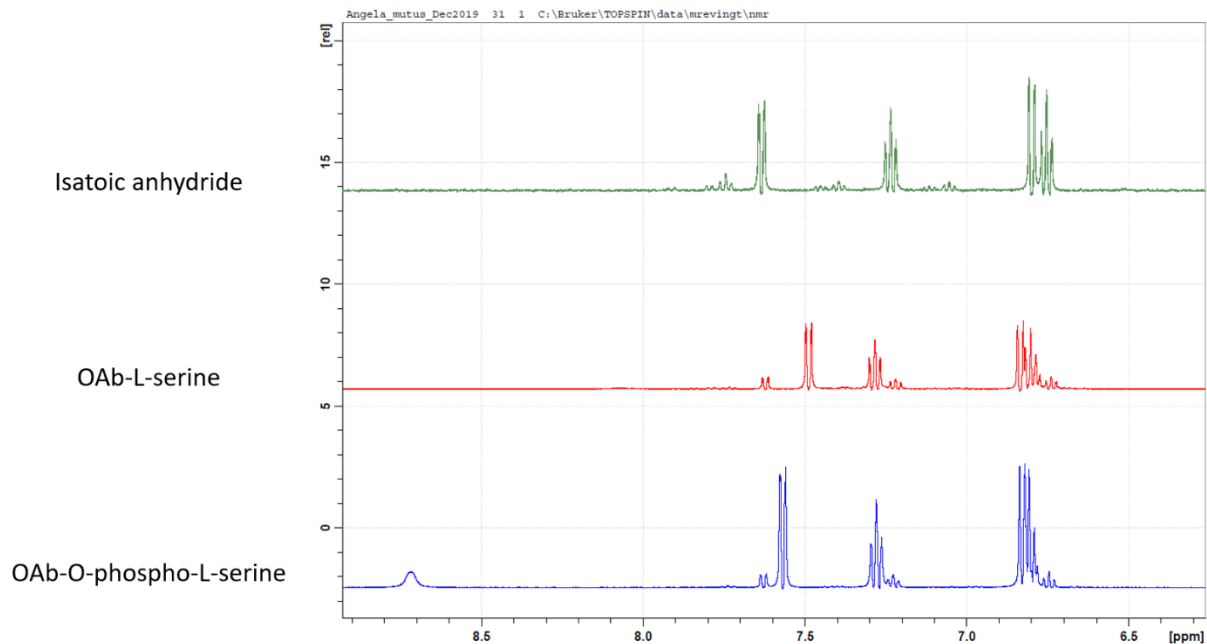


Figure 4. 40. ^1H NMR spectra of the aromatic regions of isatoic anhydride, OAb-L-serine and O-phospho-L-serine.

Samples of isatoic anhydride, OAb-L-serine and OAb-O-phospho-L-serine, were dissolved and/or synthesized in Tris-HCl (0.5 M, pH 9). Samples were subject to a Sephadex QAE column and eluted (0.5M NaCl in MilliQ) before being diluted in a Tris-HCl (0.1M, pH 9) using 1:9 dilution factor of neat sample to solvent. 600 μL of isatoic anhydride, OAb-L-serine or OAb-O-phospho-L-serine were analyzed using ^1H NMR.

4.7.2. *The normalization and fluorescence emission properties studies of OAb-S and OAb-PS*

Next, OAb-S or OAb-PS in Tris-HCl (0.1 M, pH 9) were normalized (**Abs: 0.39**, $\lambda_{\text{max}} = 312 \text{ nm}$, $\epsilon_{\text{M}} = 2800 \text{ M}^{-1} \text{ cm}^{-1}$) using UV-vis (**figure 4.41**) [72]. Samples (**153.57 μM**) were excited at 320 nm and monitored for fluorescence (**figure 4.42 (a)**).

Fluorescence emission maximums (**410 nm**) were observed at **17.6** and **22 a.u.** for OAb-S and OAb-PS, respectively. A significant difference in fluorescence properties was reported (*p-value* <0.0001) (**figure 4.42. (b)**) and a 1.25-fold change was observed.

Absorbance Spectra of the Normalization of Synthesized OAb-S/-PS in Tris buffer (0.1 M, pH 7)

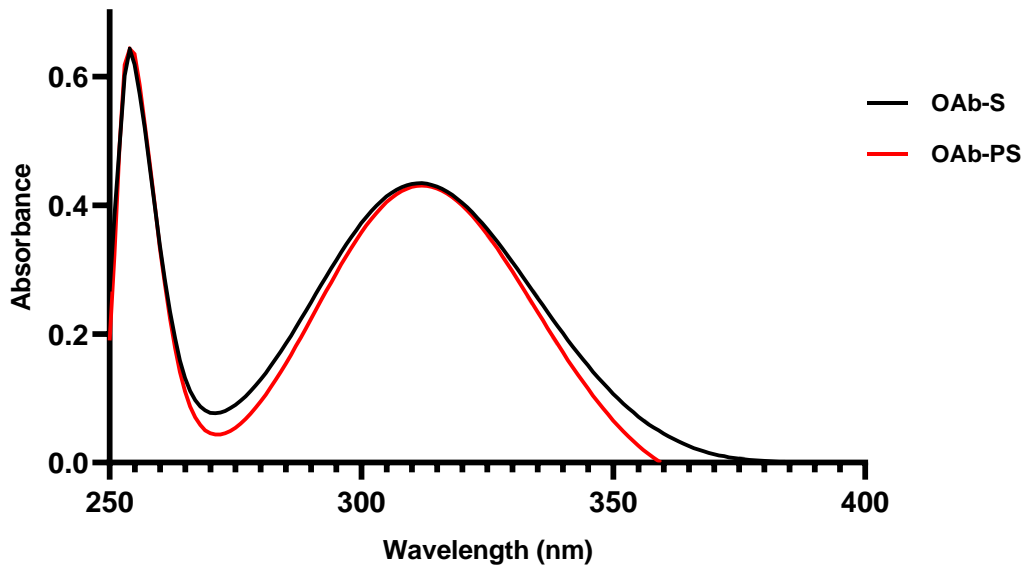
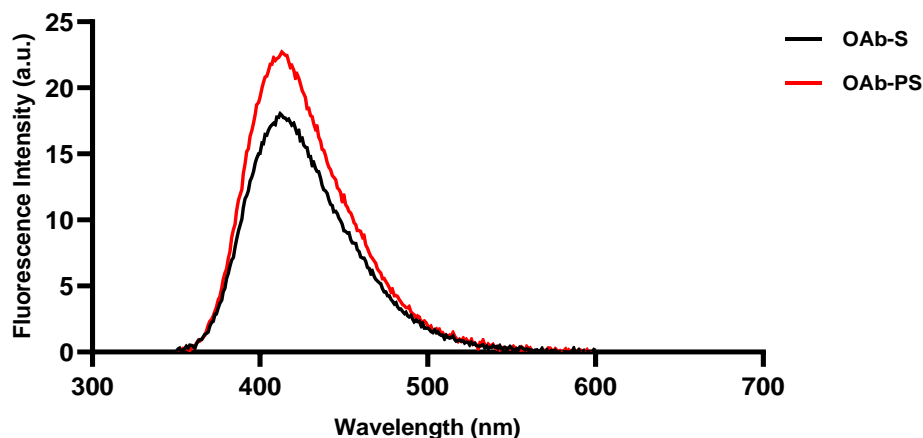


Figure 4. 41. UV/vis spectra of the normalization of OAb-L-serine and OAb-O-phospho-L-serine.

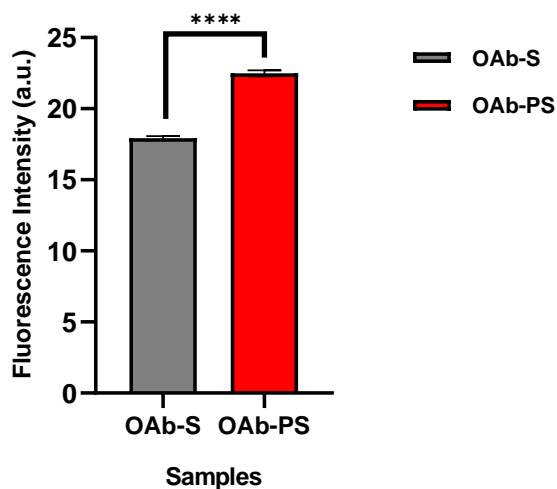
Samples of OAb-L-serine and OAb-O-phospho-L-serine were dissolved and/or synthesized in Tris-HCl (0.5 M, pH 9). Samples were subject to a Sephadex QAE column and eluted (0.5M NaCl in MilliQ) before 10 μ L of each sample was diluted in 290 μ L of Tris-HCl (0.1M, pH 9) using 1:29 dilution factor of neat sample to solvent. The samples were then monitored for absorbance using UV-vis spectroscopy. OAb-L-serine (OAb-S) was normalized to an absorbance value of 0.431 and O-phospho-L-serine (OAb-PS), 0.434. Samples were observed to have absorption values of 312 nm, $n = 3$.

Emission Spectra of Normalized OAb-S/-PS in Tris buffer (0.1 M, pH 7)



(a)

Emission Properties of Normalized OAb-S/-PS in Tris buffer (0.1 M, pH 7)



(b)

Figure 4. 42. Fluorescent emission spectra of normalized OAb-L-serine and OAb-O-phospho-L-serine.

(a) Normalized samples (Abs: 0.43, 153.57 μ M) of OAb-L-serine (OAb-S) and OAb-O-phospho-L-serine (OAb-PS) were immediately monitored for fluorescence. Samples were excited at 320 nm and an emission maximum was observed 410 nm. OAb-L-serine and OAb-O-phospho-L-serine had fluorescent intensities of 17.6 and 22 a.u., respectively. (b) Emission properties of OAb-S and OAb-PS had a p -value < 0.0001 . P -values were calculated using a unpaired t -test. The error bars represent SEM, $n = 3$.

4.7.3. Survey of fluorescence zirconium (IV) precipitation assay using OAb-S and OAb-PS

The fluorescence of OAb-S (153.57 μ M) and OAb-PS (153.57 μ M) yielded a 1.25-fold change when monitored in aqueous solutions. In the effort to increase fluorescence intensity differences of these samples, zirconium (IV) chloride (5-25 mM) in Tris-HCl (0.1 M, pH 9) was aliquoted (in triplicates) in a clear 96-well plate and incubated in OAb-S or OAb-PS (75 μ M) (**figure 4.43**) [111].

We hypothesized that the phospho-group on the OAb-PS amino acid conjugate would demonstrate a higher affinity for the precipitated zirconium (IV) chloride than OAb-S, thus, yielding higher fluorescence intensity fold changes [111–113]. Our results supported increasing fluorescence intensities for OAb-PS in the presence of zirconium (IV) chloride (5-25 mM), evidently inducing higher fold changes (**figure 4.44**). The following p-values and fold-changes were calculated at varying concentrations of $ZrCl_4$: 5 mM (**p-value: 0.0002, 1.32-fold change**) (**figure 4.44. (b)**), 10 mM (**p-value: 0.0022, 1.66-fold change**) (**figure 44.4. (d)**), 15 mM (**p-value: 0.0001, 1.922-fold change**) (**figure 4.44. (f)**), 20 mM (**p-value: 0.0001, 1.97-fold change**) (**figure 44. (h)**) and 25 mM (**p-value: 0.0009, 1.78-fold change**) (**figure 4.44. (j)**).

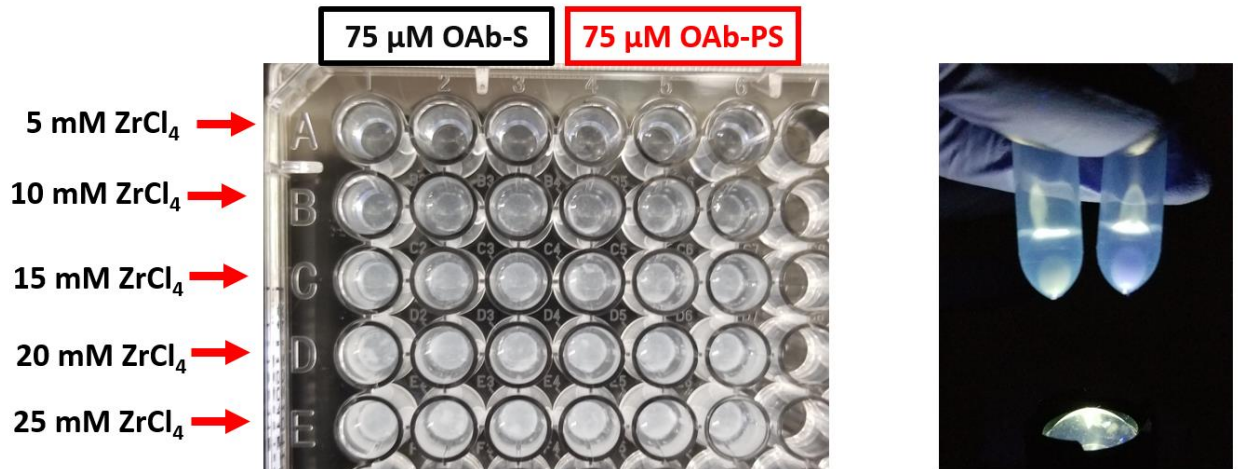
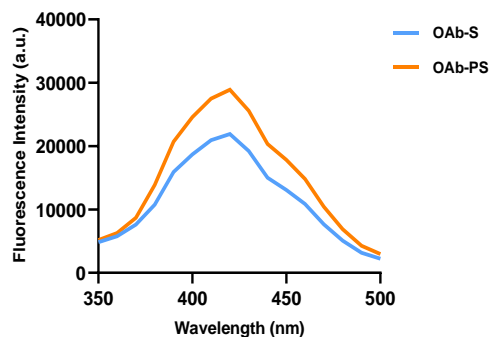


Figure 4. 43. $ZrCl_4$ precipitation assay of OAb-L-serine and OAb-O-phospho-L-serine.

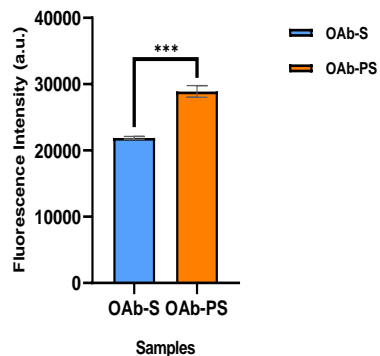
In a 96-well plate, samples of $ZrCl_4$ (5-25 mM) in Tris-HCl (0.1 M, pH 9) were made (in triplicates, A-E). Each well contained OAb-S and OAb-PS (75 μ M). Increasing concentrations of $ZrCl_4$ in pH 9 correlated to higher yields of precipitate. Samples were excited at 320 nm and monitored for fluorescence. The right image shows the survey of OAb-S (left microcentrifuge tube) and OAb-PS (right microcentrifuge tube) in Tris-HCl (0.1 M, pH 9) with precipitated zirconium (IV) chloride under fluorescent lamp.

Emission Spectra of OAb-S/-PS using $ZrCl_4$ (5 mM)
Precipitation Assay



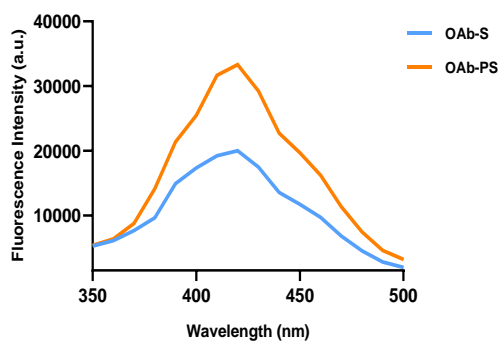
(a)

Fluorescence Comparison of OAb-S/-PS using $ZrCl_4$ (5 mM)
Precipitation Assay



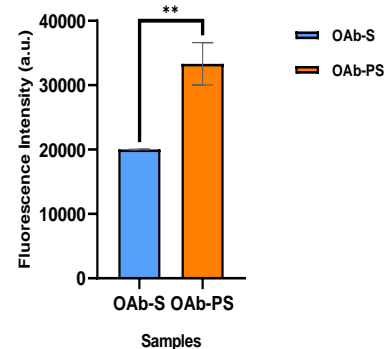
(b)

Emission Spectra of OAb-S/-PS using $ZrCl_4$ (10 mM)
Precipitation Assay



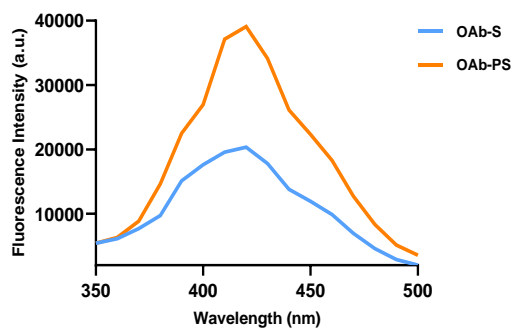
(c)

Fluorescence Comparison of OAb-S/-PS using $ZrCl_4$ (10 mM)
Precipitation Assay



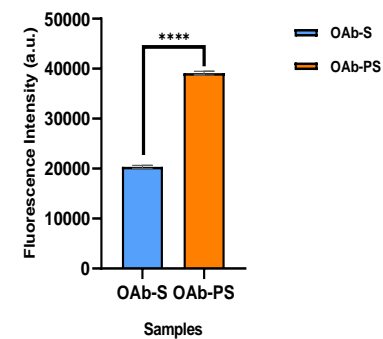
(d)

Emission Spectra of OAb-S/-PS using $ZrCl_4$ (15 mM)
Precipitation Assay



(e)

Fluorescence Comparison of OAb-S/-PS using $ZrCl_4$ (15 mM)
Precipitation Assay



(f)

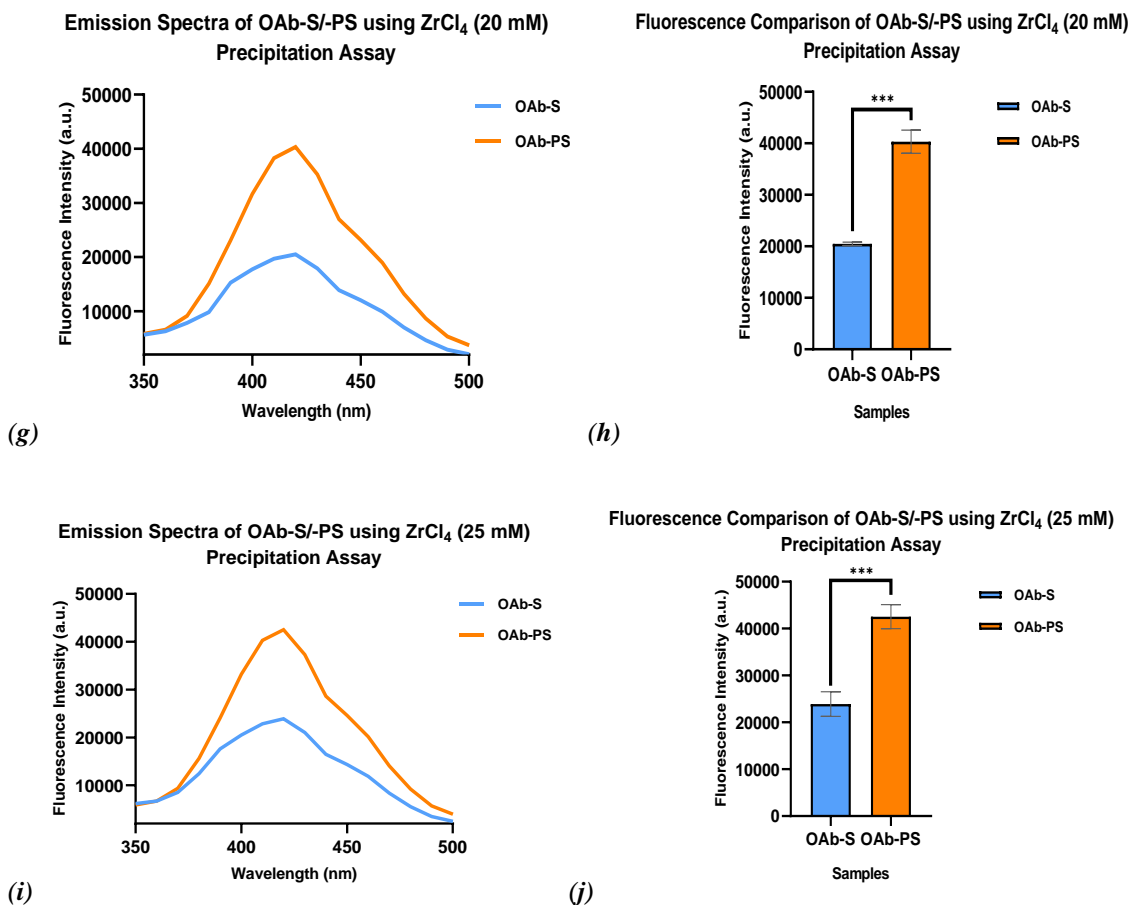


Figure 4.44. Emission properties of precipitation assay of ZrCl₄ with OAb-S and OAb-PS.

Samples of ZrCl₄ (5-25 mM) in a clear 96-well plate with triplicated samples of OAb-S and OAb-PS (75 μM) in Tris-HCl (0.1 M, pH 9) were excited for at 320 nm and monitored for fluorescence. (a) The emission spectra of samples of OAb-S and OAb-PS treated with 5 mM ZrCl₄. (b) The fluorescence emission properties of OAb-S and OAb-PS with 5 mM ZrCl₄ at 420 nm. Samples have p-values of 0.0002. (c) The emission spectra of samples of OAb-S and OAb-PS treated with 10 mM ZrCl₄. (d) The fluorescence emission properties of OAb-S and OAb-PS with 10 mM ZrCl₄ at 420 nm. Samples have p-values of 0.0022. (e) The emission spectra of samples of OAb-S and OAb-PS treated with 5 mM ZrCl₄. (f) The fluorescence emission properties of OAb-S and OAb-PS with 15 mM ZrCl₄ at 420 nm. Samples have p-values of 0.0001. (g) The emission spectra of samples of OAb-S and OAb-PS treated with 20 mM ZrCl₄. (h) The fluorescence emission properties of OAb-S and OAb-PS with 20 mM ZrCl₄ at 420 nm. Samples have p-values of 0.0001. (i) The emission spectra of samples of OAb-S and OAb-PS treated with 25 mM ZrCl₄. (j) The fluorescence emission properties of OAb-S and OAb-PS with 25 mM ZrCl₄ at 420 nm. Samples have p-values of 0.0009. P-values were calculated using an unpaired t-test. The error bars represent SEM, n = 3.

4.7.4. Fluorescence emission properties of OAb-S/-PS using lanthanides and transition metals for an aqueous phosphatase assay

Previously shown, the $ZrCl_4$ precipitation assay yielded greater fluorescence intensity differences of OAb-S and OAb-PS with an increased fold change by 0.72 (**figure 4.42. (b) & figure 4.44. (h)**). This method was conducted based on the documented and observed studies of zirconium (IV) exhibiting an affinity for phosphate, which has also been extended to lanthanide species [97, 112].

We hypothesized that an aqueous phosphatase assay could be developed by titrating OAb-S and OAb-PS to enhance the fluorescence intensity differences and fold changes. Changes would be observed based on the interactions of the metal species and phospho-group on OAb-PS [114, 115].

OAb-S/-PS (2.8 μ M) were titrated with equal concentrations of europium (III) chloride in Tris-HCl (0.1 M, pH 4, 7 or 9). Titrations were conducted until a fluorescence intensity saturation was observed. In the presence of europium (III), significant fluorescence quenching effects were reported for OAb-PS (*p-value* < 0.0001) (**figures 4.46-48**). The highest fold change of 2.4 was observed in pH 4.

Although, fluorescence quenching assays are less favourable due to possible contaminant interferences, these results do support a significant interaction between europium (III) and the *o*-aminobenzoyl phospho-amino acid conjugate. These studies could be further utilized in the development of an aqueous phosphatase assay.

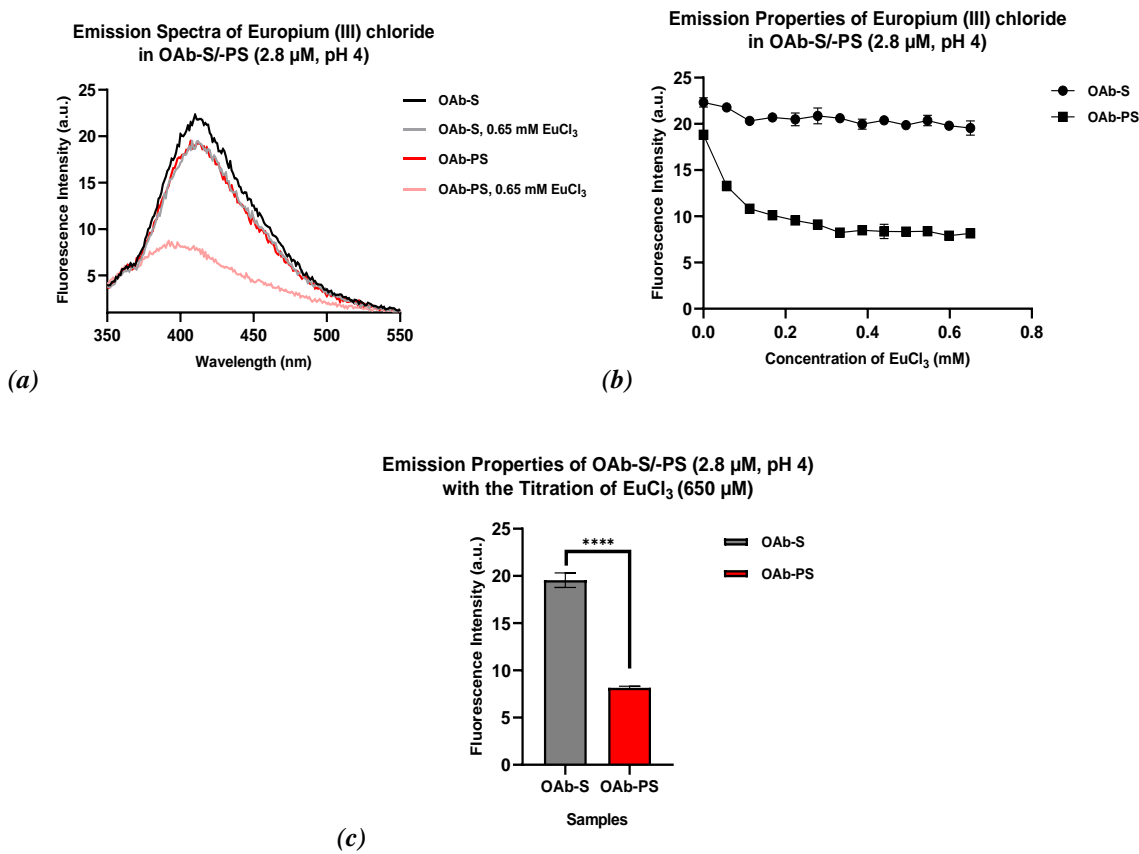


Figure 4. 45: Aqueous assay of OAb-S/-PS with the titration of europium (III) chloride (650 μ M, pH 4).

In a 1 mL cuvette OAb-S/-PS (2.8 μ M) in a Tris-HCl (0.1 M, pH 4) solvent was titrated with europium (III) chloride. (a) The emission spectral properties of OAb-S/-PS (2.8 μ M, pH 4) are shown with europium (III) chloride at 0 μ M and 650 μ M. (b) The fluorescence emission maximums of OAb-S/-PS (2.8 μ M, pH 4) titrated with europium (III) chloride (0 – 650 μ M). (c) A comparison of OAb-S and OAb-PS emission maximums at 410 nm with europium (III) chloride (650 μ M). The p -values for OAb-S and OAb-PS are <0.0001 . All samples were excited at 320 nm. P -values were calculated using a unpaired t -test. The error bars represent SEM, $n = 3$.

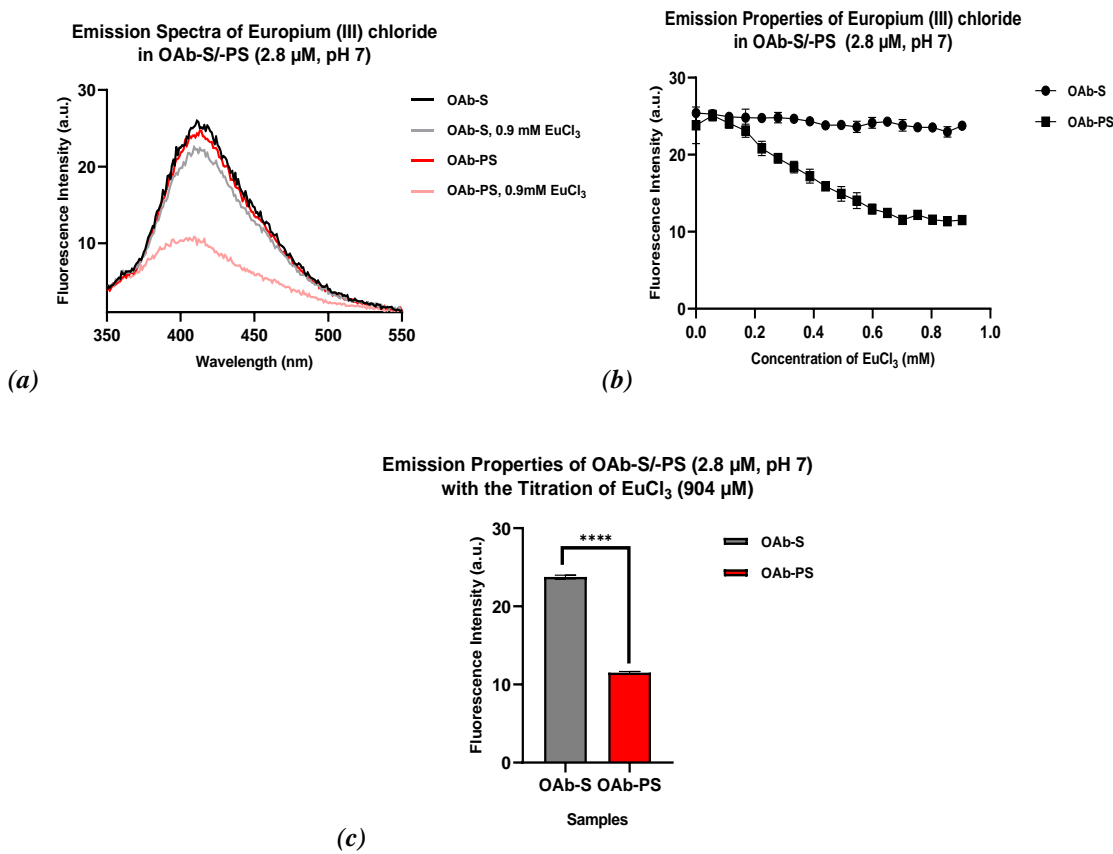


Figure 4. 46: Aqueous assay of OAb-S/-PS with the titration of europium (III) chloride (904 μ M, pH 7).

In a 1 mL cuvette OAb-S/-PS (2.8 μ M) in a Tris-HCl (0.1 M, pH 7) solvent was titrated with europium (III) chloride. (a) The emission spectral properties of OAb-S/-PS (2.8 μ M, pH 7) are shown with europium (III) chloride at 0 μ M and 904 μ M. (b) The fluorescence emission maximums of OAb-S/-PS (2.8 μ M, pH 7) titrated with europium (III) chloride (0 – 904 μ M). (c) A comparison of OAb-S and OAb-PS emission maximums at 410 nm with europium (III) chloride (904 μ M). The p -values for OAb-S and OAb-PS are <0.0001 . All samples were excited at 320 nm. P -values were calculated using a unpaired t -test. The error bars represent SEM, $n = 3$.

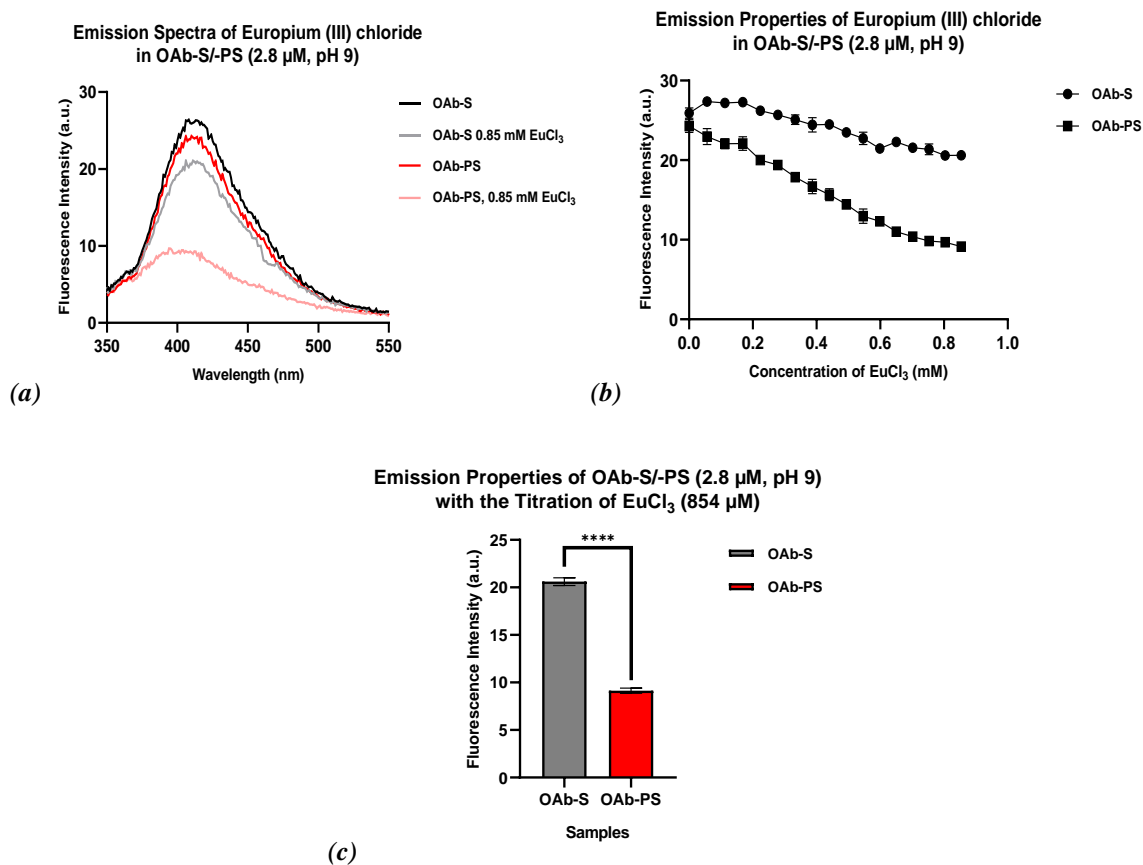


Figure 4. 47. Aqueous assay of OAb-S/-PS with the titration of europium (III) chloride (854 μM, pH 9).

In a 1 mL cuvette OAb-S/-PS (2.8 μM) in a Tris-HCl (0.1 M, pH 9) solvent was titrated with europium (III) chloride. (a) The emission spectral properties of OAb-S/-PS (2.8 μM, pH 9) are shown with europium (III) chloride at 0 μM and 854 μM. (b) The fluorescence emission maximums of OAb-S/-PS (2.8 μM, pH 9) titrated with europium (III) chloride (0 – 854 μM). (c) A comparison of OAb-S and OAb-PS emission maximums at 410 nm with europium (III) chloride (854 μM). The *p*-values for OAb-S and OAb-PS are <0.0001. All samples were excited at 320 nm. *P*-values were calculated using a unpaired *t*-test. The error bars represent SEM, *n* = 3.

4.8. Results summary

In the method development of a fluorescence inorganic phosphate assay, propidium iodide (PI), quinacrine mustard dihydrochloride (QM) and quercetin-metal complexes were used to survey fluorescence properties in the presence of P_i . Our P_i concentration detection range of interest was 0.1 to 10 μ M. Propidium iodide and quinacrine mustard dihydrochloride were found to have fluorescence quenching effects or slight intensity increases in the P_i concentrations outside our range of interest, respectively. The complexation of LH-20-QM was titrated with P_i concentrations (0.5 – 1.2 mM) and an aqueous fluorescence increase was observed. A novel method successfully synthesized solid supports of cellulose-phosphate to immobilize cationic fluorophores for sensor development. Quercetin-metal complexations with Al (III) or Zr (IV) demonstrated fluorescence quenching or enhancing effects, respectively, where quercetin-Al (III) detected P_i concentrations of 0.1-1 mM in an aqueous quenching system and the precipitation of quercetin-Zr (IV) in the presence of P_i detected increases in fluorescence detection. The quercetin-Zr (IV) probe, to the best of our knowledge, has the highest reported quercetin-metal binding affinity. Using ^1H NMR, the postulated metal binding site of zirconium (IV) on quercetin was proposed. Following these studies quercetin-Zr (IV) was explored for the potential detection of biomolecules containing phospho-groups.

Quercetin-Zr (IV) was titrated with L-serine or O-phospho-L-serine in aqueous systems of Tris-HCl (40 μ M, pH 9), this demonstrated fluorescence quenching effects in the presence of either amino acid residue. Higher binding affinities were observed as suggested by lower K_b constants for the phosphorylated amino acid residue, which led to the investigation of quercetin-Zr (IV) as a fluorescence stain for phosphorylated proteins.

Nitrocellulose membranes containing immobilized phosphorylated proteins were stained with our quercetin-Zr (IV) probe, where phosphorylated protein displayed fluorescence signaling. An alkaline phosphatase treatment was conducted on non-phosphorylated and phosphorylated proteins, both untreated and treated samples were detected for fluorescence with increased signaling for the treated samples. No fluorescence detection was monitored for the untreated non-phosphorylated protein, BSA.

Finally, an investigation for an aqueous phosphatase assay utilizing OAb conjugates of OAb-L-serine and OAb-phospho-L-serine were successfully synthesized and monitored for fluorescence. An increased fluorescence difference between the conjugated amino acid probes was observed in the presence of europium (III) in aqueous systems of pH 4, 7 and 9. Further optimization of these techniques will allow for manufacturing of sensitive and robust phosphate sensors.

CHAPTER 5

DISCUSSION

5. The investigation of an inorganic phosphate sensor

In the last 60 years, high phosphate levels have caused oxygen depletion and subsequent aquatic life toxicity in bodies of fresh water, supporting the spread and growth of algae [17, 116]. The development of cost-effective methods to monitor inorganic phosphate (P_i) concentrations would be an imperative tool assisting in wastewater treatment [46]. According to the Ontario Provincial Water Quality Objectives, systems capable of detecting 0.1-10 μM of P_i could serve as an early warning allowing prevention of harmful algal blooms, preserving water quality [28]. In attempts of developing a precise and sensitive P_i sensor, fluorescent dyes were used, taking advantage of the biochemical characteristics inherent to inorganic phosphate.

P_i possesses three potential anionic sites when fully deprotonated (**figure 1.8**), propelling the investigation of cationic fluorescence probes which would electrostatically interact with the anionic P_i [117]. The general workflow for the method development of this sensor involved binding cationic fluorescent dye to a solid support. The fluorescent probe would remain bound to the solid support until exchanged by P_i . Using this system, titrations of P_i would result in an enhanced fluorescence signal that would be produced in an aqueous medium proportional to P_i concentrations.

The survey of cationic probes began by monitoring the fluorescence emission properties of propidium iodide (PI), quinacrine mustard dihydrochloride hydrate (QM) and quercetin-metal (Q) all in the presence of P_i [37, 41, 42, 118]. These probes have previously been shown to bind phosphate, making them suitable candidates for the study. We monitored the fluorescence of each probe with P_i in aqueous solutions, desiring probes displaying a fluorescence increase within P_i concentrations of 0.1-10 μM [18, 40, 41]. Polar

probes, PI and QM did not detect P_i within this range, however, using QM, fluorescence was increased in the presence of P_i in increasing polar solvents, which have shown to increase dipole moments, thus enhancing probe sensitivity (**figure 4.1-2**) [1]. From all quercetin-metal complexes surveyed, quercetin-Al (III) and quercetin-Zr (IV) were suitable for P_i detection within our concentration range of interest (**figure 4.17**). We utilized QM and quercetin-Al for further assay development.

As a fluorescence increase of QM in the presence of P_i was observed, this probe was used in solid support systems comprising of Sephadex[®] LH-20 and calcium phosphate in an attempt to create a phosphate sensor (**figure 4.3, 4.5**) [83, 84]. While titrations of P_i in these fluorescent systems suggest that the limit of detection of these probes are outside our range of interest, Sephadex[®] – a hydrophilic/lipophilic dextran – bound QM in the presence of P_i showed an increase in fluorescence proportional P_i concentrations, while no trend was observed using calcium phosphate (**figure 4.3, 4.5**). To further refine the sensitivity of the LH-20-QM sensor, modifications to buffer volumes and addition of polar solvents can be implemented. One example being the polar solvent PSS (0.1%, pH 7), which was initially shown to enhance the fluorescence of QM in the presence of P_i (**figure 4.2**) [80].

In contrast to our QM studies, quercetin-Al (III) complexes exhibited fluorescence quenching effects within our desired P_i detection range, however challenges of using this sensor raises caution to contaminant reading interferences when measuring field samples (**figure 4.17**) [17, 82, 119, 120]. This probe's ability to bind inorganic phosphate was supported by reports using quercetin-Al (III) as a sensor to detect phospho-proteins [41]. A *cost-effective paper-based P_i sensor* was created using quercetin-Al and synthesized

cellulose-phosphate disks. The novel method of cellulose-phosphate disk production used applied techniques previously described to form crystalline cellulose-phosphate [47, 85]. Cellulose-phosphate disk production was verified using sulfuric digestion following by a total phosphate assay (Malachite Green assay), where increases of phosphate were seen following digestion, suggesting liberation of phosphate from the synthesized disks (**figure 4.9**). Other techniques used to assess the synthesis of cellulose-phosphate included FTIR (Fourier-transform infrared spectroscopy), which showed low levels of organophosphate containing compounds detected likely owed to a low concentration of phosphate on sampled portions of the cellulose-phosphate disk (**figure 4.7**). Laser ablation *trace-element* analysis techniques were used and detected significant levels of phosphorus on cellulose-phosphate disks (**figure 4.8**) [121, 122]. Taken together, findings from these experiments verify successful production of cellulose-phosphate, using our novel method. The synthesized cellulose-phosphate disks were incubated in quercetin-Al immobilizing the probe via ionic bonding between aluminum and phosphate. Applying P_i onto these fluorescent disks showed no changes in fluorescence correlating to increased P_i concentrations (**figure 4.11**). The distribution of cellulose fibres is not uniformly compact (visualized by laser ablation) leading to differences of immobilized probe between disks, accounting for our anomalous findings. It is possible that monitoring the fluorescence of the aqueous fractions of these samples would better correlate to P_i concentrations, as liberated probe would exist in the aqueous medium.

In addition to quercetin-Al, quercetin bound to zirconium (IV), nickel (II), iron (III), cobalt (III) or copper (II) were tested to binding phosphate (**figures 4.13, 4.14, 4.20-23**), see appendix A for full list. Of these complexes, quercetin-Zr (IV) displayed a

fluorescence increase proportional to P_i concentration (**figure 4.22**). This was determined by surveying all probes in varying pH environments to identify maximum absorption wavelengths, which were used to excite probes and monitor fluorescence in the presence of P_i (**figures 4.13, 4.14, 4.20-23**), see appendix A for full list. Proceeding studies characterized quercetin-Zr (IV) binding affinities and metal binding coordination site(s). Our findings yielded a binding constant of **20.0 ±0.71 nM**, which, to the best of our knowledge, is the highest metal binding affinity reported for quercetin (**figure 4.25**) [44]. Therefore, the literature should be updated to show the new ascending order of stability as $Mg^{2+} < Ca^{2+} < Al^{3+} < Ni^{2+} < Zr^{4+}$ [43, 44, 123].

Quercetin can bind metals in any of its three coordination sites, with metals bearing a 3+ charge, like aluminum (III) or chromium (III), which bind to quercetin at the site highlighted in **figure 1.11 (II)** [41, 123, 124]. To see if zirconium (IV) behaved in the same manner, 1H NMR was used to observe quercetin spectra in the presence of zirconium (**figure 4.28-29**). Our findings displayed chemical shifts of protons on C_6 and C_8 downfield (increasing in ppm) (**figure 4.29**), and are the only chemical shifts observed for quercetin [10, 125]. This leads us to believe that these carbon atoms were impacted by the binding of zirconium at the nearest metal coordination site [44]. The introduction of P_i affected the same protons which observed chemical shifts with zirconium. P_i recovered these shifts toward lower ppm values, suggesting this region of quercetin is involved with zirconium and P_i interactions. An important take away from our 1H NMR preparation, requiring a high concentration of reactions components, was a precipitation reaction upon P_i introduction [126]. This led us to conclude that the probe conditions used induced zirconium phosphate precipitation due to the stable binding of quercetin to zirconium, producing a

fluorescently labelled precipitate [127]. This phenomenon would extend to our aqueous studies of quercetin-Zr and P_i where we had monitored *precipitated* and *not* the aqueous forms of quercetin-Zr- P_i (**figure 4.21-23**). ^{31}P NMR was used to monitor phosphorus signaling in the presence of Zr, similar to our 1H NMR studies, the introduction of zirconium formed an immediate precipitate with P_i . A phase separation was observed, and the supernatant (top phase) of our sample was monitored for phosphorus signaling. No phosphorus signaling was observed, suggesting that in our working conditions, zirconium phosphate is formed and the strong binding of quercetin to zirconium, fluorescently labels the precipitate, consistent with our initial hypothesis [127, 128]. Learning about the precipitation of quercetin-Zr with free phosphate, led our research to investigate quercetin-Zr (IV) in the presence of phosphate-containing biomolecules, as groups have utilized quercetin-metals in the detection of phospho-proteins [41].

5.1. Investigating phospho-protein sensors using quercetin-Zr (IV)

Current methods using quercetin bound to metals, such as aluminum, serve as biological phosphate sensors. A facet of these sensors that requires improvement is the reduction of the long dwell times currently needed for efficient phosphate-sensor binding [41]. Biologically, phosphorylation of amino acid residues is arguably one of the most influential post-translational modifications to occur, influencing a great set of processes through various signal transduction cascades in organisms [56, 129]. Proteins become phosphorylated through the stable phosphoester formation between phosphate and a hydroxyl group of amino acid residues [54, 130]. More than one-third of proteins are phosphorylated, with an overwhelming amount, 86.4%, occurring on serine (Ser) residues found within proteins [49, 56, 57, 109, 129].

We extended the use of our quercetin-Zr (IV) probe as a potentially *rapid* and *cost-effective* fluorescent phospho-protein probe, propelling research of protein signaling and characterization [41].

We hypothesized that phospho-groups on biomolecules would be less susceptible to precipitation reactions and yield observable fluorescence relationships in aqueous solutions [41, 131]. To challenge this hypothesis, L-serine (serine) or O-phospho-L-serine (phosphoserine) were titrated into solutions of quercetin-Zr (IV) (**figure 4.32-33**).

Fluorescence quenching-effects were observed for both amino acids and lower dissociation constants were observed for phosphoserine (**figure 4.32-33**). It was apparent that two binding affinities existed for quercetin-Zr in the presence of serine, which was confirmed with the calculated set of dissociation constants, $K_{b1} = 2.7 \text{ fM}$ and $K_{b2} = 0.3 \text{ fM}$. This phenomenon was also observed for phosphoserine with the lower values of $K_{b1} = 2.2 \text{ fM}$ and $K_{b2} = 0.2 \text{ fM}$, suggesting the probe had a higher sensitivity for phospho-amino acids, as lower dissociation constants are indicative of tighter and more stable binding [94, 126]. Evidence suggests that this tighter binding is due to the phosphate group, the only distinction between serine and phosphoserine [126, 132]. Preliminary work showed maximum probe-phosphate binding at pH 9 and was used in these phospho-amino acid binding studies (**figure 4.22-24**). A drawback of these conditions would be the deprotonation of the functional groups comprising amino acids [133, 134]. Specifically, the negatively-charged carboxyl group would be accessible for probe binding [133, 134]. To determine if these quenching-effects are due to probe-carboxyl group binding, experiments should be performed under low pH conditions, allowing for carboxyl group protonation, however, using these conditions would fully protonate the phosphate group as

pK_a values required for the protonation of the carboxyl are lower than phosphate, enabling potentially less optimal conditions for probe-phosphate binding [133, 135, 136]. Because quercetin-Zr was sensitive to phosphoserine we tested its potential use in other applications. Quercetin-Al was reported to detect phospho-proteins as a stain requiring long incubation times. As such, this led our research to explore an alternative quercetin-Zr stain allowing for *simple* and *quick* detection of phosphoproteins on nitrocellulose membranes [41].

Nitrocellulose membranes use hydrophobic interactions to immobilize and cross link proteins [60, 107]. For our method development non-phosphorylated (BSA, bovine serum albumin) and phosphorylated (casein, empty vector control, MTMR2) proteins were dot blotted onto the membrane and incubated with quercetin-Zr (**figure 4.34**) [41, 137, 138]. BSA served as a nonphosphorylated protein control, because it typically shows little to no phosphorylation, while casein is heavily composed of Ca₃(PO₄)₂ and lysine residues and served as a concentrated source of phosphoproteins [106, 139, 140]. In addition, complex cell lysates were also included in the analyses, one being an empty vector control lysate containing a whole host of phosphoproteins found in cells and the other overexpressing the protein MTMR2 [141]. MTMR2 (myotubularin related-protein 2), a protein with a well characterized phosphorylation site, serine 58, which regulates endocytic events [57, 109, 141]. Phosphorylated MTMR2 detection is an example of a protein whose studies would benefit from a *simple* and *timely* phospho-protein stain [109, 141]. Our findings demonstrated significant fluorescent signaling for all phospho-proteins and no detection of non-phosphorylated protein, BSA (**figure 4.34-35**) [41, 106, 132]. To further verify probe specificity for phosphoproteins, samples were treated with alkaline

phosphatase (APP) (**figure 4.36**) [67, 78]. APP, as the name suggests, is a phosphatase that cleaves the stable phosphoester bonds, generating dephosphorylated amino acid residues [78]. Contrary to expected results, APP-treated samples displayed little to no fluorescence detection, a consistent trend of elevated fluorescence was observed when compared to untreated samples (**figure 4.37**). Following APP treatment, BSA (non-phosphorylated control) reported fluorescence signaling, suggesting APP was responsible for the fluorescence detection of treated samples. To investigate how APP causes this increase, we turned to immunoblotting, monitoring MTMR2 serine 58 phosphorylation with and without APP treatment [141]. Using an antibody specific for MTMR2 phospho-serine 58, untreated samples showed a signal, while APP treated samples showed no signal for MTMR2 phosphorylation (**appendix figure B.1**) [109]. This ratified the effectiveness of our APP; a nonspecific band was detected on the blot matching the molecular weight of APP (**appendix figure B.1**). Furthermore, this band is only observed in APP treated samples, propelling us to believe this band belongs to APP. The literature suggests that APP can be phosphorylated, explaining the fluorescence detection in *all* of our APP treated samples analyzed using quercetin-Zr [139, 141, 142]. The removal of APP would allow us to examine the probe specificity to phosphoproteins and provide insights into the effect of APP on our samples [137].

5.2. The development of a conjugated fluorescence phosphatase assay

In the pursuit of optimizing a phospho-protein assay, we reported drawbacks of APP detection on a solid support of nitrocellulose membrane (**figure 4.36**). This work led to the reconstruction of our scientific approach and a new goal: the development of a *simple, rapid* and *cost-effective* phosphatase assay [143, 144]. This assay involved forming

a fluorescent probe conjugate with protein, allowing us to detect phosphorylated or nonphosphorylated proteins based on significant fluorescent intensity differences [71, 145]. The probe utilized *o*-aminobenzoyl (OAb), reacts with nitrogen nucleophiles and forms fluorescence molecular conjugates [71, 72]. As such, we conjugated OAb with serine or phosphoserine [131, 139]. The synthesis of these fluorescently conjugated amino acids would serve as the preliminary work in the development of an OAb-dependent phosphatase assay.

OAb-serine (OAb-S) or OAb-phosphoserine (OAb-PS) were synthesized in basic conditions and purified using anion exchange chromatography [72]. Fluorescently conjugated amino acids were accessed using ¹HNMR (**figure 4.39**) and TLC (thin layer chromatography) (**appendix figure B.2-4**) [72, 146–148]. Results confirmed successful sample synthesis and purity. The concentrations of our probes were normalized using UV-vis spectroscopy (**figure 4.41**). The fluorescence of OAb displayed significant differences in emission intensities between OAb conjugated to serine or phosphoserine (**figure 4.42**) [1, 71, 72]. Our next objective was to enhance these differences, increasing the 1.25-fold change between phosphoserine and serine. Further strengthening the utility of this phosphatase assay [72].

In attempts to enhance sensitivity of the phosphatase assay, a precipitated ZrCl₄ solid support was created in Tris-HCl (0.1 M, pH 9) (**figure 4.43**) [111]. This support would ionically bind the phospho-groups of phosphoserine fluorescent conjugates and yield fluorescence probe intensity differences by a 1.97-fold change (**figure 4.44**) [56, 139]. This was further supported by the constant intensity values monitored for OAb-S and increasing intensities of OAb-PS in varying densities of ZrCl₄. Although the sensitivity of

the phosphatase assay was established, the optimization of a completely aqueous sensor was pursued to ratify an even more robust assay.

Lanthanides have been reported to induce the emission intensity changes of fluorophores and used to form more robust aqueous sensors [95]. A recent study showed the lanthanide, europium (III), displays a strong affinity for inorganic phosphate, where fluorophore quenching due to europium binding, was recovered by the introduction of P_i [17, 115]. These findings led us to examine the fluorescent conjugates of serine or phosphoserine in the presence of europium, where we expected fluorescence intensity changes of phosphoserine due to stable europium binding affinities for phosphate (phospho-groups) [115]. Ultimately, this would increase fluorescence intensity differences, thus creating a greater distinction between phosphorylated and non-phosphorylated biomolecules. Our findings using an aqueous system in pH 4 supported this; where a 2.4-fold change between OAb-S and OAb-PS was observed. Using europium, significant quenching was unique to OAb-PS likely based on the ionic bond formation between europium and the phospho-group of OAb-PS (**figure 4.45-47**) [1, 115, 149, 150].

Our aim in developing a robust phosphatase assay led to designing various methods composed of phosphate binding metals in aqueous or solid support systems. The two most effective assays proposed contained either metal aqueous solution or metal solid support. The aqueous system used comprised reaction buffer, OAb-S/-PS, and a phosphate binding metal.

We investigated nine metals known to promote phosphate binding, to better distinguish phosphoserine detection, where a europium aqueous solution showed the best

distinction over the pH range tested (see **appendix for full list and results**). Our second method utilized the formation of the $ZrCl_4$ solid – where Zr^{4+} containing probes were shown to bind phosphate - to bind phosphoserine. By comparison, the $ZrCl_4$ phosphatase assay had a 1.97-fold change, whereas the europium aqueous assay had a fold change of 2.4. The aqueous probe can be used for a phosphatase assay at different conditions owing to its simplicity of using high affinity phosphate binding metals in solution, whereas our solid support design relied on laborious techniques such as the required precipitation of $ZrCl_4$ under more stringent conditions. In contrast, the assay involving europium is amenable to being performed under a wide array of conditions without alterations to our current method; such as use of more polar and/or viscous solvents, which have been shown to increase probe detection through dipole moment alignments and retarding fluorophore decay [151]. While we were successful in distinguishing non- and phosphorylated amino acid probe conjugates in aqueous and solid support systems, future assays would require the synthesis of OAb-peptides to test the stability of this method and evaluate the fluorescence properties of phosphorylated peptides, aiding in the detection of biological phosphorylation events.

5.3. Discussion summary

Orthophosphate in waterbodies has caused harmful algal blooms which contaminate drinking water and negatively affect recreation and tourism industries [17]. To this end, a fluorescent P_i sensor was pursued to monitor orthophosphate levels in waterbodies between 0.1 and 10 μM [28]. The anionic properties of the molecular phosphate structure led to investigating cationic fluorophores in combination with different solid supports [92]. Sensors with the following compositions were able to detect P_i ; Sephadex[®] LH-20-QM, quercetin-Al and quercetin-Zr. From the surveyed probes, quercetin-Zr detected P_i in the range of interest and showed an increase in fluorescence proportional to P_i concentrations. Binding studies of quercetin-Zr (IV), yielded the highest binding affinity and stability of a quercetin-metal complex known [44]. Proceeding studies inferred a precipitation reaction with P_i yielding quercetin-Zr (IV)- P_i , transitioning the application of this probe for phosphoprotein sensing. The preliminary findings suggest quercetin-Zr (IV) can work as a phosphoprotein stain on nitrocellulose membranes. The challenges that surfaced from optimizing this stain led to the development of a third assay for the detection of phospho-biomolecules using the fluorescent probe *o*-aminobenzoyl conjugated to amino acids. This assay would distinguish phospho-amino acids in aqueous systems, and further improved with the addition of europium. Overall, the most robust and sensitive sensor developed was quercetin-Zr for the detection of phosphoproteins.

CHAPTER 6

CONCLUSION AND FUTURE DIRECTIONS

Eutrophication in water bodies has become one of the most prevalent environmental issues of today [24]. This phenomenon is a direct result of high orthophosphate concentrations supplying nutrients for the rapid growth of algae [17]. These processes have potentially dire consequences for fishing, recreation, and tourism industries [115]. Environmental agencies have been seeking precise methods to monitor inorganic phosphate levels and susceptible regions [28, 116].

We aimed to develop a fluorescent inorganic phosphate sensor allowing for the downstream analysis of P_i levels in waterbodies. Through our trials, quinacrine mustard (QM) was easily immobilized on the solid support of Sephadex[®] LH-20 and detected P_i outside our range of interest. This method could be improved by optimizing buffer volumes, pH conditions, and surveying more polar and/or viscous solvents to slow down the intramolecular rotation and non-radiative decay of our fluorophore, improving the binding of phosphate to these probes [1, 151]. While LH-20-QM methods had attractive phosphate-binding characteristics, its expense makes it impractical for use on larger scale. Cost-effective alternatives to LH-20 would possess the immobilizing characteristics of a hydrophilic and lipophilic solid support such as, carbon nanotubes [83, 152]. Since propidium iodide (PI) shares the polar properties of QM by the possession of a cationic nitrogen, this probe should be investigated using a LH-20 solid support [37, 118]. The use of LH-20 could be extended for a solid support for quercetin-Al.

In the survey of quercetin-Al (III), a P_i fluorescent quenching sensor was developed in aqueous solutions of pH 5. Challenges of using this sensor involve potential contaminant reading interferences when using field samples, contributed by compounds like nitrate and sulfate [25, 82, 120, 153]. This method development would be improved by saturating

novel cellulose-phosphate with quercetin-Al (III) in a column to thoroughly wash unbound probe. In addition, the quantity of cellulose-phosphate-probe disks per sample should be optimized until the nonuniformity of cellulose-phosphate fibres per disk is negligible, to reduce sensor imprecision [154]. A simple improvement to deepen the findings using this method could also monitor the aqueous fraction, rather than just visualizing disks for the loss of fluorescence. These applications would be further refined allowing for the development of *simple, precise, and cost-effective* devices to test orthophosphate concentrations of field samples, with the ultimate goal of constructing a hand-held device for on-site testing. These findings could easily be extended to measure inorganic phosphate levels in biological systems, such as, blood for monitoring diseases like hyperphosphatemia [155].

Proceeding studies were conducted for a quercetin-Zr (IV) probe and, to the best of our knowledge, our findings unveiled the most stable quercetin-metal complex reported [44]. This probe was observed to precipitate in the presence of P_i and as such extended our fluorescent probe studies to phosphate-containing molecules. Evaluation of quercetin-Zr (IV) as a phospho-protein stain was proven successful with the detection of phosphoproteins, casein, empty vector control samples and MTMR2 resolved on nitrocellulose membranes [41, 106, 141]. To test the phosphoprotein binding specificity of our probe, the proteins listed above were treated with APP to generate dephosphorylated proteins [156]. Our findings, however, would support the probable detection of phosphorylated APP. To circumvent the use of APP, purified protein in phospho- and nonphosphorylated forms could be used and would provide information about the probes binding specificity. It would be interesting to see if this probe had binding affinities similar between different phospho-

amino acids or certain amino acid motifs found around the phosphorylated residue [157]. This knowledge would increase the potential application of this probe, allowing researchers to use the probe on protein resolved on SDS-PAGE gels, or even perform phospho-/peptide enrichments from the complex cellular milieu.

Our next venture involved the development of an aqueous phosphatase assay using *o*-aminobenzoyl. Serine and phosphoserine were successfully conjugated to this fluorescent probe. Fluorescence monitoring showed significant differences in emission intensities of OAb-S/-PS. Differences were enhanced by addition of metal solutions and use of different pH environments. Future work would focus on improving the sensitivity and specificity of these probes by finding the optimal polar and/or viscous solvent(s) composition. Polar solvents align dipole moments, elongating emission, whereas viscous solvents retard intramolecular rotation and non-radioactive decay of the fluorophore, both allowing for more sensitive fluorescent detection and distinction [1, 151].

To satisfy the goal of using *o*-aminobenzoyl as a phosphatase assay allowing for detection of target proteins would require conjugating this probe to secondary and tertiary biomolecular structures, this would help observe the phosphorylation in aqueous systems and improve reaction conditions to ensure the stability and reactivity of proteins. Immediate work should conjugate peptides of various compositions, such as peptides mimicking known phosphorylation motifs, and multiply or differentially phosphorylated peptides. These results would assess the sensitivity and applicability of the phospho-probe in a biological context.

Ultimately, the emphasis of our studies on inorganic phosphate and phosphoprotein detection reiterates the essential demands of challenging and improving precise detection methods of phosphate. In an era of constantly evolving technologies, it is imperative that scientific methods are reflective of the times. Environmental issues and global pollution will continuously require accessible and cost-effective applications to aid the remediation of wastewater systems, while disease research will continue to seek protocols to advance the understanding of illnesses and explore preventive measures.

REFERENCES/BIBLIOGRAPHY

1. Lakowicz, J.R.: Principles of fluorescence spectroscopy, 3rd Edition, Joseph R. Lakowicz, editor. (2006)
2. Brand, L., Johnson, M.L.: An Introduction to Fluorescence Spectroscopy. 15 (2011). <https://doi.org/10.1194/jlr.M022798>
3. Mataga, N., Kaifu, Y., Koizumi, M.: Solvent Effects upon Fluorescence Spectra and the Dipolemoments of Excited Molecules. Bull. Chem. Soc. Jpn. 29, 465–470 (1956). <https://doi.org/10.1246/bcsj.29.465>
4. Scientific, H.: Fluorescence Spectroscopy - Applications and Principles. 1–8 (2018)
5. Chris, D., Joseph, R.: Topics in Fluorescence Spectroscopy. (2000)
6. Delgado-Camón, A., Garriga, R., Mateos, E., Cebolla, V.L., Galbán, J., Membrado, L., Marcos, S. De, Gálvez, E.M.: Changes in fluorescent emission of cationic fluorophores in the presence of n-alkanes and alcohols in different polarity solvents. Chem. Phys. Lett. 501, 547–553 (2011). <https://doi.org/10.1016/j.cplett.2010.11.004>
7. Acid, H., Tiie, C.: THE USE OF ISOSBESTIC POINTS IN THE FLUORE , SCENCE EXCITATION substituting Eq . 5–8 (1980)
8. Voicescu, M., Ionescu, S., Gatea, F.: Effect of pH on the fluorescence characteristics of some flavones probes. Spectrochim. Acta - Part A Mol. Biomol. Spectrosc. 123, 303–308 (2014). <https://doi.org/10.1016/j.saa.2013.12.040>
9. Ohgaki, R., Teramura, Y., Hayashi, D., Quan, L., Okuda, S., Nagamori, S., Takai, M., Kanai, Y.: Ratiometric fluorescence imaging of cell surface pH by poly(ethylene glycol)-phospholipid conjugated with fluorescein isothiocyanate. Sci. Rep. 7, 1–9 (2017). <https://doi.org/10.1038/s41598-017-17459-y>
10. Mohammed, G.I., Ahmad, W., Alwael, H., Saigl, Z.M., Al-Eryani, D.A., Bashammakh, A.S., El-Shahawi, M.S.: A quercetin based fluorescent chemical sensor for ultra-sensitive determination and speciation of tungsten species in water. Spectrochim. Acta - Part A Mol. Biomol. Spectrosc. 229, 117929 (2020). <https://doi.org/10.1016/j.saa.2019.117929>
11. Fraiji, L.K., Hayes, D.M., Werner, T.C.: Static and dynamic fluorescence quenching

- experiments for the physical chemistry laboratory. *J. Chem. Educ.* 69, 424–428 (1992).
<https://doi.org/10.1021/ed069p424>
12. Seidel, C.A.M., Schulz, A., Sauer, M.H.M.: Nucleobase-specific quenching of fluorescent dyes. 1. Nucleobase one-electron redox potentials and their Correlation with static and dynamic quenching efficiencies. *J. Phys. Chem.* 100, 5541–5553 (1996).
<https://doi.org/10.1021/jp951507c>
 13. Feng, F., Tang, Y., Wang, S., Li, Y., Zhu, D.: Continuous fluorometric assays for acetylcholinesterase activity and inhibition with conjugated polyelectrolytes. *Angew. Chemie - Int. Ed.* 46, 7882–7886 (2007). <https://doi.org/10.1002/anie.200701724>
 14. Stanisavljevic, M., Krizkova, S., Vaculovicova, M., Kizek, R., Adam, V.: Quantum dots-fluorescence resonance energy transfer-based nanosensors and their application. *Biosens. Bioelectron.* 74, 562–574 (2015). <https://doi.org/10.1016/j.bios.2015.06.076>
 15. Hussain, S.A.: *An Introduction to Fluorescence Resonance Energy Transfer (FRET)*. (2009)
 16. Selvin, P.R.: The renaissance of fluorescence resonance energy transfer. *Nat. Struct. Biol.* 7, 730–734 (2000). <https://doi.org/10.1038/78948>
 17. Sarwar, M., Leichner, J., Naja, G.M., Li, C.Z.: Smart-phone, paper-based fluorescent sensor for ultra-low inorganic phosphate detection in environmental samples. *Microsystems Nanoeng.* 5, (2019). <https://doi.org/10.1038/s41378-019-0096-8>
 18. Zhang, N., Fan, Y., Li, C., Wang, Q., Leksawasdi, N., Li, F., Wang, S.: Cell permeability and nuclear DNA staining by propidium iodide in basidiomycetous yeasts. *Appl. Microbiol. Biotechnol.* 102, 4183–4191 (2018). <https://doi.org/10.1007/s00253-018-8906-8>
 19. Mohammed, G.I., Ahmad, W., Alwael, H., Saigl, Z.M., Al-Eryani, D.A., Bashammakh, A.S., El-Shahawi, M.S.: A quercetin based fluorescent chemical sensor for ultra-sensitive determination and speciation of tungsten species in water, (2020)
 20. Saad, E.A., Khalil, L.H., Zaki, M.T.M., El-Ella, A.A.A.: Determination of zirconium (IV) and aluminium (III) in waste water. *Mikrochim. Acta.* 140, 87–91 (2002).
<https://doi.org/10.1007/s00604-001-0897-x>

21. Herrero-Foncubierta, P., Paredes, J.M., Giron, M.D., Salto, R., Cuerva, J.M., Miguel, D., Orte, A.: A red-emitting, multidimensional sensor for the simultaneous cellular imaging of biothiols and phosphate ions. *Sensors (Switzerland)*. 18, (2018).
<https://doi.org/10.3390/s18010161>
22. Wongkongkatep, J., Ojida, A., Hamachi, I.: Fluorescence Sensing of Inorganic Phosphate and Pyrophosphate Using Small Molecular Sensors and Their Applications. *Top. Curr. Chem.* 375, 1–33 (2017). <https://doi.org/10.1007/s41061-017-0120-0>
23. Berkessa, Y.W., Mereta, S.T., Feyisa, F.F.: Simultaneous removal of nitrate and phosphate from wastewater using solid waste from factory. *Appl. Water Sci.* 9, 1–10 (2019). <https://doi.org/10.1007/s13201-019-0906-z>
24. Ure, D., Awada, A., Frowley, N., Munk, N., Stanger, A., Mutus, B.: Greenhouse tomato plant roots/carboxymethyl cellulose method for the efficient removal and recovery of inorganic phosphate from agricultural wastewater. *J. Environ. Manage.* 233, 258–263 (2019). <https://doi.org/10.1016/j.jenvman.2018.12.053>
25. Burkholder, J.M.: Harmful Algal Blooms. *Encycl. Inl. Waters.* 264–285 (2009).
<https://doi.org/10.1016/B978-012370626-3.00239-8>
26. Anderson, D.M., Hoagland, P., Kaoru, Y., White, A.W.: Economic impacts from harmful algal blooms (HABs) in the United States. *Natl. Ocean. Atmos. Adm. Norman OK Natl. Sev. Storms Lab. No. WHOI-2000-11* (2000)
27. NASA: Bloom Persists in Lake Erie,
<https://landsat.visibleearth.nasa.gov/view.php?id=91038>
28. Ministry of the Environment: Rationale for the establishment of Ontario’s provincial water quality objectives. 244 (1979)
29. Buisine, E., De Villiers, K., Egan, T.J., Biot, C.: Solvent-induced effects: Self-association of positively charged π systems. *J. Am. Chem. Soc.* 128, 12122–12128 (2006).
<https://doi.org/10.1021/ja061755u>
30. Ng, J.B.S., Kamali-Zare, P., Brismar, H., Bergström, L.: Release and molecular transport of cationic and anionic fluorescent molecules in mesoporous silica spheres. *Langmuir.* 24, 11096–11102 (2008). <https://doi.org/10.1021/la801179v>

31. Liu, Y., Schanze, K.S.: Conjugated polyelectrolyte-based real-time fluorescence assay for alkaline phosphatase with pyrophosphate as substrate. *Anal. Chem.* 80, 8605–8612 (2008). <https://doi.org/10.1021/ac801508y>
32. Geddes, C.D.: *Reviews in Fluorescence 2005* Edited by Springer. (2005)
33. Goldberg, R.N., Kishore, N., Lennen, R.M.: Thermodynamic quantities for the ionization reactions of buffers. *J. Phys. Chem. Ref. Data.* 31, 231–370 (2002). <https://doi.org/10.1063/1.1416902>
34. Powell, K.J., Brown, P.L., Byrne, R.H., Gajda, T., Hefter, G., Sjöberg, S., Wanner, H.: Chemical speciation of environmentally significant heavy metals with inorganic ligands part 1: The Hg²⁺- Cl⁻, OH⁻, CO₃²⁻, SO₄²⁻, and PO₄³⁻ aqueous systems (IUPAC technical report). *Pure Appl. Chem.* 77, 739–800 (2005). <https://doi.org/10.1351/pac200577040739>
35. P, D.: *CRC Handbook of Chemistry and Physics.* *J. Mol. Struct.* (1992). [https://doi.org/10.1016/0022-2860\(92\)85083-s](https://doi.org/10.1016/0022-2860(92)85083-s)
36. Issue, V., Issn, P.--S.-: *Physicochemical Studies On Carboxymethylcellulose Sodium Salt , Dyes And Surfactants.* 2, 1860–1869 (2014)
37. Niu, Y., Li, S., Lin, Z., Liu, M., Wang, D., Wang, H., Chen, S.: Development of propidium iodide as a fluorescence probe for the on-line screening of non-specific DNA-intercalators in Fufang Banbianlian Injection. *J. Chromatogr. A.* 1463, 102–109 (2016). <https://doi.org/10.1016/j.chroma.2016.08.013>
38. Caspersson, T., Zech, L., Johansson, C., Modest, E.J.: Identification of human chromosomes by DNA-binding fluorescent agents. *Chromosoma.* 30, 215–227 (1970). <https://doi.org/10.1007/BF00282002>
39. Borgaonkar, D.S., Ebenezer, L., Scott, C.I., Golomb, H.M., Bahr, G.F.: Identification of a D/E(15/18) translocation chromosome by quinacrine fluorescence and Urea banding techniques. *Hum. Genet.* 17, 317–321 (1973). <https://doi.org/10.1007/BF00273186>
40. Sumner, A.T.: Mechanisms of quinacrine binding and fluorescence in nuclei and chromosomes. *Histochemistry.* 84, 566–574 (1986). <https://doi.org/10.1007/BF00482993>
41. Wang, X., Ni, M., Niu, C., Zhu, X., Zhao, T., Zhu, Z., Xuan, Y., Cong, W.: Simple

- detection of phosphoproteins in SDS-PAGE by quercetin. *EuPA Open Proteomics*. 4, 156–164 (2014). <https://doi.org/10.1016/j.euprot.2014.07.002>
42. Herrero-Martínez, J.M., Sanmartin, M., Rosés, M., Bosch, E., Ràfols, C.: Determination of dissociation constants of flavonoids by capillary electrophoresis. *Electrophoresis*. 26, 1886–1895 (2005). <https://doi.org/10.1002/elps.200410258>
43. Liu, Y., Guo, M.: Studies on transition metal-quercetin complexes using electrospray ionization tandem mass spectrometry. *Molecules*. 20, 8583–8594 (2015). <https://doi.org/10.3390/molecules20058583>
44. de Castilho, T.S., Matias, T.B., Nicolini, K.P., Nicolini, J.: Study of interaction between metal ions and quercetin. *Food Sci. Hum. Wellness*. 7, 215–219 (2018). <https://doi.org/10.1016/j.fshw.2018.08.001>
45. Chislock, M., Doster, E.: Eutrophication: Causes, Consequences, and Controls in Aquatic Ecosystems. *Nat. Educ.* (2013)
46. Meister, D., Ure, D., Awada, A., Barrette, J.C., Gagnon, J., Mutus, B., Trant, J.F.: Covalently Functionalized Sawdust for the Remediation of Phosphate from Agricultural Wastewater. *ACS Sustain. Chem. Eng.* 7, 20139–20150 (2019). <https://doi.org/10.1021/acssuschemeng.9b06073>
47. Bezerra, R.D.S., Morais, A.I.S., Osajima, J.A., Nunes, L.C.C., Silva Filho, E.C.: Cellulose phosphate applied in the removal of the drug acetaminophen from aqueous media. *Mater. Sci. Forum*. 869, 745–749 (2016). <https://doi.org/10.4028/www.scientific.net/MSF.869.745>
48. Kinoshita, E., Kinoshita-Kikuta, E., Koike, T.: Separation and detection of large phosphoproteins using phos-tag sds-page. *Nat. Protoc.* 4, 1513–1521 (2009). <https://doi.org/10.1038/nprot.2009.154>
49. Gao, X., Schutz-Geschwender, A., Hardwidge, P.R.: Near-infrared fluorescence detection of ATP-biotin-mediated phosphoprotein labeling. *Biotechnol. Lett.* 31, 113–117 (2009). <https://doi.org/10.1007/s10529-008-9824-0>
50. Green, K.D., Pflum, M.K.H.: Kinase-catalyzed biotinylation for phosphoprotein detection. *J. Am. Chem. Soc.* 129, 10–11 (2007). <https://doi.org/10.1021/ja066828o>

51. Kupcho, K., Hsiao, K., Bulleit, B., Goueli, S.A.: A homogeneous, nonradioactive high-throughput fluorogenic protein phosphatase assay. *J. Biomol. Screen.* 9, 223–231 (2004). <https://doi.org/10.1177/1087057103262840>
52. D'Ambrosio, C., Salzano, A.M., Arena, S., Renzone, G., Scaloni, A.: Analytical methodologies for the detection and structural characterization of phosphorylated proteins. *J. Chromatogr. B Anal. Technol. Biomed. Life Sci.* 849, 163–180 (2007). <https://doi.org/10.1016/j.jchromb.2006.06.033>
53. Krutzik, P.O., Nolan, G.P.: Intracellular phospho-protein staining techniques for flow cytometry: Monitoring single cell signaling events. *Cytometry.* 55A, 61–70 (2003). <https://doi.org/10.1002/cyto.a.10072>
54. Cieśla, J., Fraczyk, T., Rode, W.: Phosphorylation of basic amino acid residues in proteins: Important but easily missed. *Acta Biochim. Pol.* 58, 137–148 (2011). https://doi.org/10.18388/abp.2011_2258
55. In, P.P.: Protein phosphorylation in prokaryotes. *Biochimie.* 71, 987–1105 (1989). <https://doi.org/10.1146/annurev.mi.42.100188.000525>
56. Macek, B., Mijakovic, I., Olsen, J. V., Gnad, F., Kumar, C., Jensen, P.R., Mann, M.: The serine/threonine/tyrosine phosphoproteome of the model bacterium *Bacillus subtilis*. *Mol. Cell. Proteomics.* 6, 697–707 (2007). <https://doi.org/10.1074/mcp.M600464-MCP200>
57. Ardito, F., Giuliani, M., Perrone, D., Troiano, G., Muzio, L. Lo: The crucial role of protein phosphorylation in cell signaling and its use as targeted therapy (Review). *Int. J. Mol. Med.* 40, 271–280 (2017). <https://doi.org/10.3892/ijmm.2017.3036>
58. Vlastaridis, P., Kyriakidou, P., Chaliotis, A., Van de Peer, Y., Oliver, S.G., Amoutzias, G.D.: Estimating the total number of phosphoproteins and phosphorylation sites in eukaryotic proteomes. *Gigascience.* 6, 1–11 (2017). <https://doi.org/10.1093/gigascience/giw015>
59. Chang, C., Stewart, R.C.: The two-component system: Regulation of diverse signaling pathways in prokaryotes and eukaryotes. *Plant Physiol.* 117, 723–731 (1998). <https://doi.org/10.1104/pp.117.3.723>
60. Goodman, T., Schulenberg, B., Steinberg, T.H., Patton, W.F.: Detection of

- phosphoproteins on electroblot membranes using a small-molecule organic fluorophore. *Electrophoresis*. 25, 2533–2538 (2004). <https://doi.org/10.1002/elps.200406008>
61. Martin, K., Steinberg, T.H., Cooley, L.A., Gee, K.R., Beechem, J.M., Patton, W.F.: Quantitative analysis of protein phosphorylation status and protein kinase activity on microarrays using a novel fluorescent phosphorylation sensor dye. *Proteomics*. 3, 1244–1255 (2003). <https://doi.org/10.1002/pmic.200300445>
 62. An, J.S., Carmichael, W.W.: Use of a colorimetric protein phosphatase inhibition assay and enzyme linked immunosorbent assay for the study of microcystins and nodularins. *Toxicon*. 32, 1495–1507 (1994). [https://doi.org/10.1016/0041-0101\(94\)90308-5](https://doi.org/10.1016/0041-0101(94)90308-5)
 63. Montalibet, J., Skorey, K.I., Kennedy, B.P.: Protein tyrosine phosphatase: Enzymatic assays. *Methods*. 35, 2–8 (2005). <https://doi.org/10.1016/j.ymeth.2004.07.002>
 64. Galvan, B., Christopoulos, T.K.: Fluorometric and time-resolved immunofluorometric assays for protein-tyrosine phosphatase activity. *Clin. Biochem*. 29, 125–131 (1996). [https://doi.org/10.1016/0009-9120\(95\)02026-8](https://doi.org/10.1016/0009-9120(95)02026-8)
 65. Wright, D.E., Noimant, E.S., Chockt, P.B., Chautt, V.: Dependent Protein Kinase and Phosphoprotein Phosphatase Activities. 78, 6048–6050 (1981)
 66. Yang, J., Guo, J., Yuan, J.: In vitro antioxidant properties of rutin. *LWT - Food Sci. Technol*. 41, 1060–1066 (2008). <https://doi.org/10.1016/j.lwt.2007.06.010>
 67. Sharma, U., Pal, D., Prasad, R.: Alkaline phosphatase: An overview. *Indian J. Clin. Biochem*. 29, 269–278 (2014). <https://doi.org/10.1007/s12291-013-0408-y>
 68. Self, C.H.: Enzyme amplification - A general method applied to provide an immunoassisted assay for placental alkaline phosphatase. *J. Immunol. Methods*. 76, 389–393 (1985). [https://doi.org/10.1016/0022-1759\(85\)90316-3](https://doi.org/10.1016/0022-1759(85)90316-3)
 69. Kumar, D., Jadhavar, P.S., Nautiyal, M., Sharma, H., Meena, P.K., Adane, L., Pancholia, S., Chakraborti, A.K.: Convenient synthesis of 2,3-disubstituted quinazolin-4(3H)-ones and 2-styryl-3-substituted quinazolin-4(3H)-ones: Applications towards the synthesis of drugs. *RSC Adv*. (2015). <https://doi.org/10.1039/c5ra03888j>
 70. Staigerl, R.P., Miller, E.B., Staigerl, R.P., Miller, E.B.: Isatoic Anhydride. IV. Reactions with Various Nucleophiles. *J. Org. Chem*. (1959). <https://doi.org/10.1021/jo01091a013>

71. Abbas, S.Y., El-Bayouki, K.A.M., Basyouni, W.M.: Utilization of isatoic anhydride in the syntheses of various types of quinazoline and quinazolinone derivatives. *Synth. Commun.* 46, 993–1035 (2016). <https://doi.org/10.1080/00397911.2016.1177087>
72. Onukwue, N., Ventimiglia, L., Potter, M., Aljoudi, S., Mutus, B.: Simple fluorescent reagents for monitoring disulfide reductase and S-nitroso reductase activities in vitro and in live cells in culture. *Methods.* 168, 29–34 (2019). <https://doi.org/10.1016/j.ymeth.2019.06.028>
73. Heilig, M.L.: United States Patent Office. *ACM SIGGRAPH Comput. Graph.* 28, 131–134 (1994). <https://doi.org/10.1145/178951.178972>
74. Ma, X., Liu, C., Anderson, D.P., Chang, P.R.: Porous cellulose spheres: Preparation, modification and adsorption properties. *Chemosphere.* 165, 399–408 (2016). <https://doi.org/10.1016/j.chemosphere.2016.09.033>
75. Stanley, I., Stevens, M.: (12) United States Patent. 2, (2009)
76. Yen, C.H., Lin, Y.S., Tu, C.F.: A novel method for separation of caseins from milk by phosphates precipitation. *Prep. Biochem. Biotechnol.* 45, 18–32 (2015). <https://doi.org/10.1080/10826068.2013.877030>
77. Paulista, U.E., Em, P.D.E.P., Biológicas, C.: 6X SDS Protein Loading Buffer. 100
78. Thermo Scientific: Product information: Thermo Scientific FastAP Thermosensitive Alkaline Phosphatase. *Protocol.* 1–4 (2016)
79. Karupiah, N., Mutus, B.: Selective adsorption of 2'-O-anthraniloyl-AMP on DEAE-Sephadex: The basis of a direct, fluorescent assay for cyclic nucleotide phosphodiesterase. *Anal. Biochem.* 149, 202–208 (1985). [https://doi.org/10.1016/0003-2697\(85\)90496-8](https://doi.org/10.1016/0003-2697(85)90496-8)
80. Tian, E., Hu, C., Qin, Y., Ren, Y., Wang, X., Wang, X., Xiao, P., Yang, X.: A study of poly (sodium 4-styrenesulfonate) as draw solute in forward osmosis. *Desalination.* 360, 130–137 (2015). <https://doi.org/10.1016/j.desal.2015.01.001>
81. Stankovich, S., Piner, R.D., Chen, X., Wu, N., Nguyen, S.T., Ruoff, R.S.: Stable aqueous dispersions of graphitic nanoplatelets via the reduction of exfoliated graphite oxide in the presence of poly(sodium 4-styrenesulfonate). *J. Mater. Chem.* (2006). <https://doi.org/10.1039/b512799h>

82. MacKenzie, D.S., Graham, G., Jankowski, J.: Effect of contamination on the cooling rate of quench oils. In: Quenching Control and Distortion - Proceedings of the 6th International Quenching and Control of Distortion Conference, Including the 4th International Distortion Engineering Conference (2012)
83. GE Healthcare: Sephadex LH-20. GE Healthc. (2006)
84. LeGeros, R.Z.: Calcium phosphate-based osteoinductive materials, (2008)
85. Bezerra, R.D.S., Silva, M.M.F., Morais, A.I.S., Osajima, J.A., Santos, M.R.M.C., Airoidi, C., Silva Filho, E.C.: Phosphated cellulose as an efficient biomaterial for aqueous drug ranitidine removal. *Materials (Basel)*. 7, 7907–7924 (2014). <https://doi.org/10.3390/ma7127907>
86. Merck: IR Spectra Table & Chart | Sigma-Aldrich. Sigmaaldrich. (2020)
87. Zhang, D., Guan, L.: Laser Ablation. In: *Comprehensive Materials Processing* (2014)
88. Russo, R.E., Mao, X., Gonzalez, J.J., Zorba, V., Yoo, J.: Laser ablation in analytical chemistry. *Anal. Chem.* (2013). <https://doi.org/10.1021/ac4005327>
89. Source, L.: Technical specifications. *Hydraul. Fill Man.* 433–475 (2013). <https://doi.org/10.1201/b13077-13>
90. Stewart, R., Li, L., Thomas, D.: Laser ablation of multilayers of ink from a paper substrate for tactile printing. *Opt. Laser Technol.* (2000). [https://doi.org/10.1016/S0030-3992\(00\)00067-0](https://doi.org/10.1016/S0030-3992(00)00067-0)
91. Sahrawat, K.L., Kumar, G.R., Murthy, K.V.S.: Sulfuric acid-selenium digestion for multi-element analysis in a single plant digest. *Commun. Soil Sci. Plant Anal.* 33, 3757–3765 (2002). <https://doi.org/10.1081/CSS-120015920>
92. Baykov, A.A., Evtushenko, O.A., Avaeva, S.M.: A malachite green procedure for orthophosphate determination and its use in alkaline phosphatase-based enzyme immunoassay. *Anal. Biochem.* 171, 266–270 (1988). [https://doi.org/10.1016/0003-2697\(88\)90484-8](https://doi.org/10.1016/0003-2697(88)90484-8)
93. Rasband, W.: ImageJ [Software]. U. S. Natl. Institutes Heal. Bethesda, Maryland, USA. (2015)

94. Sonu, V.K., Rajkumar, I., Bhattacharjee, K., Joshi, S.R., Mitra, S.: Interaction of caffeine and sulfadiazine with lysozyme adsorbed at colloidal metal nanoparticle interface: influence on drug transport ability and antibacterial activity. *J. Biomol. Struct. Dyn.* 37, 321–335 (2019). <https://doi.org/10.1080/07391102.2018.1426497>
95. Wiikinkoski, E.W., Xu, J., Zhang, W., Hietala, S., Koivula, R.T.: Modification of α -Zirconium Phosphate Synthesis – Effects of Crystallinity and Acidity on Eu(III) and Am(III) Ion Exchange. *ChemistrySelect.* (2018). <https://doi.org/10.1002/slct.201801601>
96. Material, E.S., This, C.C., Society, T.R.: General method of UV-Vis and fluorescence titration. (2013)
97. He, H., Li, C., Tian, Y., Wu, P., Hou, X.: Phosphorescent Differential Sensing of Physiological Phosphates with Lanthanide Ions-Modified Mn-Doped ZnCdS Quantum Dots. *Anal. Chem.* 88, 5892–5897 (2016). <https://doi.org/10.1021/acs.analchem.6b00780>
98. Kaskel, S. et al.: 5.62 Physical Chemistry II. (2008)
99. Bakhmutov, V.I., Clearfield, A.: ^{31}P Solid-State NMR Relaxation in the Zirconium Phosphate Network in the Presence of Paramagnetic Centers: A Detailed Relaxation Study in Static and Rotating Samples of Layered Zirconium Phosphate Materials. *J. Phys. Chem. C.* 121, 7372–7378 (2017). <https://doi.org/10.1021/acs.jpcc.7b01466>
100. National Center for Biotechnology Information. Presented at the (2019)
101. Sridharan, K.: Chapter 5 – NMR Spectroscopy. (2016)
102. Stanford, S.M., Panchal, R.G., Walker, L.M., Wu, D.J., Falk, M.D., Mitra, S., Damle, S.S., Ruble, D., Kaltcheva, T., Zhang, S., Zhang, Z.Y., Bavari, S., Barrios, A.M., Bottini, N.: High-throughput screen using a single-cell tyrosine phosphatase assay reveals biologically active inhibitors of tyrosine phosphatase CD45. *Proc. Natl. Acad. Sci. U. S. A.* 109, 13972–13977 (2012). <https://doi.org/10.1073/pnas.1205028109>
103. von Stechow, L.: Preface. *Methods Mol. Biol.* 1355, v (2016). <https://doi.org/10.1007/978-1-4939-3049-4>
104. Wiesner, C., Vliet, V. Van, Butt, E., Pavensta, H., Sto, M., Linder, S., Kremerskothen, J.: Lasp-1 Regulates Podosome Function. *PLoS One.* 7, 1–10 (2012). <https://doi.org/10.1371/Citation>

105. De Muro, M.A.: Probe design, production, and applications. In: *Molecular Biomethods Handbook: Second Edition* (2008)
106. Albumin, B.P.: Albumin from bovine serum. SigmaAldrich. (1990)
107. Brown, T.: Dot and Slot Blotting of DNA. *Curr. Protoc. Mol. Biol.* 21, 2.9.15-2.9.20 (1993). <https://doi.org/10.1002/0471142727.mb0209bs21>
108. Wong, I., Lohman, T.M.: A double-filter method for nitrocellulose-filter binding: Application to protein-nucleic acid interactions. *Proc. Natl. Acad. Sci. U. S. A.* (1993). <https://doi.org/10.1073/pnas.90.12.5428>
109. Franklin, N.E., Bonham, C.A., Xhabija, B., Vacratsis, P.O.: Differential phosphorylation of the phosphoinositide 3-phosphatase MTMR2 regulates its association with early endosomal subtypes. *J. Cell Sci.* (2013). <https://doi.org/10.1242/jcs.113928>
110. Zhang, Z.H., Lü, H.Y., Yang, S.H., Gao, J.W.: Synthesis of 2,3-dihydroquinazolin-4(1H)-ones by three-component coupling of isatoic anhydride, amines, and aldehydes catalyzed by magnetic Fe₃O₄ nanoparticles in water. *J. Comb. Chem.* (2010). <https://doi.org/10.1021/cc100047j>
111. Stenina, I.A., Voropaeva, E.Y., Veresov, A.G., Kapustin, G.I., Yaroslavtsev, A.B.: Effect of precipitation pH and heat treatment on the properties of hydrous zirconium dioxide. *Russ. J. Inorg. Chem.* (2008). <https://doi.org/10.1134/s0036023608030029>
112. Pica, M., Donnadio, A., Casciola, M.: From microcrystalline to nanosized α -zirconium phosphate: Synthetic approaches and applications of an old material with a bright future. *Coord. Chem. Rev.* 374, 218–235 (2018). <https://doi.org/10.1016/j.ccr.2018.07.002>
113. Costantino, U., Nocchetti, M., Marmottini, F., Vivani, R.: Amino Acid Derivatives of Layered Zirconium Phosphates – α -Zirconium L-(+)-Serinephosphate and Zirconium L-(+)-Serinephosphate Phosphates. *Eur. J. Inorg. Chem.* 1998, 1447–1452 (1998). [https://doi.org/10.1002/\(sici\)1099-0682\(199810\)1998:10<1447::aid-ejic1447>3.3.co;2-2](https://doi.org/10.1002/(sici)1099-0682(199810)1998:10<1447::aid-ejic1447>3.3.co;2-2)
114. Patra, C.R., Bhattacharya, R., Patra, S., Basu, S., Mukherjee, P., Mukhopadhyay, D.: Inorganic phosphate nanorods are a novel fluorescent label in cell biology. *J. Nanobiotechnology.* 4, 1–15 (2006). <https://doi.org/10.1186/1477-3155-4-11>
115. Borse, V., Jain, P., Sadawana, M., Srivastava, R.: “Turn-on” fluorescence assay for

- inorganic phosphate sensing. *Sensors Actuators, B Chem.* 225, 340–347 (2016).
<https://doi.org/10.1016/j.snb.2015.11.054>
116. Flemming, R., Fraser, H.: Nitrate and Phosphorous Levels in Selected Surface Water Sites in Southern Ontario – 1964-1994. *Surf. Water Qual.* 16 (1999)
117. Geelhoed, J.S., Hiemstra, T., Van Riemsdijk, W.H.: Phosphate and sulfate adsorption on goethite: Single anion and competitive adsorption. *Geochim. Cosmochim. Acta.* (1997).
[https://doi.org/10.1016/S0016-7037\(97\)00096-3](https://doi.org/10.1016/S0016-7037(97)00096-3)
118. Selander, R.K.: Interaction of quinacrine mustard with mononucleotides and polynucleotides. *Biochem. J.* 131, 749–755 (1973). <https://doi.org/10.1042/bj1310749>
119. Solscheid, C., Kunzelmann, S., Davis, C.T., Hunter, J.L., Nofer, A., Webb, M.R.: Development of a Reagentless Biosensor for Inorganic Phosphate, Applicable over a Wide Concentration Range. *Biochemistry.* 54, 5054–5062 (2015).
<https://doi.org/10.1021/acs.biochem.5b00449>
120. Hernandez-Ruiz, S., Abrell, L., Wickramasekara, S., Chefetz, B., Chorover, J.: Quantifying PPCP interaction with dissolved organic matter in aqueous solution: Combined use of fluorescence quenching and tandem mass spectrometry. *Water Res.* 46, 943–954 (2012). <https://doi.org/10.1016/j.watres.2011.11.061>
121. Cremers, D.A., Chinni, R.C.: Laser-induced breakdown spectroscopy-capabilities and limitations. *Appl. Spectrosc. Rev.* 44, 457–506 (2009).
<https://doi.org/10.1080/05704920903058755>
122. Baudalet, M., Boueri, M., Yu, J., Mao, X., Mao, S.S., Russo, R.: Laser ablation of organic materials for discrimination of bacteria in an inorganic background. *Ultrafast Phenom. Semicond. Nanostructure Mater.* XIII. 7214, 72140J (2009).
<https://doi.org/10.1117/12.808485>
123. Hajji, H. El, Nkhili, E., Tomao, V., Dangles, O.: Interactions of quercetin with iron and copper ions: Complexation and autoxidation. *Free Radic. Res.* 40, 303–320 (2006).
<https://doi.org/10.1080/10715760500484351>
124. Panhwar, Q.K., Memon, S.: Synthesis, characterisation, and antioxidant study of Cr(III)-rutin complex. *Chem. Pap.* 68, 614–623 (2014). <https://doi.org/10.2478/s11696-013-0494->

125. Thermo Scientific: NMR Spectra of Quercetin, <https://www.thermofisher.com/ca/en/home/industrial/spectroscopy-elemental-isotope-analysis/spectroscopy-elemental-isotope-analysis-learning-center/spectroscopy-elemental-isotope-analysis-resource-library/nmr-tech-talk/nmr-tech-talk-february-2015/nmr-spect>
126. Zhang, G.Y., Zhuang, Y.H., Shan, D., Su, G.F., Cosnier, S., Zhang, X.J.: Zirconium-based porphyrinic metal-organic framework (PCN-222): Enhanced photoelectrochemical response and its application for label-free phosphoprotein detection. *Anal. Chem.* 88, 11207–11212 (2016). <https://doi.org/10.1021/acs.analchem.6b03484>
127. Feng, Y., He, W., Zhang, X., Jia, X., Zhao, H.: The preparation of nanoparticle zirconium phosphate. *Mater. Lett.* 61, 3258–3261 (2007). <https://doi.org/10.1016/j.matlet.2006.11.132>
128. Bakhmutov, V.I., Clearfield, A.: ³¹P NMR Relaxation and Motions of Phosphate Groups in Layered Zirconium Phosphate Materials. *J. Phys. Chem. C.* 120, 19225–19233 (2016). <https://doi.org/10.1021/acs.jpcc.6b06417>
129. Amoutzias, G.D., He, Y., Gordon, J., Mossialos, D., Oliver, S.G., Van De Peer, Y.: Posttranslational regulation impacts the fate of duplicated genes. *Proc. Natl. Acad. Sci. U. S. A.* 107, 2967–2971 (2010). <https://doi.org/10.1073/pnas.0911603107>
130. Haystead, T. a J., Garrison, J.C.: Study of protein phosphorylation in intact cells. *Protein Phosphorylation.* 1–31 (1999)
131. Barragan, P., Bouvier, J.L., Roquebert, P.O., Macaluso, G., Commeau, P., Comet, B., Lafont, A., Camoin, L., Walter, U., Eigenthaler, M.: Resistance to thienopyridines: Clinical detection of coronary stent thrombosis by monitoring of vasodilator-stimulated phosphoprotein phosphorylation. *Catheter. Cardiovasc. Interv.* 59, 295–302 (2003). <https://doi.org/10.1002/ccd.10497>
132. Zhao, L., Wu, R., Han, G., Zhou, H., Ren, L., Tian, R., Zou, H.: The Highly Selective Capture of Phosphopeptides by Zirconium Phosphonate-Modified Magnetic Nanoparticles for Phosphoproteome Analysis. *J. Am. Soc. Mass Spectrom.* 19, 1176–1186 (2008). <https://doi.org/10.1016/j.jasms.2008.04.027>

133. Hofer, F., Kraml, J., Kahler, U., Kamenik, A.S., Liedl, K.R.: Catalytic Site pKa Values of Aspartic, Cysteine, and Serine Proteases: Constant pH MD Simulations. *J. Chem. Inf. Model.* 60, 3030–3042 (2020). <https://doi.org/10.1021/acs.jcim.0c00190>
134. Kahyaoglu, A.: Direct proton magnetic resonance determination of the pKa of the active center histidine in thiolsubtilisin. *Protein Sci.* 11, 965–973 (2002). <https://doi.org/10.1110/ps.3890102>
135. Campbell, N.A.: *Campbell Biology 10th Edition*, (2013)
136. Voet, D., Voet, J.G.: *Biochemistry and*. (1995)
137. Abeyrathne, P.D., Lam, J.S.: Conditions that allow for effective transfer of membrane proteins onto nitrocellulose membrane in Western blots. *Can. J. Microbiol.* 53, 526–532 (2007). <https://doi.org/10.1139/W07-007>
138. Feng, S., Ye, M., Zhou, H., Jiang, X., Jiang, X., Zou, H., Gong, B.: Immobilized zirconium ion affinity chromatography for specific enrichment of phosphopeptides in phosphoproteome analysis. *Mol. Cell. Proteomics.* 6, 1656–1665 (2007). <https://doi.org/10.1074/mcp.T600071-MCP200>
139. Stevens, S.M., Chung, A.Y., Chow, M.C., McClung, S.H., Strachan, C.N., Harmon, A.C., Denslow, N.D., Prokai, L.: Enhancement of phosphoprotein analysis using a fluorescent affinity tag and mass spectrometry. *Rapid Commun. Mass Spectrom.* 19, 2157–2162 (2005). <https://doi.org/10.1002/rcm.2027>
140. Lee, B.S., Lasanthi, G.D., Jayathilaka, P., Huang, J.S., Gupta, S.: Immobilized metal affinity electrophoresis: A novel method of capturing phosphoproteins by electrophoresis. *J. Biomol. Tech.* 19, 106–108 (2008)
141. Franklin, N.E., Taylor, G.S., Vacratsis, P.O.: Endosomal targeting of the phosphoinositide 3-phosphatase MTMR2 is regulated by an N-terminal phosphorylation site. *J. Biol. Chem.* 286, 15841–15853 (2011). <https://doi.org/10.1074/jbc.M110.209122>
142. SCHWARTZ, J.H.: The phosphorylation of alkaline phosphatase. *Proc. Natl. Acad. Sci. U. S. A.* 49, 871–878 (1963). <https://doi.org/10.1073/pnas.49.6.871>
143. Kumar, D., Jadhavar, P.S., Nautiyal, M., Sharma, H., Meena, P.K., Adane, L., Pancholia, S., Chakraborti, A.K.: Convenient synthesis of 2,3-disubstituted quinazolin-4(3H)-ones

- and 2-styryl-3-substituted quinazolin-4(3H)-ones: Applications towards the synthesis of drugs. *RSC Adv.* 5, 30819–30825 (2015). <https://doi.org/10.1039/c5ra03888j>
144. Cao, X.Y., Kong, F.Z., Zhang, Q., Liu, W.W., Liu, X.P., Li, G.Q., Zhong, R., Fan, L.Y., Xiao, H., Cao, C.X.: iPhone-imaged and cell-powered electrophoresis titration chip for the alkaline phosphatase assay in serum by the moving reaction boundary. *Lab Chip.* 18, 1758–1766 (2018). <https://doi.org/10.1039/c8lc00163d>
145. Staigerl, R.P., Miller, E.B., Staigerl, R.P., Miller, E.B.: Isatoic Anhydride. IV. Reactions with Various Nucleophiles. *J. Org. Chem.* 24, 1214–1219 (1959). <https://doi.org/10.1021/jo01091a013>
146. Osterval, E.: Sephadex Information Brochure. GE Healthc. (2007)
147. Marston, A.: Thin-layer chromatography with biological detection in phytochemistry, (2011)
148. PubChem: Isatoic anhydride, <s://pubchem.ncbi.nlm.nih.gov/compound/Isatoic-anhydride>.
149. Karvinen, J., Laitala, V., Mäkinen, M.L., Mulari, O., Tamminen, J., Hermonen, J., Hurskainen, P., Hemmi, I.: Fluorescence Quenching-Based Assays for Hydrolyzing Enzymes. Application of Time-Resolved Fluorometry in Assays for Caspase, Helicase, and Phosphatase. *Anal. Chem.* 76, 1429–1436 (2004). <https://doi.org/10.1021/ac030234b>
150. Song, X., Ma, Y., Ge, X., Zhou, H., Wang, G., Zhang, H., Tang, X., Zhang, Y.: Europium-based infinite coordination polymer nanospheres as an effective fluorescence probe for phosphate sensing. *RSC Adv.* 7, 8661–8669 (2017). <https://doi.org/10.1039/C6RA27819A>
151. Vyšniauskas, A., Qurashi, M., Gallop, N., Balaz, M., Anderson, H.L., Kuimova, M.K.: Unravelling the effect of temperature on viscosity-sensitive fluorescent molecular rotors. *Chem. Sci.* 6, 5773–5778 (2015). <https://doi.org/10.1039/c5sc02248g>
152. Rigi, M.R., Farahbakhsh, M., Rezaei, K.: Use of solid phase extraction with hydrophilic-lipophilic balance (HLB) cartridge as the appropriate option for metribuzin extraction from contaminated soils. *J. Braz. Chem. Soc.* 26, 156–164 (2015). <https://doi.org/10.5935/0103-5053.20140232>
153. Hao, T. wei, Xiang, P. yu, Mackey, H.R., Chi, K., Lu, H., Chui, H. kwong, van Loosdrecht, M.C.M., Chen, G.H.: A review of biological sulfate conversions in

wastewater treatment, (2014)

154. Varanasi, S., Batchelor, W.: Superior non-woven sheet forming characteristics of low-density cationic polymer-cellulose nanofibre colloids. *Cellulose*. 21, 3541–3550 (2014). <https://doi.org/10.1007/s10570-014-0370-8>
155. Askar, A.M.: Hyperphosphatemia: The hidden killer in chronic kidney disease. *Saudi Med. J.* 36, 13–19 (2015). <https://doi.org/10.15537/smj.2015.1.9843>
156. Coleman, J.E.: Structure and mechanism of alkaline phosphatase, (1992)
157. He, Z., Yang, C., Guo, G., Li, N., Yu, W.: Motif-All: Discovering all phosphorylation motifs. *BMC Bioinformatics*. 12, S22 (2011). <https://doi.org/10.1186/1471-2105-12-S1-S22>

APPENDICES

Appendix A (Chapter 1 supplementary material)

Emission Spectra of P_i Titrations of 25 μM Quercetin
(pH 4, excited at 375 nm)

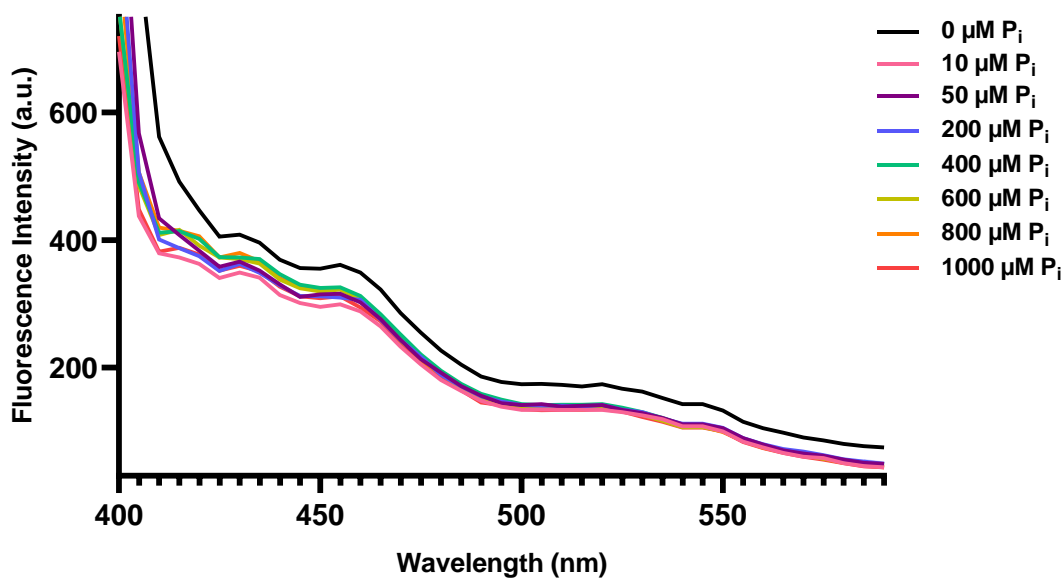


Figure A. 1: Fluorescence emission spectra of quercetin (25 μM , pH 4) with P_i titrations (ex: 375 nm).

Quercetin (25 μM , 40% MeOH, 20% 1,2-propanediol) was made in Tris-HCl (40 mM, pH 4). In a clear 96-well plate, triplicates of each sample were aliquoted (180 μL) and stock concentrations of P_i (0-1mM, 20 μL) were added. Samples were excited at 375 nm and monitored for fluorescence emission between 400 – 590 nm, every 5 seconds.

**Emission Spectra of P_i Titrations of Quercetin-Ni (II)
(pH 2, excited at 335 nm)**

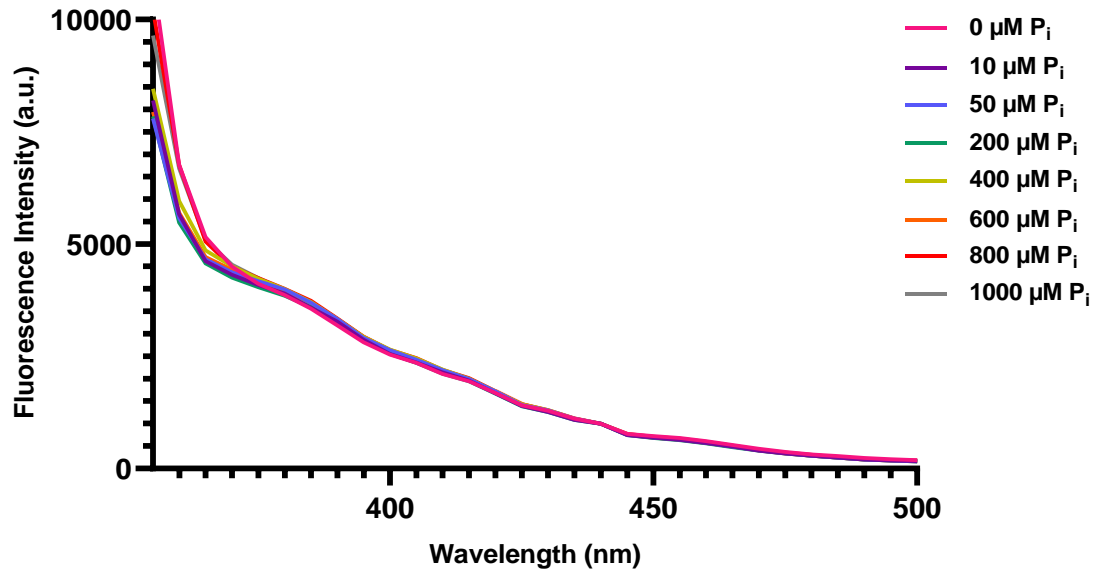


Figure A. 2: Fluorescence emission spectra of quercetin-Ni (II) (25 μ M, 50 μ M, pH 2) with P_i titrations (ex: 335 nm).

Quercetin-Ni (II) (25 μ M, 50 μ M, 40% MeOH, 20% 1,2-propanediol) was made in Tris-HCl (40 mM, pH 2). In a clear 96-well plate, triplicates of each sample were aliquoted (180 μ L) and stock concentrations of P_i (0-1mM, 20 μ L) were added. Samples were excited at 335 nm and monitored for fluorescence emission between 355 – 500 nm, every 5 seconds.

**Emission Spectra of P_i Titrations of Quercetin-Ni (II)
(pH 9, excited at 335 nm)**

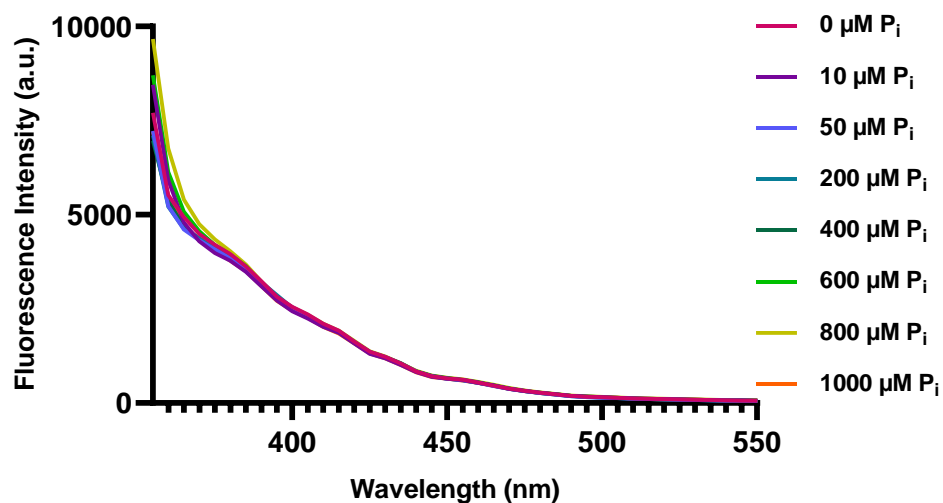


Figure A. 3: Fluorescence emission spectra of quercetin-Ni (II) (25 μM , 50 μM , pH 9) with P_i titrations (ex: 335 nm).

Quercetin-Ni (II) (25 μM , 50 μM , 40% MeOH, 20% 1,2-propanediol) was made in Tris-HCl (40 mM, pH 9). In a clear 96-well plate, triplicates of each sample were aliquoted (180 μL) and stock concentrations of P_i (0-1mM, 20 μL) were added. Samples were excited at 335 nm and monitored for fluorescence emission between 355 – 550 nm, every 5 seconds.

**Emission Spectra of P_i Titrations of Quercetin-Ni (II)
(pH 5, excited at 335 nm)**

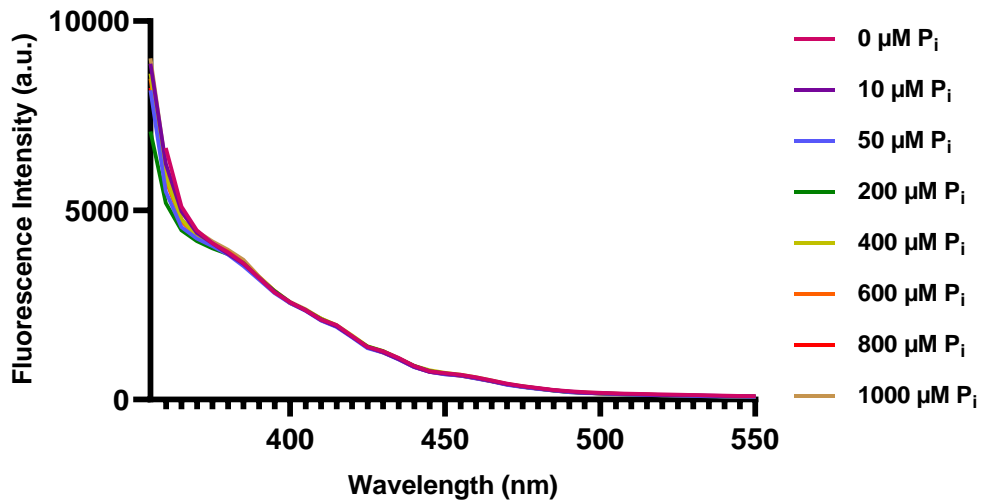


Figure A. 4: Fluorescence emission spectra of quercetin-Ni (II) (25 μM , 50 μM , pH 5) with P_i titrations (ex: 335 nm).

Quercetin-Ni (II) (25 μM , 50 μM , 40% MeOH, 20% 1,2-propanediol) was made in Tris-HCl (40 mM, pH 5). In a clear 96-well plate, triplicates of each sample were aliquoted (180 μL) and stock concentrations of P_i (0-1mM, 20 μL) were added. Samples were excited at 335 nm and monitored for fluorescence emission between 355 – 550 nm, every 5 seconds.

**Emission Spectra of P_i Titrations of Quercetin-Ni (II)
(pH 2, excited at 380 nm)**

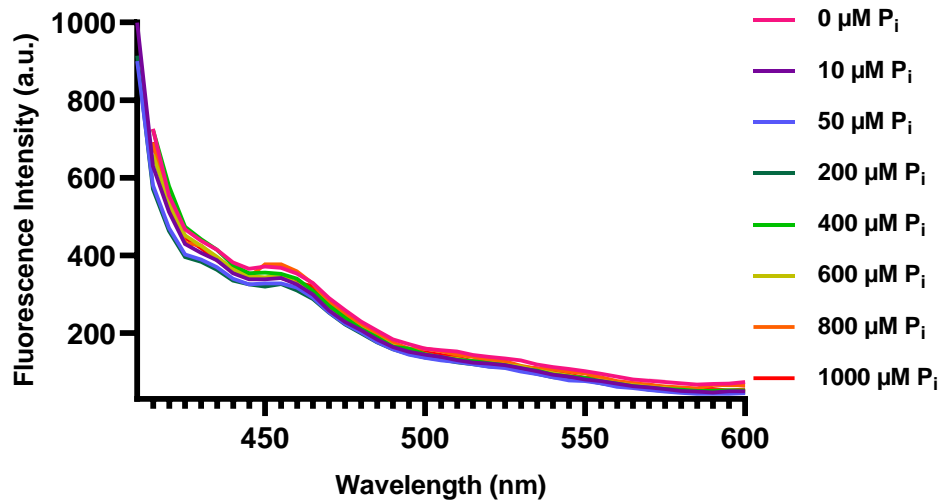


Figure A. 5: Fluorescence emission spectra of quercetin-Ni (II) (25 μM , 50 μM , pH 2) with P_i titrations (ex: 380 nm).

Quercetin-Ni (II) (25 μM , 50 μM , 40% MeOH, 20% 1,2-propanediol) was made in Tris-HCl (40 mM, pH 2). In a clear 96-well plate, triplicates of each sample were aliquoted (180 μL) and stock concentrations of P_i (0-1mM, 20 μL) were added. Samples were excited at 380 nm and monitored for fluorescence emission between 410 – 600 nm, every 5 seconds.

**Emission Spectra of P_i Titrations of Quercetin-Ni (II)
(pH 5, excited at 380 nm)**

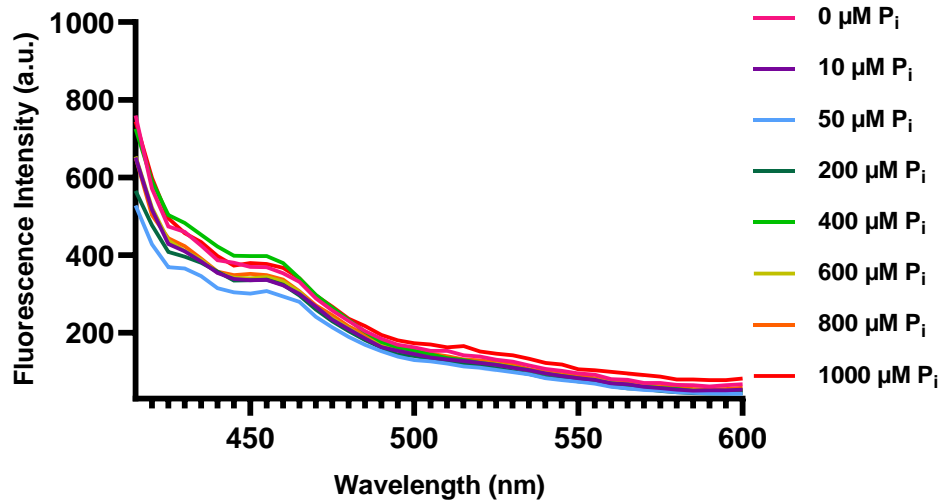


Figure A. 6: Fluorescence emission spectra of quercetin-Ni (II) (25 μM , 50 μM , pH 5) with P_i titrations (ex: 380 nm).

Quercetin-Ni (II) (25 μM , 50 μM , 40% MeOH, 20% 1,2-propanediol) was made in Tris-HCl (40 mM, pH 5). In a clear 96-well plate, triplicates of each sample were aliquoted (180 μL) and stock concentrations of P_i (0-1mM, 20 μL) were added. Samples were excited at 380 nm and monitored for fluorescence emission between 415 – 600 nm, every 5 seconds.

**Emission Spectra of P_i Titrations of Quercetin-Ni (II)
(pH 9, excited at 380 nm)**

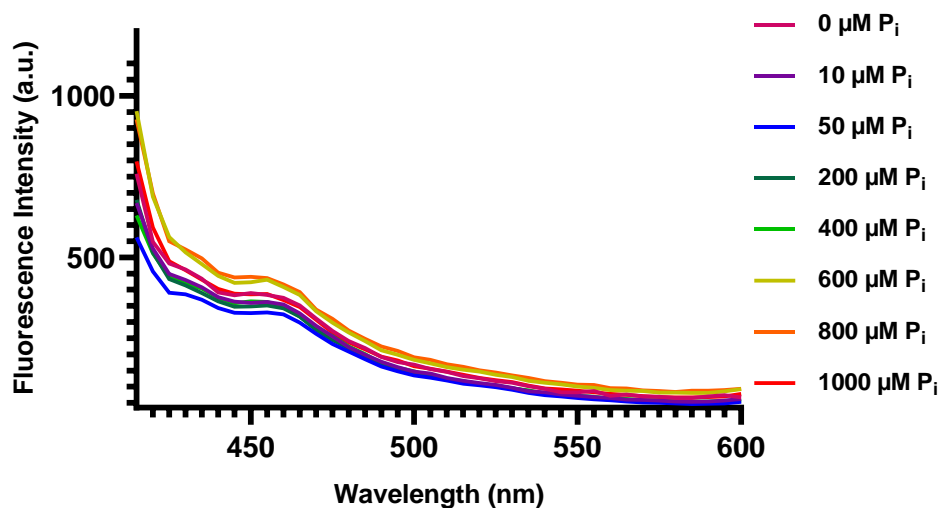


Figure A. 7: Fluorescence emission spectra of quercetin-Ni (II) (25 μM , 50 μM , pH 9) with P_i titrations (ex: 380 nm).

Quercetin-Ni (II) (25 μM , 50 μM , 40% MeOH, 20% 1,2-propanediol) was made in Tris-HCl (40 mM, pH 9). In a clear 96-well plate, triplicates of each sample were aliquoted (180 μL) and stock concentrations of P_i (0-1mM, 20 μL) were added. Samples were excited at 380 nm and monitored for fluorescence emission between 415 – 600 nm, every 5 seconds.

**Emission Spectra of P_i Titrations of Quercetin-Al (III)
(pH 2, excited at 320 nm)**

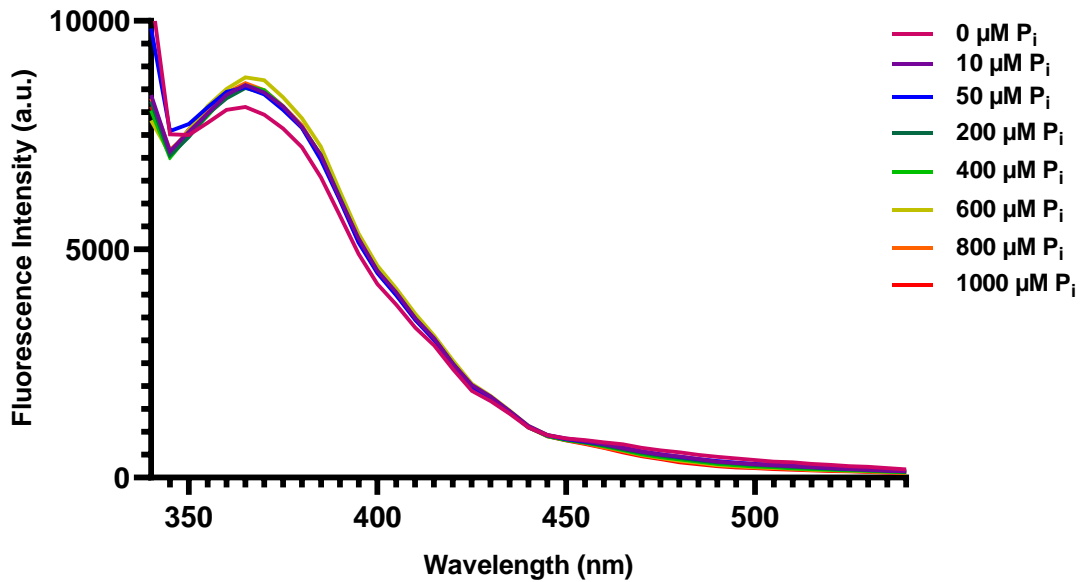


Figure A. 8: Fluorescence emission spectra of quercetin-Al (III) (25 μM , 50 μM , pH 2) with P_i titrations (ex: 320 nm).

Quercetin-Al (III) (25 μM , 50 μM , 40% MeOH, 20% 1,2-propanediol) was made in Tris-HCl (40 mM, pH 2). In a clear 96-well plate, triplicates of each sample were aliquoted (180 μL) and stock concentrations of P_i (0-1mM, 20 μL) were added. Samples were excited at 320 nm and monitored for fluorescence emission between 340 – 540 nm, every 5 seconds.

**Emission Spectra of P_i Titrations of Quercetin-Al (III)
(pH 5, excited at 320 nm)**

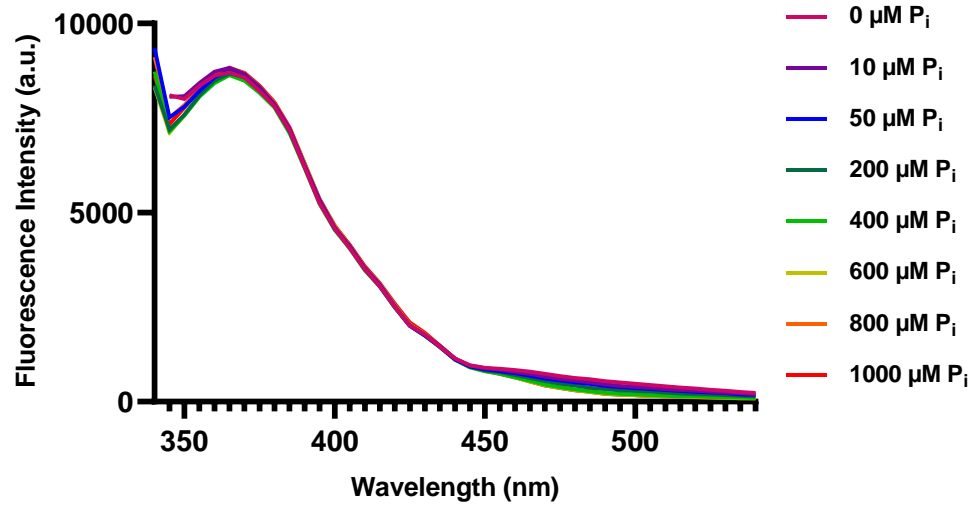


Figure A. 9: Fluorescence emission spectra of quercetin-Al (III) (25 μ M, 50 μ M, pH 5) with P_i titrations (ex: 320 nm).

Quercetin-Al (III) (25 μ M, 50 μ M, 40% MeOH, 20% 1,2-propanediol) was made in Tris-HCl (40 mM, pH 5). In a clear 96-well plate, triplicates of each sample were aliquoted (180 μ L) and stock concentrations of P_i (0-1mM, 20 μ L) were added. Samples were excited at 320 nm and monitored for fluorescence emission between 340 – 540 nm, every 5 seconds.

**Emission Spectra of P_i Titrations of Quercetin-Al (III)
(pH 9, excited at 320 nm)**

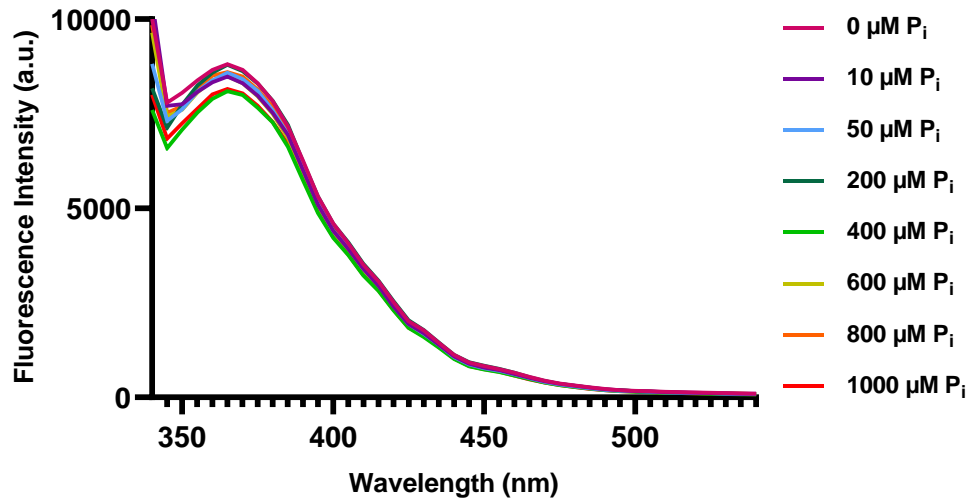


Figure A. 10: Fluorescence emission spectra of quercetin-Al (III) (25 μM , 50 μM , pH 9) with P_i titrations (ex: 320 nm).

Quercetin-Al (III) (25 μM , 50 μM , 40% MeOH, 20% 1,2-propanediol) was made in Tris-HCl (40 mM, pH 9). In a clear 96-well plate, triplicates of each sample were aliquoted (180 μL) and stock concentrations of P_i (0-1mM, 20 μL) were added. Samples were excited at 320 nm and monitored for fluorescence emission between 340 – 540 nm, every 5 seconds.

**Emission Spectra of P_i Titrations of Quercetin-Al (III)
(pH 12, excited at 320 nm)**

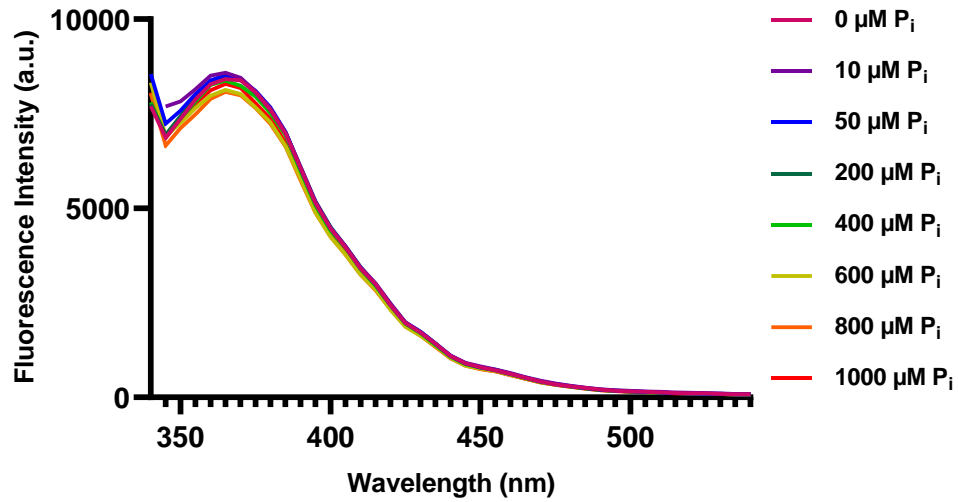


Figure A. 11: Fluorescence emission spectra of quercetin-Al (III) (25 μM , 50 μM , pH 12) with P_i titrations (ex: 320 nm).

Quercetin-Al (III) (25 μM , 50 μM , 40% MeOH, 20% 1,2-propanediol) was made in Tris-HCl (40 mM, pH 12). In a clear 96-well plate, triplicates of each sample were aliquoted (180 μL) and stock concentrations of P_i (0-1mM, 20 μL) were added. Samples were excited at 320 nm and monitored for fluorescence emission between 340 – 540 nm, every 5 seconds.

**Emission Spectra of P_i Titrations of Quercetin-Al (III)
(pH 2, excited at 380 nm)**

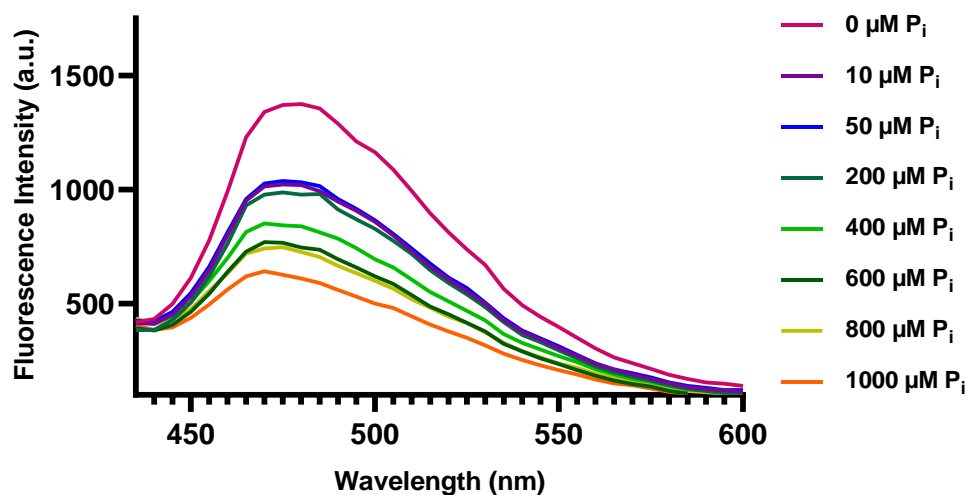


Figure A. 12: Fluorescence emission spectra of quercetin-Al (III) (25 μM , 50 μM , pH 2) with P_i titrations (ex: 380 nm).

Quercetin-Al (III) (25 μM , 50 μM , 40% MeOH, 20% 1,2-propanediol) was made in Tris-HCl (40 mM, pH 2). In a clear 96-well plate, triplicates of each sample were aliquoted (180 μL) and stock concentrations of P_i (0-1mM, 20 μL) were added. Samples were excited at 380 nm and monitored for fluorescence emission between 435 – 600 nm, every 5 seconds.

**Emission Spectra of P_i Titrations of Quercetin-Al (III)
(pH 5, excited at 380 nm)**

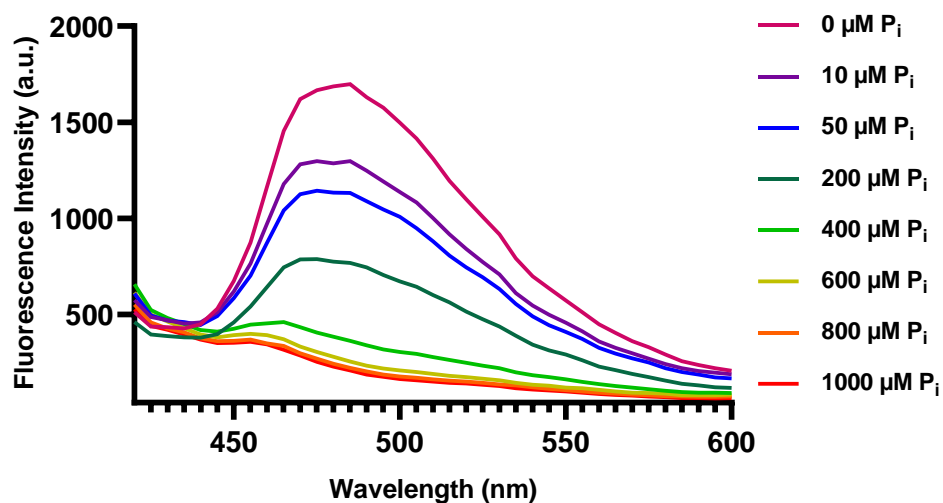


Figure A. 13: Fluorescence emission spectra of quercetin-Al (III) (25 μM , 50 μM , pH 5) with P_i titrations (ex: 380 nm).

Quercetin-Al (III) (25 μM , 50 μM , 40% MeOH, 20% 1,2-propanediol) was made in Tris-HCl (40 mM, pH 5). In a clear 96-well plate, triplicates of each sample were aliquoted (180 μL) and stock concentrations of P_i (0-1mM, 20 μL) were added. Samples were excited at 380 nm and monitored for fluorescence emission between 430 – 600 nm, every 5 seconds.

**Emission Spectra of P_i Titrations of Quercetin-Al (III)
(pH 9, excited at 380 nm)**

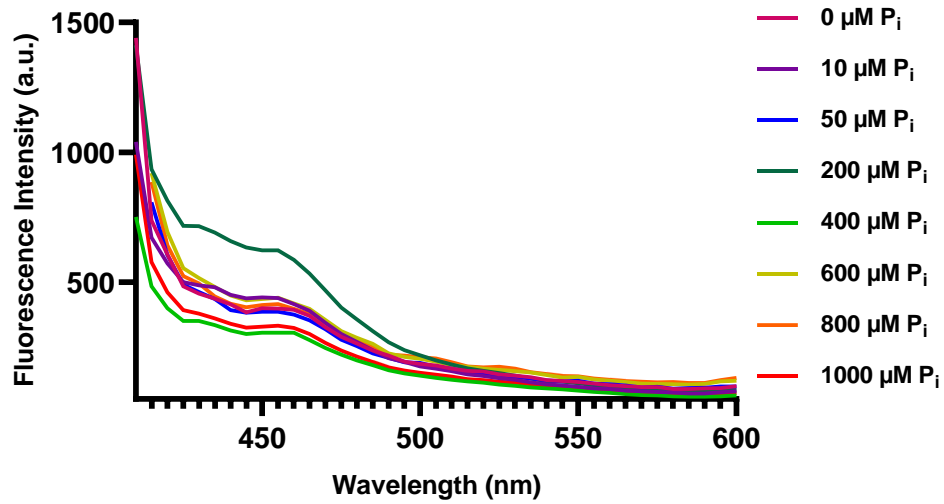


Figure A. 14: Fluorescence emission spectra of quercetin-Al (III) (25 μM , 50 μM , pH 9) with P_i titrations (ex: 380 nm).

Quercetin-Al (III) (25 μM , 50 μM , 40% MeOH, 20% 1,2-propanediol) was made in Tris-HCl (40 mM, pH 9). In a clear 96-well plate, triplicates of each sample were aliquoted (180 μL) and stock concentrations of P_i (0-1mM, 20 μL) were added. Samples were excited at 380 nm and monitored for fluorescence emission between 410 – 600 nm, every 5 seconds.

**Emission Spectra of P_i Titrations of Quercetin-Al (III)
(pH 12, excited at 380 nm)**

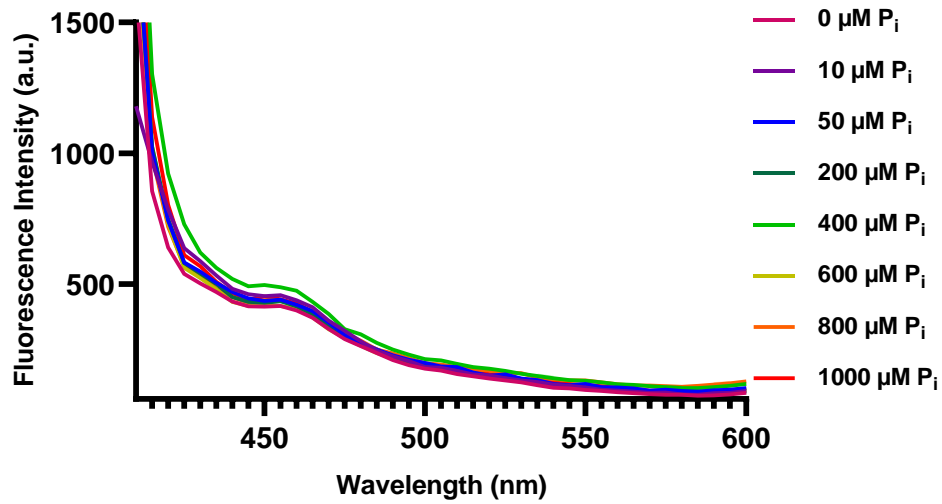


Figure A. 15: Fluorescence emission spectra of quercetin-Al (III) (25 μM , 50 μM , pH 12) with P_i titrations (ex: 380 nm).

Quercetin-Al (III) (25 μM , 50 μM , 40% MeOH, 20% 1,2-propanediol) was made in Tris-HCl (40 mM, pH 12). In a clear 96-well plate, triplicates of each sample were aliquoted (180 μL) and stock concentrations of P_i (0-1mM, 20 μL) were added. Samples were excited at 380 nm and monitored for fluorescence emission between 410 – 600 nm, every 5 seconds.

**Emission Spectra of P_i Titrations of Quercetin-Al (III)
(pH 9, excited at 425 nm)**

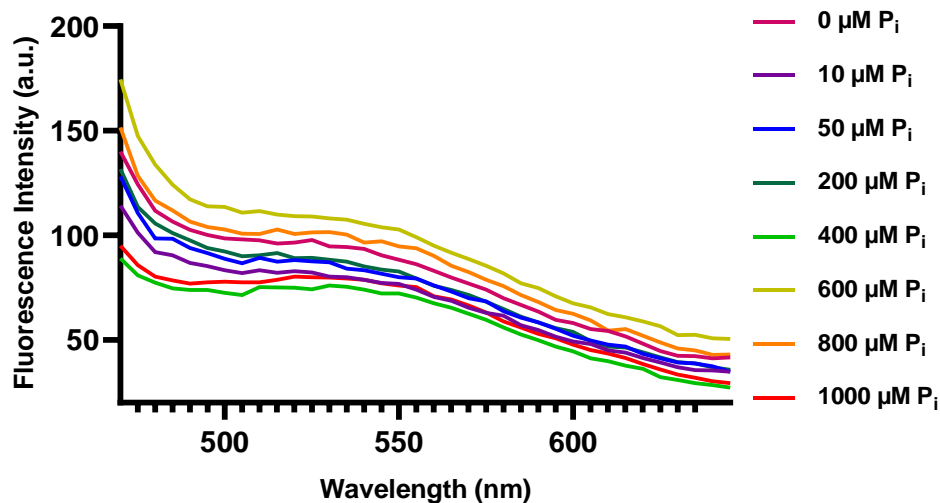


Figure A. 16: Fluorescence emission spectra of quercetin-Al (III) (25 μM , 50 μM , pH 9) with P_i titrations (ex: 425 nm).

Quercetin-Al (III) (25 μM , 50 μM , 40% MeOH, 20% 1,2-propanediol) was made in Tris-HCl (40 mM, pH 9). In a clear 96-well plate, triplicates of each sample were aliquoted (180 μL) and stock concentrations of P_i (0-1mM, 20 μL) were added. Samples were excited at 425 nm and monitored for fluorescence emission between 470 – 640 nm, every 5 seconds.

**Emission Spectra of P_i Titrations of Quercetin-Al (III)
(pH 12, excited at 425 nm)**

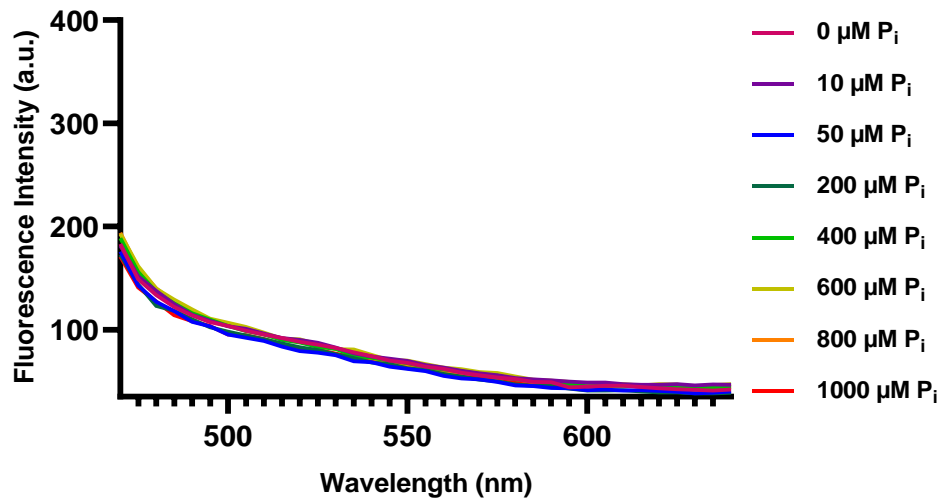


Figure A. 17: Fluorescence emission spectra of quercetin-Al (III) (25 μM , 50 μM , pH 12) with P_i titrations (ex: 425 nm).

Quercetin-Al (III) (25 μM , 50 μM , 40% MeOH, 20% 1,2-propanediol) was made in Tris-HCl (40 mM, pH 12). In a clear 96-well plate, triplicates of each sample were aliquoted (180 μL) and stock concentrations of P_i (0-1mM, 20 μL) were added. Samples were excited at 425 nm and monitored for fluorescence emission between 470 – 640 nm, every 5 seconds.

**Emission Spectra of P_i Titrations of Quercetin-Al (III)
(pH 9, excited at 440 nm)**

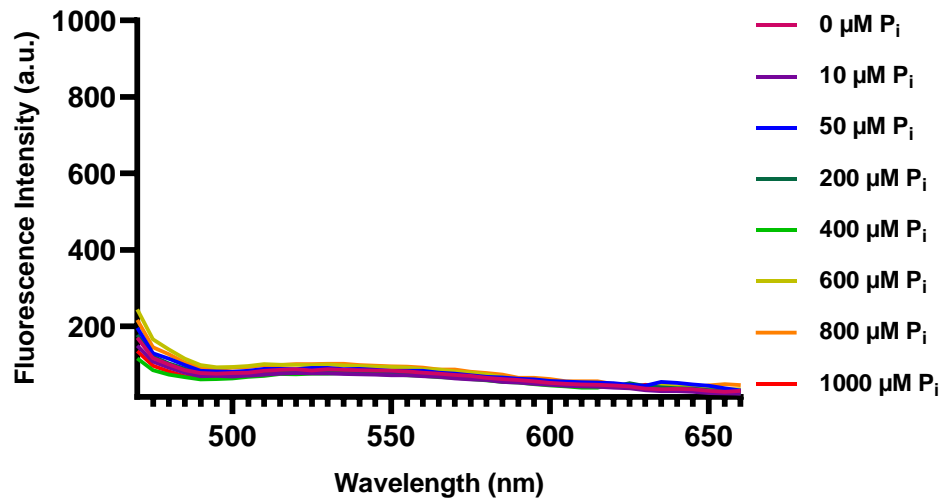


Figure A. 18: Fluorescence emission spectra of quercetin-Al (III) (25 μM , 50 μM , pH 9) with P_i titrations (ex: 440 nm).

Quercetin-Al (III) (25 μM , 50 μM , 40% MeOH, 20% 1,2-propanediol) was made in Tris-HCl (40 mM, pH 9). In a clear 96-well plate, triplicates of each sample were aliquoted (180 μL) and stock concentrations of P_i (0-1mM, 20 μL) were added. Samples were excited at 440 nm and monitored for fluorescence emission between 470 – 660 nm, every 5 seconds.

**Emission Spectra of P_i Titrations of Quercetin-Al (III)
(pH 12, excited at 440 nm)**

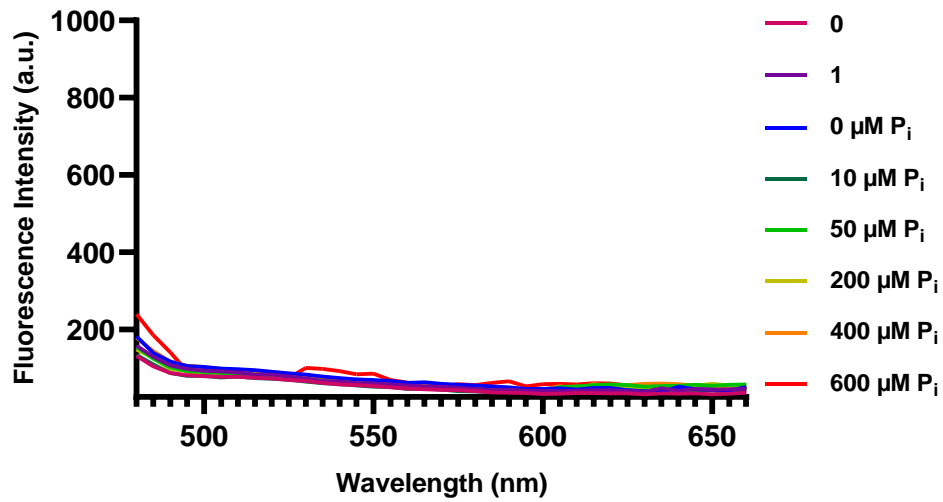


Figure A. 19: Fluorescence emission spectra of quercetin-Al (III) (25 μM , 50 μM , pH 12) with P_i titrations (ex: 440 nm).

Quercetin-Al (III) (25 μM , 50 μM , 40% MeOH, 20% 1,2-propanediol) was made in Tris-HCl (40 mM, pH 12). In a clear 96-well plate, triplicates of each sample were aliquoted (180 μL) and stock concentrations of P_i (0-1mM, 20 μL) were added. Samples were excited at 440 nm and monitored for fluorescence emission between 480 – 660 nm, every 5 seconds.

**Emission Spectra of P_i Titrations of Quercetin-Fe (III)
(pH 7, excited at 330 nm)**

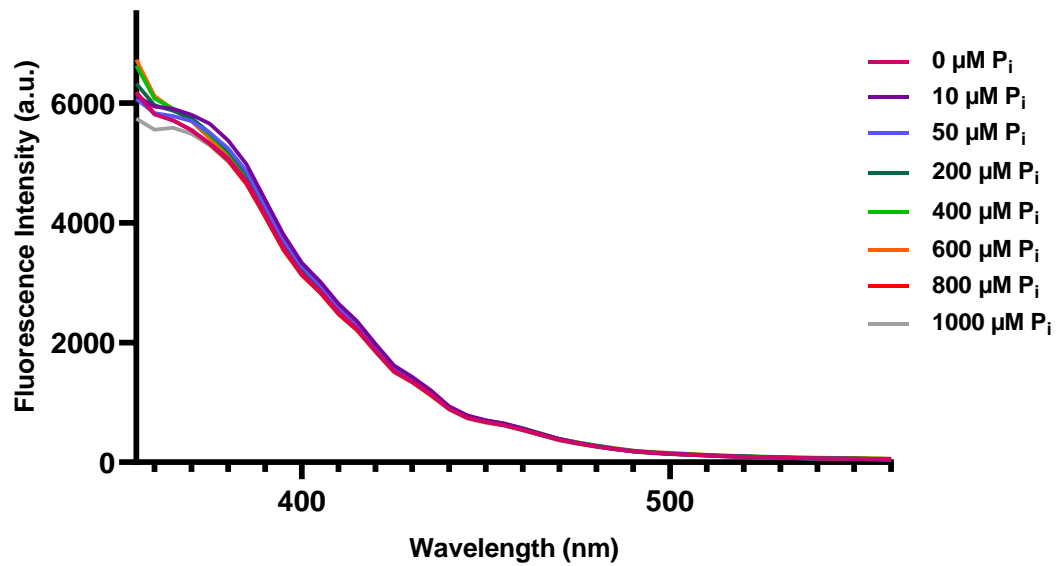


Figure A. 20: Fluorescence emission spectra of quercetin-Fe (III) (25 μM , 50 μM , pH 7) with P_i titrations (ex: 330 nm).

Quercetin-Fe (III) (25 μM , 50 μM , 40% MeOH, 20% 1,2-propanediol) was made in Tris-HCl (40 mM, pH 7). In a clear 96-well plate, triplicates of each sample were aliquoted (180 μL) and stock concentrations of P_i (0-1mM, 20 μL) were added. Samples were excited at 330 nm and monitored for fluorescence emission between 365 – 560 nm, every 5 seconds.

**Emission Spectra of P_i Titrations of Quercetin-Fe (III)
(pH 11, excited at 330 nm)**

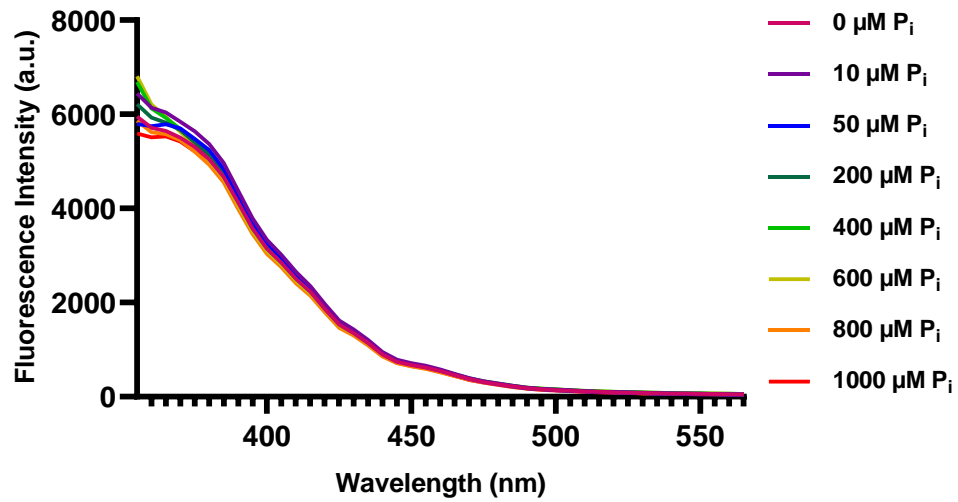


Figure A. 21: Fluorescence emission spectra of quercetin-Fe (III) (25 μM , 50 μM , pH 11) with P_i titrations (ex: 330 nm).

Quercetin-Fe (III) (25 μM , 50 μM , 40% MeOH, 20% 1,2-propanediol) was made in Tris-HCl (40 mM, pH 11). In a clear 96-well plate, triplicates of each sample were aliquoted (180 μL) and stock concentrations of P_i (0-1mM, 20 μL) were added. Samples were excited at 330 nm and monitored for fluorescence emission between 355 – 565 nm, every 5 seconds.

**Emission Spectra of P_i Titrations of Quercetin-Fe (III)
(pH 7, excited at 445 nm)**

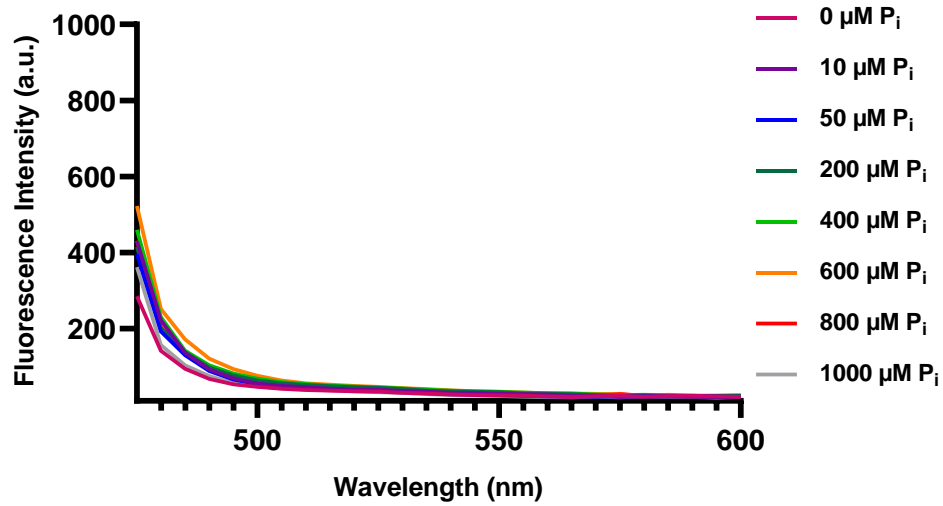


Figure A. 22: Fluorescence emission spectra of quercetin-Fe (III) (25 μM , 50 μM , pH 7) with P_i titrations (ex: 445 nm).

Quercetin-Fe (III) (25 μM , 50 μM , 40% MeOH, 20% 1,2-propanediol) was made in Tris-HCl (40 mM, pH 7). In a clear 96-well plate, triplicates of each sample were aliquoted (180 μL) and stock concentrations of P_i (0-1mM, 20 μL) were added. Samples were excited at 445 nm and monitored for fluorescence emission between 475 – 600 nm, every 5 seconds.

**Emission Spectra of P_i Titrations of Quercetin-Fe (III)
(pH 11, excited at 445 nm)**

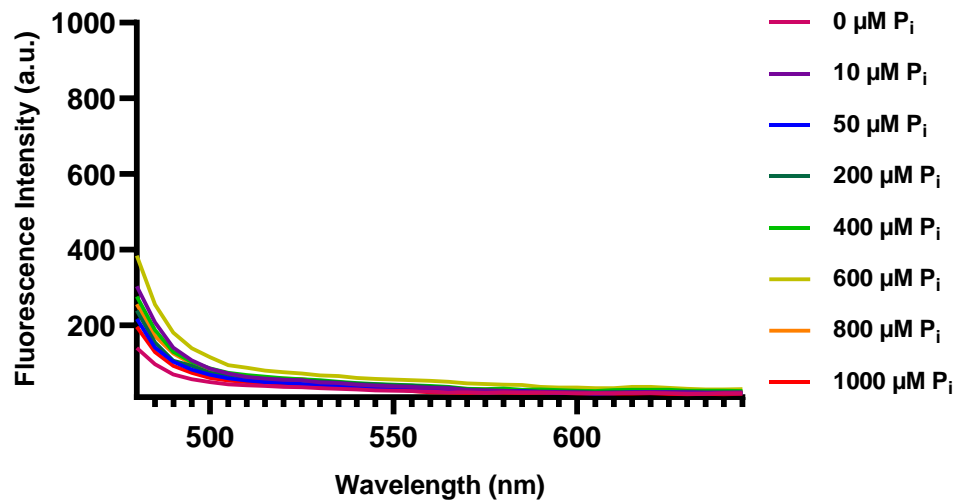


Figure A. 23: Fluorescence emission spectra of quercetin-Fe (III) (25 μM , 50 μM , pH 11) with P_i titrations (ex: 445 nm).

Quercetin-Fe (III) (25 μM , 50 μM , 40% MeOH, 20% 1,2-propanediol) was made in Tris-HCl (40 mM, pH 11). In a clear 96-well plate, triplicates of each sample were aliquoted (180 μL) and stock concentrations of P_i (0-1mM, 20 μL) were added. Samples were excited at 445 nm and monitored for fluorescence emission between 485 – 645 nm, every 5 seconds.

**Emission Spectra of P_i Titrations of Quercetin-Zr (IV)
(pH 3, excited at 325 nm)**

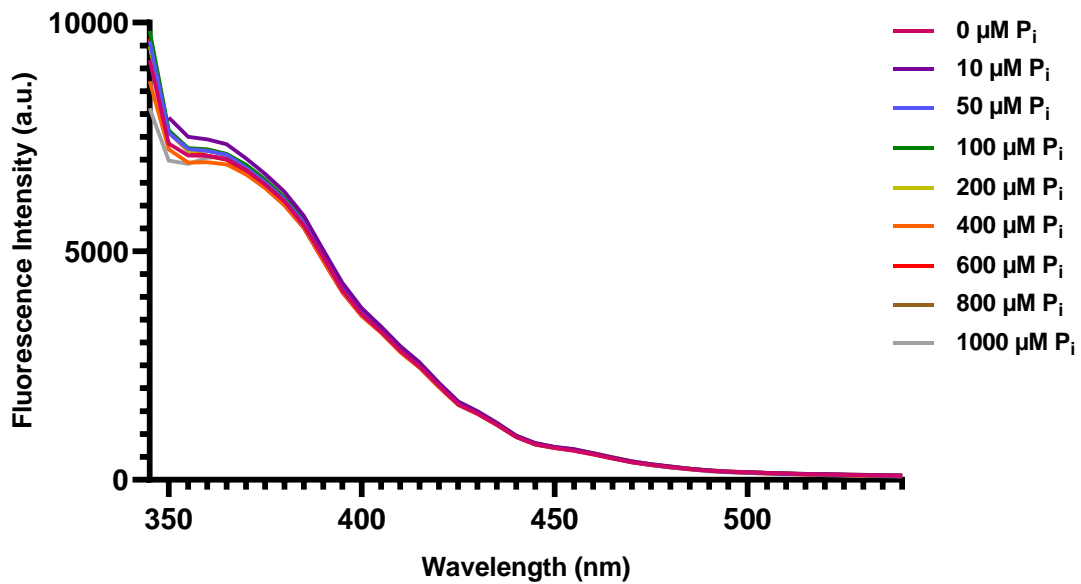


Figure A. 24: Fluorescence emission spectra of quercetin-Zr (IV) (25 μM , 50 μM , pH 3) with P_i titrations (ex: 325 nm).

Quercetin-Zr (IV) (25 μM , 50 μM , 40% MeOH, 20% 1,2-propanediol) was made in Tris-HCl (40 mM, pH 3). In a clear 96-well plate, triplicates of each sample were aliquoted (180 μL) and stock concentrations of P_i (0-1mM, 20 μL) were added. Samples were excited at 325 nm and monitored for fluorescence emission between 345 – 550 nm, every 5 seconds.

**Emission Spectra of P_i Titrations of Quercetin-Zr (IV)
(pH 9, excited at 325 nm)**

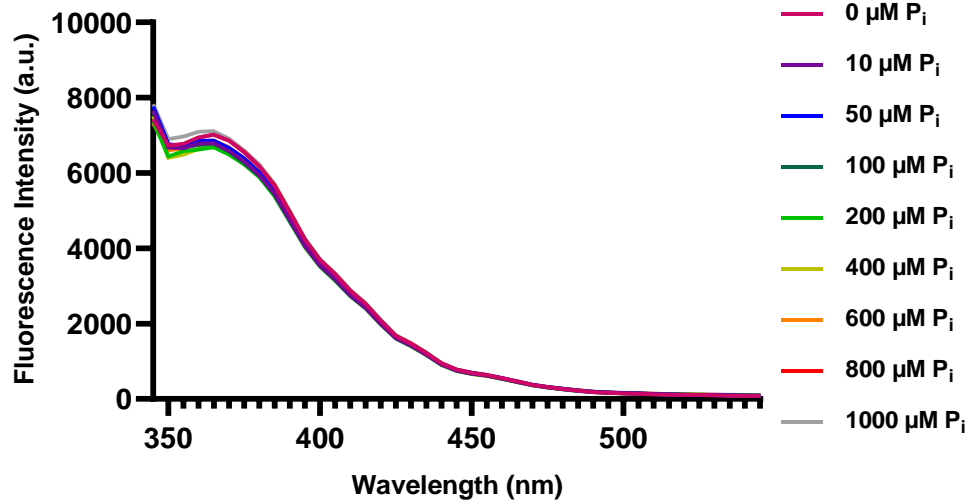


Figure A. 25: Fluorescence emission spectra of quercetin-Zr (IV) (25 μM , 50 μM , pH 9) with P_i titrations (ex: 325 nm).

Quercetin-Zr (IV) (25 μM , 50 μM , 40% MeOH, 20% 1,2-propanediol) was made in Tris-HCl (40 mM, pH 9). In a clear 96-well plate, triplicates of each sample were aliquoted (180 μL) and stock concentrations of P_i (0-1mM, 20 μL) were added. Samples were excited at 325 nm and monitored for fluorescence emission between 345 – 550 nm, every 5 seconds.

**Emission Spectra of P_i Titrations of Quercetin-Zr (IV)
(pH 12, excited at 325 nm)**

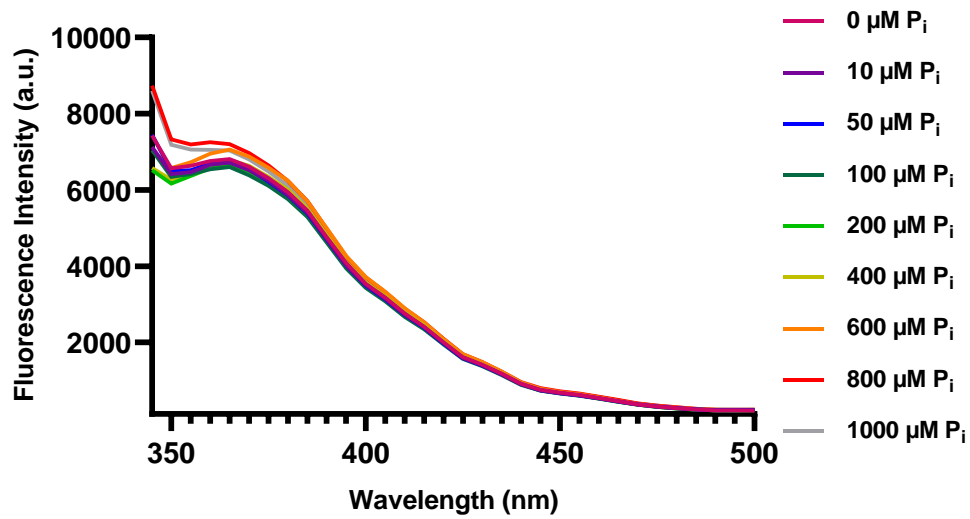


Figure A. 26: Fluorescence emission spectra of quercetin-Zr (IV) (25 μM , 50 μM , pH 12) with P_i titrations (ex: 325 nm).

Quercetin-Zr (IV) (25 μM , 50 μM , 40% MeOH, 20% 1,2-propanediol) was made in Tris-HCl (40 mM, pH 12). In a clear 96-well plate, triplicates of each sample were aliquoted (180 μL) and stock concentrations of P_i (0-1mM, 20 μL) were added. Samples were excited at 325 nm and monitored for fluorescence emission between 345 – 550 nm, every 5 seconds.

**Emission Spectra of P_i Titrations of Quercetin-Zr (IV)
(pH 3, excited at 455 nm)**

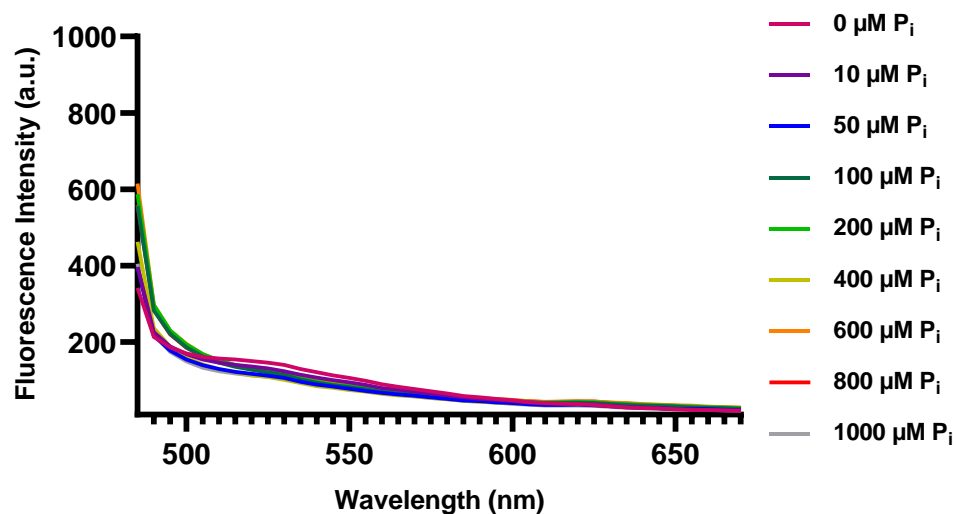


Figure A. 27: Fluorescence emission spectra of quercetin-Zr (IV) (25 μ M, 50 μ M, pH 3) with P_i titrations (ex: 455 nm).

Quercetin-Zr (IV) (25 μ M, 50 μ M, 40% MeOH, 20% 1,2-propanediol) was made in Tris-HCl (40 mM, pH 3). In a clear 96-well plate, triplicates of each sample were aliquoted (180 μ L) and stock concentrations of P_i (0-1mM, 20 μ L) were added. Samples were excited at 455 nm and monitored for fluorescence emission between 485 – 670 nm, every 5 seconds.

**Emission Spectra of P_i Titrations of Quercetin-Zr (IV)
(pH 12, excited at 455 nm)**

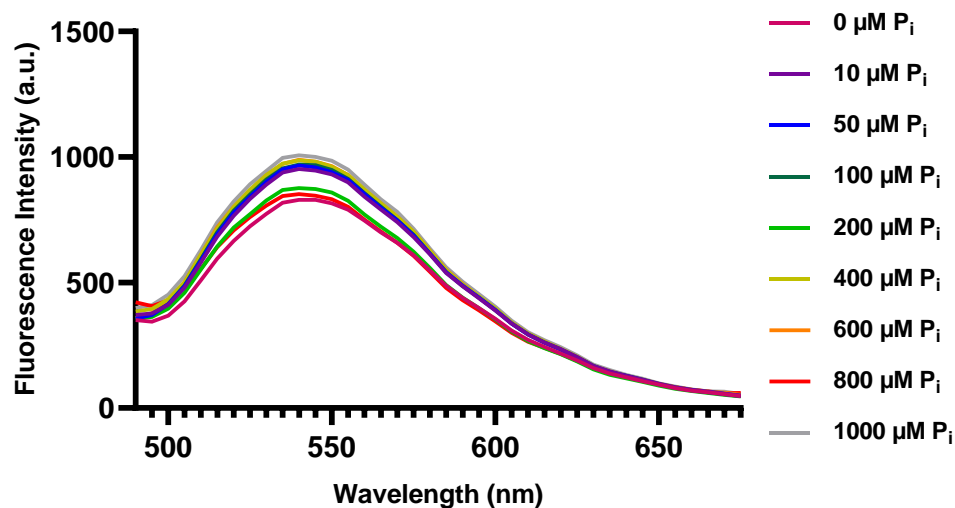


Figure A. 28: Fluorescence emission spectra of quercetin-Zr (IV) (25 μM , 50 μM , pH 12) with P_i titrations (ex: 455 nm).

Quercetin-Zr (IV) (25 μM , 50 μM , 40% MeOH, 20% 1,2-propanediol) was made in Tris-HCl (40 mM, pH 12). In a clear 96-well plate, triplicates of each sample were aliquoted (180 μL) and stock concentrations of P_i (0-1mM, 20 μL) were added. Samples were excited at 455 nm and monitored for fluorescence emission between 490 – 675 nm, every 5 seconds.

**Emission Spectra of P_i Titrations of Quercetin-Zr (IV)
(pH 3, excited at 465 nm)**

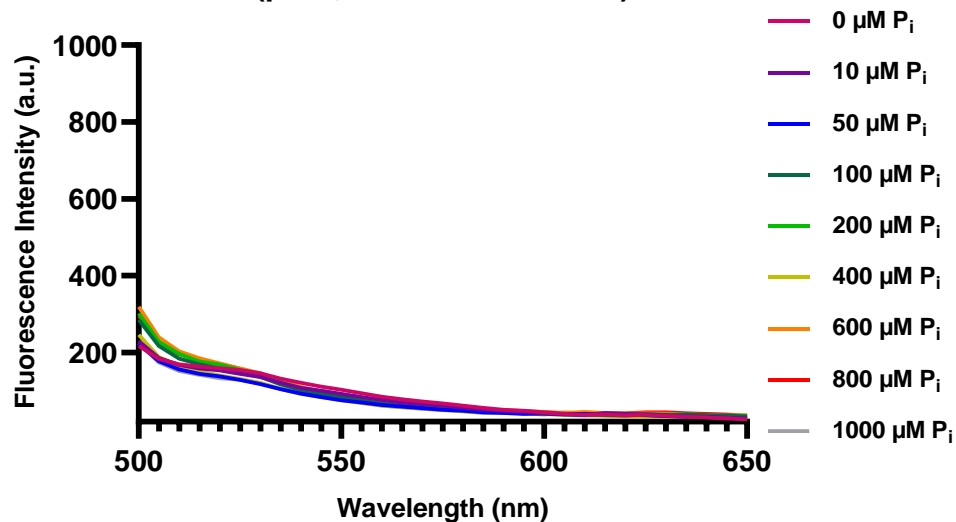


Figure A. 29: Fluorescence emission spectra of quercetin-Zr (IV) (25 μM , 50 μM , pH 3) with P_i titrations (ex: 465 nm).

Quercetin-Zr (IV) (25 μM , 50 μM , 40% MeOH, 20% 1,2-propanediol) was made in Tris-HCl (40 mM, pH 3). In a clear 96-well plate, triplicates of each sample were aliquoted (180 μL) and stock concentrations of P_i (0-1mM, 20 μL) were added. Samples were excited at 465 nm and monitored for fluorescence emission between 500 – 650 nm, every 5 seconds.

**Emission Spectra of P_i Titrations of Quercetin-Zr (IV)
(pH 12, excited at 465 nm)**

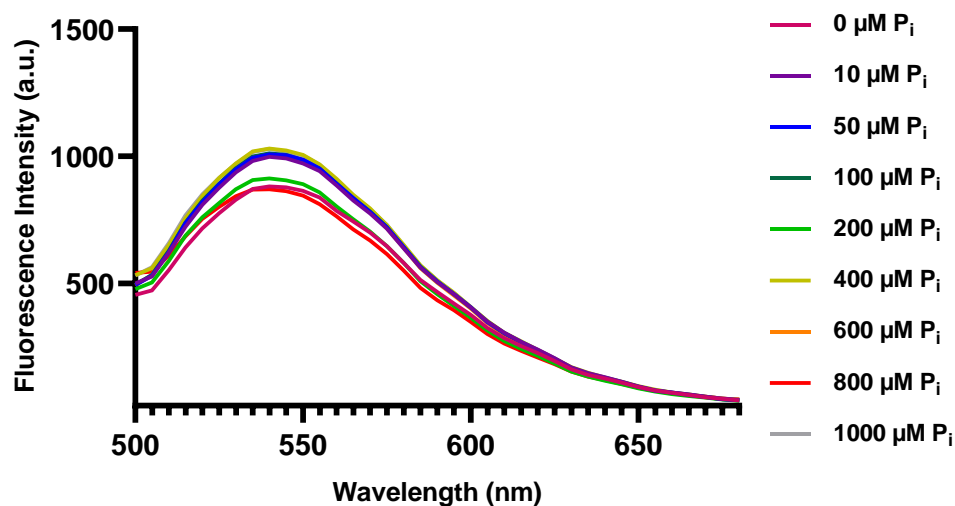


Figure A. 30: Fluorescence emission spectra of quercetin-Zr (IV) (25 μM , 50 μM , pH 12) with P_i titrations (ex: 465 nm).

Quercetin-Zr (IV) (25 μM , 50 μM , 40% MeOH, 20% 1,2-propanediol) was made in Tris-HCl (40 mM, pH 12). In a clear 96-well plate, triplicates of each sample were aliquoted (180 μL) and stock concentrations of P_i (0-1mM, 20 μL) were added. Samples were excited at 465 nm and monitored for fluorescence emission between 500 – 650 nm, every 5 seconds.

**Emission Spectra of P_i Titrations of Quercetin-Zr (IV)
(pH 3, excited at 470 nm)**

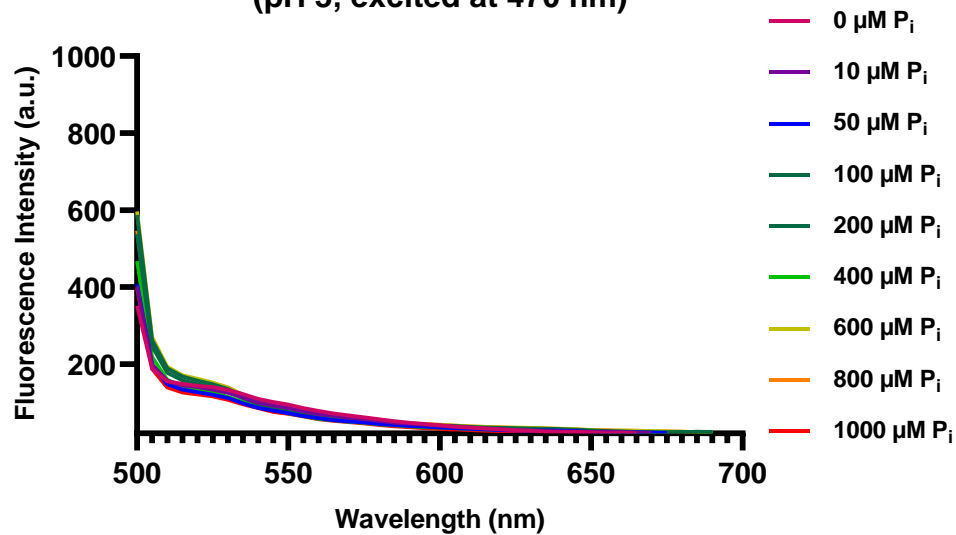


Figure A. 31: Fluorescence emission spectra of quercetin-Zr (IV) (25 μ M, 50 μ M, pH 3) with P_i titrations (ex: 470 nm).

Quercetin-Zr (IV) (25 μ M, 50 μ M, 40% MeOH, 20% 1,2-propanediol) was made in Tris-HCl (40 mM, pH 3). In a clear 96-well plate, triplicates of each sample were aliquoted (180 μ L) and stock concentrations of P_i (0-1mM, 20 μ L) were added. Samples were excited at 470 nm and monitored for fluorescence emission between 500 – 700 nm, every 5 seconds.

**Emission Spectra of P_i Titrations of Quercetin-Zr (IV)
(pH 12, excited at 470 nm)**

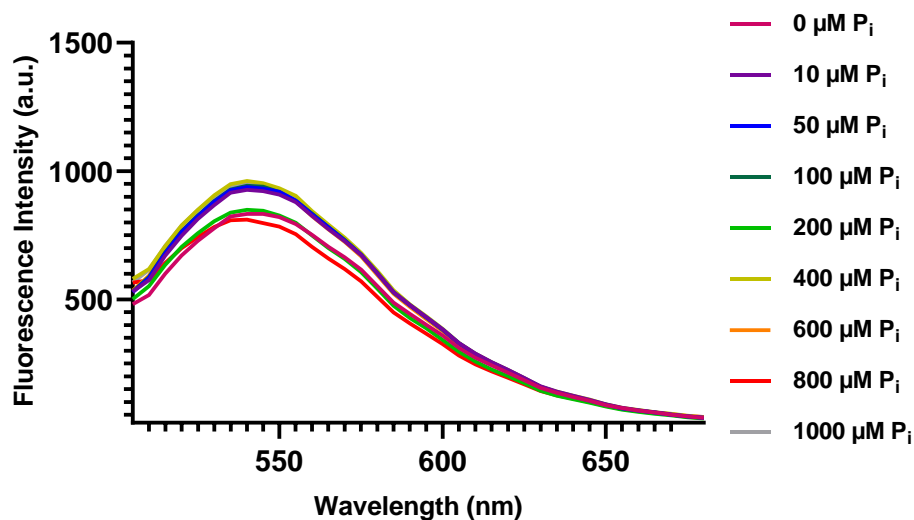


Figure A. 32: Fluorescence emission spectra of quercetin-Zr (IV) (25 μM , 50 μM , pH 12) with P_i titrations (ex: 470 nm).

Quercetin-Zr (IV) (25 μM , 50 μM , 40% MeOH, 20% 1,2-propanediol) was made in Tris-HCl (40 mM, pH 12). In a clear 96-well plate, triplicates of each sample were aliquoted (180 μL) and stock concentrations of P_i (0-1mM, 20 μL) were added. Samples were excited at 470 nm and monitored for fluorescence emission between 505 – 680 nm, every 5 seconds.

Appendix B (Chapter 2 supplementary material)

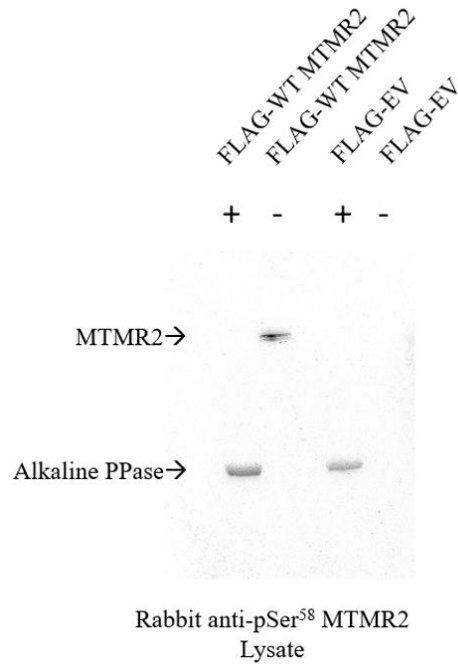


Figure B. 1: Immunoblot of alkaline phosphatase treated MTMR2 using rabbit anti-pSer⁵⁸ antibody.

WT (wild-type) MTMR2 (myotubularin-related protein 2) and empty vector (control) samples were subject to alkaline phosphatase treatment. Blot was incubated with rabbit anti-pSer⁵⁸ (anti-phosphoserine 58) MTMR2 specific antibody and visualized for chemiluminescence. Procedure performed by Justin Roberto of the Vacratsis research group.

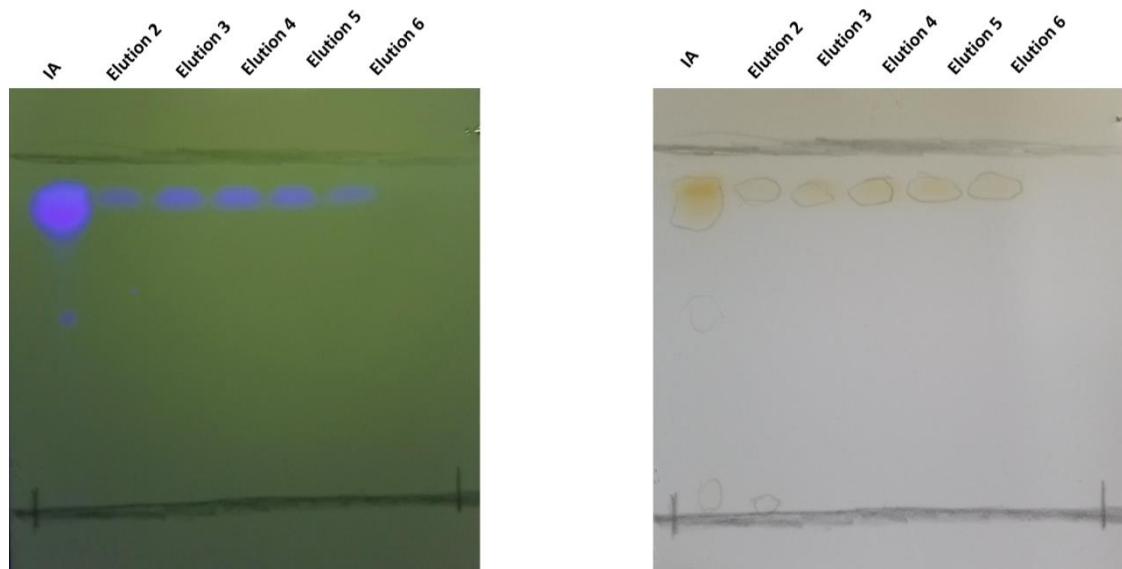


Figure B. 2: Thin Layer Chromatography performed on SiliaPlate™ TLC aluminum backed TLC plates for IA (isatoic anhydride).

Isatoic anhydride was applied to a packed Sephadex® QAE column, washed with MilliQ (100 mL) and eluted with NaCl (0.1 M, pH 7). Thin Layer Chromatography was performed on SiliaPlate™ TLC aluminum backed TLC plates for IA and elution samples (shown from left to right) from Sephadex-QAE Econo-Column® [72].

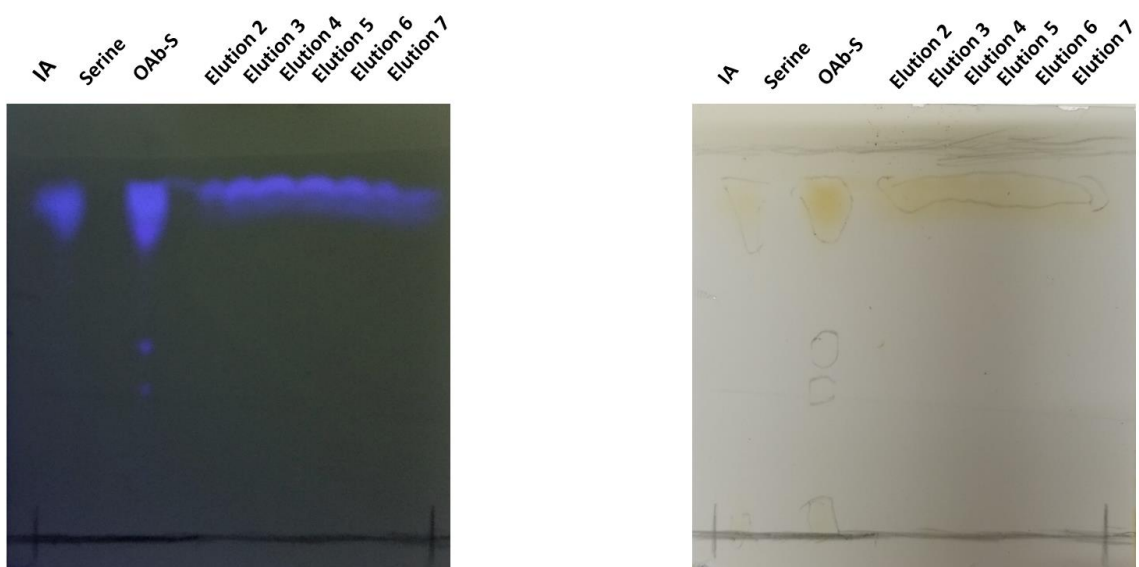


Figure B. 3: Thin Layer Chromatography performed on SiliaPlate™ TLC aluminum backed TLC plates for *o*-aminobenzoyl-*L*-serine.

o-aminobenzoyl-*L*-serine (OAb-S) was applied to a packed Sephadex® QAE column, washed with MilliQ (100 mL) and eluted with NaCl (0.1 M, pH 7). Thin Layer Chromatography was performed on SiliaPlate™ TLC aluminum backed TLC plates for (from left to right) isatoic anhydride, *L*-serine, synthesized OAb-S and elution samples 2-7 from a Sephadex-QAE Econo-Column®.

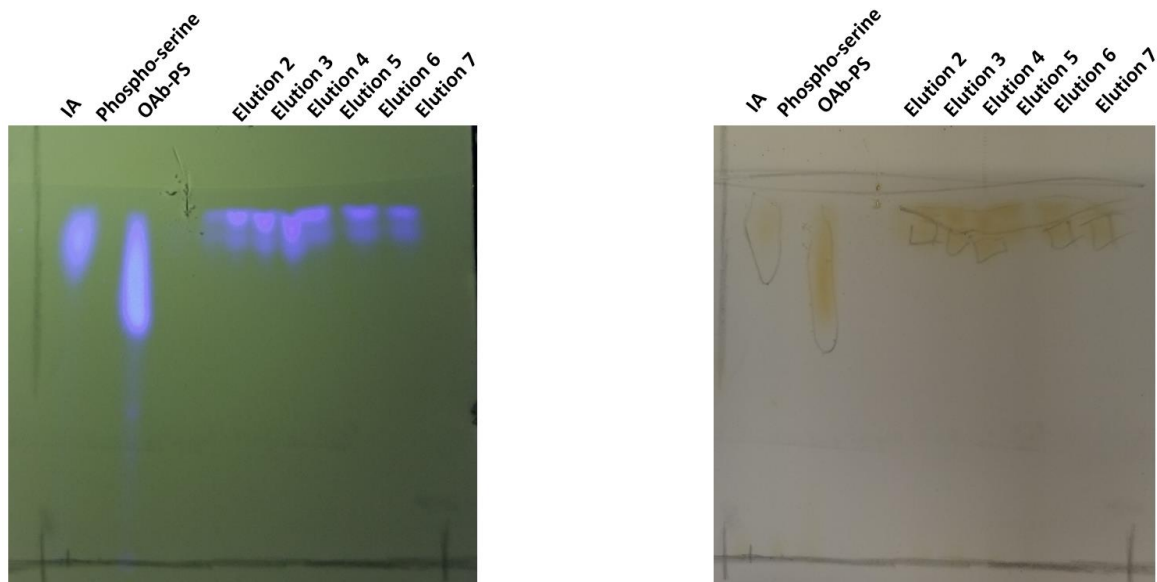


Figure B. 4: Thin Layer Chromatography performed on SiliaPlate™ TLC aluminum backed TLC plates for *o*-aminobenzoyl-phospho-L-serine.

o-aminobenzoyl-phospho-L-serine (OAb-PS) was applied to a packed Sephadex® QAE column, washed with MilliQ (100 mL) and eluted with NaCl (0.1 M, pH 7). Thin Layer Chromatography was performed on SiliaPlate™ TLC aluminum backed TLC plates for (from left to right) isatoic anhydride, *O*-phospho-L-serine, synthesized OAb-PS and elution samples 2-7 from a Sephadex-QAE Econo-Column®.

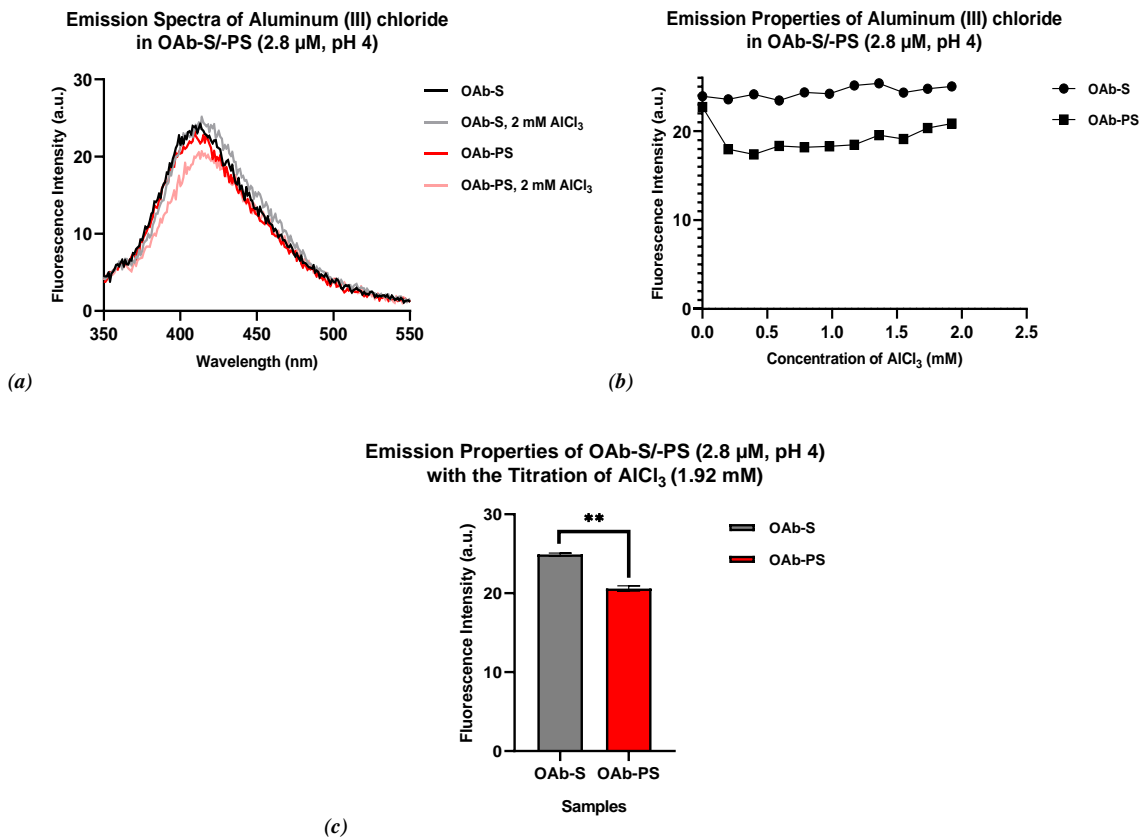


Figure B. 5: Aqueous assay of OAb-S/-PS with the titration of aluminum (III) chloride (1.92 mM, pH 4).

In a 1 mL cuvette OAb-S/-PS (2.8 μ M) in a Tris-HCl (0.1 M, pH 4) solvent was titrated with aluminum (III) chloride. (a) The emission spectral properties of OAb-S/-PS (2.8 μ M, pH 4) are shown with aluminum (III) chloride at 0 μ M and 1.92 mM. (b) The fluorescence emission maximums of OAb-S/-PS (2.8 μ M, pH 4) titrated with aluminum (III) chloride (0 – 1.92 mM). (c) A comparison of OAb-S and OAb-PS emission maximums at 410 nm with aluminum (III) chloride (1.92 mM) (p -value: 0.0041). All samples were excited at 320 nm. P -values were calculated using an unpaired t -test. The error bars represent SEM, $n = 3$.

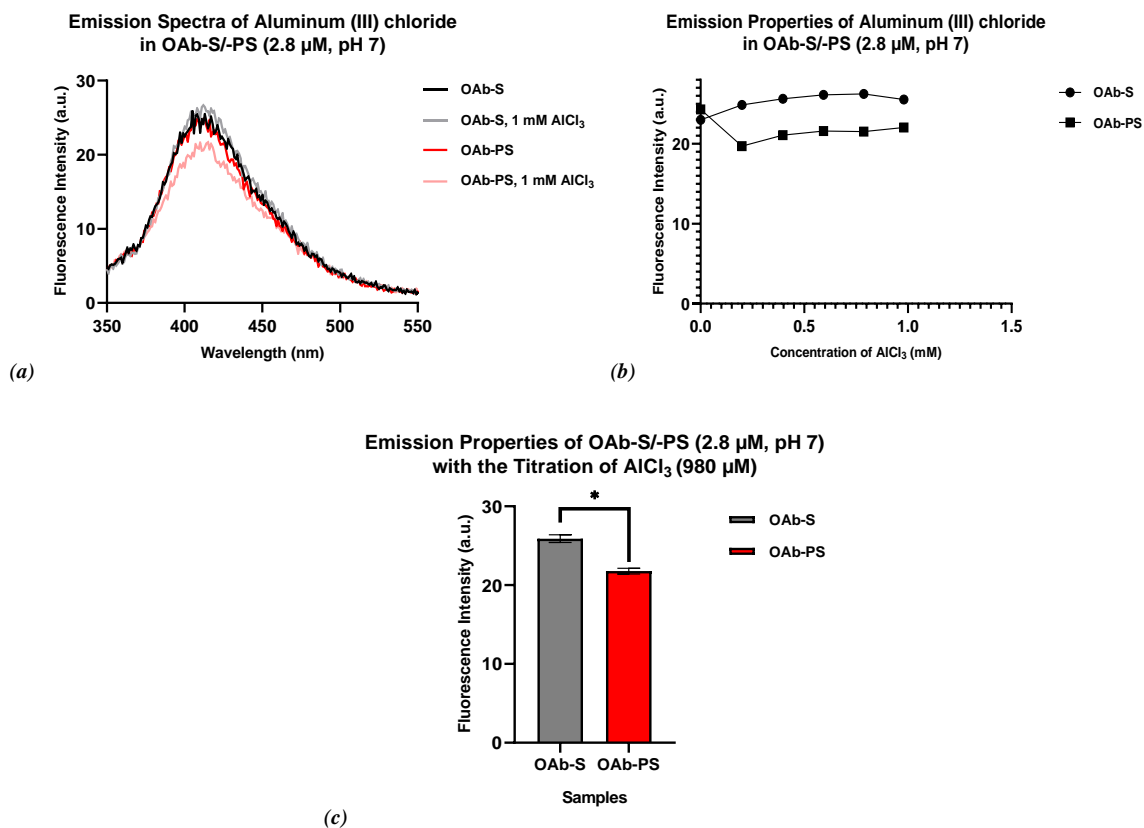


Figure B. 6: Aqueous assay of OAb-S/-PS with the titration of aluminum (III) chloride (980 μ M, pH 7).

In a 1 mL cuvette OAb-S/-PS (2.8 μ M) in a Tris-HCl (0.1 M, pH 7) solvent was titrated with aluminum (III) chloride. (a) The emission spectral properties of OAb-S/-PS (2.8 μ M, pH 7) are shown with aluminum (III) chloride at 0 μ M and 980 μ M. (b) The fluorescence emission maximums of OAb-S/-PS (2.8 μ M, pH 7) titrated with aluminum (III) chloride (0 – 980 μ M). (c) A comparison of OAb-S and OAb-PS emission maximums at 410 nm with aluminum (III) chloride (980 μ M) (p -value: 0.0107). All samples were excited at 320 nm. P -values were calculated using an unpaired t -test. The error bars represent SEM, $n = 3$.

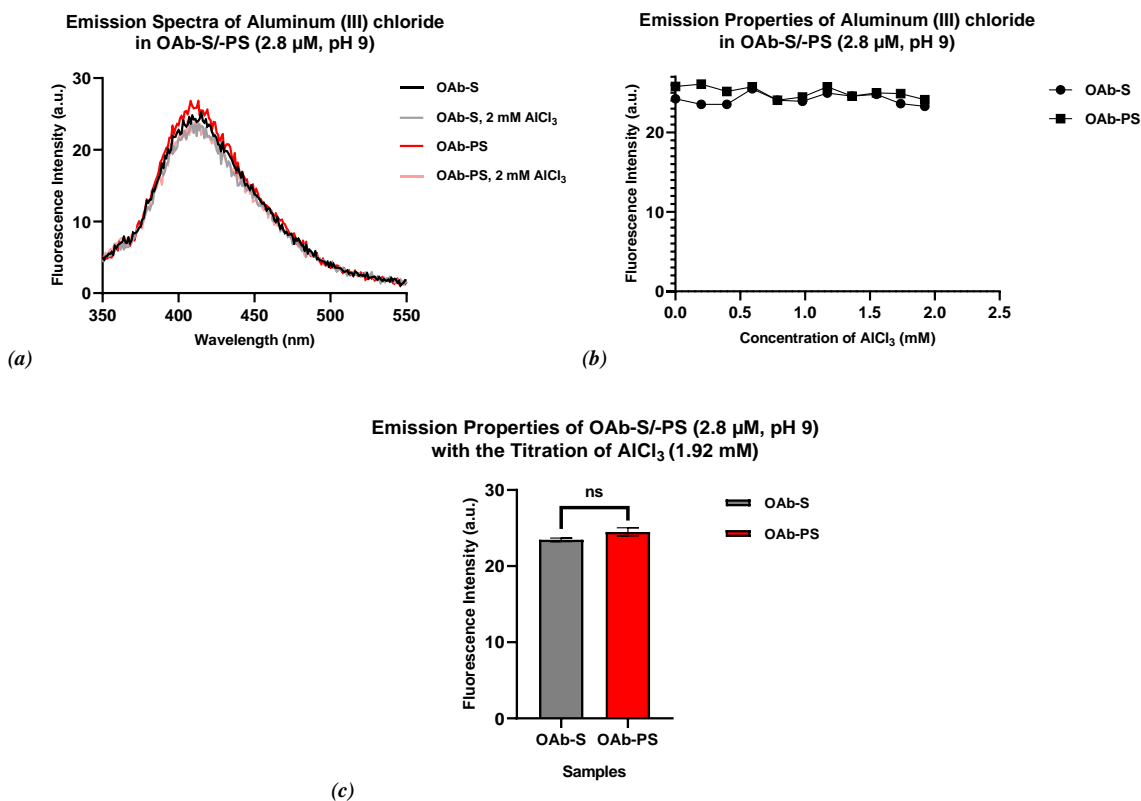


Figure B. 7: Aqueous assay of OAb-S/-PS with the titration of aluminum (III) chloride (1.92 mM, pH 9).

In a 1 mL cuvette OAb-S/-PS (2.8 μ M) in a Tris-HCl (0.1 M, pH 9) solvent was titrated with aluminum (III) chloride. (a) The emission spectral properties of OAb-S/-PS (2.8 μ M, pH 9) are shown with aluminum (III) chloride at 0 μ M and 1.92 mM. (b) The fluorescence emission maximums of OAb-S/-PS (2.8 μ M, pH 9) titrated with aluminum (III) chloride (0 – 1.92 mM). (c) A comparison of OAb-S and OAb-PS emission maximums at 410 nm with aluminum (III) chloride (1.92 mM) (p -value: 0.1295). All samples were excited at 320 nm. P -values were calculated using an unpaired t -test. The error bars represent SEM, $n = 3$.

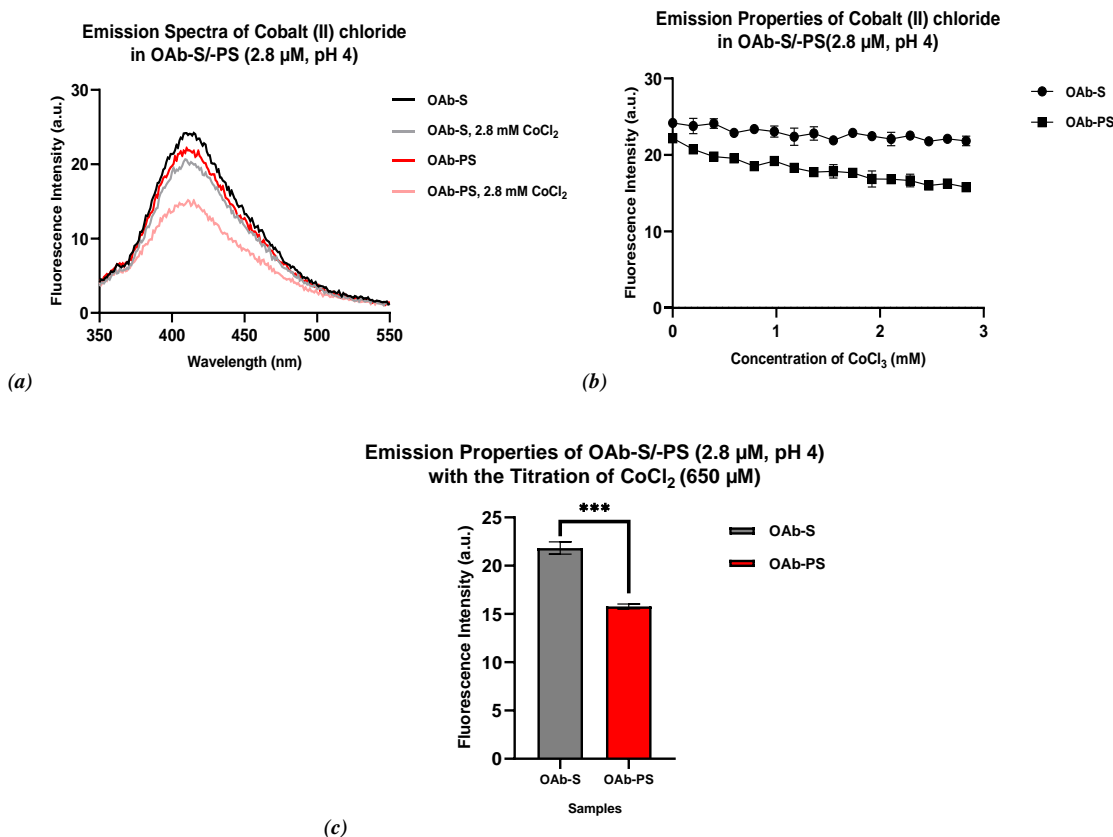


Figure B. 8: Aqueous assay of OAb-S/-PS with the titration of cobalt (II) chloride (650 μM, pH 4).

In a 1 mL cuvette OAb-S/-PS (2.8 μM) in a Tris-HCl (0.1 M, pH 4) solvent was titrated with cobalt (II) chloride. (a) The emission spectral properties of OAb-S/-PS (2.8 μM, pH 4) are shown with cobalt (II) chloride at 0 μM and 650 μM. (b) The fluorescence emission maximums of OAb-S/-PS (2.8 μM, pH 4) titrated with cobalt (II) chloride (0 – 650 μM). (c) A comparison of OAb-S and OAb-PS emission maximums at 410 nm with cobalt (II) chloride (650 μM) (p-value: 0.0001). All samples were excited at 320 nm. P-values were calculated using an unpaired t-test. The error bars represent SEM, n = 3.

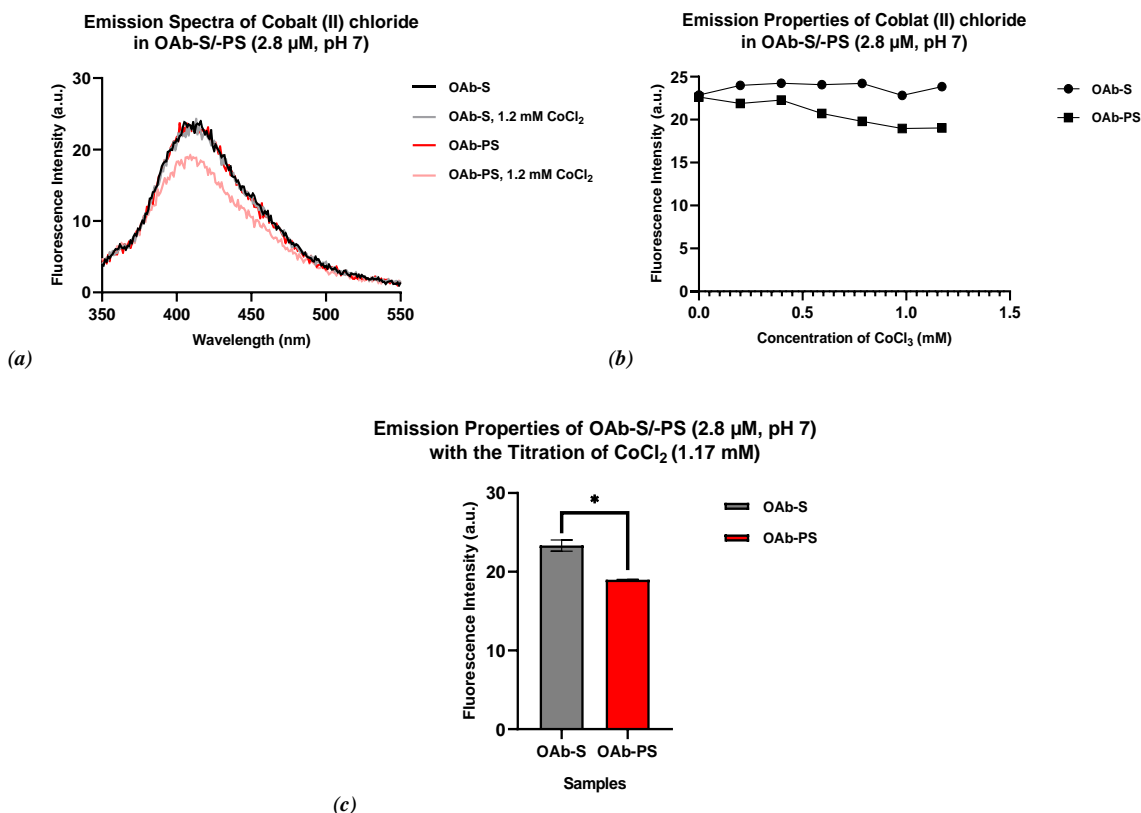


Figure B. 9: Aqueous assay of OAb-S/-PS with the titration of cobalt (II) chloride (1.17 mM, pH 7).

In a 1 mL cuvette OAb-S/-PS (2.8 μ M) in a Tris-HCl (0.1 M, pH 7) solvent was titrated with cobalt (II) chloride. (a) The emission spectral properties of OAb-S/-PS (2.8 μ M, pH 7) are shown with cobalt (II) chloride at 0 μ M and 1.17 mM. (b) The fluorescence emission maximums of OAb-S/-PS (2.8 μ M, pH 7) titrated with cobalt (II) chloride (0 – 1.17 mM). (c) A comparison of OAb-S and OAb-PS emission maximums at 410 nm with cobalt (II) chloride (1.17 mM) (*p*-value: 0.0135). All samples were excited at 320 nm. *P*-values were calculated using an unpaired *t*-test. The error bars represent SEM, *n* = 3.

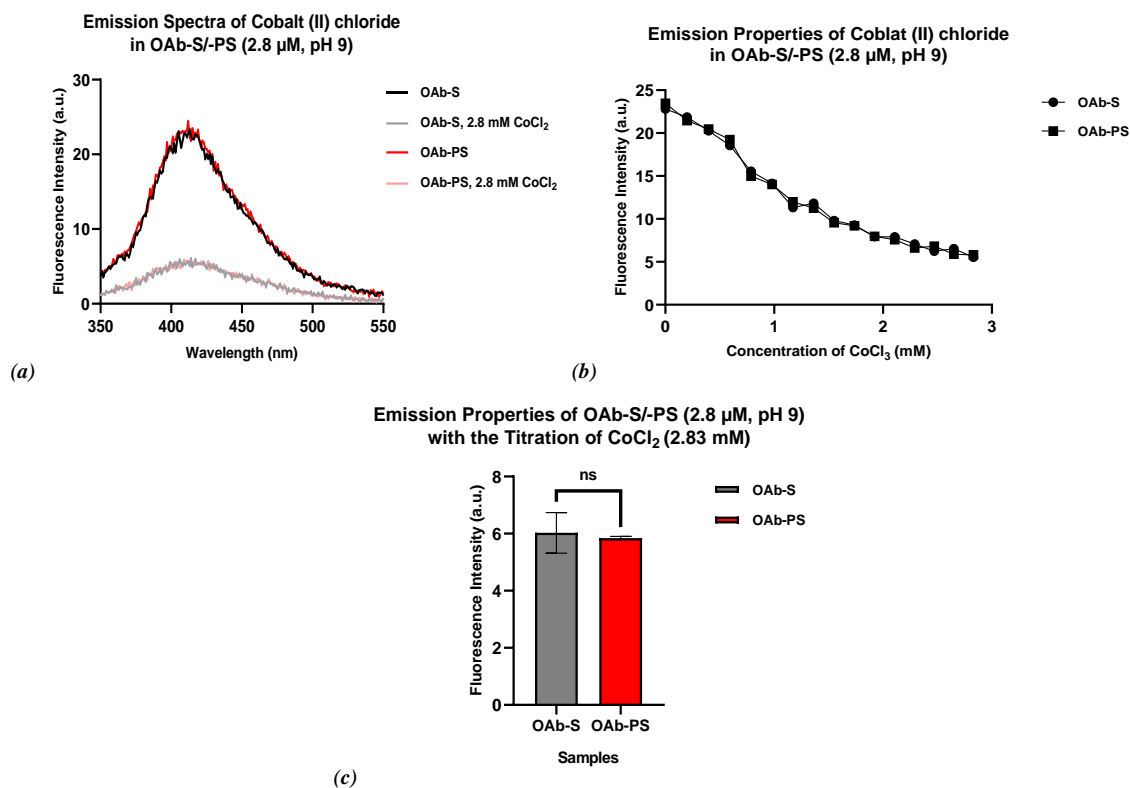


Figure B. 10: Aqueous assay of OAb-S/-PS with the titration of cobalt (II) chloride (2.83 mM, pH 9).

In a 1 mL cuvette OAb-S/-PS (2.8 μ M) in a Tris-HCl (0.1 M, pH 9) solvent was titrated with cobalt (II) chloride. (a) The emission spectral properties of OAb-S/-PS (2.8 μ M, pH 9) are shown with cobalt (II) chloride at 0 μ M and 2.83 mM. (b) The fluorescence emission maximums of OAb-S/-PS (2.8 μ M, pH 7) titrated with cobalt (III) chloride (0 – 2.83 mM). (c) A comparison of OAb-S and OAb-PS emission maximums at 410 nm with cobalt (II) chloride (2.83 mM) (p -value: 0.7525). All samples were excited at 320 nm. P -values were calculated using an unpaired t -test. The error bars represent SEM, $n = 3$.

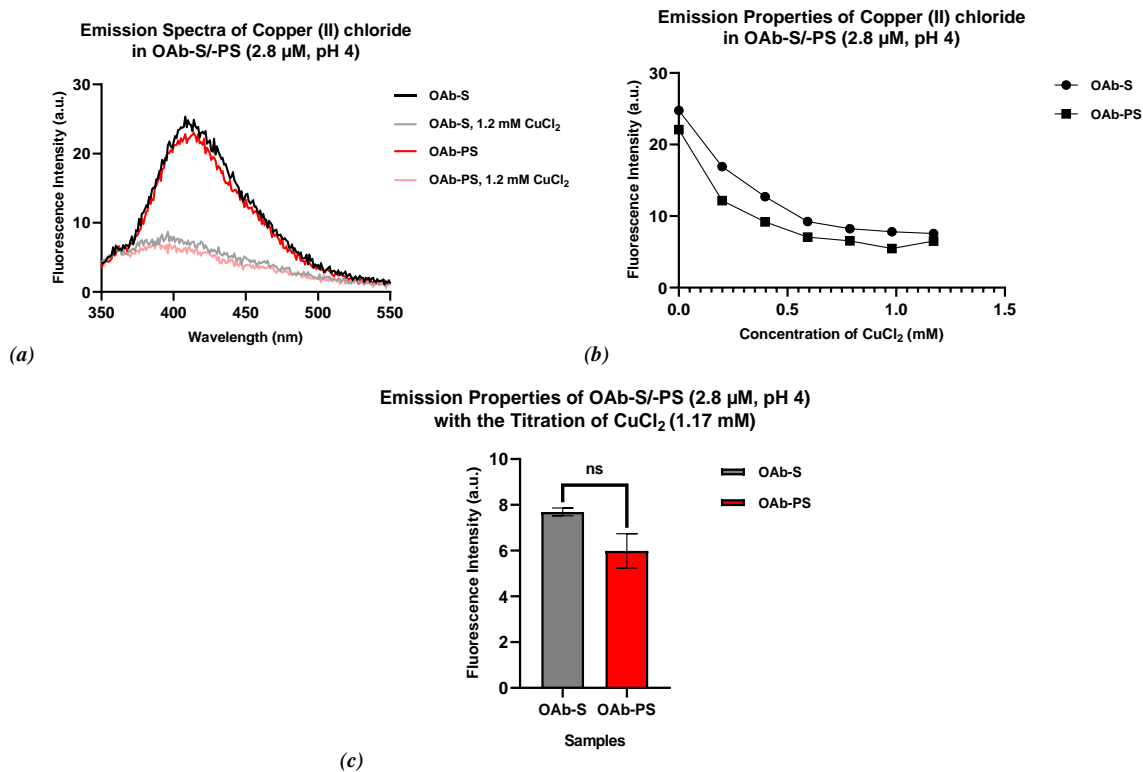


Figure B. 11: Aqueous assay of OAb-S/-PS with the titration of copper (II) chloride (1.17 mM, pH 4).

In a 1 mL cuvette OAb-S/-PS (2.8 μM) in a Tris-HCl (0.1 M, pH 4) solvent was titrated with copper (II) chloride. (a) The emission spectral properties of OAb-S/-PS (2.8 μM, pH 4) are shown with copper (II) chloride at 0 μM and 1.17 mM. (b) The fluorescence emission maximums of OAb-S/-PS (2.8 μM, pH 4) titrated with copper (II) chloride (0 – 1.17 mM). (c) A comparison of OAb-S and OAb-PS emission maximums at 410 nm with copper (II) chloride (1.17 mM) (*p*-value: 0.0887). All samples were excited at 320 nm. *P*-values were calculated using an unpaired *t*-test. The error bars represent SEM, *n* = 3.

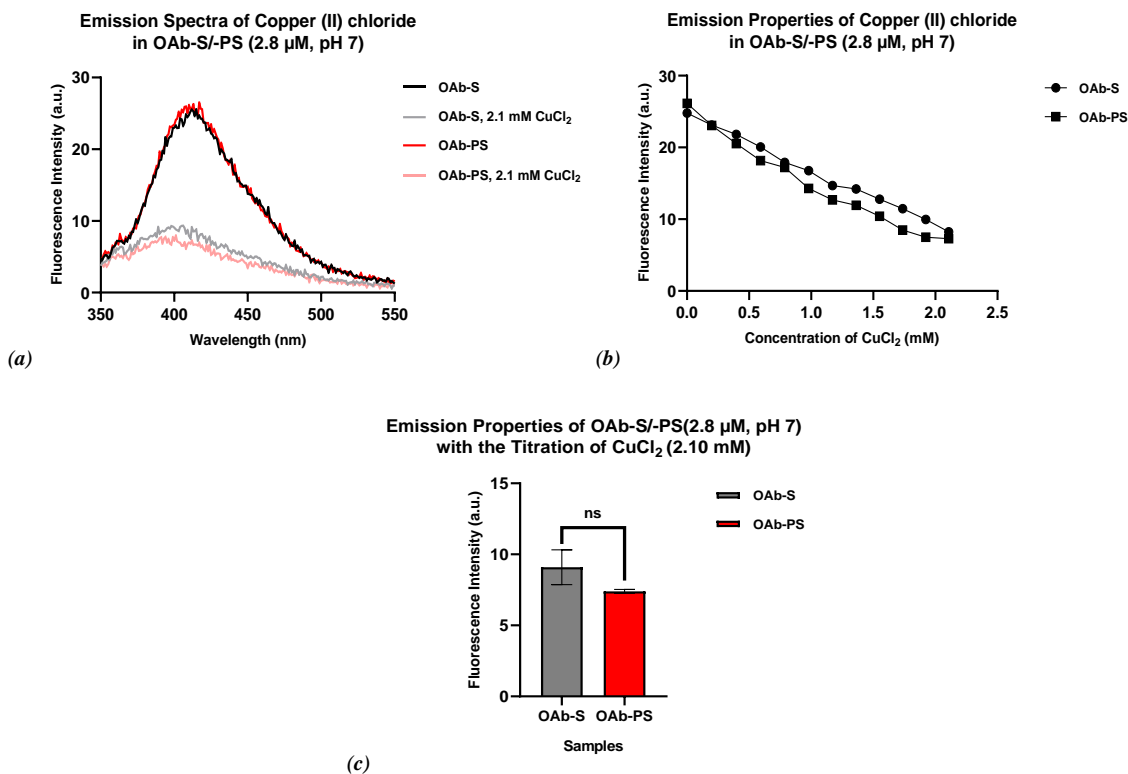


Figure B. 12: Aqueous assay of OAb-S/-PS with the titration of copper (II) chloride (2.10 mM, pH 7).

In a 1 mL cuvette OAb-S/-PS (2.8 μM) in a Tris-HCl (0.1 M, pH 7) solvent was titrated with copper (II) chloride. (a) The emission spectral properties of OAb-S/-PS (2.8 μM, pH 7) are shown with copper (II) chloride at 0 μM and 2.10 mM. (b) The fluorescence emission maximums of OAb-S/-PS (2.8 μM, pH 7) titrated with copper (II) chloride (0 – 2.10 mM). (c) A comparison of OAb-S and OAb-PS emission maximums at 410 nm with copper (II) chloride (2.10 mM) (p-value: 0.1890). All samples were excited at 320 nm. P-values were calculated using an unpaired t-test. The error bars represent SEM, n = 3.

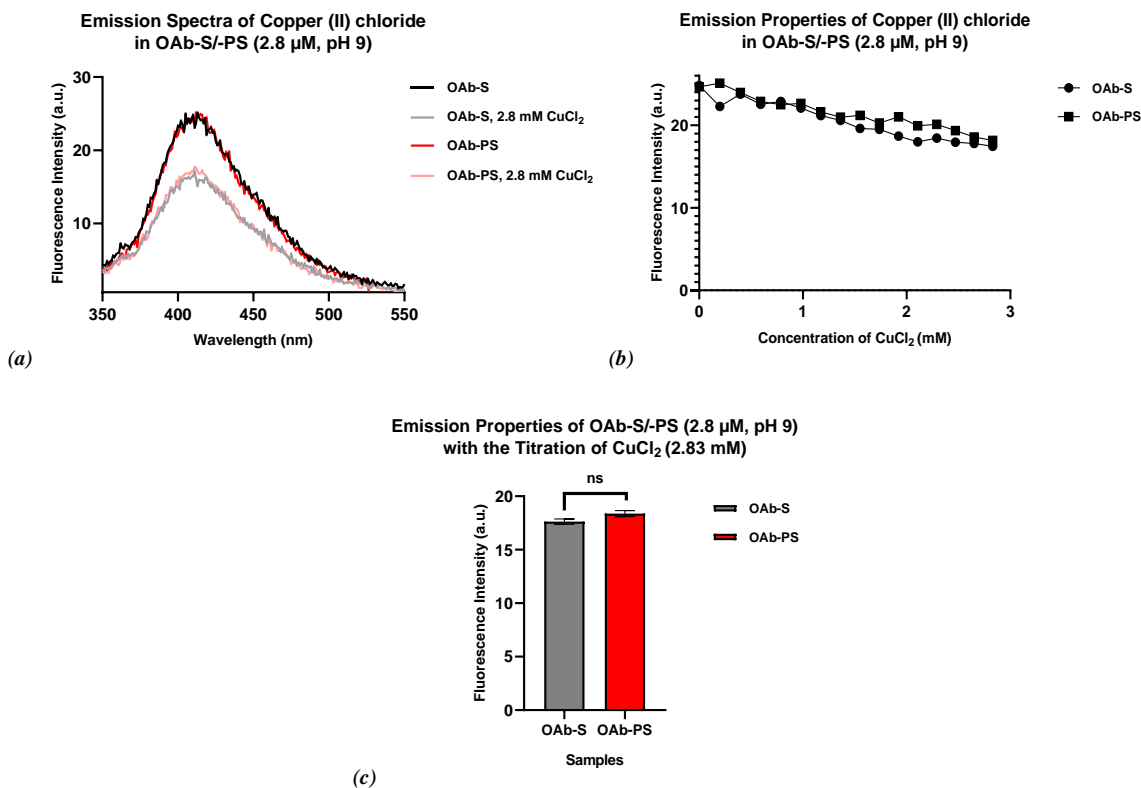


Figure B. 13: Aqueous assay of OAb-S/-PS with the titration of copper (II) chloride (2.83 mM, pH 9).

In a 1 mL cuvette OAb-S/-PS (2.8 μ M) in a Tris-HCl (0.1 M, pH 9) solvent was titrated with copper (II) chloride. (a) The emission spectral properties of OAb-S/-PS (2.8 μ M, pH 9) are shown with copper (II) chloride at 0 μ M and 2.83 mM. (b) The fluorescence emission maximums of OAb-S/-PS (2.8 μ M, pH 9) titrated with copper (II) chloride (0 – 2.83 mM). (c) A comparison of OAb-S and OAb-PS emission maximums at 410 nm with copper (II) chloride (2.83 mM) (p -value: 0.1112). All samples were excited at 320 nm. P -values were calculated using an unpaired t -test. The error bars represent SEM, $n = 3$.

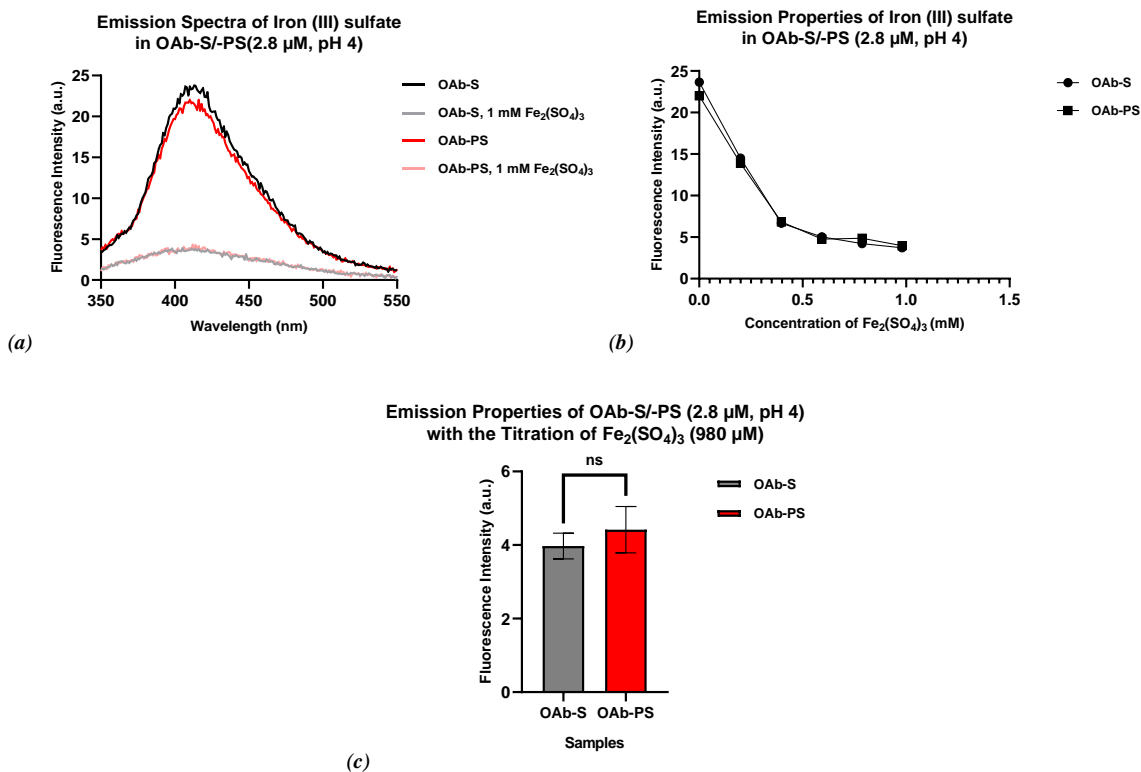


Figure B. 14: Aqueous assay of OAb-S/-PS with the titration of iron (III) sulfate (980 μM, pH 4).

In a 1 mL cuvette OAb-S/-PS (2.8 μM) in a Tris-HCl (0.1 M, pH 4) solvent was titrated with iron (III) sulfate. (a) The emission spectral properties of OAb-S/-PS (2.8 μM, pH 4) are shown with iron (III) sulfate at 0 μM and 980 μM. (b) The fluorescence emission maximums of OAb-S/-PS (2.8 μM, pH 4) titrated with iron (III) sulfate (0 – 980 μM). (c) A comparison of OAb-S and OAb-PS emission maximums at 410 nm with iron (III) sulfate (980 μM) (*p*-value: 0.4758). All samples were excited at 320 nm. *P*-values were calculated using an unpaired *t*-test. The error bars represent SEM, *n* = 3.

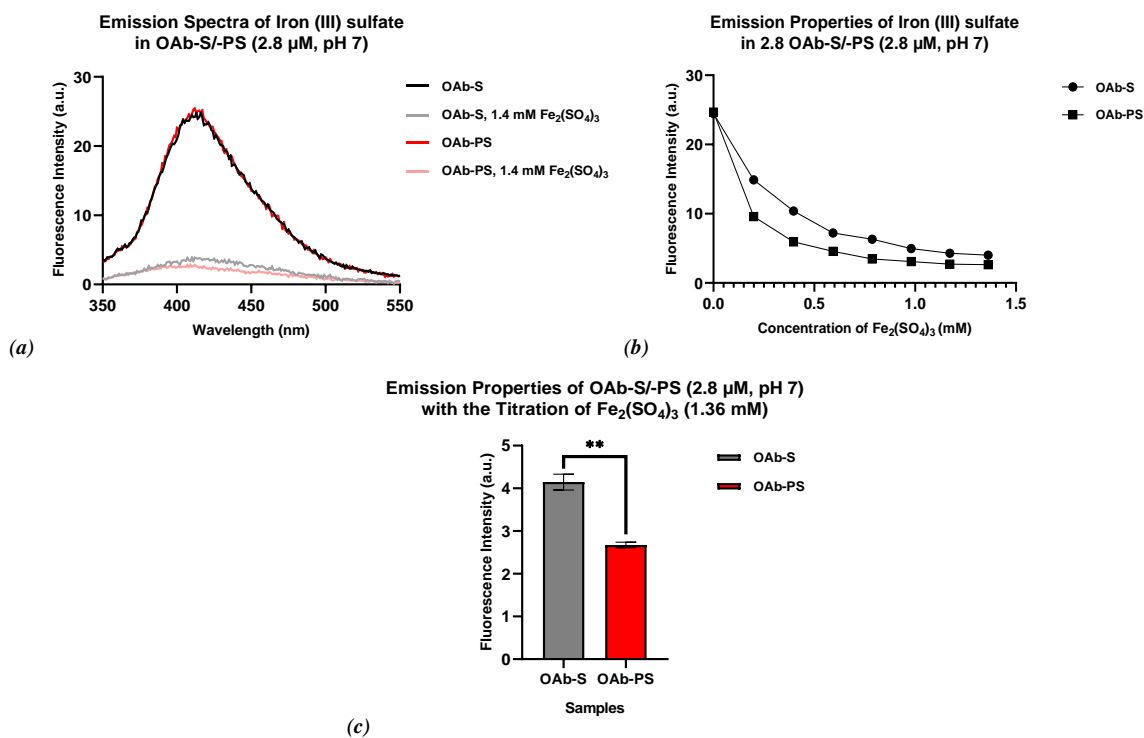


Figure B. 15: Aqueous assay of OAb-S/-PS with the titration of iron (III) sulfate (1.36 mM, pH 7).

In a 1 mL cuvette OAb-S/-PS (2.8 μ M) in a Tris-HCl (0.1 M, pH 7) solvent was titrated with iron (III) sulfate. (a) The emission spectral properties of OAb-S/-PS (2.8 μ M, pH 7) are shown with iron (III) sulfate at 0 μ M and 1.36 mM. (b) The fluorescence emission maximums of OAb-S/-PS (2.8 μ M, pH 7) titrated with iron (III) sulfate (0 – 1.36 mM). (c) A comparison of OAb-S and OAb-PS emission maximums at 410 nm with iron (III) sulfate (1.36 mM) (p -value: 0.0088). All samples were excited at 320 nm. P -values were calculated using an unpaired t -test. The error bars represent SEM, $n = 3$.

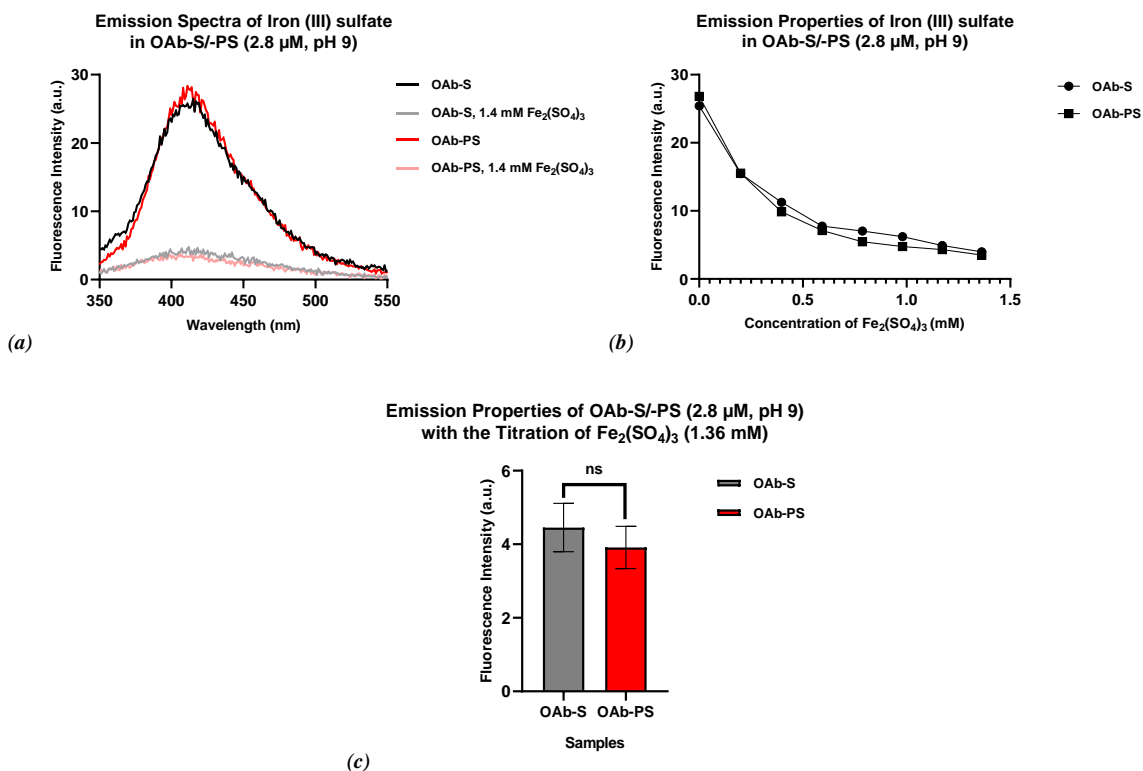


Figure B. 16: Aqueous assay of OAb-S/-PS with the titration of iron (III) sulfate (1.36 mM, pH 9).

In a 1 mL cuvette OAb-S/-PS (2.8 μM) in a Tris-HCl (0.1 M, pH 9) solvent was titrated with iron (III) sulfate. (a) The emission spectral properties of OAb-S/-PS (2.8 μM, pH 9) are shown with iron (III) sulfate at 0 μM and 1.36 mM. (b) The fluorescence emission maximums of OAb-S/-PS (2.8 μM, pH 9) titrated with iron (III) sulfate (0 – 1.36 mM). (c) A comparison of OAb-S and OAb-PS emission maximums at 410 nm with iron (III) sulfate (1.36 mM) (*p*-value: 0.4752). All samples were excited at 320 nm. *P*-values were calculated using an unpaired *t*-test. The error bars represent SEM, *n* = 3.

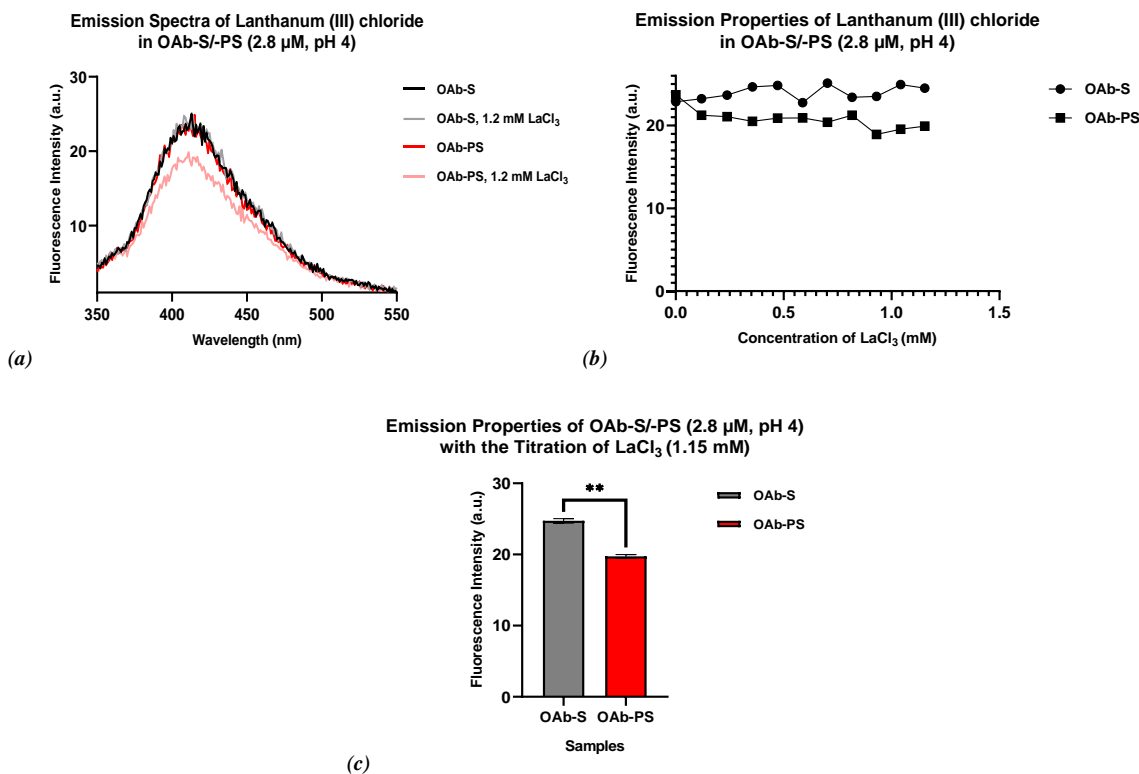


Figure B. 17: Aqueous assay of OAb-S/-PS with the titration of lanthanum (III) chloride (1.15 mM, pH 4).

In a 1 mL cuvette OAb-S/-PS (2.8 μ M) in a Tris-HCl (0.1 M, pH 4) solvent was titrated with lanthanum (III) chloride. (a) The emission spectral properties of OAb-S/-PS (2.8 μ M, pH 4) are shown with lanthanum (III) chloride at 0 μ M and 1.15 mM. (b) The fluorescence emission maximums of OAb-S/-PS (2.8 μ M, pH 4) titrated with lanthanum (III) chloride (0 – 1.15 mM). (c) A comparison of OAb-S and OAb-PS emission maximums at 410 nm with lanthanum (III) chloride (1.15 mM) (*p*-value: 0.0031). All samples were excited at 320 nm. *P*-values were calculated using an unpaired *t*-test. The error bars represent SEM, *n* = 3.

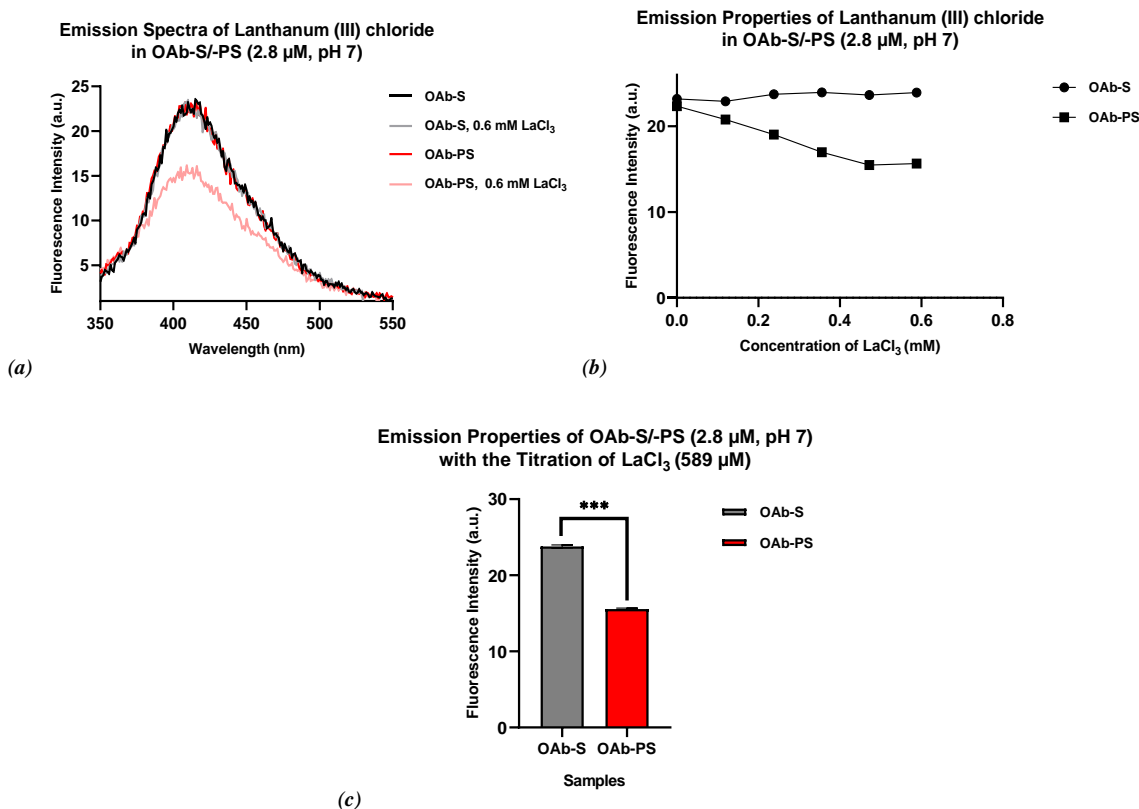


Figure B. 18: Aqueous assay of OAb-S/-PS with the titration of lanthanum (III) chloride (589 μM, pH 7).

In a 1 mL cuvette OAb-S/-PS (2.8 μM) in a Tris-HCl (0.1 M, pH 7) solvent was titrated with lanthanum (III) chloride. (a) The emission spectral properties of OAb-S/-PS (2.8 μM, pH 7) are shown lanthanum (III) chloride at 0 μM and 589 μM. (b) The fluorescence emission maximums of OAb-S/-PS (2.8 μM, pH 7) titrated with lanthanum (III) chloride (0 – 589 μM). (c) A comparison of OAb-S and OAb-PS emission maximums at 410 nm with lanthanum (III) chloride (589 μM) (*p*-value: 0.0004). All samples were excited at 320 nm. *P*-values were calculated using an unpaired *t*-test. The error bars represent SEM, *n* = 3.

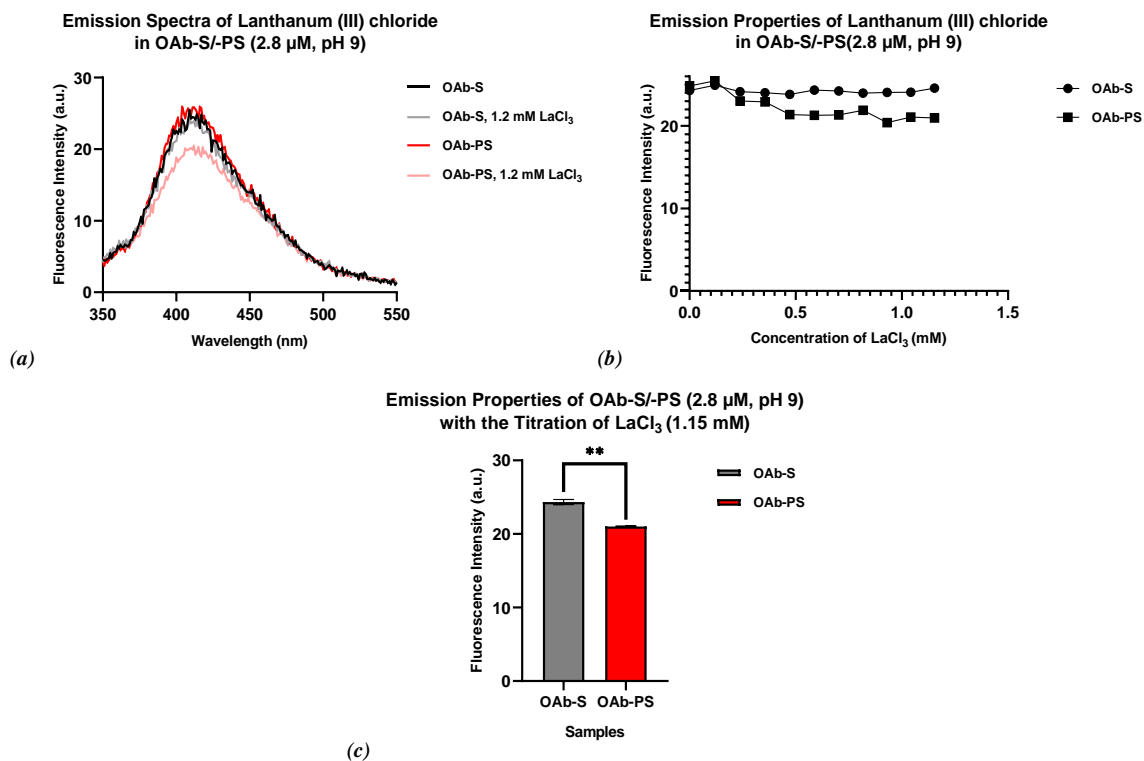


Figure B. 19: Aqueous assay of OAb-S/-PS with the titration of lanthanum (III) chloride (1.15 mM, pH 9).

In a 1 mL cuvette OAb-S/-PS (2.8 μM) in a Tris-HCl (0.1 M, pH 9) solvent was titrated with lanthanum (III) chloride. (a) The emission spectral properties of OAb-S/-PS (2.8 μM, pH 9) are shown with lanthanum (III) chloride at 0 μM and 1.15 mM. (b) The fluorescence emission maximums of OAb-S/-PS (2.8 μM, pH 9) titrated with lanthanum (III) chloride (0 – 1.15 mM). (c) A comparison of OAb-S and OAb-PS emission maximums at 410 nm with lanthanum (III) chloride (1.15 mM) (*p*-value: 0.0058). All samples were excited at 320 nm. *P*-values were calculated using an unpaired *t*-test. The error bars represent SEM, *n* = 3.

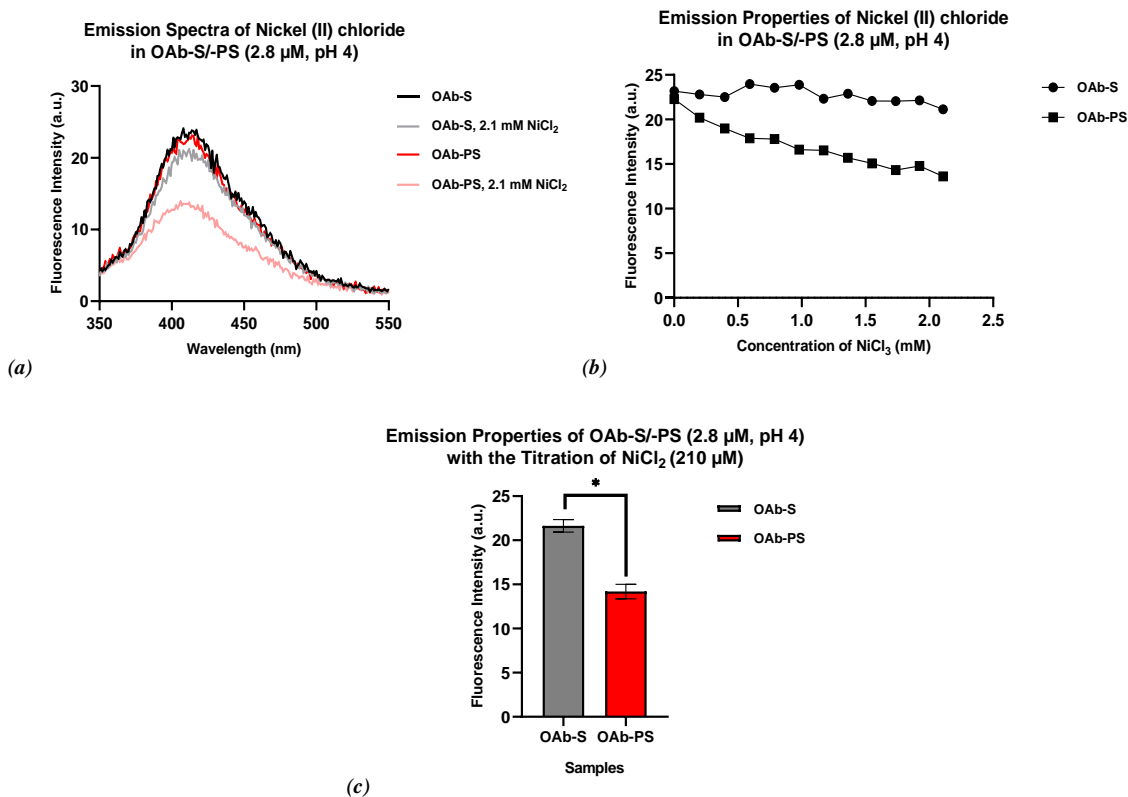


Figure B. 20: Aqueous assay of OAb-S/-PS with the titration of nickel (II) chloride (210 μM, pH 4).

In a 1 mL cuvette OAb-S/-PS (2.8 μM) in a Tris-HCl (0.1 M, pH 4) solvent was titrated with nickel (II) chloride. (a) The emission spectral properties of OAb-S/-PS (2.8 μM, pH 4) are shown with nickel (II) chloride at 0 μM and 210 μM. (b) The fluorescence emission maximums of OAb-S/-PS (2.8 μM, pH 4) titrated with nickel (II) chloride (0 – 210 μM). (c) A comparison of OAb-S and OAb-PS emission maximums at 410 nm with nickel (II) chloride (210 μM) (*p*-value: 0.0105). All samples were excited at 320 nm. *P*-values were calculated using an unpaired *t*-test. The error bars represent SEM, *n* = 3.

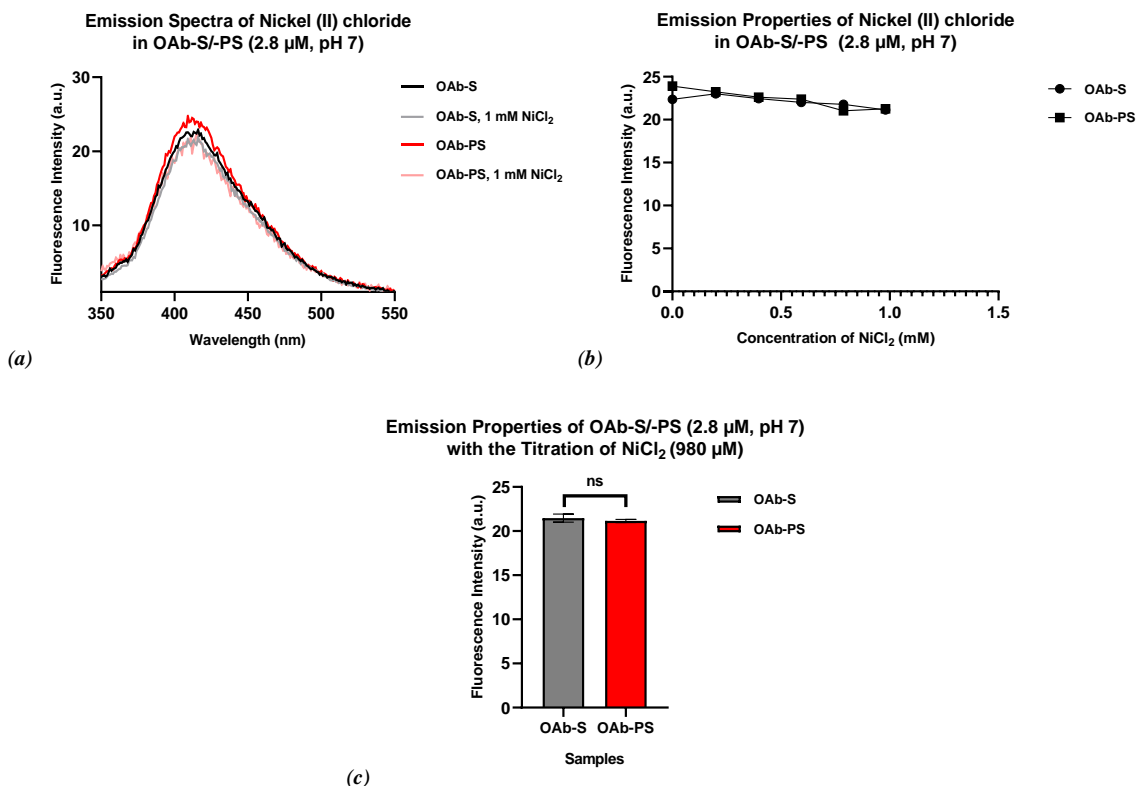


Figure B. 21: Aqueous assay of OAb-S/-PS with the titration of nickel (II) chloride (980 μM, pH 7).

In a 1 mL cuvette OAb-S/-PS (2.8 μM) in a Tris-HCl (0.1 M, pH 7) solvent was titrated with nickel (II) chloride. (a) The emission spectral properties of OAb-S/-PS (2.8 μM, pH 7) are shown with nickel (II) chloride at 0 μM and 980 μM. (b) The fluorescence emission maximums of OAb-S/-PS (2.8 μM, pH 7) titrated with nickel (II) chloride (0 – 980 μM). (c) A comparison of OAb-S and OAb-PS emission maximums at 410 nm with nickel (II) chloride (980 μM) (*p*-value: 0.4503). All samples were excited at 320 nm. *P*-values were calculated using an unpaired *t*-test. The error bars represent SEM, *n* = 3.

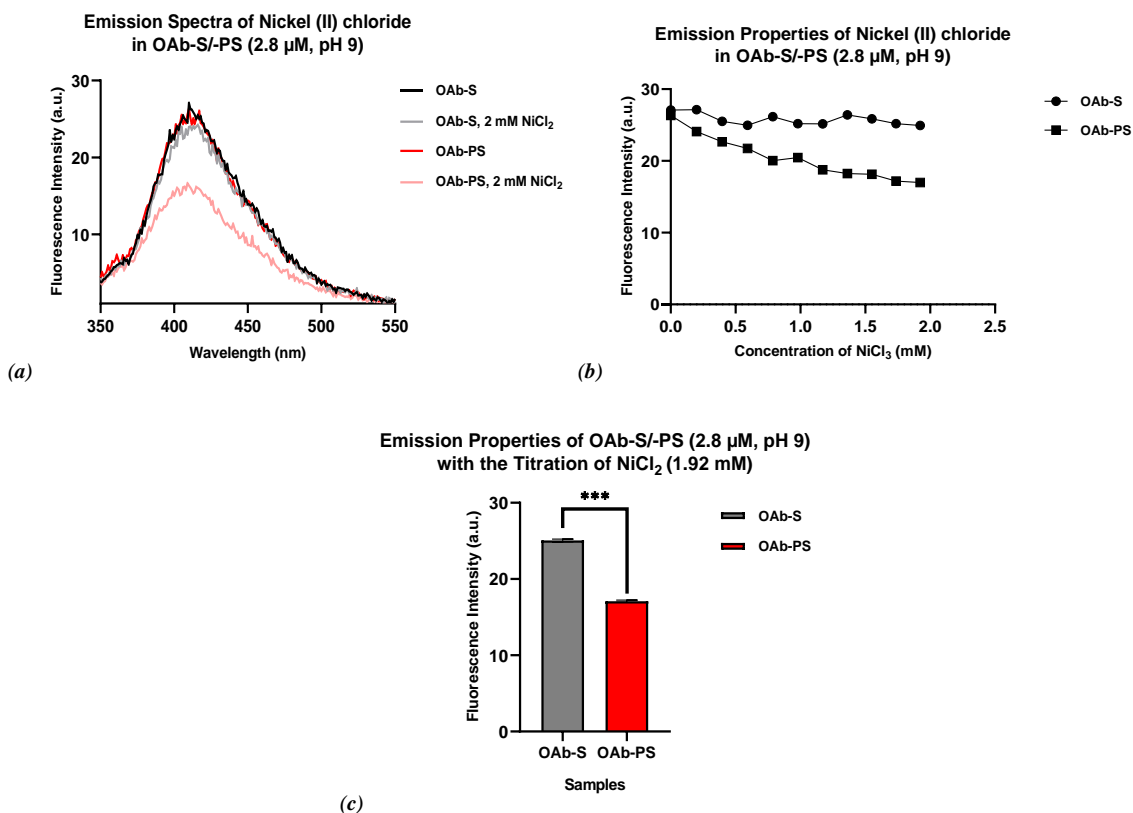


Figure B. 22: Aqueous assay of OAb-S/-PS with the titration of nickel (II) chloride (1.92 mM, pH 9).

In a 1 mL cuvette OAb-S/-PS (2.8 μ M) in a Tris-HCl (0.1 M, pH 9) solvent was titrated with nickel (II) chloride. (a) The emission spectral properties of OAb-S/-PS (2.8 μ M, pH 9) are shown with nickel (II) chloride at 0 μ M and 1.92 mM. (b) The fluorescence emission maximums of OAb-S/-PS (2.8 μ M, pH 9) titrated with nickel (II) chloride (0 – 1.92 mM). (c) A comparison of OAb-S and OAb-PS emission maximums at 410 nm with nickel (II) chloride (1.92 mM) (*p*-value: 0.0004). All samples were excited at 320 nm. *P*-values were calculated using an unpaired *t*-test. The error bars represent SEM, *n* = 3.

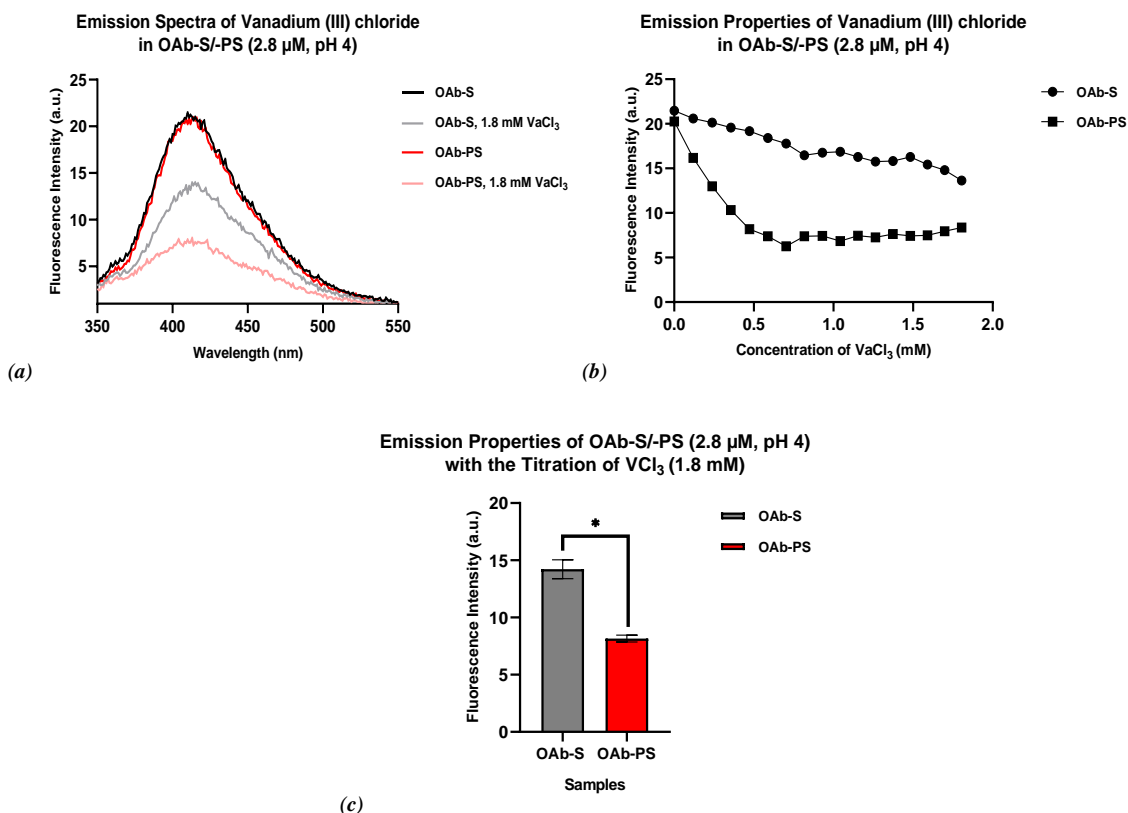


Figure B. 23: Aqueous assay of OAb-S/-PS with the titration of vanadium (III) chloride (1.8 mM, pH 4).

In a 1 mL cuvette OAb-S/-PS (2.8 μ M) in a Tris-HCl (0.1 M, pH 4) solvent was titrated with vanadium (III) chloride. (a) The emission spectral properties of OAb-S/-PS (2.8 μ M, pH 4) are shown with vanadium (III) chloride at 0 μ M and 1.8 mM. (b) The fluorescence emission maximums of OAb-S/-PS (2.8 μ M, pH 4) titrated with vanadium (III) chloride (0 – 1.8 mM). (c) A comparison of OAb-S and OAb-PS emission maximums at 410 nm with vanadium (III) chloride (1.8 mM) (*p*-value: 0.0103). All samples were excited at 320 nm. *P*-values were calculated using an unpaired *t*-test. The error bars represent SEM, *n* = 3.

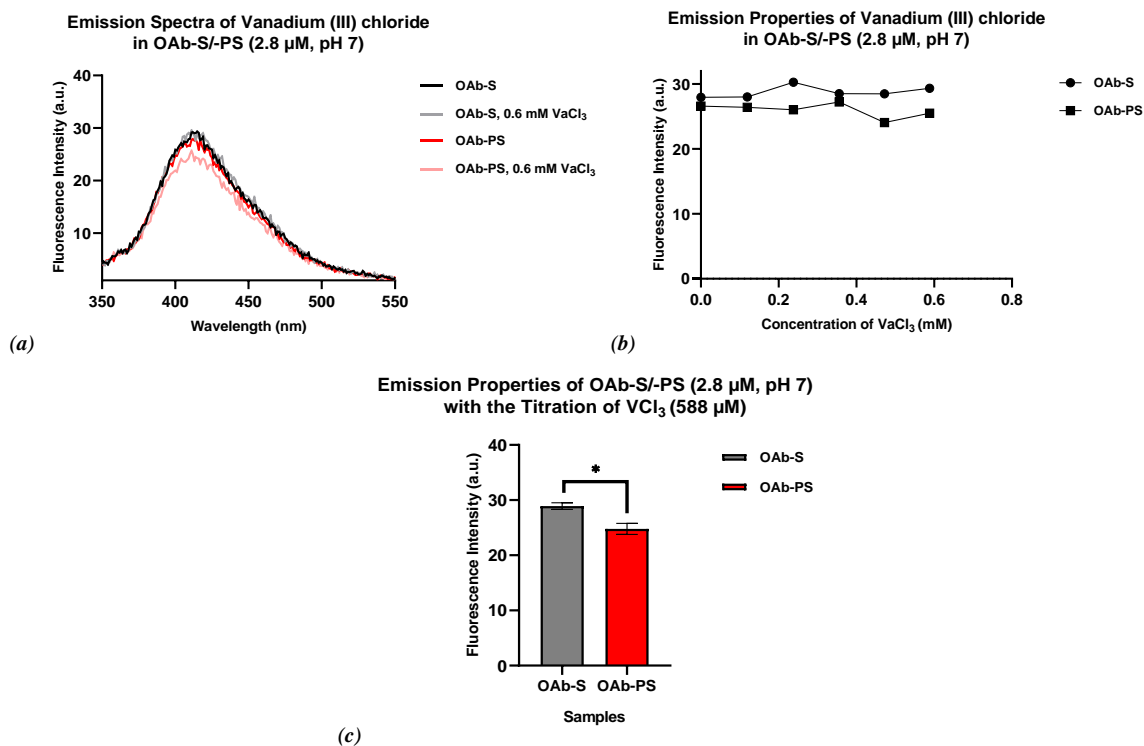


Figure B. 24: Aqueous assay of OAb-S/-PS with the titration of vanadium (III) chloride (588 μM, pH 7).

In a 1 mL cuvette OAb-S/-PS (2.8 μM) in a Tris-HCl (0.1 M, pH 7) solvent was titrated with vanadium (III) chloride. (a) The emission spectral properties of OAb-S/-PS (2.8 μM, pH 7) are shown with vanadium (III) chloride at 0 μM and 588 μM. (b) The fluorescence emission maximums of OAb-S/-PS (2.8 μM, pH 7) titrated with vanadium (III) chloride (0 – 588 μM). (c) A comparison of OAb-S and OAb-PS emission maximums at 410 nm with vanadium (III) chloride (588 μM) (*p*-value: 0.0381). All samples were excited at 320 nm. *P*-values were calculated using an unpaired *t*-test. The error bars represent SEM, *n* = 3.

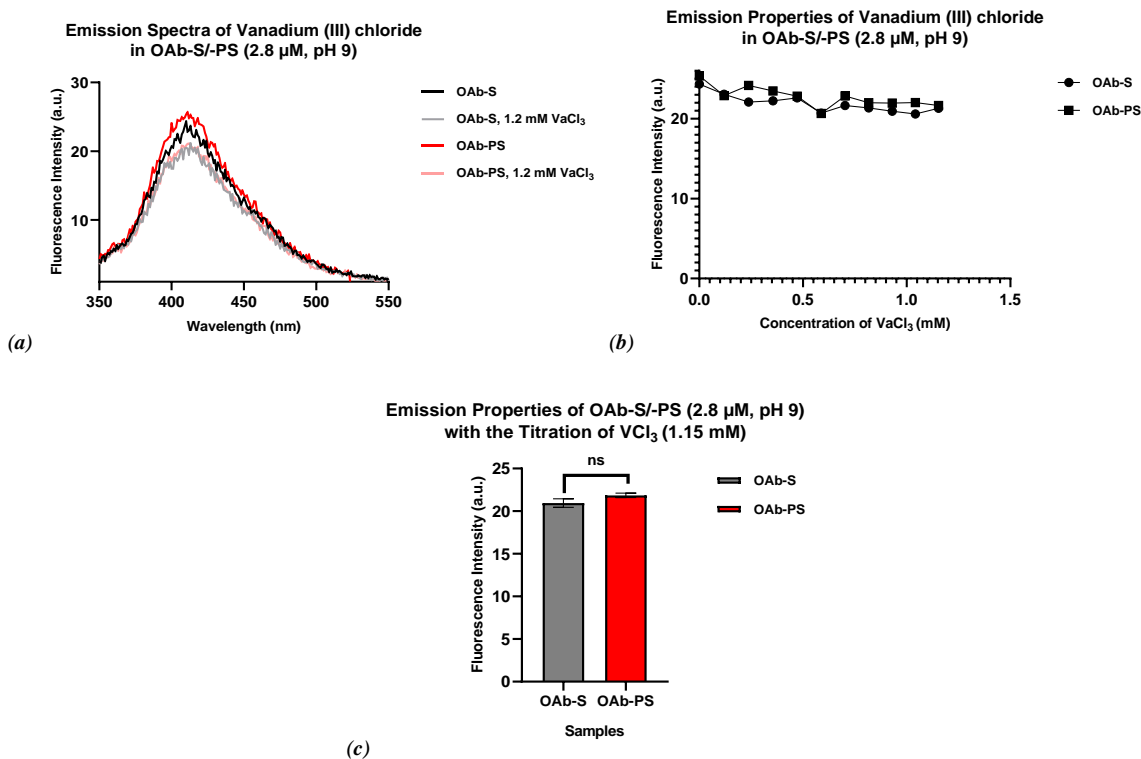


Figure B. 25: Aqueous assay of OAb-S/-PS with the titration of vanadium (III) chloride (1.15 mM, pH 9).

In a 1 mL cuvette OAb-S/-PS (2.8 μM) in a Tris-HCl (0.1 M, pH 9) solvent was titrated with vanadium (III) chloride. (a) The emission spectral properties of OAb-S/-PS (2.8 μM, pH 9) are shown with vanadium (III) chloride at 0 μM and 1.15 mM. (b) The fluorescence emission maximums of OAb-S/-PS (2.8 μM, pH 9) titrated with vanadium (III) chloride (0 – 1.15 mM). (c) A comparison of OAb-S and OAb-PS emission maximums at 410 nm with vanadium (III) chloride (1.15 mM) (*p*-value: 0.1535). All samples were excited at 320 nm. *P*-values were calculated using an unpaired *t*-test. The error bars represent SEM, *n* = 3.

Appendix C (Copyright permissions)

SPRINGER NATURE LICENSE TERMS AND CONDITIONS

Jul 15, 2020

This Agreement between University of Windsor -- Angela Awada ("You") and Springer Nature ("Springer Nature") consists of your license details and the terms and conditions provided by Springer Nature and Copyright Clearance Center.

License Number	4870001323037
License date	Jul 15, 2020
Licensed Content Publisher	Springer Nature
Licensed Content Publication	Analytical and Bioanalytical Chemistry
Licensed Content Title	Joseph R. Lakowicz: Principles of fluorescence spectroscopy, 3rd Edition
Licensed Content Author	Christiane Albrecht
Licensed Content Date	Jan 16, 2008
Type of Use	Thesis/Dissertation
Requestor type	academic/university or research institute
Format	print and electronic
Portion	figures/tables/illustrations
Number of figures/tables/illustrations	3

Will you be translating?	no
Circulation/distribution	1 - 29
Author of this Springer Nature content	no
Title	Graduate student
Institution name	University of Windsor
Expected presentation date	Sep 2020
Portions	Figure 1.24. Figure 6.2. Figure 8.43.
Requestor Location	University of Windsor 401 Sunset Ave Essex Hall, 274-3 Windsor, ON N9B 3P4 Canada Attn: University of Windsor
Total	0.00 CAD
Terms and Conditions	

VITA AUCTORIS

NAME: Angela Awada

PLACE OF BIRTH: Ottawa, ON

YEAR OF BIRTH: 1995

EDUCATION: Hon. W.C. Kennedy Collegiate Institute, Windsor, ON, 2013

University of Windsor, B.Sc., Windsor, ON, 2018

University of Windsor, M.Sc., Windsor, ON, 2020

PUBLICATIONS: Meister, D., Ure, D., **Awada, A.**, Barrette, J.C., Gagnon, J., Mutus, B., Trant, J.F.: Covalently Functionalized Sawdust for the Remediation of Phosphate from Agricultural Wastewater. ACS Sustain. Chem. Eng. 7, 20139–20150 (2019). <https://pubs.acs.org/doi/10.1021/acssuschemeng.9b06073>

Ure, D., **Awada, A.**, Frowley, N., Munk, N., Stanger, A., Mutus, B.: Greenhouse tomato plant roots/carboxymethyl cellulose method for the efficient removal and recovery of inorganic phosphate from agricultural wastewater. J. Environ. Manage. 233, 258–263 (2018). <https://doi.org/10.1016/j.jenvman.2018.12.053>